

**Evaluation of LIMD1-VHL targeting microRNA as
biomarker in Uterine Cervical Carcinogenesis**

**THESIS SUBMITTED FOR THE DEGREE OF
DOCTOR OF PHILOSOPHY (SCIENCE)**

OF

JADAVPUR UNIVERSITY

2025



BY

FARHIN SULTANA

**DEPARTMENT OF ONCOGENE REGULATION
CHITTARANJAN NATIONAL CANCER INSTITUTE
KOLKATA-700026**

Index No: 117/21/Life Sc./27



चितरंजन राष्ट्रीय कैंसर संस्थान
CHITTARANJAN NATIONAL CANCER INSTITUTE

(An Autonomous Institute under Ministry of Health and Family Welfare, Govt. of India)

(स्वास्थ्य और परिवार कल्याण मंत्रालय, भारत सरकार के अधीन एक स्वायत्त संस्थान)

प्रथम कैंपस – 37, एस.पी. मुखर्जी रोड, कोलकाता-700026/1st Campus – 37, S. P. Mukherjee Road, Kolkata - 700 026

द्वितीय परिसर - स्ट्रीट नंबर 299, प्लॉट नंबर डीजे - 01, परिसर नंबर 02-0321, एक्शन एरिया 1डी, न्यू टाउन, कोलकाता – 700160

2nd Campus - Street No.299, Plot No. DJ – 01, Premises No. 02-0321, Action Area 1D, New Town, Kolkata – 700160

CERTIFICATE FROM THE SUPERVISORS

This is to certify that the thesis entitled "Evaluation of LIMD1-VHL targeting microRNA as biomarker in Uterine Cervical Carcinogenesis", submitted by Smt. Farhin Sultana who got her name registered on 26.11.2021 (Index No: 117/21/Life Sc./27) for the award of Ph. D. (Science) Degree of Jadavpur University, is absolutely based upon her own work under the supervision of Dr. Sankhadeep Dutta and Dr. Chinmay Kumar Panda (Co-supervisor) and that neither this thesis nor any part of it has been submitted for either any degree / diploma or any other academic award anywhere before.


17/03/2025

(Supervisor)

Dr. Sankhadeep Dutta, Ph.D.
Senior Scientific Officer, Grade-II
Dept. of Oncogene Regulation
CHITTARANJAN NATIONAL CANCER INSTITUTE
37, S. P. Mukherjee Road, Kolkata-700 026


17/03/2025

(Co-Supervisor)

Dr. Chinmay Kumar Panda, Ph.D, FNASc, FAScT
NASI Senior Scientist Platinum Jubilee Fellow
Officer-in-charge (Research)- Former
Senior Assistant Director Grade- Retired
Dept. of Oncogene Regulation
CHITTARANJAN NATIONAL CANCER INSTITUTE
37, S. P. Mukherjee Road, Kolkata-700 026

***Dedicated to
my beloved family...***

<u>Contents</u>	Page No.
Acknowledgement	i-iii
List of Abbreviations	iv-v
Summary	vi-viii
Chapter 1- General Introduction	1-53
1.1 Cervical Cancer: an overview	1-31
1.1.1 Histopathogenesis of CaCx:	3-5
1.1.2 Etiology of CaCx:	5-6
1.1.3 Association of Human Papillomavirus with Cervical Carcinogenesis:	6-22
1.1.4 CaCx early detection for prevention: The screen-triage-treat model	23-31
1.2 Molecular basis of Uterine Cervical Carcinogenesis:	31-45
1.2.1 Chromosomal alteration during cervical carcinogenesis: effect on coding, non-coding RNA expression and altered pathways	31-41
1.2.2. Contribution of onco-miR during carcinogenesis of uterine cervix:	41-44
1.2.3 miRNA as triage biomarker for CaCx: A non-invasive approach	44-45
1.3 Importance of miRNAs targeting LIMD1-VHL associated hypoxic stress response pathway during Cervical Carcinogenesis	46-53
1.3.1 Hypoxia, role of LIMD1-VHL and cervical carcinogenesis	46-50
1.3.2 MiRNAs as master player in the hypoxic stress response pathway	50-53
Chapter 2- Scope of the study	54-58
Chapter 3- Analysis of the expression profiles of LIMD1, VHL and their targeting miRNA(s) along with genetic alteration mechanism of the frequently deregulated miRNA, during development of CaCx	59-82
3.1 Introduction	60-61
3.2 Objective of the study	61
3.3 Materials and Methods	61-72
3.4 Result	72-80
3.5 Discussion	81-82
3.6 Inference points	82
Chapter 4 Evaluation of the candidate miRNA(s) as molecular biomarkers in cervical swabs from population-based cancer screening	83-111
4.1 Introduction	84-85

4.2 Objective of the study	85
4.3 Materials and Methods	85-98
4.4 Result	99-108
4.5 Discussion	109-110
4.6 Inference points	111
Chapter 5 <i>In vitro</i> functional validation of the candidate miRNA(s) in target gene expression	112-135
5.1 Introduction	113-114
5.2 Objective of the study	114
5.3 Materials and Methods	115-121
5.4 Result	122-132
5.5 Discussion	132-134
5.6 Inference points	135
Chapter 6- General Discussion	136-141
References	142-173
Papers published/ communicated	174-176
Seminar/ Conferences attended	177-178

Acknowledgement

On the verge of completion of my doctoral work, I would like to express my sincere gratitude to everyone who has contributed to the successful completion of this thesis, titled "Evaluation of LIMD1-VHL targeting microRNA as biomarker in Uterine Cervical Carcinogenesis". This research was conducted in the Department of Oncogene Regulation at Chittaranjan National Cancer Institute (CNCI), Kolkata, under the esteemed supervision of Dr. Sankhadeep Dutta.

First and foremost, I extend my deepest gratitude to my supervisor, Dr. Sankhadeep Dutta, for his unwavering support, patience, and insightful guidance throughout my academic journey. His vast knowledge, meticulous research approach, and constructive criticism have been instrumental in shaping my scientific perspective and maintaining my enthusiasm. I consider myself extremely fortunate to have had him as my mentor—one who not only cared deeply about my work but also inspired me to strive for excellence. Sir, I am profoundly grateful for your invaluable mentorship; this thesis would not have been possible without you. I am also immensely thankful to my co-supervisor, Dr. Chinmay Kumar Panda, for his constant guidance, immense attention to the research work, constructive criticism, speculative outlook and research insights. Sir, your encouragement and guidance have been truly invaluable—thank you for always being there for me.

I would also like to extend my heartfelt gratitude to all the patients and their families who participated in our study. Their contributions have been invaluable, and I sincerely hope that their efforts will pave the way for new possibilities, bringing hope and smiles to many others facing similar challenges.

I am deeply thankful to The Director of CNCI, Kolkata, for granting me the opportunity to conduct my research at this esteemed institution. Additionally, I am profoundly grateful to CSIR, Government of India, for providing me the fellowship support, which made this research possible.

It is my pleasure to thank our academic coordinator, Dr. Ugir Hossain for his selfless support. I am thankful to Dr. Shyamsundar Mandal for his excellent guidance in statistical analysis. I would like to thank Dr. Sutapa Mukherjee and Dr. Saptak Banerjee for letting me use their instruments and lab space whenever needed. I would like to extend my special thanks to Prof. Bishnupada Chatterjee, whose constant encouragement and motivation have been instrumental in the completion of my research. His guidance and unwavering support have truly been a driving force throughout this journey.

I sincerely acknowledge the support of Dr. Ranajit Kumar Mandal, Dr. Manisha Vernekar, Dr. Sreeya Bose, Dr. Puja Chatterjee, Dr. Dipanwita Banerjee, Rakiba Begam, Masmuda Khatun (Department of Gynecological Oncology, CNCI) for their invaluable guidance and assistance during the sample collection

phase of my research. Their constant encouragement played a crucial role in the smooth execution of this study.

I extend my heartfelt gratitude to all **CNCI members** who have contributed, directly or indirectly, to fostering a seamless research environment at our institution. I sincerely extend my gratitude to all the members of the Central Research Instrumentation Facility (CRIF), the library, the office of the director, as well as the accounts and administrative sections for their unwavering support, cooperation, and assistance throughout my research journey.

Research is a collective endeavour, and its success relies on the collaboration of numerous dedicated individuals. I am thankful to **Dr. Somsubhra Nath** (Presidency University, Kolkata), **Dr. Anusri Tripathi** (CSTM, Kolkata), **Dr. Soma Banerjee** (IPGMER, Kolkata) for their kind suggestions during my work.

Having good friends during a Ph.D. journey is truly a blessing. In this regard, I would like to express my heartfelt gratitude to my senior **Dr. Debolina Pal** (Debolina Di) and **Rituparna Roy** (Rituparna Di), **Dr. Priyanka Dutta** (Priyanka Di), **Dr. Mukta Basu** (Mukta Di), **Dr. Balarko Chakraborty** (Balarko Da) and **Dr. Debolina Mukhopadhyay** (D2 Di) for their support during my experimental work. I am also deeply grateful to **Mrs. Nilanjana Chatterjee**, **Mr. Sadi Khan** (Papai), and **Ms. Debica Mukherjee**. They have been my pillars of strength, offering scientific advice, sharing in my struggles, and helping me navigate the challenges of this journey. Because of these incredible friends, my Ph.D. journey has been filled with joy, and I deeply cherish the bond we share. I firmly believe that our friendship will continue beyond this academic milestone, and together, we will create many more wonderful memories in the years to come.

It is impossible to express the depth of my gratitude to my family in just a few words. I am eternally thankful to my parents, **Sk. Ahammad Hossain** (Abbu) and **Mrs. Jebunnessa Begum** (Maa), for their unwavering love, sacrifices, and lifelong support. Their constant encouragement and motivation have shaped my journey, both academically and personally. I will always cherish the immense love and affection they have shown me, knowing that no words or actions can ever truly repay their kindness. With immense gratitude, I would like to mention my late grandfather, **Sk. Abul Hossain** (dadu), who always wished to see his grandchildren successful and established. I know that had he been here with us, he would have been one of the happiest people celebrating my achievements. None the less, I hope he is looking down at me with pride and happiness.

A special note of gratitude to my sisters, **Mrs. Asmantara Sultana** (didi) and **Ms. Nasreen Sultana** (buni), who has been my pillar of strength, offering unwavering support through every academic and personal challenge. Their unwavering support in moments of stress, disappointment, insecurity, and uncertainty has made this journey truly meaningful. I am also deeply grateful to my hostel mates, **Vatsata Khatoor**, **Anjali Kumari** and **Tanima Gupta** for their encouragement and support throughout my research journey. My

heartfelt regards also go to my new family, my father-in-law (Md. Kasfuddoza Hazari) and my mother-in-law (Mrs. Arufa Hazari) for their cooperation and understanding during the phase of Thesis-writing.

Last but not most importantly, I owe my deepest gratitude to my husband, Md. Asrafuddoza Hazari (Rahul). He has been incredibly supportive, kind, and encouraging throughout this journey. His constant motivation and academic support have been invaluable, giving me the strength to persevere through every challenge of my PhD journey. You were always there during moments when I felt it was impossible to continue, helping me regain perspective and persevere. I deeply appreciate your unwavering belief in me and truly value your invaluable support and encouragement throughout this journey.

Lastly, I would like to extend my heartfelt gratitude to all the friends, family members, and well-wishers whom I may have unintentionally missed mentioning. Your support, whether direct or indirect, has played a significant role in the successful completion of my research, and for that, I am truly grateful.

Farhin Sultana

List of Abbreviations

ASO: Antisense Oligonucleotides
CaCx: Cervical Cancer
CGH: Comparative Genome Hybridization
Chr: Chromosome
CIN: Cervical Intraepithelial Neoplasia
CNV: Copy Number Variation
DEPC: Diethyl Pyro carbonate
DMSO: Dimethyl Sulfoxide
DNA: Deoxy Ribose nucleic acid
DNase: Deoxy Ribonuclease
EDTA: Ethylene-Diamine-Tetra Acetic acid
FACS: Fluorescence-activated Cell Sorting
FBS: Foetal Bovine Serum
FFPE: Formalin-Fixed and Paraffin-Embedded
GEO: Gene Expression Omnibus
HE: Haematoxylin- Eosin
HPV: Human Papilloma Virus
HR-HPV: High-risk Human Papillomavirus
HR-HPV: High-risk Human papillomavirus
HSIL: High-grade Squamous Intraepithelial Lesions
IHC: Immunohistochemistry
kb: Kilo Base pairs
KD: Kilo Daltons
LCR: Long Control Region
LMIC: Low- and Middle-Income Countries
LNA: Locked Nucleic Acid
MiR: MicroRNA
PBL: Peripheral Blood Lymphocytes
PBS: Phosphate Buffered Saline
PCR: Polymerase Chain Reaction

PCR: Polymerase Chain Reaction

PI: Propidium iodide

pRB: Retinoblastoma protein

qRT-PCR: Quantitative real-time PCR

RNA: Ribonucleic Acid

RNase: Ribonuclease

SDS: Sodium dodecyl Sulphate

SIL: Squamous Intraepithelial Lesions

STS: Short Tandem Sequence

TCGA: The Cancer Genome Atlas

TE: Tris EDTA

TEMED: N' N' N' N' -Tetramethylene Diamine

TSG: Tumor Suppressor Gene

TSG: Tumour Suppressor Gene

VHL: von Hippel-Lindau suppressor

μM: Micromolar

Summary

Summary:

Cervical cancer (CaCx) remains a major public health challenge, especially in low- and middle-income countries (LMICs), where limited screening and treatment drive high mortality rates. It is the fourth most common cancer globally and the second most prevalent in India. Persistent high-risk human papillomavirus (HR-HPV) infection is the primary driver of CaCx, with HR-HPV-induced stabilization of hypoxia-inducible factor-1 alpha (HIF-1 α) promoting early tumor progression via the regulation of some angiogenic factors transcription. Under normal oxygen conditions, HIF-1 α is regulated by two key tumor suppressor genes (TSGs) LIMD1 and VHL, frequently altered in CaCx. While their downregulation is often linked to promoter methylation or genetic deletions, some cases show reduced expression without detectable genetic or epigenetic modifications, hinting at additional regulatory mechanisms.

Hence, we hypothesized microRNAs (miRNAs), key post-transcriptional regulators, may contribute to LIMD1 and VHL suppression. Through *in silico* analysis, our study first identified two miRNAs: miR-135b-5p (which targets LIMD1) and miR-21-5p (which targets VHL). We demonstrated that the overexpression of miR-135b-5p and miR-21-5p correlates with progressive cervical lesion severity, transitioning from normal epithelium to cervical intraepithelial neoplasia (CIN) to CaCx. This progression was inversely correlated with downregulation of LIMD1 and VHL in the corresponding samples, implicating these miRNAs in HIF-1 α pathway dysregulation and tumor progression. Additionally, we uniquely decipher MIR135B locus amplification as a primary genetic mechanism for the miRNA upregulation in CaCx.

Given their expression patterns in tissue, we further hypothesized miR-135b-5p and miR-21-5p could serve as triage biomarkers in cervical swabs for detecting clinically relevant high-grade cervical dysplasia. Validation in a large cohort of cervical swabs (N=243) revealed consistent overexpression of these miRNAs and downregulation of their target genes in HR-HPV-positive high-grade squamous intraepithelial lesions (HSIL) compared to earlier clinical stages. This finding highlights the potential of miR-135b-5p and miR-21-5p as triage biomarkers capable of distinguishing low-grade squamous intraepithelial lesions (LSIL) from HSIL, addressing the limitations of current diagnostic tools in differentiating lesion severity. Receiver operating characteristic (ROC) curve analysis further demonstrated that combining these two miRNAs as a biomarker panel improved triage sensitivity (90.4%) and specificity (94%) for distinguishing HR-HPV+ve HSIL from HR-HPV+ve LSIL. This refined risk

stratification approach could minimize overtreatment in women with non-progressive lesions while ensuring timely intervention for high-risk cases.

To improve accessibility, we developed a novel fluorescence-based miRNA detection technique for miR-135b-5p in cervical swabs through a pilot study. A sensor-oligo-based miR-135b-5p detection assay in clinical settings demonstrated its potential in high-throughput cervical cancer screening and precise clinical decision-making. This method offers a rapid and cost-effective alternative to quantitative real-time PCR (qRT-PCR), which requires specialized equipment and expertise. These findings emphasize the translational significance of our approach.

Furthermore, we explored the mechanistic role of these miRNAs in regulating two key tumor suppressor genes (LIMD1 and VHL) during CaCx progression and demonstrated their impact on cervical cancer cell proliferation, apoptosis, migration, and invasion. At first, we experimentally validated LIMD1 as a direct target of miR-135b-5p through dual-luciferase reporter assay. Dual inhibition of miR-135b-5p and miR-21-5p led to G0/G1 cell cycle arrest through the restoration of LIMD1 and VHL expression, enhanced apoptosis, and reduced migration and invasion of CaCx cell line, SiHa. These effects were mediated by the downregulation of HIF-1 α target genes, including VEGF, MMP9, TGF- α , and CCND1, elucidating their roles in CaCx progression.

By bridging the gap between HR-HPV screening and clinical interventions, miR135b-5p and miR-21-5p-based triaging hold significant potential in early detection of clinically relevant cervical lesions, thereby, minimizing overtreatment in low resource settings. Ultimately, our study significantly contributes to the global cervical cancer control strategies.

CHAPTER 1

General Introduction

Chapter 1

General Introduction

1.1 Cervical Cancer: an overview

According to the **GLOBOCAN 2022** database, Cervical Cancer (CaCx) is the fourth most prevalent cancer among women worldwide, in both incidence and cancer-related mortality. It was estimated to cause approximately 6,62,301 new cases (6.9% of the total) and 3,48,874 deaths (8.1% of the total) globally [Bray et al., 2024]. The situation is further concerning in India, where CaCx is the second most common cancer among women, after breast cancer. It accounts for 1,27,526 new cases (17.7% of the total) and 79,906 deaths (17.9% of the total), highlighting its significant health burden in the region (**Figure 1.1**) [Bray et al., 2024]. Based on GLOBOCAN 2022 report, the global age-standardized mortality rate (ASMR) for CaCx is approximately 7.1 per 1,00,000 women. In India, however, the ASMR for CaCx is significantly higher, at about 11.2 per 1,00,000 women, highlighting a markedly elevated mortality rate in comparison to the global average [Bray et al., 2024].

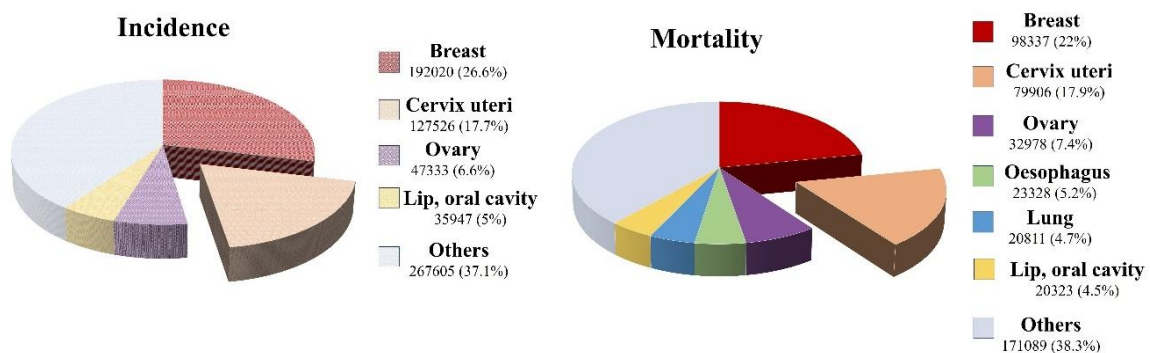


Figure 1.1: Incidence and mortality of CaCx among the most common cancers in Indian women (GLOBOCAN, 2022)

1.1.1 Histopathogenesis of CaCx:

The cervix, constituting the lower portion of the uterus, is cylindrical or conical in shape. Histologically, it is composed of two parts (**Figure 1.2**) [Sankaranarayanan et al., 2003]:

- a. **Ectocervix:** It protrudes into the vagina and is covered with a stratified, non-keratinizing squamous epithelium.
- b. **Endocervix:** It forms the canal connecting the ectocervix to the uterine cavity and is lined with tall, glandular columnar epithelium.

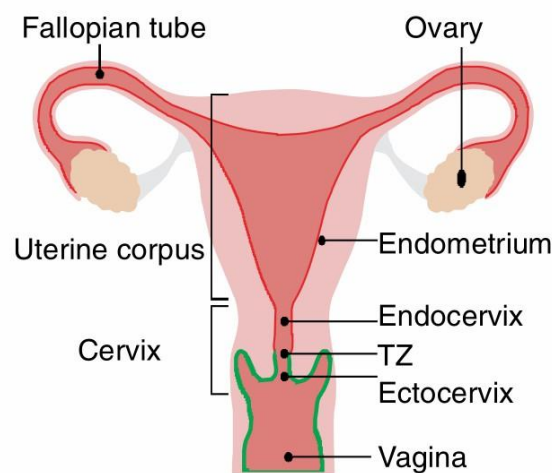


Figure 1.2 Anatomy of uterine cervix (Adapted from Gurumurthy et al., 2022)

These two epithelial types meet at the **squamocolumnar junction** [Sankaranarayanan et al., 2003]. At birth, the columnar epithelium extends into the ectocervix, but as a woman ages, it recedes back into the endocervical canal through a process called **squamous metaplasia**. This dynamic area, where the squamous and columnar epithelium interface, is known as the **transformation zone (TZ)**, which is highly prone to neoplastic changes (**Figure 1.3**) [Moscicki et al., 2006].

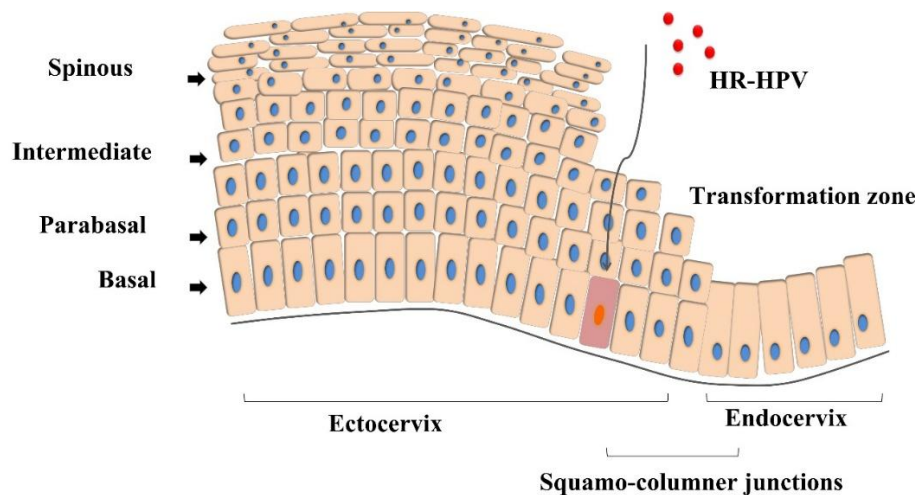


Figure 1.3 Schematic representation of the transformation zone of uterine cervical epithelium.

Premalignant changes in the cervix, termed **Cervical Intraepithelial Neoplasia (CIN)**, may remain in a non-invasive stage for an extended period before evolving into invasive carcinoma. CINs are categorized based on the degree of epithelial dysplasia. This classification is determined through cervical biopsies and histological evaluations, dividing lesions into three grades: **CIN I (mild dysplasia)**, **CIN II (moderate dysplasia)**, and **CIN III (severe dysplasia)**. These categories are represented in **Figure 1.4** [Montz, 2000].

- **CIN I** is characterized by dysplasia confined to the lower third of the epithelium or less.
- **CIN II** indicates dysplasia affecting two third of the epithelial layers.
- **CIN III** involves dysplasia spanning the full thickness of the epithelium.

Progression beyond CIN III, where dysplastic cells invade the basal membrane, is classified as full-grown cancer of cervix (**Figure 1.4**) [Montz, 2000].

In 1988, the **Bethesda System** was introduced to cytological reporting to improve classification. This system groups precancerous lesions into two categories: **Low-Grade Squamous Intraepithelial Lesions (LSIL)** and **High-Grade Squamous Intraepithelial Lesions (HSIL)** [WHO]. CIN I aligns with LSIL, while CIN II and CIN III are combined under HSIL due to challenges in differentiating their cytological features (**Figure 1.4**).

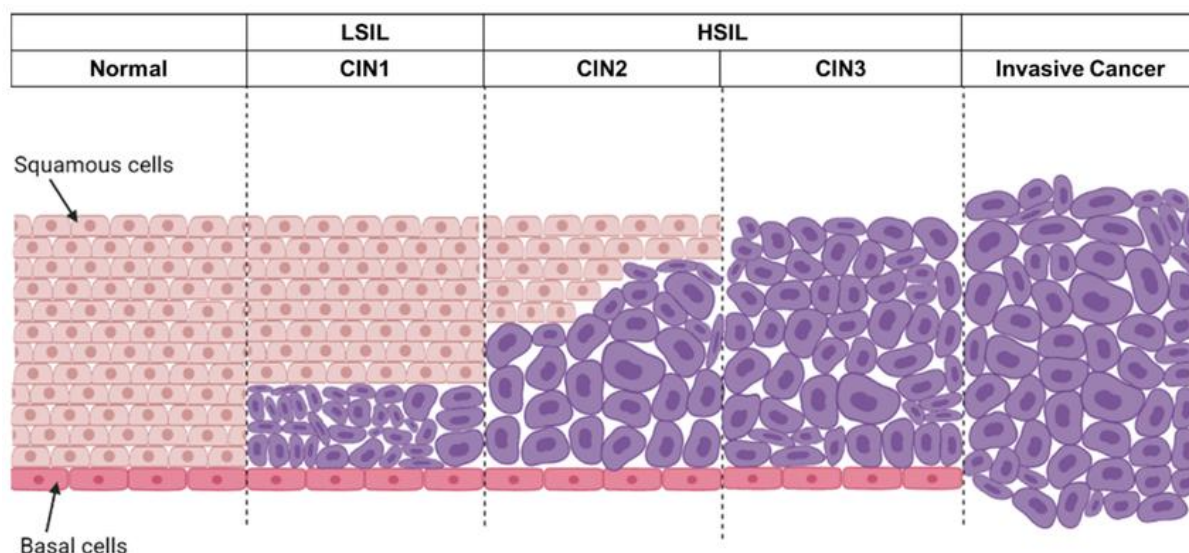


Figure 1.4 Diagram showing the progression of CaCx. The normal cervix has a layer of squamous cells on the outer surface and a single basal cell layer attached to the basement membrane. Under persistent HR-HPV infection, CIN can develop, potentially progressing from CIN I (LSIL) to CIN II/ III (HSIL) and eventually to invasive cancer [Adopted from Boon et al., 2022].

Histologically, these premalignant lesions are identified by the increasing atypia of epithelial cells from the lower parabasal layers to the entire thickness of the squamous epithelium, depending on the grade [Pontén and Guo, 1998].

Epithelial tumors of the cervix are classified into three main types based on their origin and cellular characteristics [Wright et al., 1994]:

- Squamous Cell Carcinoma:** This is the most common form, accounting for 85-90% of CaCx cases. It originates from the squamous epithelial cells of the ectocervix.
- Adenocarcinoma:** These tumors arise from the glandular epithelium of the endocervix and represent 10-15% of CaCx cases.
- Adenosquamous Carcinoma:** A rare form, constituting less than 1% of cases, characterized by features of both squamous cell carcinoma and adenocarcinoma.

1.1.2 Etiology of CaCx:

The major etiological factor for CaCx development is **Human Papillomavirus (HPV)** infection. However, among the high-risk HPV (HR-HPV) types, HPV16 is consistently the most common type associated with the development of CaCx [Crow, 2012; Bhatla et al., 2008]. According to the **IARC Monographs**, out of 448 identified HPV strains, 12 are classified as

group 1 carcinogens, which means that HPV is a necessary but insufficient cause of CaCx [Walboomers et al., 1999]. Other significant risk factors include smoking, high parity (a greater number of childbirths), long-term use of oral contraceptives, and certain sexually transmitted infections (STIs), such as HIV and *Chlamydia trachomatis* [Thun et al., 2017]. The incidence and mortality rates of CaCx are notably higher in transitioning countries (Low-middle-income countries; LMICs) compared to transitioned countries, with rates of 19.3 vs. 12.1 per 1,00,000 for incidence and 12.4 vs. 4.8 per 1,00,000 for mortality, respectively [Bray et al., 2022]. This disparity is partly due to a higher prevalence of persistent HPV infections and limited access to effective screening and treatment programs in LMICs [Bray et al., 2022].

1.1.3 Association of Human Papillomavirus with Cervical Carcinogenesis:

1.1.3.1 Prevalence and Natural History of HPV Infections

Studies indicate that HPV infection is extremely common among sexually active women. Over 50% of young women are estimated to acquire HPV infection following their first sexual encounter, and more than 80% of women are likely to be infected at some point during their lifetime [Sasagawa et al., 2012]. In most cases (about 90%), the infection is cleared naturally within three years; however, around 10% of infections persist, and fewer than 1% of these progress to CaCx (**Figure 1.5**). The prevalence of any HPV infection was estimated to be 9.9% in rural districts surrounding the city of Kolkata in eastern India [Dutta et al., 2012]. The prevalence of HPV infection among women in Western Tamil Nadu (South India) was 10.5% [Sureshkumar et al., 2015]. A study conducted in northeast India examined the presence of HPV DNA in cervical scrape samples from married women in Manipur and Sikkim, comparing the findings with data from women in West Bengal, located in eastern India. The results indicated that HPV infection was less prevalent in Manipur (7.4%) than in Sikkim (12.5%) and West Bengal (12.9%) [Laikangbam et al., 2007]. Additionally, research reported an overall HPV prevalence of 10.3% in western India [Sankaranarayanan et al., 2005] and 14% in southern India [Franceschi et al., 2005].

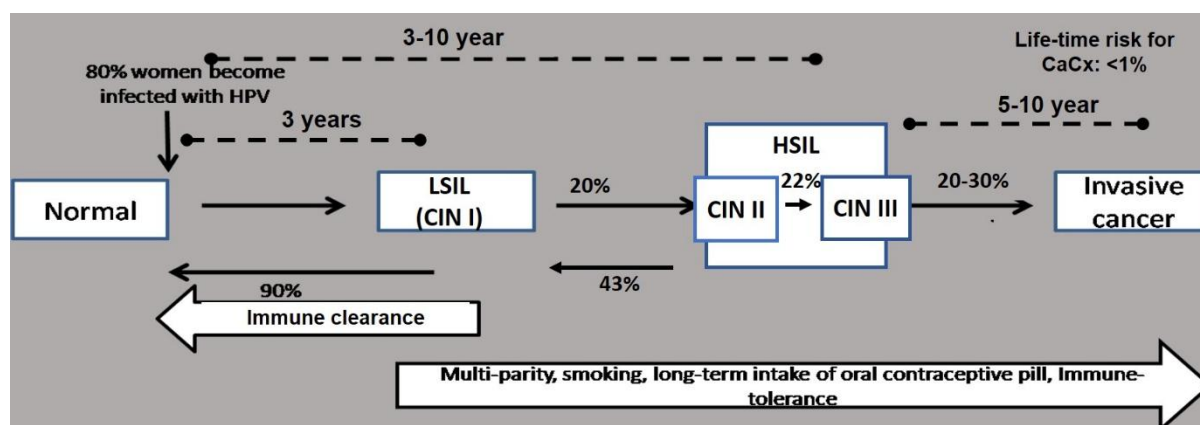


Figure 1.5: The natural history of HR-HPV infection and its potential clearance or persistence, leading to cervical carcinogenesis (Modified after Sasagawa et al., 2012).

1.1.3.2 Morphology of HPV:

HPVs are small, non-enveloped viruses characterized by an icosahedral capsid and a closed, double-stranded circular DNA genome (**Figure 1.6**). The capsid is composed of 72 capsomeres, each formed by a pentamer of the major capsid protein, L1, organized into a T=7 icosahedral surface lattice [Baker et al., 1991; Sapp et al., 1995]. Of these capsomeres, 60 are hexavalent, while the remaining 12 are pentavalent. Additionally, the capsid includes a minor protein, L2, which constitutes approximately 2–5% of the total capsid protein, likely represented by 12 copies of L2 [Doorbar, 2006; Sapp et al., 1995; Modis et al., 2002].

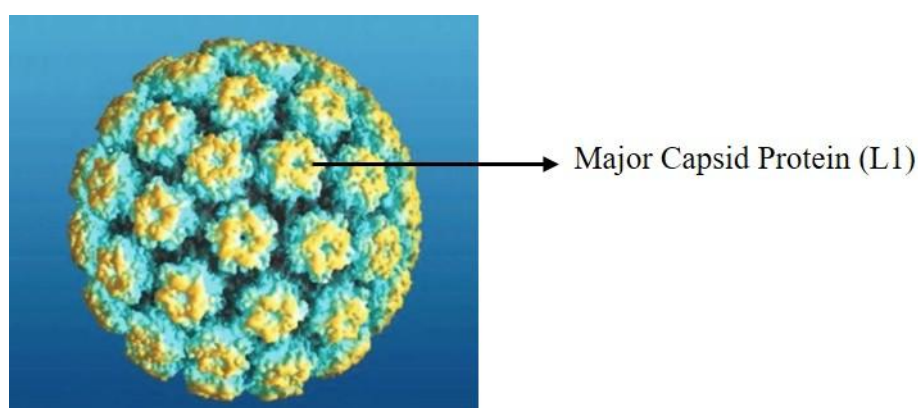


Figure 1.6 Structure of the Human Papillomavirus (HPV) Capsid: This illustration represents the structural organization of the HPV capsid, as determined through cryo-electron microscopy. The capsid is composed of 72 pentameric capsomeres, arranged in a symmetrical pattern. Of these, 12 capsomeres (orange) are each linked to five neighboring capsomeres, while the remaining 60 capsomeres (red) are each connected to six adjacent capsomeres (Adopted from Modis et al., 2002).

1.1.3.3 Classification of Human Papillomaviruses

HPVs belong to the family Papillomaviridae [De Villiers et al., 2004]. HPVs have been classified based on nucleotide sequence homology, evolutionary relationships, and biological characteristics. The L1 open reading frame (ORF) is the most conserved gene within the genome and is utilized for identifying new HPV types. A novel PV type is recognized if the L1 ORF sequence differs by more than 10% from the nearest known PV type. Variations in homology between 2-10% define a subtype, while less than 2% indicate a variant [De Villiers et al., 2004]. Based on the L1 ORF sequence, HPVs are phylogenetically classified into 5 major genera, viz. Alpha, Beta, Gamma, Mu, and Nu- papillomavirus (**Figure 1.7**). Among the five genera, members of Alpha-HPVs infect mucosal or cutaneous epithelium, and having oncogenic association.

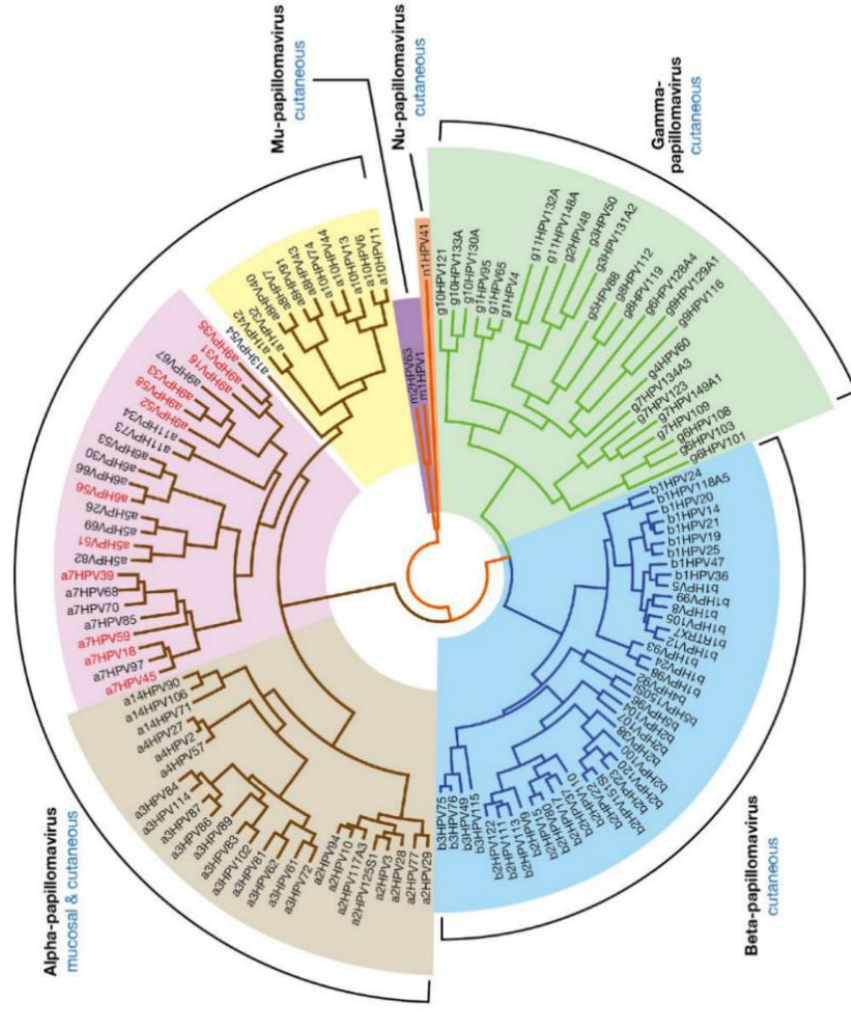


Figure 1.7 Evolutionary Relationship between Human Papillomaviruses: Human papillomaviruses (HPV[s]) are categorized into five genera, with Alpha-papillomavirus [Low-risk cutaneous HPV's (light brown); Low-risk mucosal HPV's (yellow); HR-HPV's (pink)], Beta-papillomavirus (blue), and Gamma-papillomavirus (green), Mu-papillomavirus (violet) and Nu-papillomavirus (orange). The HR-HPV types, particularly those highlighted in red text, are confirmed as human carcinogens based on epidemiological evidence. Other high-risk types are classified as probable or possible carcinogens based on their potential to contribute to cancer development [Adopted from Egawa et al., 2015].

Based on their disease association, the Alpha-HPVs are further classified into high-risk types (HR-HPV; refers to specific HPV types that have strong oncogenic potential and are linked to the development of cervical, anogenital, and oropharyngeal cancers through persistent infection and disruption of normal cell regulation), low-risk types (LR-HPV; refers to HPV types that are not associated with cancer but can cause benign conditions such as genital warts and mild cellular abnormalities), Probable high-risk types (refers to HPV types that are suspected to have oncogenic potential but have not been definitively classified as high-risk, as they are associated with some cancer cases but have weaker or less consistent evidence linking them to malignant transformation) and Undetermined-risk types (refers to HPV types with unclear oncogenic potential due to insufficient evidence, as they are not consistently linked to cancer, may cause benign infections or remain asymptomatic) **Table 1.1** [Muñoz et al., 2003].

Table 1.1: Classification of different types of HPV based on oncogenic association (adopted from Muñoz et al., 2003)

Risk	Types
High-risk	16, 18, 31, 33, 35, 39, 45, 51, 52, 56, 58, 59, 68, 73, 82
Probable high-risk	26, 53, 66
Low-risk	6, 11, 32, 40, 42, 43, 44, 54, 61, 70, 72, 81
Undetermined-risk	34, 57, 83

Among the high-risk types, HPV16 and HPV18 are most closely associated with CaCx [Walboomers et al. 1999].

1.1.3.4 Genome structure of HPV:

HPVs have circular, double-stranded DNA genomes of approximately 7.9 kilobases [Doorbar, 2006]. These genomes comprise an upstream regulatory region (URR), an intergenic noncoding region (NCR) characterized by simple (AT)_n and poly-T repeats, and eight primary protein-coding open reading frames (ORFs). The ORFs are named based on their temporal expression during the viral life cycle: "E" denotes early genes, while "L" represents late genes. The ORFs include E6, E7, E1, E2, E4, E5, L2, and L1 in the 5'–3' orientation (**Figure 1.8**). Additionally, an auxiliary sequence, E8, comprising 12 2/3 codons, is spliced to E2 during specific infection stages to form the E8[^]E2 fusion [Nelson and Mirabello., 2023]. All ORFs are located on the forward (sense) strand and are expressed as polycistronic (multi-ORF)

mRNAs [Doorbar, 2006; Nelson and Mirabello., 2023]. The functions of viral proteins were given in **Table 1.2** [Nelson and Mirabello., 2023].

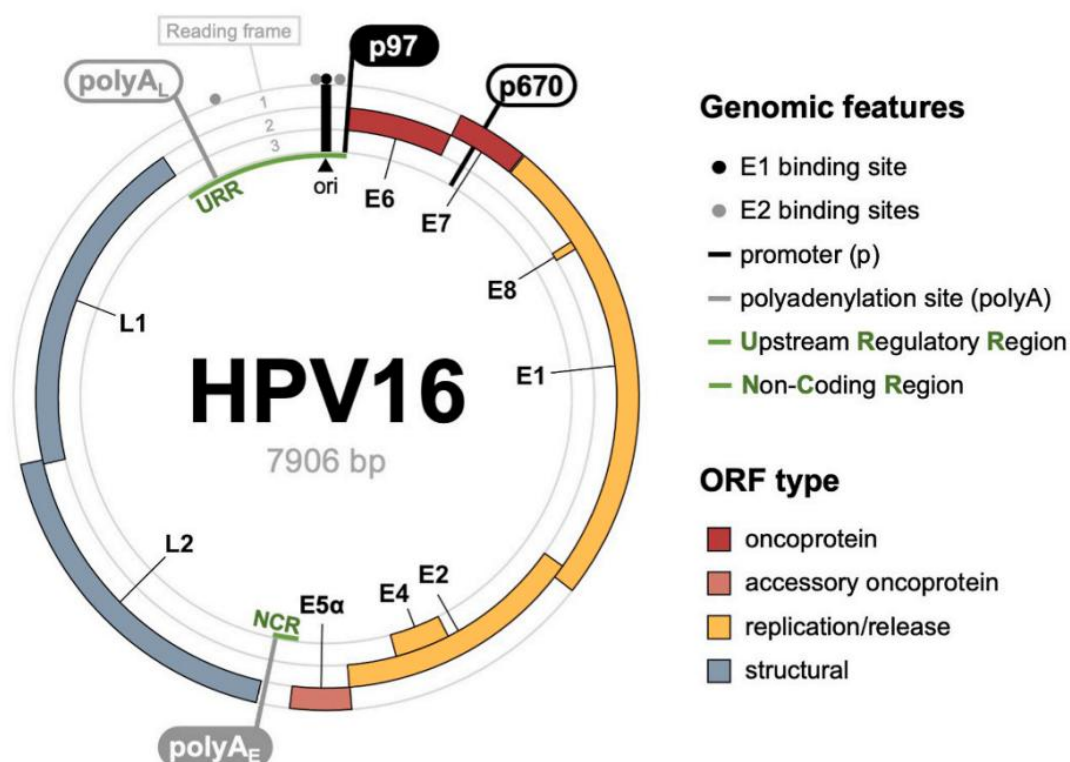


Figure 1.8 Genome organization of HPV-16: The structure of the HPV genome enables it to efficiently utilize its small size by encoding multiple regulatory and structural proteins necessary for the viral life cycle. The early genes (E1–E7) are primarily expressed during the initial stages of infection, contributing to viral replication and cellular transformation, while the late genes (L1 and L2) are expressed during the later stages, facilitating viral particle assembly [Adopted from Nelson and Mirabello., 2023].

Table 1.2: List of proteins synthesized from HR-HPV genome and their functions

HPV Protein	Function	Details
E6	Degrades p53	- Binds to tumor suppressor protein p53, thereby, promoting its degradation
		- inhibits apoptosis and contributes to cell transformation.
		- E6 interacts with various host cell proteins to inhibit differentiation, promote DNA replication, and evade immune surveillance."

		- Persistent E6 expression is essential for the sustained progression and maintenance of CaCx.
E7	Degrades pRb	- Binds to and inactivates the retinoblastoma protein (pRb), disrupting cell cycle control.
		- leads to uncontrolled cell division, a hallmark of cancer.
		- interacts with various other host proteins to enhance viral replication and survival.
		- Persistent E7 expression is required for the maintenance of CaCx.
E5	Accessory oncoprotein	- plays a contributory role in oncogenesis but is not essential for tumor development.
		- is highly hydrophobic and possesses transmembrane domains.
		- downregulates MHC/HLA class I molecules, impairing antigen presentation to cytotoxic (CD8 ⁺) T cells, thereby facilitating immune evasion.
		- E5 α is the group present in carcinogenic HPVs.
E1	Helicase	- A core viral protein essential for replication and genome maintenance
E8 (E8 [^] E2)	Suppresses viral replication	- Undergoes splicing with E2 to generate the E8 [^] E2 fusion protein
E2	DNA binding protein	- Core viral protein involved in replication and genome maintenance.
		- The full-length E2 protein tethers viral genomes to host chromosomes, ensuring their distribution to daughter cells during cell division
		- Downregulates E6 and E7 expression at specific stages of the viral life cycle
		- The shorter E8 [^] E2 splice variant is expressed in the basal epithelium to suppress viral replication and maintain low viral copy numbers, possibly avoiding immune detection.

E4	Assists genome amplification and virion release	- involves in genome amplification and virion release.
		- E4 is one of the most highly expressed ORFs in HPV.
		- E4 is an overlapping ORF encoded in an alternative reading frame within the E2 ORF.
L1	Major structural protein	- Major structural protein of the viral icosahedral capsid.
		- L1 is the most conserved open reading frame (ORF) and serves as the basis for defining HPV types
		- Contains five highly variable regions that encode outward-facing loops, which harbor L1's neutralizing antibody epitopes, crucial for vaccine-induced immunity
		- Genetic differences in L1 correspond to antigenic differences, possibly reflecting natural selection for immune escape.
L2	Minor structural protein	- Minor structural protein of the viral icosahedral capsid.
		- Assists in the assembly of the capsid and the encapsidation of the viral genome.

1.1.3.5 HR-HPV and CaCx Progression

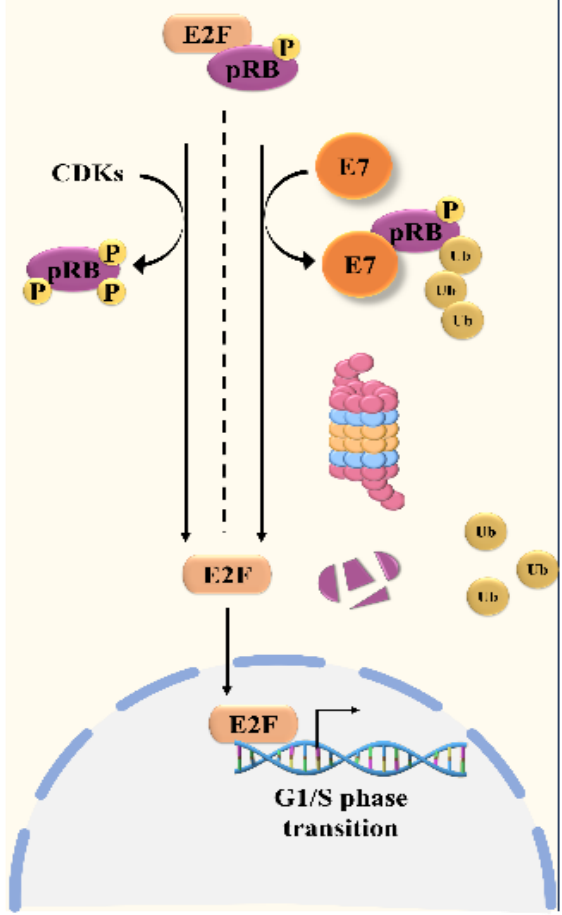
A persistent HR-HPV infection, with special attention to HPV16, is a critical factor in the development of cervical malignancies. The viral oncoproteins E6 and E7 of HPV16 play a central role in this process, often requiring a decade or more to transform normal cervical epithelial cells into cancerous ones (**Figure 1.5**). The initial phase of this transformation is marked by the onset of CIN I, which typically occurs after a persistent HR-HPV (HR-HPV) infection lasting approximately four to five years [Hausen, 2000]. In CIN I, the HR-HPV infection targets the proliferative basal and parabasal cells of the cervical epithelium, triggering both genetic and epigenetic changes. These basal cells, which are actively dividing, begin to exhibit abnormal cellular phenotypes (dysplasia) due to the increased expression of the E6 and E7 oncoproteins. The E6 oncoprotein facilitates the degradation of tumor suppressor protein p53, while E7 protein inactivates the retinoblastoma (Rb1) protein, disrupting normal cell cycle regulation and promoting cellular proliferation [Mazumder et al., 2011].

As the infection persists, the dysplastic changes expand beyond the basal layer to the differentiated spinous layer, marking the transition from CIN I (LSIL) to CIN II-III (HSIL). With each progression from CIN II to CIN III and eventually to invasive cervical carcinoma, additional genetic and cellular alterations accumulate, further transforming the epithelial cells. The interplay between HPV16 E6/E7 oncoproteins and cellular targets like p53 and Rb1 is fundamental to this stepwise transformation, leading to uncontrolled cell division and malignant progression [Mazumder et al., 2011].

HR-HPV promotes a selective growth advantage by either inhibiting or inducing key proteins which lead to alteration of critical cellular pathways [**Table 1.3**]. These disruptions affect three fundamental cellular processes: cell fate, cell survival, and genome maintenance [Vogelstein et al., 2013].

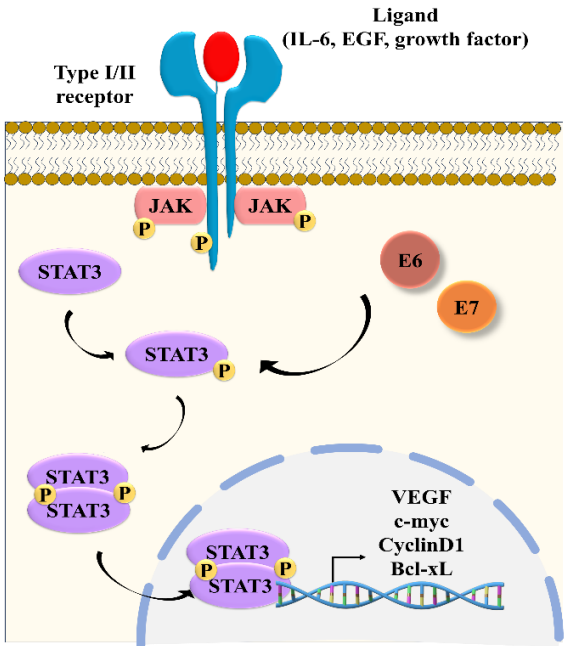
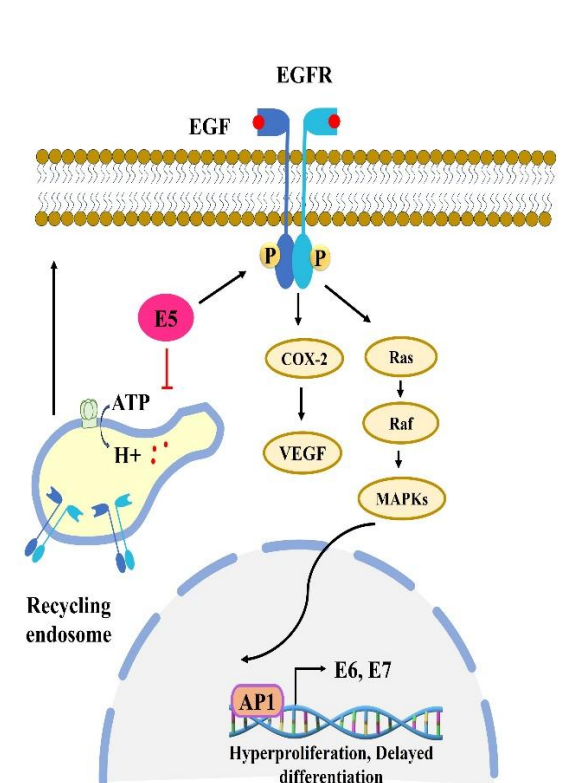
Table 1.3: Signalling Pathways and HPV:

Viral proteins	Target	Mechanism	Diagram
HR-HPV E6	P53	<ul style="list-style-type: none"> ○ E6 interacts with p53 and the ubiquitin E3 ligase, E6-associated protein (E6AP), to form a ternary complex ○ Ubiquitinates p53, leading to its proteasome-mediated degradation ○ Evade apoptosis and cell cycle arrest <p>[Scheffner et al., 1990]</p>	<p>The diagram illustrates the mechanism of E6-mediated ubiquitination of p53. It shows E6 (red circle) and E6AP (blue oval) forming a complex. p53 (green hexagon) then joins to form a ternary complex. Ubiquitin (Ub, yellow circles) is added to p53, forming a polyubiquitin chain. This complex is targeted to the Proteasome System (pink and blue barrel structure). The diagram shows two outcomes: Apoptosis (indicated by a red T-bar) and Cell survival (indicated by a black arrow).</p>

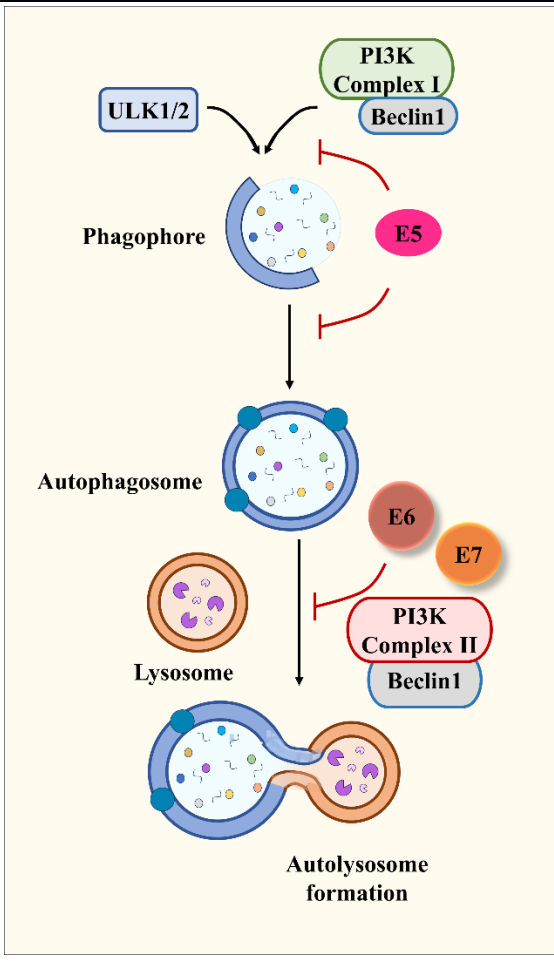
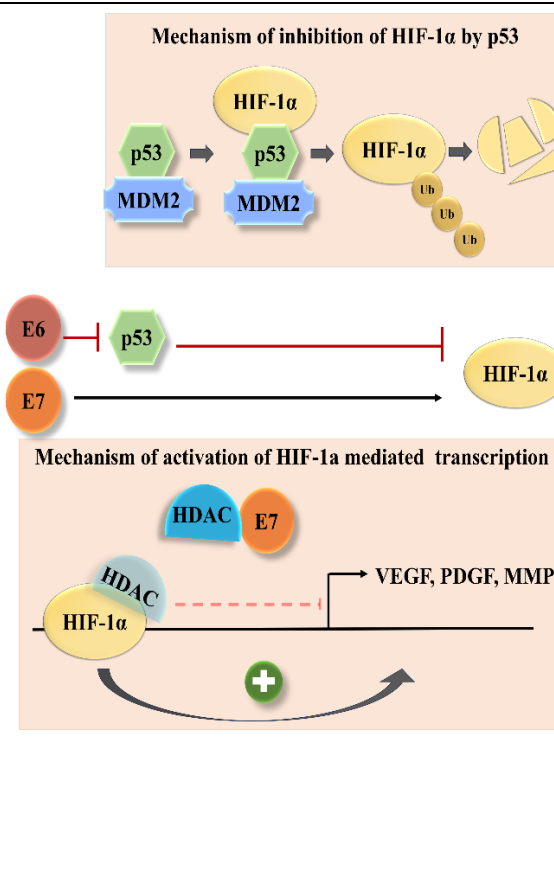
<p>HR-HPV E7</p>	<p>pRb</p>	<ul style="list-style-type: none"> ○ interacts with retinoblastoma protein (pRb), leading to the release of E2F. ○ inactivate and destabilize pRb independently of cyclin-dependent kinases (CDKs), promoting its degradation via the proteasomal pathway ○ promoting uncontrolled cell cycle progression <p>[Tommasino et al., 1995]</p>	
-------------------------	-------------------	--	---

<p>HPV16 E6 and E7</p>	<p>Akt, TSC2</p>	<ul style="list-style-type: none"> ○ can directly activate Akt or bind to (Tuberous sclerosis complex 2) TSC2, promoting its degradation. ○ enhances the activity of the mechanistic target of rapamycin complex 1 (mTORC1). ○ promoting cellular growth and metabolism <p>[Contreras-Paredes et al., 2009]</p>	<p>The diagram illustrates the signaling pathways involving Akt. At the top, the cell membrane contains GPCR and RTK. GPCR activates PI3K, which generates PIP3. RTK, upon activation, also produces PIP3. PIP3 recruits Akt, leading to its activation (Akt-P). PTEN acts as a negative regulator of PI3K. E7 promotes Akt activation. E6 inhibits the TSC2/TSC1 complex, which normally inhibits mTORC1. mTORC1 promotes Akt activation. mTORC2 also promotes Akt activation. Akt-P leads to gene regulation, cell proliferation, and cancer progression.</p>
--------------------------------	------------------------------------	--	---

<p>HPV16 E6 and E7</p>	<p>APC</p>	<ul style="list-style-type: none"> ○ inhibits the activity of APC (a component of β-catenin degradation complex), thereby, increasing β-catenin levels ○ induces cancer cell proliferation and differentiation <p>[Pim et al., 2005]</p>	<p>The diagram illustrates the Wnt signaling pathway and its inhibition by HPV16 E6 and E7. At the cell membrane, E-cadherin (blue) is linked to p120, γ-catenin (yellow), and α-catenin (yellow). The Wnt receptor (Fzd) (pink) is also at the membrane. In the cytoplasm, the β-catenin destruction complex consists of APC (brown), GSK3β (blue), and Axin (purple). Siah-1 (green) is shown inhibiting GSK3β. HPV16 E6 (red) and E7 (orange) are shown inhibiting the destruction complex, leading to the accumulation of β-catenin (yellow). Accumulated β-catenin then moves into the nucleus, where it binds to TCF/LCF (brown), leading to the transcription of genes like VEGF, c-myc, and MMP7. Siah-1 (green) is also shown in the nucleus.</p>
------------------------	-------------------	--	---

<p>HPV16 E6 and E7</p>	<p>STAT3</p>	<ul style="list-style-type: none"> ○ increases high STAT3 phosphorylation, mediating expression of genes VEGF, c-myc, CyclinD1, Bcl-xL ○ induces tumor growth, proliferation and angiogenesis <p>[Morgan and Macdonald, 2020]</p>	
<p>HPV16 and HPV6 E5</p>	<p>EGFR</p>	<ul style="list-style-type: none"> ○ HPV16 and HPV 6 E5 binds to the 16K subunit of the v-ATPase pump of endosome <p>[Conrad et al., 1993]</p> <ul style="list-style-type: none"> ○ HPV16 E5 disrupts endosomal acidification, thereby, increasing EGFR activation. <p>[Disbrow et al., 2005].</p>	

		<ul style="list-style-type: none">○ HPV16 E5 oncoproteins upregulates the expression of VEGF and COX2 through EGFR. <p>[Kim et al., 2006]</p> <ul style="list-style-type: none">○ HPV16 E5 activates multiple proto-oncogenes, particularly mitogen-activated protein kinases (MAPKs) and activating protein-1 (AP-1) components, leading to the induction of viral oncoproteins E6/E7 expression <p>[Kim et al., 2009; Ilahi et al., 2020]</p>	
--	--	---	--

<p>HPV16 E5</p> <p>HPV16 E6/E7</p>	<p>ATG5, LC3, ULK1, ULK2, Beclin 1, and ATG7</p>	<ul style="list-style-type: none"> ○ downregulate phagophore assembly ○ inhibit autophagosome-lysosome fusion ○ induce tumor cell proliferation <p>[Mattosio et al., 2018]</p>	
<p>HPV16 E6/E7</p>	<p>HIF-1α</p>	<ul style="list-style-type: none"> ○ HPV16 E6 oncoprotein functions to counteract p53-mediated HIF-1α degradation ○ HPV16 E7 oncoprotein enhances HIF-1α transcriptional activity by blocking the interaction of HDAC with HIF-1α. 	

		<ul style="list-style-type: none"> ○ promote angiogenesis and cancer development <p>[Bodily et al., 2011; Ravi et al., 2000]</p>	
--	--	---	--

Genes denoted in ORANGE indicate activation and BLUE indicate inhibition

1.1.4 CaCx early detection for prevention: The screen-triage-treat model

1.1.4.1 CaCx Screening and treatment:

In 2022, cancer-related deaths reached an estimated nearly 10 million globally, making the cancer one of the leading causes of mortality worldwide [Bray et al., 2024]. This number is projected to rise further, with a significant increase anticipated in LMICs, like India which currently face the greatest obstacles in managing the cancer burden [Bray et al., 2024; WHO]. Early detection through screening is key to CaCx prevention. Cervical screening tests, including conventional cytology (PAP smear), liquid-based cytology (LBC), HPV testing, and visual inspection with acetic acid (VIA), are effective in detecting precancerous cervical lesions in asymptomatic women who appear healthy.

1.1.4.1.1 Cytology based screening:

Cytology is the most commonly employed method for CaCx screening. In high-income countries, cytology-based screening has been integrated into healthcare systems, achieving high coverage through effective program organization. This integration has significantly reduced both the incidence and mortality rates of CaCx over time [IARC, 2005]. Some middle-income countries in regions like South and Central America and Asia have also adopted population-based CaCx screening using cytology. However, these programs have generally had limited success in reducing the CaCx burden due to challenges such as inadequate coverage, follow-up care, treatment, and lack of quality control [Murillo et al., 2008].

In most LMICs, cytology-based screening has yet to be established on a large scale. These nations often lack the resources and infrastructure to implement and maintain quality-assured cytology screening within their under-resourced and fragmented healthcare

systems, which are often burdened by competing healthcare priorities and limited trained personnel. Effective cytology screening requires well-equipped laboratory facilities, systematic monitoring, skilled technicians or pathologists, and reliable follow-up systems for individuals with positive screening results—all of which present significant challenges in resource-limited settings [Murillo et al., 2008].

Cytology findings are typically categorized using The Bethesda System (TBS) [Nayar & Wilbur, 2015]. In many healthcare settings, a threshold for positive cytology findings requiring further diagnostic investigation, such as colposcopy, is set at the level of Atypical Squamous Cells of Undetermined Significance (ASCUS) or LSIL. Women who receive results indicating atypical squamous cells that cannot rule out a high-grade lesion (ASC-H), LSIL, or HSIL require additional evaluation via colposcopy. Some of the well-established cytological techniques for CaCx screenings are:

A. Pap test:

Cytology smears are prepared by spreading cervical cell samples, collected using a spatula and cervical brush, onto a glass slide. These smears are then fixed and stained using the Papanicolaou (PAP) staining method. Pap test considered some key cytological features, such as cellular morphology, nuclear abnormalities (enlarged nuclei, hyperchromasia, irregular nuclear membranes, multinucleation), cytoplasmic features (cytoplasmic vacuolization, keratinization in squamous cells), koilocytosis (HPV-related changes). Cytology is a highly subjective test, with results often varying between laboratories and depending on the expertise of the cytologists interpreting the smears. In developing countries, the high prevalence of cervical inflammation contributes to significant inflammatory debris in PAP smears, presenting substantial challenges for interpretation and accurate reporting. The false-negative rate for PAP smears is relatively high (ranging from 14–33%), primarily due to limitations in sampling and smear preparation techniques. Quality assurance across all stages, viz. preparation, fixation, staining, analysis, and reporting, is essential to obtain reliable results. When quality control is rigorously maintained, a single PAP smear has a sensitivity of approximately 60–95% for detecting CIN II+ lesions, along with a comparable specificity [Cuzick et al., 2014; Nanda et al., 2000]. Furthermore, inadequate healthcare infrastructure and the absence of effective awareness programs hinder the development of a robust cytology-based screening program, particularly in rural populations [Srivastava et al., 2018].

B. Liquid-based cytology (LBC):

It enhances specimen collection, resulting in a lower rate of unsatisfactory smears, reduced debris, and a shorter time required for interpretation compared to conventional cytology. This represents the first significant technical advancement in cervical cytology in over 50 years. In LBC, cervical cell samples are collected into a vial containing a liquid transport medium, then filtered, allowing for a random sample to be presented as a thin layer on a slide, which minimizes cell overlap. Additionally, LBC samples can be utilized for reflex HPV testing and other molecular analyses, particularly for triaging cases with ASCUS. However, the sensitivity and specificity of LBC are generally comparable to those of traditional cytology in detecting CIN II or worse lesions [Whitlock et al., 2011].

1.1.4.1.2 Visual screening tests:**A. Visual inspection with acetic acid (VIA):**

It involves colposcopic examination of cervix one minute after applying a 3–5% dilute acetic acid solution under bright lighting [Sankaranarayanan et al., 2003]. A positive result is indicated by the presence of a well-defined, dense acetowhite area adjacent to the SCJ within the TZ of the cervix. This test is particularly effective for premenopausal women under 50 years of age when the TZ is clearly visible on the ectocervix. However, interpreting the results becomes challenging in postmenopausal and older women. VIA is not recommended for women over 50 years of age or in cases where the SCJ is not fully visible.

VIA is a simple, feasible, and cost-effective point-of-care test that provides immediate results, allowing for diagnosis and/or treatment during the same visit for women who test positive. A wide range of healthcare professionals, including doctors, nurses, and primary healthcare workers, can be trained to perform VIA with minimal training. The infrastructural requirements are low, and the necessary consumables are widely accessible.

The efficacy of VIA has been thoroughly evaluated across diverse settings. A pooled analysis revealed that the sensitivity and specificity of VIA for detecting CIN II or higher (CIN II+) were 80–92% [Sauvaget et al., 2011]. However, these values exhibited significant variability across different environments due to the subjective and provider-dependent nature of the test, the varying quality of reference standard investigations, and the differing age groups included in the studies. Additionally, VIA is associated

with a high rate of false positives. Despite these limitations, implementing VIA screening in low-income countries represents a pragmatic approach to build the necessary infrastructure and human resources, potentially facilitating the future introduction of affordable HPV screening.

B. Visual Inspection with Lugol's iodine (VILI):

Another straightforward and inexpensive visual screening method is visual inspection with Lugol's iodine (VILI). This test relies on identifying iodine-negative areas on the cervix following the application of Lugol's iodine. However, VILI has not been extensively evaluated and is known for its high rate of false positives. The consumables required for this test can be costly and may not be readily available. Consequently, the World Health Organization (WHO) does not currently recommend VILI for routine CaCx screening.

World Health Organization, in its recent guidelines for the screening and treatment of cervical pre-cancer lesions to prevent CaCx, has recommended HPV DNA testing as the primary screening method [WHO, 2021]. This recommendation marks a shift away from traditional methods such as VIA and cytology. The transition is driven by several challenges, including a shortage of trained healthcare professionals, limited awareness of screening practices among women, and the technical constraints of VIA. The WHO emphasizes that HPV DNA testing should serve as Gold Standard test for the general population and high-risk groups (e.g. women living with HIV) [WHO, 2021].

1.1.4.1.3 HPV Testing for cervical screening:

HPV testing involves the detection of HPV DNA or the mRNA of two oncoproteins (E6 and E7) in cervical cell samples collected either through pelvic examination or self-sampling. This method is considered the most accurate and reproducible cervical screening test, independent of the provider. Its sensitivity for detecting CIN II+ lesions exceed 90%, while that for CIN III+ lesions exceed 95%. Although it is more sensitive than cytology, HPV testing has lower specificity [Arbyn et al., 2012]. For women over the age of 30, HPV testing is the most suitable screening option, as HPV-negative individuals can safely be monitored for at least 7–10 years, given the high negative predictive value of a negative HPV test for CIN III and CaCx [Schiffman et al., 2011; Sankaranarayanan et al., 2009]. HPV tests have undergone extensive evaluation and comparison with cytology in numerous randomized controlled trials. A cluster randomized trial in India involving approximately 1,35,000 women aged 30–59 years

found that a single round of HPV testing resulted in a significant 53% reduction in the incidence of advanced cancer (stage II+) and a 48% reduction in CaCx mortality [Sankaranarayanan et al., 2009]. In four European randomized trials with 1,76,464 women aged 20–64 years, HPV testing was compared to cytology screening. These participants were followed for a median of 6.5 years, revealing that HPV testing offered 60–70% greater protection against invasive cervical carcinoma compared to cytology [Ronco et al., 2014]. The data from randomized trials in Europe and India support the initiation of HPV-based screening and extending screening intervals to at least five years. The WHO recommends repeat screening after 10 years for HPV-negative women in resource-limited settings [WHO, 2013].

1.1.4.2 The “Screen and Treat model” for CaCx

The effectiveness of a successful screening program relies on its widespread uptake and linkage to treatment of women who screen positive, a strategy known as the **"Screen and Treat"** model (**Figure 1.9**). In this approach, women are screened for cervical abnormalities, typically using an HPV test. If the test result is positive, they receive immediate treatment for precancerous lesions, often on the same day. This method eliminates the need for additional confirmatory tests or follow-up visits, ensuring early detection and prompt intervention to prevent the progression of CaCx. To effectively reduce the burden of CaCx, it is crucial to appropriately treat screen-detected CIN lesions, particularly CIN II and CIN III. These lesions can be managed through two main approaches: ablation and excision. Ablative techniques are cost-effective, simpler to perform, and associated with minimal complications, making them accessible to trained non-clinicians. Two widely used ablative methods are cryotherapy and thermocoagulation, both of which have been demonstrated to be equally safe and effective, even when performed by nurses [Dolman et al., 2014]. Excisional techniques, on the other hand, include large loop excision of the transformation zone (LLETZ) and cold knife conization (CKC). These procedures involve the complete removal of the TZ, which is then submitted for histopathological examination [WHO, 2013].

1.1.4.3 Limitations of cervical “Screen and Treat Model” in LMICs:

A "screen-and-treat" approach generally imposes a higher patient burden due to the potential for unnecessary treatment in women with positive screening results that may not progress to a serious condition. This is because all conventional screening methods have their own limitations, viz., cytology lacks sensitivity, whereas VIA has only moderate sensitivity and

specificity [Kiviat et al., 2008; Poli et al., 2015]. Furthermore, although high-risk (HR) HPV DNA testing is considered the Gold Standard, it lacks specificity for identifying CIN II+/ HSIL [Kiviat et al., 2008]. This is because most HPV infections are transient and do not lead to clinical consequences. Only a small proportion of HR-HPV infections initiate an oncogenic process that ultimately leads to the progression of precancerous lesions into invasive CaCx [Koliopoulos et al., 2017]. However, treatment is generally indicated for CIN II/III, as this stage represents the final opportunity to prevent cancer development [Snijders et al., 2006].

Since not all CIN lesions progress to cancer, there is a critical need for risk stratification in HR-HPV-positive women with CIN II+/HSIL. Identifying those at high risk of CaCx progression versus those unlikely to develop malignancy can help reduce overtreatment, minimize patient anxiety, and lower healthcare costs by limiting unnecessary diagnostic procedures, especially in LMICs such as India, where healthcare resources are often constrained.

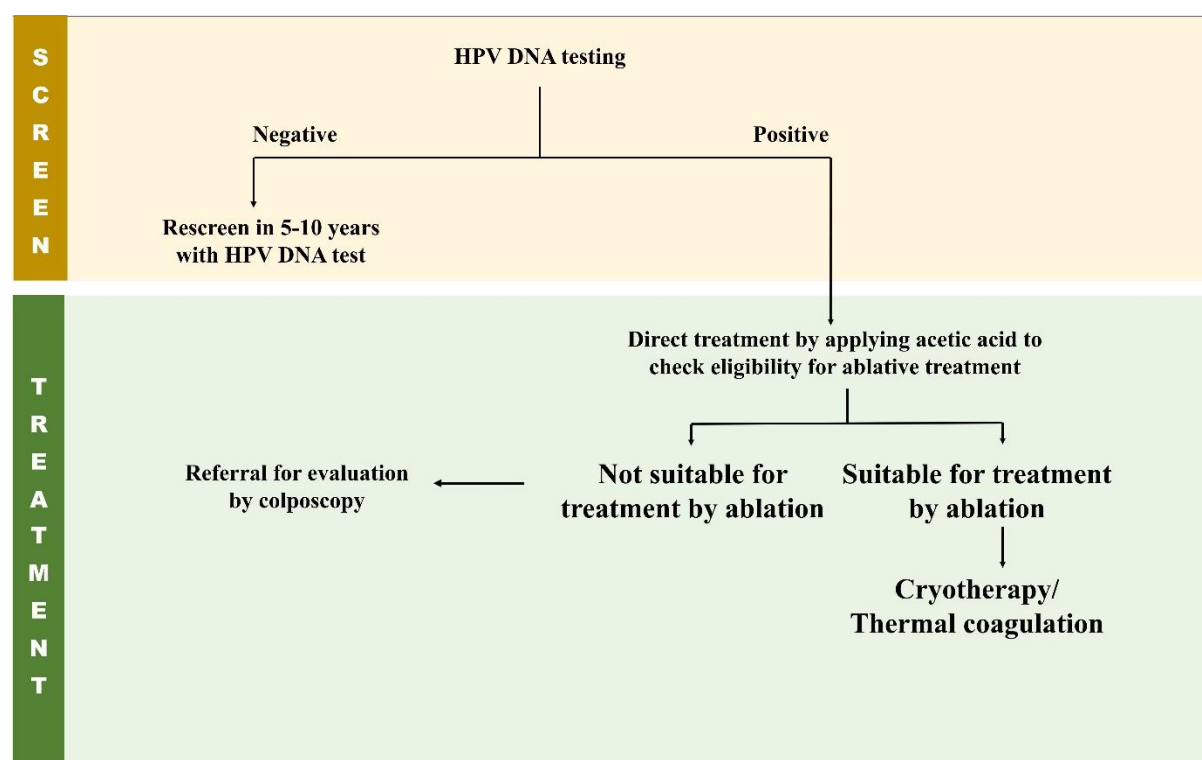


Figure 1.9 Screen and Treat model for CaCx screening

1.1.4.4 “Screen, Triage, and Treat” model for CaCx:

To address the challenges of “Screen and Treat Model”, the World Health Organization (WHO) introduced a “screen, triage, and treat” approach in 2021 (Figure 1.10). In this strategy, treatment decisions are based on a positive result from primary HPV screening, followed by a confirmatory triage test to guide clinical management [WHO, 2021]. Such

molecular triage biomarker tests can interpose between screening and treatment for prioritization of clinically relevant HSIL, thereby reducing over-treatment of non-relevant ones in countries with low-resource set-ups, such as India.

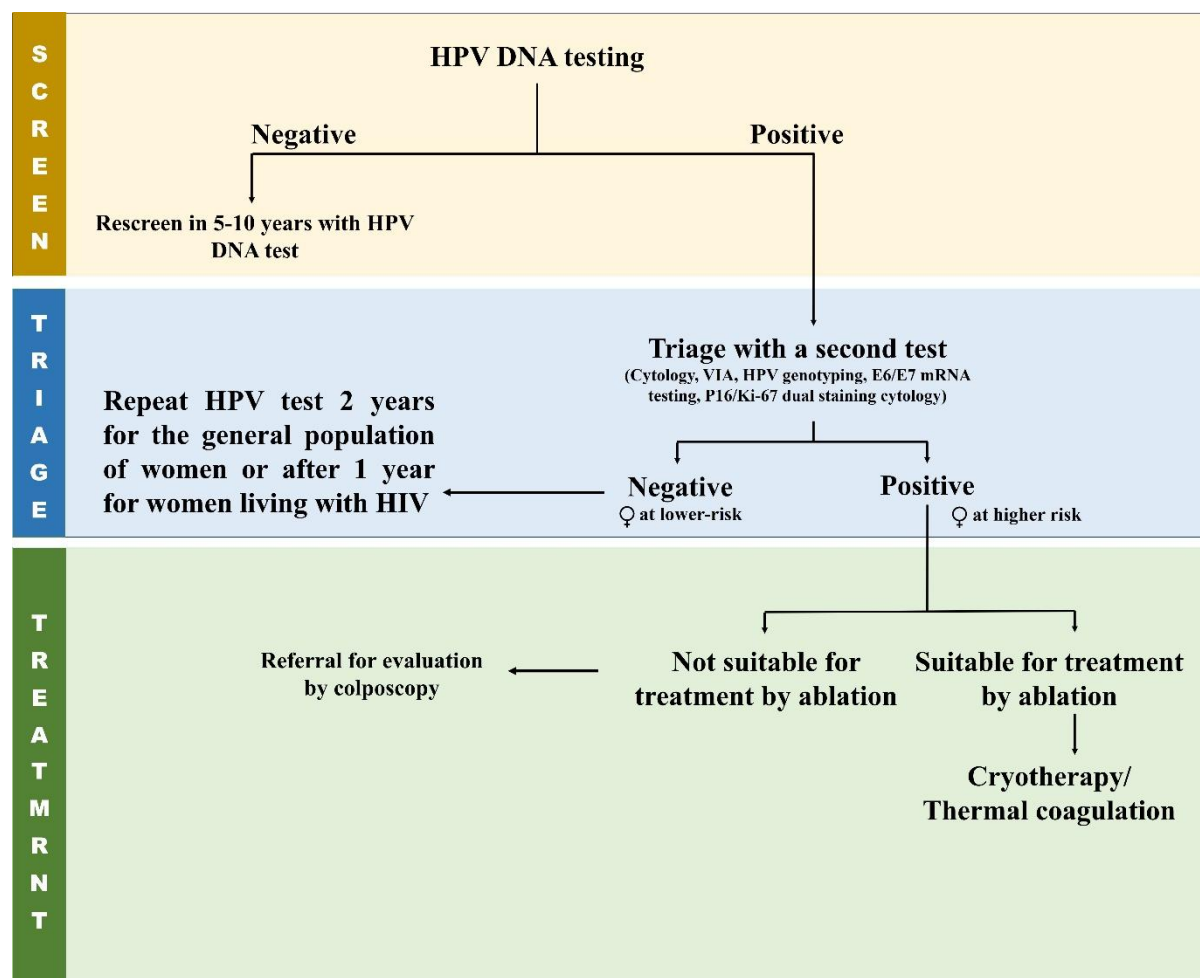


Figure 1.10 Screen, Triage, and Treat approach for CaCx screening

These strategies rely on assessing risk thresholds to identify the small subset of women likely to progress to advanced disease compared to the other screen-positive women. The most commonly employed triage tests include **Cytology, HPV Genotyping, VIA/ VILI**. In addition to these widely used methods, several other triage tests are available for enhanced risk stratification, including:

a. Triage with p16/Ki-67 dual staining:

The p16 protein is a reliable biomarker for cervical precancer, particularly in HPV infections [Bergeron et al., 2015]. Initial p16 assays required subjective evaluation, prompting the development of a dual stain assay combining p16 with Ki-67, a proliferation marker. This method detects co-stained cells, requires minimal training,

and is highly reproducible [Wentzensen et al., 2014]. Studies, including those from Italy and Kaiser Permanente Northern California (KPNC), have shown the dual stain assay to be more sensitive and specific than traditional cytology, with fewer colposcopy referrals [Wentzensen et al., 2015].

b. E6/E7 mRNA Triage biomarkers:

DNA-based HPV tests struggle with specificity, as they cannot distinguish between transient and persistent infections. The upregulation of E6 and E7 mRNA is crucial in HPV-related cellular transformation [Origoni et al., 2015]. E6/E7 mRNA tests demonstrate high sensitivity and specificity for detecting high-grade CIN (CIN II/III) [Haedicke and Iftner, 2016].

c. Other mRNA Triage biomarkers:

Beyond E6/E7, host gene expression profiles change during CaCx progression. Studies comparing CIN lesions, CaCx, and normal tissues have identified several candidate genes for further research, including HOXC10, BPA1, HIF-1 α , PTP, HME1, HNT1, and PHGDH [Zhai et al., 2007; Kendrick et al., 2007; Sopov et al., 2004; Rotondo et al., 2015]. Recent research has focused on the feasibility of using mRNA-based biomarkers from liquid-based cytology (LBC) samples to detect HSIL and CaCx. Key biomarkers studied include CDKN2A/p16, BIRC5, MMP9, TOP2A, MCM5, and MKI67. Among these, TOP2A exhibited the highest sensitivity (97%) for detecting HSIL. CDKN2A/p16 was the most specific (78%). A combined marker approach using TOP2A and CDKN2A/p16 demonstrated high sensitivity (96%) and acceptable specificity (71%), making it a promising strategy for identifying HSIL with enhanced accuracy [Del Pino et al., 2015].

d. HPV E6 Protein as Triage biomarkers:

E6 protein biomarkers derived from mRNA testing face challenges like susceptibility to degradation. New ELISA-based methods using monoclonal antibodies for HPV E6 detection show improved specificity but reduced sensitivity, requiring enhancements to increase coverage of more HPV types for broader clinical applicability [Yang et al., 2012; Valdez et al., 2016; Qiao et al., 2014].

e. Methylation based Triage Biomarker:

Abnormal DNA methylation, both in viral and host genes, is a common event in carcinogenesis. Methylation in specific HPV DNA regions (e.g., L1, E2) correlates with high-risk lesions and persistence of the infection [Clarke et al., 2012; Mirabello et al., 2012]. Host gene methylation panels (e.g., CADM1/MAL, FAM19A4/miR124-2) show potential in triaging HR-HPV-positive women, though challenges like high referral rates and inconsistent detection limit their current clinical use [Bierkens et al., 2013; De Strooper et al., 2014].

f. CNV as Triage biomarkers:

Alterations in chromosomal regions, particularly gains in 3q26 (linked to the hTERT gene), are frequently observed in HPV16-positive CaCx. These markers show promise in identifying low-grade CIN lesions but require larger, prospective studies for validation [Caraway et al., 2008].

g. miRNA as Triage biomarker:

miRNAs regulate mRNA stability and translation, influencing cellular processes like proliferation and apoptosis. Meta-analyses have identified specific miRNAs associated with CaCx, such as upregulated miR-20a, miR-21 and downregulated miR-145, miR-103, miR-143 [Li and Hu, 2015]. Changes in miRNA expression across CIN stages could help classify disease progression [He et al., 2016], although further large-scale studies are needed.

These molecular biomarkers have become a significant focus of CaCx research, particularly for triaging HR-HPV-positive women. Though these biomarkers offer the potential to distinguish between productive HPV infections and those transforming into high-grade lesions, most of them have their own limitations. Methylation-based biomarkers have insufficient sensitivity and specificity, as well as test assays need modest improvement [Lorincz et al., 2016], mRNA-based biomarkers are more prone to degradation [Del Pino et al., 2015], whereas protein-based biomarkers have turned out to be an expensive and time-taking procedure [Torres-Poveda et al., 2020]. By contrast, miRNAs possess an array of advantages. It is a highly stable molecule because of its smaller size (18-25 nt) and is easily detected by PCR techniques; it has high tissue sensitivity and specificity, and its expression varies with disease stages [Condrat et al., 2020]. Therefore, it may have the potential to be part of new triage marker for HR-HPV+ve women [Condrat et al., 2020].

1.2 Molecular basis of Uterine Cervical Carcinogenesis:

1.2.1 Chromosomal alteration during cervical carcinogenesis: effect on coding, non-coding RNA expression and altered pathways

Persistent infection with HR-HPVs, followed by viral DNA integration into the host genome, is considered a major risk factor for the development of CaCx. In approximately 66% of cases, integration occurs either within (34%) or adjacent to (32%) fragile sites in the genome [Schiffman & Wentzensen, 2013; Pett & Coleman, 2007]. HPV DNA integration directly induces genomic instability, leading to chromosomal aberrations. Additionally, it deregulates the expression of genes located at or near the integration sites, contributing to the malignant transformation of host cells [Schmitz et al., 2012; Akagi et al., 2014; Hu et al., 2015].

CNV analysis using microsatellite or sequence-tagged site (STS) markers in primary cervical lesions has revealed loss of heterozygosity (LOH) (>25%) on various chromosomal arms, including 1q, 2q, 3p, 4p, 4q, 5q, 6p, 10q, 11p, 11q, 13q, 16p, 18p, 19p, and Xq [Mitra et al., 1994; Mullokandov et al., 1996]. Detailed investigations have identified LOH during CaCx progression in regions such as 3p14.1–p22 (48%), 4p16 (40%), 4q21–35 (32%), 5p13–15 (17%), 6p21.3–22 (41%), 11p15 (28%), 11q23 (38%), 17p13.3 (24%), and 18q12.2–22 (24%) [Lazo, 1999]. Further studies have linked deletions at regions 2q34–37, 3p21.2–21.31, 3p25–pter, 4p15.31, 4p16.2, 4q34.2–34.3, 4q35.1–35.2, 8p21.3–22, 8p23.1, 9q22.32, 11q22.3–23.1, and 11q23.3–24.1 with premalignant cervical lesions. Meanwhile, deletions in 3p13, 3p22.3, 3p26.1, 4p15.2, 4q23.3–24, 6p24.3–25.1, 9p21.3, 11p15.5, 11q23.1, 11q24.2, 13q14.2, 17p13, and 18q22–qter have been associated with invasive CaCx [Kersemaekers et al., 1999; Dasgupta et al., 2003; Singh et al., 2005 & 2007]. Gains in regions such as 3q25.31, 8q24.2, and 11q13.3 have also been observed in invasive CaCx [Bhattacharya et al., 2004; Mitra et al., 2010; Singh et al., 2005].

Comparative genomic hybridization (CGH) analysis has identified multiple chromosomal regions exhibiting copy number alterations in precancerous cervical lesions, CaCx samples, and CaCx cell lines, as listed in the **Table 1.4**.

Table 1.4: List of frequently altered chromosomal loci as evident from CGH microarray analysis.

<i>Sample type</i>	<i>Loss of chromosomal loci</i>	<i>Gain of chromosomal loci</i>	<i>References</i>
precancerous lesions or CIN	2q35–qter, 3p12–p21, 3p14.1–p24, 4p16.3–p16.1, 4q31.21, 4q35.2, 11q13.3, 11q23–qter, 16q24.2–q24.3, 17p13.3, 17q25.3, and 19p13.11–q12	1p36.11–p35.2, 1p31.3–p21.1, 1q25.3–q32.1, 1q32.2–q44, 3p26.3–p26.1, 3p14.3–p14.2, 3q11.2–q29, 7q31.1–q31.2, 20p13–p11.21, and 20q12.	Narayan & Murty, 2010
Invasive CaCx	1q21–42, 2q22.2, 2q33–q37, 3p12–p23.1, 4q, 4q28.3–q32.1, 6p22–24, 6q, 8p23.3, 8p12–21.3, 8q23.2–q23.3, 9p, 10p, 10p11.23–q21.3, 10q23.3, 11p15.5, 11q13.3, 11q22.3–q25, 13q12.11–14.3, 13q14.3–q21.33, 13q31.1–q31.3, 17p13.3, and 18q11.2–q23	1p33–35, 1p36, 1p31.3–p21.1, 1q12–q44, 3p14.3–p14.2, 3p26.3–p26.1, 3q13–q29, 5p12–p13, 6p, 7p11.2, 7q11.22–q11.23, 7q31.1–q31.2, 8q24.13–q24.22, 9p22, 9q33.2–q34.3, 15q, 16p, 16p11.2, 16q22.1–q23.2, 17q21–q22, 17q25.1–q25.2, 19q13.3, 20q11.21–q13.33, 22q11.23, Xp11.2–p11.3, Xq12, Xq22, and Xq28	Narayan & Murty, 2010
Advanced stage (stage III/IV) CaCx patients	2q34–2q37.3, 4p16.3–4p12, 4q21.3, 8p23.3, 8p23.2, 8p11.22, 11q14.1–11q25, 13q13.3–13q14.3, and 19p13.3	1p36.11–1p31.1, 1q21.1–1q44, 3q13.13–3q29, 5p15.33–5p12, 8q24.3, 16q22.2, 19q13.13–19q13.2, Xp22.33–Xp11.21 and Xq11.2–Xq12	Roychowdhury et al., 2017
HeLa (CaCx cell line)	4q32.3–qter, 7q35–qter, 11q23–qter, 13q10–q14, and 20p	1q, 2q31–q36, 3pter–p21, 5p, 5q11–q32, 7pter–q35, 8q24–qter, 9p, 9q34–qter, 11p14–	Macville et al., 1999

		p11, 11q13-q22, 12p-q15, 15q, 16p, and 20q	
ME-180, MS751, SiHa, CaSki, C-4I, DoTc2 4510, SW756 and HeLa (CaCx cell lines)	2q34-2q36.1, 2q36.1-2q37.1, 3p23-3p21.3, 3p21.1-3p12.2, 4p, 4q28.3, 4q31.3-4q32.1, 8p21.3-8p12, 11p15.5, 13q12.11-13q14.3, 18q11.2-18q12.1, 18q12.2-18q23	3q26.33-3q27.2, 3q29, 5p, 7q11.22-7q11.23, 8q24.13-8q24.22, 9q33.2-9q33.3, 9q34.11-9q34.3, 12p13, 16q22.1-16q23.1, 16q23.2, 17q25.1-17q25.2, 19q13.13-19q13.32, 19q13.41, 20q11.21-20q12, 20q13.12-20q13.31	Lockwood et al., 2007
CaSki, C-33A, C-4I, HT-3, ME-180, MS751, SiHa, and SW756 (CaCx cell lines)	1p (38%), 2q (100%), 3p (62%), 4q (88%), 6q (63%), 8p (75%), 9p (38%), 10p (63%), 10q (38%), 11p (38%), 11q (38%), 13q (75%), and 18q (88%)	1p (38%), 3q (50%), 5p (63%), 5q (38%), 7p (63%), 7q (63%), 9q (88%), 11q (50%), 14q (50%), 15q (38%), 16q (50%), 17q (63%), 19q (50%), 20p (25%), 20q (88%), and Xq (38%)	Harris et al., 2003

1.2.1.1: Deregulation of mRNA and miRNA expression during the development of Cervical Carcinoma:

Frequent alterations in chromosomal regions during the development of CaCx lead to the deregulation of several candidate genes involved in cervical carcinogenesis. As shown in **Figure 1.11**, the most common genetic changes observed during the transition from normal cervical epithelium to CIN include the downregulation of some key TSGs such as RBSP3, RASSF1A, CHEK1, and LIMD1 etc [Mitra et al., 2012; Chakraborty et al., 2018; Chakraborty et al., 2016]. The progression from CIN to CaCx is associated with the downregulation of PTCH1, SLIT2, ROBO1, ROBO2, CADM1, MLH1, and VHL, primarily through gene deletion or promoter methylation (**Figure 1.11**) [Mitra et al., 2012; Indra et al., 2011; Chakraborty et al., 2018; Dutta et al., 2023]. Conversely, the transition from normal cervical epithelium to CIN is marked by the upregulation of some oncogenes such as AKT1, EPHB2, SMARCA4, and PIK3CR4. Further progression from CIN to CaCx involves the upregulation

of BCL9, NOTCH2, GLI2, CCND1, c-MYC, ERBB2, LIG4, and KIF4A through gene amplification or overexpression (Figure 1.12) [Mitra et al., 2010, 2012; Indra et al., 2011; Singh et al., 2007].

Gene expression studies have further highlighted significant dysregulation during CaCx development. Downregulation of genes such as CADM1, CDH1, FHIT, MLH1, ATM, CHEK1, E2F4, CACNA2D2, RASSF1A, ROBO1, ROBO2, APC, PTCH1, SLIT2, SFRP1, SFRP2, SFRP4, and SFRP5 has been frequently observed. In contrast, overexpression of Cyclin L1, Cyclin D1, c-MYC, and EGFR has been consistently reported in CaCx samples [Kersemakers et al., 1999; Bhattacharya et al., 2004; Singh et al., 2005; Narayan & Murty, 2010; Mazumder Indra et al., 2011a, 2011b; Mitra et al., 2010, 2012a, 2012b; Ojesina et al., 2014; Burk et al., 2017].

On the other hand, promoter hypermethylation has been reported in multiple tumor suppressor and regulatory genes at different stages of cervical carcinogenesis. Genes commonly hypermethylated in CIN include CDKN2A, CCNA1, CADM1, CTDSPL, CDH1, CDH13, FHIT, MLH1, PCDH10, RASSF1A, ROBO1, ROBO2, SLIT1, SLIT2, SLIT3, and WT1 [Narayan & Murty, 2010; Mitra et al., 2012a, 2012b; Ojesina et al., 2014; Burk et al., 2017]. Invasive CaCx exhibits frequent promoter hypermethylation in genes such as APC, CADM1, CDH1, CDH13, COX2, DAPK, FHIT, RASSF1A, THBS1, STAC, TPOU2F3, PTCH1, PTEN, SOCS1, TERT, HSPA2, MLH1, SLIT2, ROBO1, SFRP1, SFRP2, SFRP4, and SFRP5 (**Figure 1.11**) [Narayan & Murty, 2010; Mitra et al., 2012a, 2012b; Ojesina et al., 2014; Burk et al., 2017]. Mutations in genes such as PIK3CA, EP300, FBXW7, PTEN, HLA-A, ARID1A, NFE2L2, HLA-B, KRAS, ERBB3, MAPK1, CASP8, TGFBR2, SHKBP1, STK11, ELF3, CBFB, and TP53 have been identified in invasive CaCx [Ojesina et al., 2013; Burk et al., 2017].

According to Pardini et al. (2018), certain miRNAs were also deregulated during the progression of CaCx. Several qRT-PCR and microarray analyses revealed the upregulation of miR-10a, miR-34b, miR-34c, miR-338, miR-345, miR-424, miR-512-5p, miR-518a, let-7g, miR-26a, miR-29a, miR-29b, miR-29c, miR-30a, miR-34c-5p, miR-101, miR-125a-5p, miR-135b, miR-143, and miR-145 in CIN II/III stages compared to CIN I or normal tissue samples [Wilting et al., 2013; Cheung et al., 2012]. In contrast, miR-16, miR-27a, miR-197, miR-106a, miR-142-5p, miR-205, miR-7d, miR-9, miR-15a, miR-15b, miR-17, miR-18a, miR-19a, miR-20b, miR-24, miR-27, miR-30d, miR-93, miR-107, miR-130b, miR-141, miR-151-3p, miR-155, miR-185, miR-200c, miR-331-3p, miR-339-5p, miR-363, miR-425, and miR-652 were

upregulated in squamous cell carcinoma (SCC) samples compared to CIN II/III stages [Wilting et al., 2013; Pereira et al., 2010]. A stage-wise progressive upregulation of specific miRNAs such as miR-15b, miR-16, miR-17, miR-20a, miR-20b, miR-25, miR-31, miR-92a, miR-92b, miR-93, miR-106a, miR-182, miR-185, miR-155, miR-221, miR-222, and miR-224 was observed from normal tissue to CIN to SCC [Li et al., 2011].

Conversely, microarray data indicated that miR-193a-3p, miR-205, miR-212, miR-221, miR-27a, miR-27b, miR-484, miR-636, and miR-770-5p were downregulated in CIN I or normal samples compared to CIN II/III stages. Additionally, miR-100, miR-125b, miR-148a, miR-188-5p, miR-195, miR-199a-5p, miR-199b-3p, miR-218, miR-26b, miR-375, miR-376a, miR-378, miR-486-5p, miR-494, miR-497, miR-513b, miR-660, and miR-671-5p were downregulated in CIN II/III samples compared to SCC samples [Wilting et al., 2013]. Moreover, the expression of let-7b, miR-10b, miR-29a, miR-29c, miR-99a, miR-100, miR-125b, miR-126, miR-145, miR-195, miR-199a-3p, miR-218, miR-375, and miR-424 was progressively downregulated during the transition from normal tissue to CIN II/III and eventually to SCC (**Figure 1.11**) [Li et al., 2011]

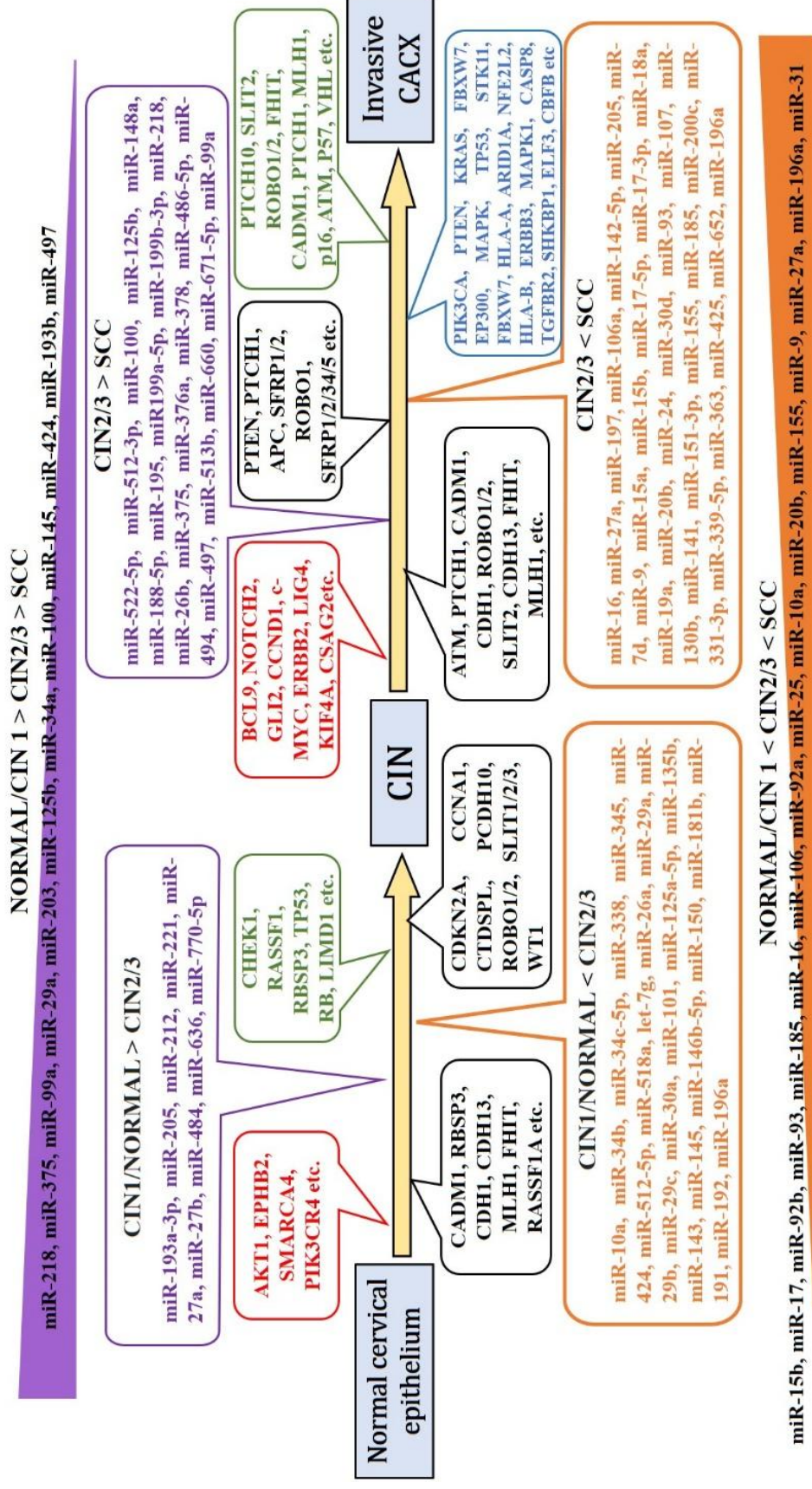


Figure 1.11 Alteration of coding (mRNA) and non-coding (miRNA) genes during molecular progression of uterine cervical carcinoma. Upregulated genes are denoted in RED. Downregulated genes are denoted in GREEN. Methyalted genes are denoted in BLACK. Mutated genes are denoted in BLUE. Upregulated miRNAs are denoted in ORANGE and downregulated miRNAs are denoted in VIOLET.

1.2.2.2 miRNA-Mediated mRNA Decay

miRNAs predominantly regulate gene expression mostly by binding to complementary sequences in the 3' untranslated region (UTR) of its target mRNAs. This interaction typically results in mRNA degradation, or translational repression [Huntzinger & Izaurralde, 2011; Ipsaro & Joshua-Tor, 2015]. Initially, it was believed that miRNAs primarily inhibit translation without significantly affecting mRNA stability [Olsen & Ambros, 1999; Wightman et al., 1993]. Subsequent studies, however, revealed that miRNAs can destabilize mRNAs by recruiting deadenylase complexes through interactions with GW182 proteins [Mishima et al., 2006; Behm-Ansmant et al., 2006; Till et al., 2007].

In mammals, GW182 proteins (also referred to as TNRC6) serve as molecular bridges linking Argonaute proteins, a key component of the RNA-induced silencing complex (RISC), to deadenylase complexes, thereby facilitating mRNA degradation [Chen et al., 2009]. The glycine-tryptophan (GW) repeats of GW182 are recognized by the PIWI domain of Argonaute proteins, creating a recruitment platform for deadenylase complexes such as CCR4–NOT and PAN2–PAN3 [Behm-Ansmant et al., 2006; Till et al., 2007]. Among these, CCR4–NOT plays a dominant role in miRNA-induced deadenylation, whereas PAN2–PAN3 provides a supplementary function (**Figure 1.12**) [Fabian et al., 2009; Huntzinger et al., 2010; Braun et al., 2011].

Deadenylation, the process of poly(A) tail shortening, is often preceded by the dissociation of poly(A)-binding protein (PABP). The recruitment of CCR4–NOT facilitates access to the poly(A) tail, accelerating mRNA decay [Behm-Ansmant et al., 2006; Fukaya & Tomari, 2012]. Following deadenylation, the mRNA undergoes decapping, wherein the DCP2 enzyme removes the 5' cap structure. This step is supported by decapping activators such as DDX6, DCP1, and EDC4, which are recruited to Ago-bound mRNAs (**Figure 1.12**) [Pillai et al., 2005; Chu & Rana, 2006; Nishihara et al., 2013]. Once the cap is removed, the mRNA is degraded in a 5'-to-3' direction by the exonuclease XRN1 (**Figure 1.12**) [Subtelny et al., 2014].

Although, deadenylation typically precedes decapping, certain miRNAs can induce decapping independently, bypassing poly(A) tail shortening [Makino et al., 2015]. Structural studies suggest that CCR4–NOT interactions with decapping activators such as DDX6 further enhance this process [Chen et al., 2009; Mathys et al., 2014]. In humans, additional proteins such as 4E-T serve as molecular bridges connecting the deadenylation and decapping machinery [Nishimura et al., 2015].

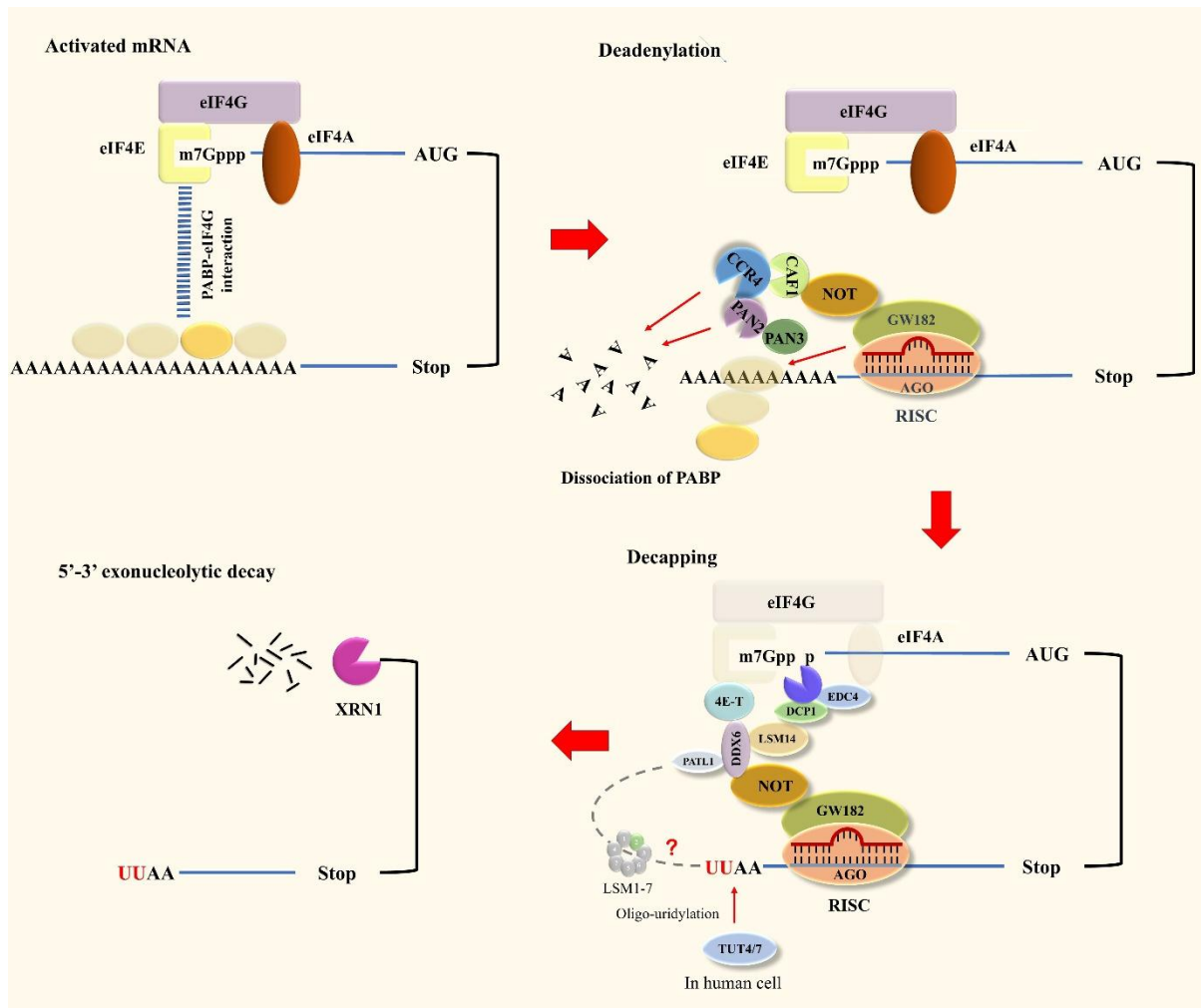


Figure 1.12 *miRNA-Mediated mRNA Decay Pathway in Animals (Adapted and modified after Iwakawa & Tomari, 2015).*

1.2.2.3 Oncogenic and Tumor suppressive miRNA during CaCx development

OncomiRs are miRNAs that promote cancer progression by downregulating tumor suppressor genes or enhancing oncogenic signaling pathways, whereas tumor-suppressive (TS) miRNAs prevent cancer by inhibiting oncogenes or controlling cell cycle progression, differentiation, and apoptosis [Wang et al., 2019]. Oncogenic and tumor-suppressive (TS) miRNAs are key components among dysregulated miRNAs. These distinct classes play crucial roles in various

biological processes, including the invasion, growth, and progression of CaCx. Such contributions highlight their significance in the molecular mechanisms underlying cancer development (**Figure 1.13**) [Wang et al., 2019].

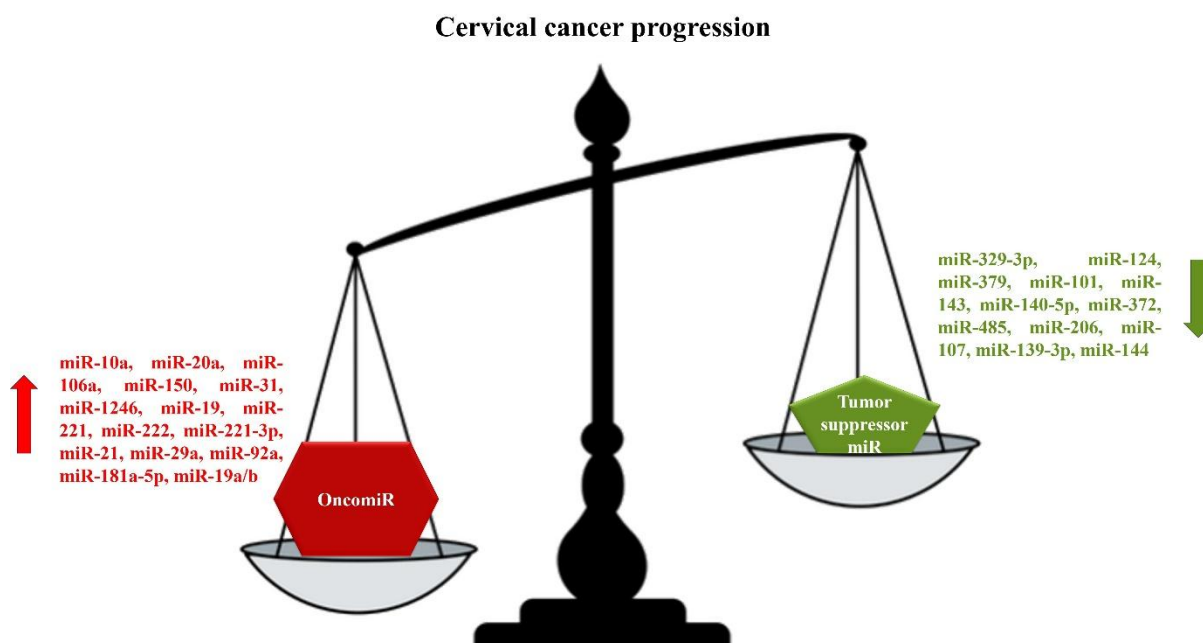


Figure 1.13 miRNAs as oncogenes or tumor suppressors in cervical carcinogenesis. RED up arrow indicates upregulations and GREEN down arrow indicates downregulation.

1.2.1.4 Alteration in signalling pathways associated with deregulation of miRNA/ mRNA during CaCx development

The aberrant expression of specific miRNAs in CaCx significantly contributes to the activation of key signalling pathways involved in tumor progression through their respective target genes expression alterations. Prominent pathways regulated by miRNAs include the PI3K/AKT/mTOR, Wnt/ β -catenin, MAPK/ERK, and JAK/STAT cascades, underscoring the crucial role of miRNAs in the cancer pathogenesis (**Figure 1.14**) [Hasan et al., 2023]. A comprehensive list of miRNAs, their target genes, and associated signalling pathways is presented in **Table 1.5**, further emphasizing their importance in the progression of CaCx.

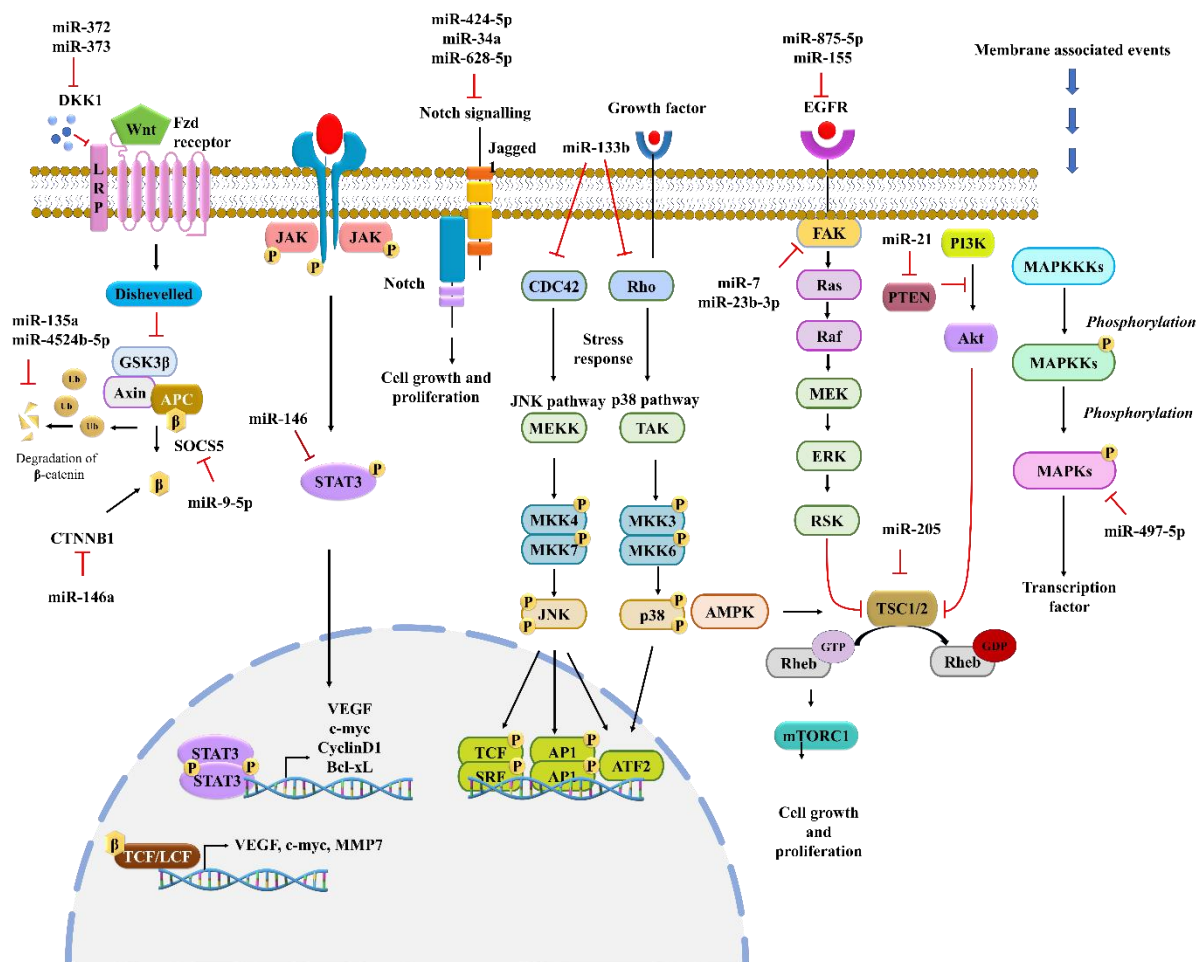


Figure 1.14 miRNA mediated regulation of key cellular pathways associated with CaCx development (Modified after Doghish et al., 2023)

Table 1.5: miRNA mediated regulation of important signalling pathways associated with CaCx development. miRNA/ mRNA denoted in RED indicates upregulation and GREEN indicates downregulation.

<i>miRNA (s)</i>	<i>Target genes (s)</i>	<i>Associated Pathways</i>	<i>References</i>
miR-372, miR-373	DKK1	Wnt signaling pathway	Zhou et al., 2012
miR-135a, miR-4524b-5p	β-catenin		Leung et al., 2014; Li et al., 2019
miR-146a	CTNNB1		

miR-9-5p	SOCS5		Sathyanarayanan et al., 2016 Wei et al., 2019
miR-146	STAT3	JAK-STAT signaling pathway	Sathyanarayanan et al., 2016
miR-424-5p	KDM5B	NOTCH signaling pathway	Zhou et al., 2017
miR-34a	UPA		Pang et al., 2010
miR-628-5p	Jagged 1		Chen et al., 2010
miR-875-5p	EGFR	EGFR pathway	Liang et al., 2021
miR-7, miR-23b-3p	FAK		Campos-Viguri et al., 2020; Hao et al., 2015
miR-21	PTEN	PI3K-Akt pathway	Xu et al., 2015
miR-205	TSC1/2		Zhang et al., 2019
miR-497-5p	MAPK1	MAPK pathway	Lu et al., 2022
miR-133b	CDC42 Rho	JNK pathway P38 pathway	Qin et al., 2012

1.2.2. Contribution of onco-miR during carcinogenesis of uterine cervix:

The inactivation of tumor-suppressor (TS) proteins often arises from genetic modifications. However, numerous studies have revealed that epigenetic silencing, rather than genetic deletion, is a more common mechanism behind TS protein loss [Wang et al., 2019]. OncomiRs have been shown to regulate the expression of TS genes across various cancer types. Evidence

suggests that oncomiRs facilitate tumor progression by downregulating TS genes associated with cellular proliferation and apoptosis. This is consistent with the pivotal roles that proliferation and apoptosis play as checkpoints in the development of nearly all cancers [Finkel et al., 2007]. A list of oncogenic miRNAs, their target genes and their mechanism of action during development of CaCx were tabulated in **Table 1.6**.

Table 1.6: Role of oncomiRs during uterine cervix carcinogenesis

<i>OncomiR</i>	<i>Target genes</i>	<i>Mechanism of action</i>	<i>References</i>
miR-34a	<i>P18Ink4c, CDK4, CDK6, Cyclin A, E2, E2F1, BCL2, BIRC3</i>	<ul style="list-style-type: none"> i. <i>p53-dependent pathway</i> ii. <i>Cell cycle progression</i> iii. <i>Cellular senescence</i> 	<i>Li et al., 2010</i>
miR-20a	<i>ATG7 and TIMP2</i>	<ul style="list-style-type: none"> i. <i>Promotes lymph node metastasis</i> 	<i>Bao et al., 2013</i>
miR-182	<i>FOXO1</i>	<ul style="list-style-type: none"> i. <i>Induce cellular proliferation</i> ii. <i>Inhibit apoptosis of cells</i> iii. <i>Regulate cell cycle pathways</i> 	<i>Tang et al., 2013</i>
miR-200b	<i>FoxG1</i>	<ul style="list-style-type: none"> i. <i>Inhibit cellular apoptosis</i> ii. <i>Induce cell migration and invasion</i> 	<i>Choi et al., 2022</i>
miR-499a	<i>SOX6</i>	<ul style="list-style-type: none"> i. <i>Enhanced cellular proliferation</i> ii. <i>Regulate cell cycle</i> iii. <i>Induce colony formation</i> iv. <i>Inhibit cellular apoptosis</i> v. <i>Induce cell migration and invasion</i> 	<i>Chen et al., 2020</i>
miR-137	<i>EZH2</i>	<ul style="list-style-type: none"> i. <i>Cell proliferation and migration</i> 	<i>Zhang et al., 2018</i>

<i>miR-133b</i>	<i>MST2, CDC42, ERK1 and ERK2, RHOA, AKT1</i>	<ul style="list-style-type: none"> i. Enhances cell proliferation ii. Induces colony formation 	<i>Qin et al., 2012</i>
<i>miR-886-5p</i>	<i>AX</i>	<ul style="list-style-type: none"> i. Cell transformation 	<i>Li et al., 2011</i>
<i>miR-873-5p</i>	<i>ZEB1</i>	<ul style="list-style-type: none"> i. promotes CaCx progression by notch signalling pathway 	<i>Wen et al., 2021</i>
<i>miR-224</i>	<i>RASSF8</i>	<ul style="list-style-type: none"> i. Associated with aggressive disease progression and poor prognosis 	<i>Huang et al., 2016</i>
<i>miR-214</i>	<i>Bcl2l2</i>	<ul style="list-style-type: none"> i. facilitates the progression of CC by activating PI3K/AKT/mTOR pathway 	<i>Wang et al., 2013</i>
<i>miR-9-5p</i>	<i>CDH1</i> <i>TWIST1</i> <i>SOC5</i>	<ul style="list-style-type: none"> i. Involved in angiogenesis ii. Facilitates metastasis iii. Regulates epithelial-mesenchymal transition (EMT) and tube formation 	<i>Farzanehpour et al., 2019</i> <i>Babion et al., 2019</i> <i>Wei et al., 2019</i>
<i>miR-21-5p</i>	<i>PTEN</i>	<ul style="list-style-type: none"> i. Encourages proliferative signalling via. PI3K pathway ii. Induces cell migration and invasion 	<i>Bumrungthai et al., 2015</i>
<i>miR-155-5p</i>	<i>TP53INP1</i>	<ul style="list-style-type: none"> i. Induces tumor progression 	<i>Li et al., 2019a</i>
<i>miR-301b</i>	<i>RASAL1</i>	<ul style="list-style-type: none"> i. Increase RAS activation 	<i>McBee Jr et al., 2011</i>

		ii. Promotes CaCx progression	
--	--	-------------------------------	--

1.2.3 miRNA as triage biomarker for CaCx: A non-invasive approach

The use of circulatory body fluid biomarkers is gaining traction in clinical settings for the early detection of cancer, prognosis evaluation, and treatment monitoring [Lazaros et al., 2025]. Although invasive diagnostic procedures offer crucial insights into disease mechanisms, they are often costly, pose procedural risks, and cause discomfort to patients. In contrast, non-invasive biomarkers provide a promising alternative, enabling precise disease assessment through easily obtainable biological samples. These innovative approaches employ diverse analytical techniques, each offering distinct contributions to understanding health status and disease progression [Lazaros et al., 2025].

Although, several potential miRNA-based triage biomarkers for CaCx screening have been identified in various body fluids, including plasma, urine, and cervical scrapes [Xin et al., 2016; Aftab et al., 2021; Kawai et al., 2018; Ivanov et al., 2018], the identification of miRNAs from exfoliated cervical cells would be more suitable. This is because exfoliated cervical cells are already extensively used in CaCx screening and represent a minimally invasive method [Kawai et al., 2018; Ivanov et al., 2018].

Differentially expressed miRNAs could serve as a potential molecular triage strategy in HR-HPV-based cervical screening programs as it is easily accessible, has high tissue sensitivity and specificity, expression varies with disease stages, moreover, needs less time and lower cost [Condrat et al., 2020]. miRNAs are either genetically or epigenetically deregulated and play a direct role in disease progression, hold significant promise as biomarkers for detecting HSIL [Babion et al., 2018]. Furthermore, the detection of HSIL was enhanced by incorporating HPV16/18 genotyping into the screening process [Babion et al., 2018]. A subset of miRNA-based triage biomarkers for CaCx screening are listed in **Table 1.7**

Table 1.7: List of miRNA-based triage biomarkers used for CaCx screening

Sl. No.	miRNA (s)	Sample type	Detection stage	Sensitivity and Specificity	
1	miR-15b-5p and miR-375	HR-HPV+ve cervical scrapes	CIN III	Specificity 70%	[Babion et al., 2018]
2	let-7b, miR-15b, miR-20a, miR-93, and miR-222	HR-HPV+ve cervicovaginal self-samples	CIN III	Sensitivity 67% Specificity 65%	[Snoek et al., 2019]
3	miR-424/375/218 miR-424/375	HR-HPV+ve Cervical exfoliated cells	CIN II+ CIN III+	Sensitivity: 74% Specificity: 85% Sensitivity: 78% Specificity: 80%	[Tian et al., 2014]
4	miR-205	HR-HPV+ve Liquid-based cytology (LBC) samples	CIN II+ CIN III+	Specificity: 63% Specificity: 57%	[Xie et al., 2017]
5	FAM19A4/miR124-2 methylation	HR-HPV+ve Cervical scrape	CIN III	Sensitivity 77%	[Bonde et al., 2021]
6	miR-126-3p	Cervical mucus	CIN II+	Sensitivity 66% Specificity 82%	[Kawai et al., 2018]
	miR-20b-5p			Sensitivity 74% Specificity 70%	
	miR-451			Sensitivity 76% Specificity 82%	
	miR-144-3p			Sensitivity 68% Specificity 89%	

1.3 Importance of miRNAs targeting LIMD1-VHL associated hypoxic stress response pathway during Cervical Carcinogenesis

From the initial stages of infection to the development of cervical lesions and eventually, to the progression of CaCx, HPV modulates the cellular response to hypoxia by inhibiting Hypoxia-inducible factor (HIF-1 α) ubiquitylation or inducing HIF-1 α stabilization [Nakamura et al., 2009]. It has been reported that HPV E6 oncoprotein functions to counteract p53-mediated HIF-1 α degradation, [Bodily et al., 2011] whereas HPV E7 oncoprotein enhances HIF-1 α transcriptional activity by blocking the interaction of HDAC with HIF-1 α , as indicated in **Table 1.3** [Bodily et al., 2011; Ravi et al., 2000].

1.3.1 Hypoxia, role of LIMD1-VHL and cervical carcinogenesis:

HIF-1 α is a key regulator of tumor angiogenesis. Under normal oxygen levels, prolyl hydroxylase (PHD), an oxygen-sensing enzyme, hydroxylates the Pro-564 residue of HIF-1 α . This modification facilitates recognition by the von Hippel-Lindau (VHL) protein, which subsequently ubiquitinates and targets HIF-1 α for proteasomal degradation, preventing the activation of hypoxia-inducible genes (Fedele et al., 2002). LIMD1, a potential tumor suppressor gene (TSG), interacts with PHDs and VHL to enhance HIF-1 α degradation under normoxic or mild stress conditions [Foxler et al., 2012] (**Figure 1.15**).

Under hypoxic conditions, the hydroxylation of HIF-1 α is inhibited, preventing VHL-mediated ubiquitination and degradation [Fedele et al., 2002] (**Figure 1.15**). Additionally, factor-inhibiting HIF-1 (FIH), an oxygen-dependent asparaginyl hydroxylase, is unable to hydroxylate the Asn-803 residue of HIF-1 α . As a result, co-activators CBP/p300 and HIF-1 β associate with HIF-1 α , triggering the transcription of hypoxia-responsive genes such as vascular endothelial growth factor (VEGF), platelet-derived growth factor (PDGF), and matrix metalloproteinase-9 (MMP-9) [Fedele et al., 2002; Patel et al., 2005; Diez et al., 2007]. VHL is inactivated in cancer, particularly kidney cancer, which stabilizes HIF-1 α and leads to tumour angiogenesis, even in normoxia [Latif et al., 1992; Herman et al., 1994; Gnarr et al., 1994; Prowse et al., 1997; Banks et al., 2006]. LIMD1 is inactivated in HNSCC and lung carcinoma, resulting in tumour development [Sharp et al., 2008]. The structure and function of LIMD1 and VHL are discussed below:

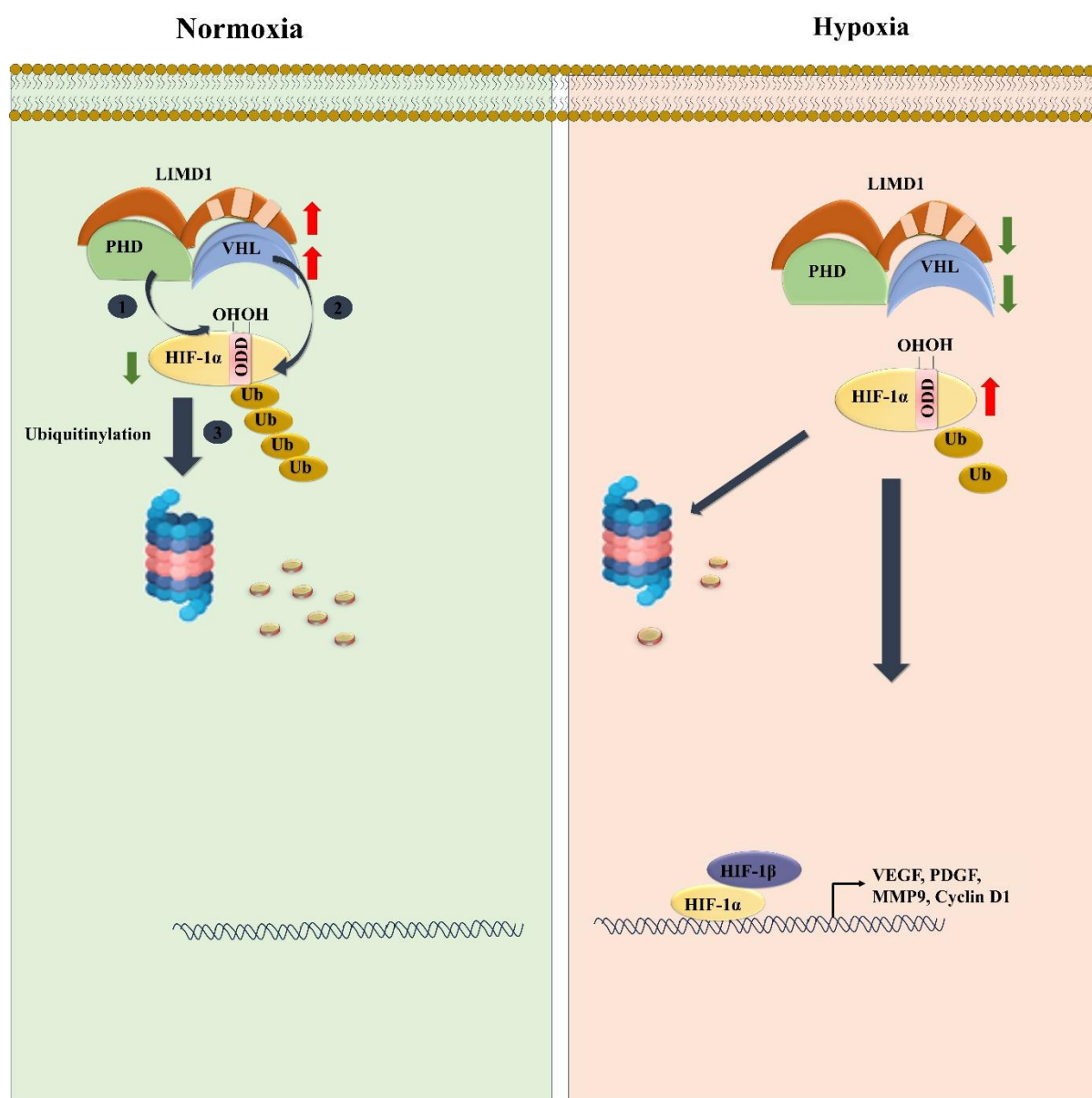


Figure 1.15 Schematic representation of the mechanism of HR-HPV induced LIMD1-VHL-HIF-1 α stress response pathway

A. LIMD1:

LIMD1 (676 amino acids, 72 kDa, NCBI ID: NP_055055.1) belongs to the Ajuba LIM protein subgroup within the Ajuba/Zyxin family. The gene spans 91,591 bp on the plus strand, located from 45,594,751- 45,686,341 bp from the p-terminus (p-ter) in the C3CER1 region at chromosome 3p21.31, commonly deleted in solid tumors (ensemble.org version 112) (**Figure 1.16**). The 5' promoter region includes a negative regulatory element, a CpG island, which includes a putative TATA box and an experimentally validated 21-bp core basal promoter region [Sharp et al., 2008]. The transcript is 11,442 bp long, consists of eight exons, and has most miRNA binding sites in the 3' UTR of the eighth exon. The first

exon encodes the N-terminal pre-LIM region (residues 1–471), each coordinating two zinc ions in a tandem zinc-finger topology (InterPro ID: IPR001781) [Kadmas and Beckerle, 2004]; while exons 2 to 8 encode three tandem LIM domains (residues 472–676) and mediate protein-protein interactions [Kadmas and Beckerle, 2004]. The pre-LIM region contains a proline/serine-rich segment (residues 69–471), a LEM-like domain (residues 18–68), a nuclear export signal (NES, residues 54–134), and the binding site for pRB (residues 404–442). The three LIM domains also function as an inherent nuclear localization signal (NLS, residues 472–676). Additionally, VHL interacts with LIMD1 in the LIM2 domain. LIMD1 shuttles between the cytoplasm and nucleus, but is not found in the nucleoli [Sharp et al., 2004]. In the cytoplasm, LIMD1 colocalises with focal adhesions [Huggins and Andrulis, 2008; Petit et al., 2005], adherens junctions [Thakur et al., 2010] and mRNA processing bodies (P-bodies) [James et al., 2010].

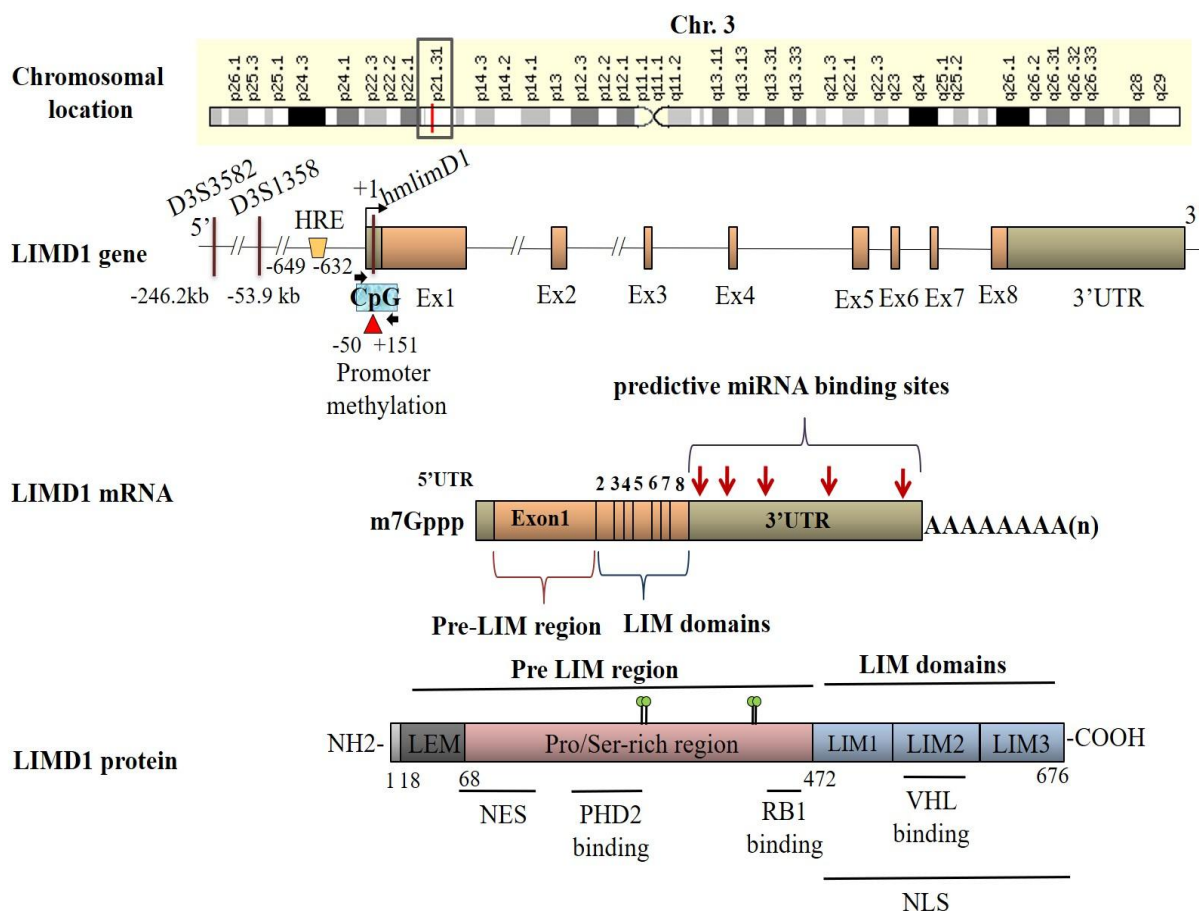


Figure 1.16 Schematic representation of *LIMD1* chromosomal location, DNA structure, transcript and its protein structure.

LIMD1 can repress cell cycle progression through pRb-dependent and pRb-independent inhibition of E2F [Sharp et al., 2004] and regulates Hippo signalling by

binding to LATS, causing sequestration of the Hippo kinase complex [Thakur et al., 2010]. LIMD1 is also part of the Slug/Snail complex that regulates E-cadherin transcription [Langer et al., 2008] in addition to facilitating centrosomal localisation of BRCA2 to prevent aberrant cellular proliferation [Hou et al., 2016].

B. VHL:

The von Hippel Lindau or VHL gene is located in the forward strand of chromosome 3 (3p25.3); ranging from 10,141,778-10,153,676 bp (**Figure 1.17**) (ensemble.org version 112). It contains only 3 exons, with a transcript size of 4414 bp. This gene codes for a protein of 213 amino acid residues and 24 kD molecular weight. This protein comprises of two functionally distinct domains: amino terminal β -domain and the carboxy terminal α -domain. The α -domain (157-189 amino acid residues) of VHL mainly interacts with ElonginB, ElonginC, Cullin2 and Rbx, resulting in the assembly of a multiprotein VBC/Cul2 complex with the function of E3-ubiquitin ligase, that targets and degrades the α -subunit of HIF-1 α , in oxygen dependent manner [Maxwell et al., 1999; Nguyen et al., 2015]. The β -domain (64-155 amino acid residues) of VHL has two major functions firstly, binding the substrates; HIF- 1 α and fibronectin (for assembly of extracellular fibronectin matrix) and secondly, nuclear/cytoplasmic trafficking of the VBC/Cul2 ubiquitin ligase. The VHL mediated degradation of HIF-1 α is facilitated by interaction of the former with Tid-1L, thereby antagonizing angiogenesis. VHL has been elaborately studied in association with renal cell carcinoma (Maranchie et al., 2002). However, the involvement of its downregulation with the development of other cancers like cervix, oral etc. has now been reported (Zhang et al., 2014; Chakraborty et al., 2018).

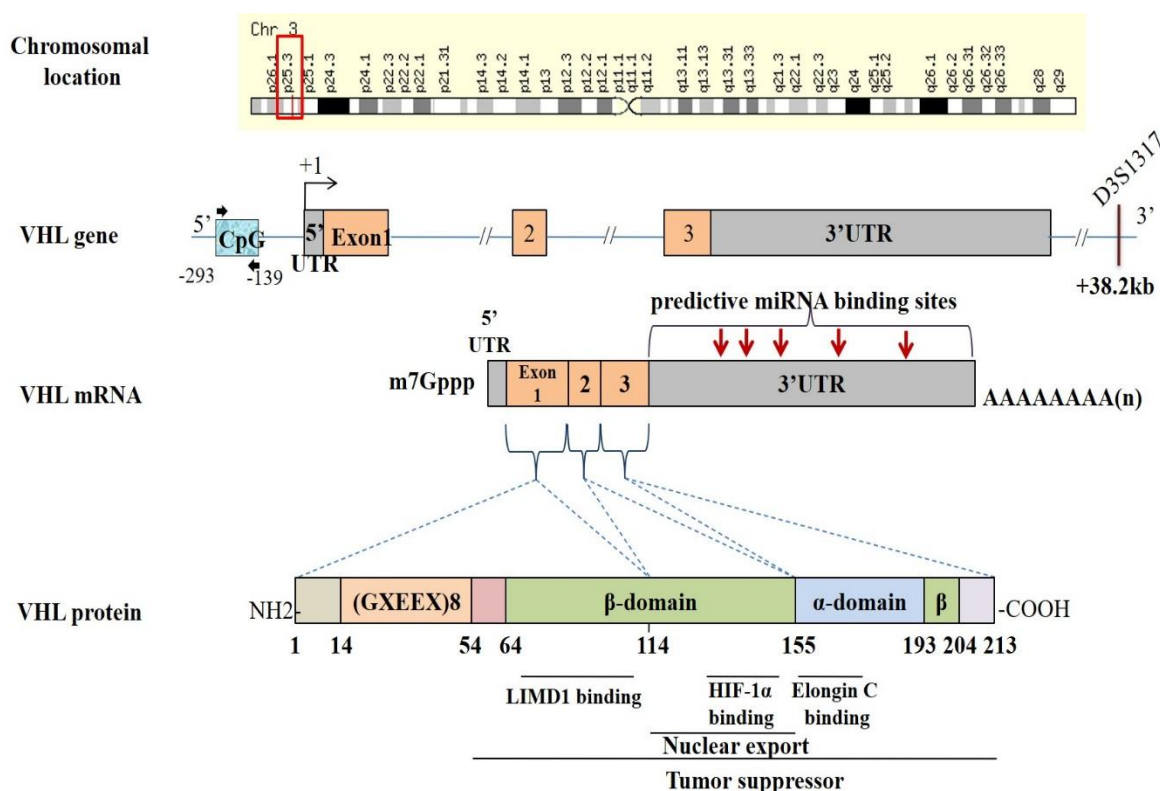


Figure 1.17 Schematic representation of *VHL* chromosomal location, DNA structure, mRNA structure and protein structure.

1.3.2 MiRNAs as master player in the hypoxic stress response pathway:

The link between hypoxia and miRNAs was first established by Kulshreshtha et al. (2007), who identified multiple hypoxia-responsive miRNAs (HRMs) through microarray-based expression analysis. These included miR-21, -23, -24, -26, -27, -30, -93, -103, -106, -107, -125, -181, -192, -195, -210, and -213, all of which were upregulated under normoxic conditions. Among them, the promoter regions of miR-210, -26, and -181c were found to be directly regulated by hypoxia-inducible factors (HIFs) [Kulshreshtha et al., 2007].

Advancements in miRNA research have led to the identification of approximately 2,300 mature human miRNAs [Alles et al., 2019]. However, only a limited number have been extensively studied and experimentally validated in the context of hypoxia-driven tumor development. Recent findings suggest that specific miRNAs play a pivotal role in cellular responses to hypoxia (**Table 1.8**). Notably, several HRMs are frequently overexpressed across different stages of cancer, underscoring their potential involvement in tumor progression [Kulshreshtha et al., 2008].

Table 1.8: List of miRNAs involved in regulating HIFs and HIF regulatory gene levels. miRNAs proven to directly bind HIF mRNAs are in bold, and indirect effects are marked with "*" (Modified after Serocki et al., 2018)

miRNA	Cell line (Cancer type)	Effect of hypoxia on miRNA expression	miRNA target(s) (direct or indirect*)	Cellular process altered	References
miR-18a	MGC-803, HGC-27 (Gastric Carcinoma)	Downregulation	<i>HIF1A</i>	Apoptosis and invasion	Wu et al., 2015
	MDA-MB-231 cells (orthotopic metastatic (Breast Cancer)	Not shown	<i>HIF1A</i>	Metastasis	Krutilina et al., 2014
miR-20b	HepG2 cells (Hepatocellular Carcinoma)	Downregulated	<i>HIF1A</i> <i>VEGF</i>	Invasion	Xue et al., 2015
miR-31	Fadu, OECM-1, SAS cells (head and neck squamous cell carcinoma – HNSCC)	Not shown	<i>HIF1A</i> <i>HIF1A</i> *	Tumour development	Liu et al., 2010
miR-33a	A375 cells (Melanomas)	Not shown	<i>HIF1A</i>	Proliferation invasion metastasis	Zhou et al., 2015
miR-33b	U2OS cells (Osteosarcoma)	Not shown	<i>HIF1A</i>	Proliferation migration	Zhou et al., 2017
miR-107	HCT116 cells (Colon Cancer)	Not shown	<i>ARNT</i>	Angiogenesis	Yamakuchi et al., 2010
miR-135b	RPMI8226 cells (Multiple myeloma)	Upregulation	<i>HIF1A</i> <i>HIF1A</i> *	Angiogenesis	Umezumi et al., 2014
miR-138	786-O cells (Clear Cell Renal Cell Carcinoma)	Not shown	<i>HIF1A</i>	Apoptosis migration	Song et al., 2011
	SKOV-3, TOV-112D cells (Ovarian Cancer)	Not shown	<i>HIF1A</i> <i>SOX4</i>	Invasion metastasis	Yeh et al., 2013
miR-142	PANC-1, SW1990, Hup, CFPAC-1 cells (Pancreatic Cancer)	Downregulation	<i>HIF1A</i>	Proliferation invasion	Lu et al., 2017
miR-145	SW1116, SW480 cells (Colon Cancer)	Not shown	<i>RPS6KB1</i> <i>HIF1A</i> *	Growth angiogenesis	Xu et al., 2012
	SW1116 cells (Colorectal Cancer), OVCAR-3, A2780 cells (Ovarian Cancer)	Not shown	<i>NRAS</i> <i>IRS-1</i> <i>HIF1A</i> *	Cancer progression	Yin et al., 2013
miR-147a	HeLa cells (CaCx)	Upregulation	<i>HIF3A</i> <i>HIF1A</i> *	Proliferation	Wang et al., 2016

miR-155	HeLa (CaCx) and CaCo-2 cells (Colon Cancer)	Upregulation	<i>HIF1A</i>	Hypoxia	Bruning et al., 2011
miR-182	786-O, OS-RC-2, Caki-1 ccRCC cells (Clear Cell Renal Cell Carcinoma)	Not shown	<i>EPAS1</i> <i>DICER1</i> *	Cancer progression	Fan et al., 2016
	PC-3, DU145 cells (Prostate Cancer)	Upregulation	<i>EGLN1</i> <i>HIF1AN</i> <i>HIF1A</i> *	Hypoxia	Li et al., 2015
miR-186	MKN45; SGC7901 cells (Gastric Cancer)	Not shown	<i>HIF1A</i>	Glycolysis	Liu et al., 2016
MiR-206	A59, NCI-H520 cells (Non-small Cell Lung Carcinoma)	Downregulation	<i>YWHAZ</i> <i>HIF1A</i> *	Growth and angiogenesis	Xue et al., 2016
miR-210	SMMC-7721, PLC/PRF/5, MHCC-97L, BEL-7402 cells (Hepatocellular Carcinoma)	Upregulation	<i>HIF3A</i> <i>HIF1A</i> *	Metastasis	Kai et al., 2016
miR-374b	PC-3 cells (Prostate Cancer)	Downregulation	<i>HIF1A</i> <i>EPAS1</i>	Angiogenesis	Sohn et al., 2015
miR-497	MCF-7 cells (Breast Cancer)	Downregulation	<i>HIF1A</i> * <i>VEGF</i> *	Angiogenesis	Wu et al., 2016
miR-519c	CL1-0 and CL1-5 cells (Lung Adenocarcinoma)	Not shown	<i>HIF1A</i>	Angiogenesis	Cha et al., 2010
miR-526b-3p	HT-29 and SW480 cells (Colon Cancer)	Not shown	<i>HIF1A</i>	Cancer development and progression	Zhang et al., 2016
miR-622	A549 and H1299 cells (Lung Cancer)	Not shown	<i>HIF1A</i>	Metastasis	Cheng et al., 2015
miR-675-5p	SW480 and SW620 cells (Colon Cancer)	Not shown	<i>DDB2</i> <i>HIF1A</i> *	Hypoxia and epithelial to mesenchymal transition	Costa et al., 2017
miR-3195	PC-3 cells (Prostate Cancer)	Not shown	<i>HIF1A</i> <i>EPAS1</i>	Angiogenesis	Sohn et al., 2015

Although miRNAs regulating HIFs and their associated genes have been identified across various cancers, as shown in **Table 1.7**, research specifically addressing LIMD1 and VHL, two key TSGs that regulate HIF-1 α under normoxic conditions, remains limited. To date, only one study has reported miR-550-5p-mediated regulation of LIMD1, exclusively in lung adenocarcinoma [Guo et al., 2020]. In contrast, multiple studies have documented miRNA-mediated regulation of VHL in various cancers [Kong et al., 2014; Zang et al., 2019; Liu et al.,

2019; Xiao et al., 2016; Liu et al., 2014; Zou et al., 2020; Liu et al., 2016]. However, only one study has linked miR-21-5p to VHL regulation in CaCx development [Cai et al., 2018]. Despite these insights, comprehensive investigations into miRNA-mediated knockdown of LIMD1 and VHL, as well as their synergistic role in modulating the LIMD1-VHL-HIF-1 α stress response pathway and its downstream effects in CaCx progression, remain scarce.

CHAPTER 2

Scope of the study

Chapter 2

Scope of the study

In 2022, global cancer-related death reached an estimate of nearly 10 million, making cancer one of the leading causes of mortality [Bray et al., 2024]. This number is projected to rise further, with a significant increase anticipated in Low- and Middle-Income Countries (LMICs), like India, facing the greatest obstacle in managing cancer burden [Bray et al., 2024]. Cervical Cancer (CaCx) is the fourth most common cancer globally, however, in India, it is the second most prevalent cancer, despite notable advancements in the screening and treatment procedures [Bray et al., 2024]. Epidemiological and functional studies have identified high-risk Human Papillomavirus (HR-HPV) infection, particularly HPV16 and HPV18, along with genetic/epigenetic factors transform the normal cervical epithelium to cancer, through preneoplastic (Cervical Intraepithelial Neoplasia I/II/III (CIN I/II/III)) stages (**Figure 2.1A**) [de Freitas et al., 2012, Doorbar et al., 2006]. World Health Organization (WHO) has set the mission for eradication of CaCx by 2030, that can be achieved through early detection of CIN stages and thereby prevention of CaCx [WHO, 2020; Snijders et al., 2006]. Though, WHO has set HR-HPV DNA testing as gold standard test for CaCx early detection, majority (90%) of HR-HPV+ve CIN I and a considerable fraction of CIN II/III (43%) does not progress to CaCx (**Figure 1.5**). Moreover, in low resource countries like India with large population size, the burden of HR-HPV+ve CIN II/III is huge. Despite this fact, no stable molecular triage biomarker is available with enough specificity and sensitivity for LMICs (with special attention to India) to discern the “high-risk” CIN II/III cases for prioritized treatment (and thereby sparing the “low-risk” CIN I cases from overtreatment) (Refer to **section 1.1.4.4**).

Upon infecting the basal cells, HR-HPV induces cellular stress in the transforming cervical epithelium and modulates the cellular response to hypoxia by inhibiting HIF-1 α ubiquitylation, as outlined in **Figure 2.1B & C**; **Table 1.3** [Nakamura et al., 2009; Bodily et al., 2011; Ravi et al., 2000]. Stabilized HIF-1 α , being a transcription factor, induces expression of some angiogenic factors contributing to the carcinogenesis [Ziello et al., 2007]. Hence, to identify early transformation (CIN II/III) specific triage biomarker, it is pertinent to evaluate the key

regulators of HIF-1 α . Among different regulators, LIMD1-VHL, the two tumor suppressors (TS) mediated regulations are at the leading edge (as described in **section 1.3** and **Figure 1.14**). LIMD1 enables efficient degradation of HIF-1 α by bridging an association between VHL and prolyl hydroxylase domain protein (PHD), leading to efficient ubiquitination and degradation of HIF-1 α during normoxic condition (**Figure 2.1B**) [Foxler et al., 2012]. Deregulation of LIMD1 and VHL was also reported to play a pivotal role during cervical carcinogenesis [Chakraborty et al., 2018]. Although, lower expression of LIMD1 and VHL is often associated with promoter methylation or genetic deletion in CaCx samples, a certain percentage of the samples still show lower expression of these two TSGs, without any detectable genetic deletion/ promoter methylation [Chakraborty et al., 2018]. Moreover, recent scientific evidences suggest existence of additional epigenetic regulatory mechanism for LIMD1 and VHL expression [Guo et al., 2020; Kong et al., 2014; Zang et al., 2019; Liu et al., 2019] apart from deletion and methylation, however, yet not well explored. This study postulates the role of non-coding RNA (especially, miRNA) in the deregulation of LIMD1 and VHL during cervical carcinogenesis (**Figure 2.1D**).

Therefore, this study will effectively focus on two aspects: first, to identify miRNAs associated with LIMD1-VHL-HIF-1 α stress response pathway that could serve as triage biomarker for CaCx detection at early stages (**Figure 2.1E**). Globally, several miRNA-based biomarkers were already reported in CaCx because of their easy accessibility, high sensitivity and specificity, stage-dependent expression variation, cost-effectiveness, and rapid detection [Condrat et al., 2020, Ivanov et al., 2018; Kotani et al., 2022]. There is, however, paucity of studies on miRNA triage biomarkers in the Indian population to discern CIN I (or Low-grade Squamous Intraepithelial Lesion (LSIL)) from CIN II/III (or High-grade Squamous Intraepithelial Lesion (HSIL)). As LIMD1-VHL-HIF-1 α stress response pathway is activated during HR-HPV induced cervical carcinogenesis; this pathway-associated miRNA-based triage biomarker could elementally aid in control of CaCx incidence.

On the other hand, focusing on molecular aspects, while several HIF-1 α regulatory miRNAs have been implicated in cancer development [Sawai et al., 2022; Valencia-Cervantes and Sierra-Vargas, 2024], the comprehensive regulatory mechanism of the LIMD1-VHL-HIF-1 α pathway via miRNAs and their impact on different cellular phenotypes remains inadequately studied in the context of CaCx development, as highlighted in **Figure 2.1F**.

2. OBJECTIVES:

Thus, to understand the key genetic/epigenetic mechanisms involved in altered miRNA expression and their effect on LIMD1 and VHL expression deregulation during CaCx development, in this study, we performed:

1. Analysis of the expression profiles of LIMD1, VHL and their targeting miRNA(s) along with genetic alteration mechanism of the frequently deregulated miRNA, during development of CaCx.
2. Evaluation of the candidate miRNA(s) as molecular biomarkers in cervical swabs from population-based cancer screening.
3. *In vitro* functional validation of the candidate miRNA(s) in target gene expression.

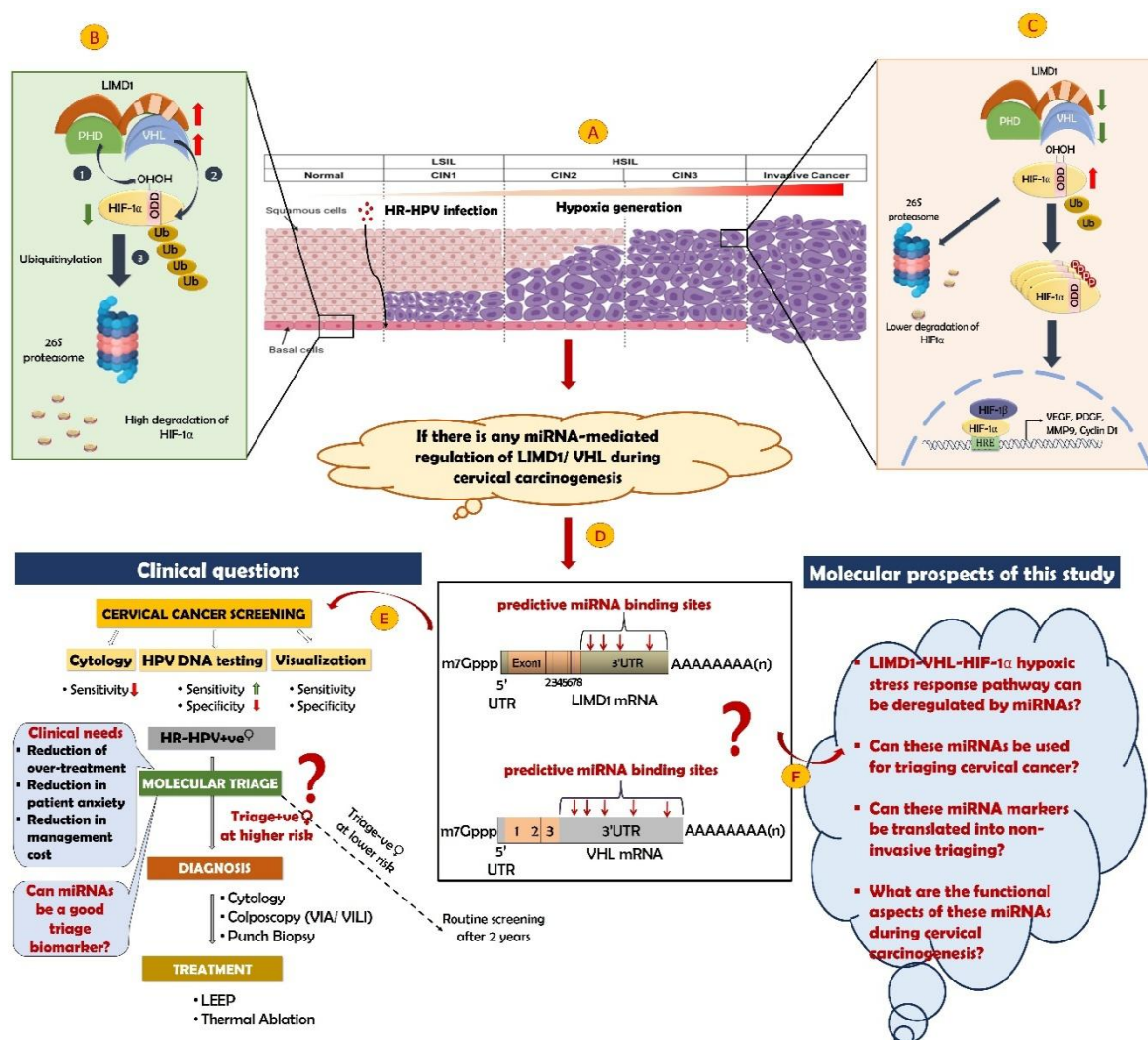


Figure 2.1 Research gap of this study: (A) Persistent HR-HPV mediated hypoxia generation and CaCx progression. (B-C) HIF-1 α regulation by LIMD1 and VHL in normal cervical epithelium (B) and in cervical cancer cells (C). (D) Prediction of miRNA mediated regulation of LIMD1/ VHL during cervical carcinogenesis. (E) Clinical question regarding the application of miRNAs associated with LIMD1-VHL-HIF-1 α stress response pathway as molecular triage biomarker for early detection of CaCx. (F) Molecular queries regarding the functional role of candidate miRNAs during HR-HPV induced cervical carcinogenesis.

CHAPTER 3

**Analysis of the expression profiles
of LIMD1, VHL and their
targeting miRNA(s) along with
genetic alteration mechanism of
the frequently deregulated
miRNA, during development of
CaCx**

Chapter 3

Analysis of the expression profiles of LIMD1, VHL and their targeting miRNA(s) along with genetic alteration mechanism of the frequently deregulated miRNA, during development of CaCx

3.1 Introduction:

Persistent high-risk HPV (HR-HPV) infection is a prerequisite for cervical cancer (CaCx) development [Doorbar et al., 2006; Wright et al., 2013; Dueñas-González et al., 2005]. HR-HPV-mediated stabilization of HIF-1 α , previously discussed in **Section 1.1.3.5** and **Table 1.3**, plays a crucial role in tumor progression [Nakamura et al., 2009; Bodily et al., 2011; Ravi et al., 2000]. As a transcription factor, HIF-1 α regulates the expression of various angiogenic factors, thereby promoting tumor growth [Ziello et al., 2007].

Under normoxic conditions, HIF-1 α is regulated by two key tumor suppressor genes (TSGs), LIMD1 and its interacting partner VHL, as discussed in **Section 1.3.1** [Foxler et al., 2012]. Alterations in these TSGs have been implicated in cervical carcinogenesis [Chakraborty et al., 2018]. While reduced expression of LIMD1 and VHL, along with promoter methylation and genetic deletions, has been observed in CaCx samples, a subset of samples exhibits low expression of these TSGs without detectable genetic (deletion) or epigenetic (promoter methylation) alterations [Chakraborty et al., 2018]. This suggests the involvement of additional regulatory mechanisms, an area that remains largely unexplored.

Beyond promoter methylation and deletion, miRNAs—small, evolutionarily conserved, non-coding RNAs—play a crucial role in post-transcriptional gene regulation, as discussed in **Section 1.2.2.2** [Huntzinger & Izaurralde, 2011; Ipsaro & Joshua-Tor, 2015]. miRNAs target numerous genes involved in signal transduction pathways [Ramírez-Moya & Santisteban, 2019], and their deregulation has been linked to cancer development and chemoresistance

[Correia de Sousa et al., 2019]. Depending on their targets, miRNAs can function as oncogenes or tumor suppressors, as described in **Section 1.2.2.3** [Wang et al., 2019].

Given this knowledge gap, we hypothesize that identifying miRNAs involved in LIMD1 and VHL deregulation could provide novel insights into the HR-HPV-induced HIF-1 α stress response pathway during cervical carcinogenesis.

3.2 Objective of the study:

Thus, our study has been focused on the following aspects:

- (a) *In silico* identification of LIMD1 and VHL targeting upregulated miRNAs during development of CaCx.
- (b) Analysis of expression status of LIMD1, VHL and their targeting miRNAs during development of CaCx.
- (c) Correlation analysis between LIMD1/ VHL and their targeting miRNAs during cervical carcinogenesis.
- (d) Analysis of molecular alteration of the candidate miRNA(s) during the development of CaCx.

3.3 Materials and Methods:

3.3.1 Chemical and reagents:

3.3.1.1 Fine chemicals (molecular biology grade) used in the study:

Formamide (Invitrogen, San Diego, CA, USA); Agarose (Lonza, Basel, Switzerland); Deoxynucleotide triphosphate (dNTPs) (Thermo Fisher Scientific, Massachusetts, United States); Diethyl pyrocarbonate (DEPC) (Sigma Aldrich, USA); TRIzol (Invitrogen, San Diego, CA, USA)/ (Ambion Inc., USA.); Power SYBR-green PCR master mix (Applied Biosystem Inc, Foster City, CA, USA) Sodium dodecyl sulphate (SDS) (Invitrogen, San Diego, CA, USA); 3,3'-Diaminobenzidine tetrachloride (DAB, sc-24982) (Santa Cruz Biotechnology, CA, USA).

3.3.1.2 Enzymes

Proteinase-K (Invitrogen, San Diego, CA, U.S.A.); DNaseI (Fermentas, USA); RNase-A (Invitrogen, San Diego, CA, USA.); Taq DNA polymerase (Promega, Wisconsin, US); Reverse Transcriptase (Promega, Wisconsin, US); RNaseOUT (Invitrogen, San Diego, USA).

3.3.1.3 Primers: List of primers used for this study have been listed in Table 3.1

Table 3.1a: Details of primers used DNA integrity checking, HPV detection, CNV and mRNA expression analysis

Gene Name	Forward Primers (5'-3')	Reverse Primer (5'-3')	Primer location	PCR conditions	Product Size (bp)
RAR β 2 (K2)	5'- AGAGTTTGATGGAG TTGGG-3'	5'- CATTCGGTTTGGG TCAATCC-3'	Exon 1	58°C/35cy	229
MY09/11	5'- GCMCAGGGWCATA AYAATGG-3'	5'- CGTCCMARRGGA WACTGATC-3'	consensus L1 region of HPV 16	54°C/35cy/2mM	445
HPV 16 typing	5'- AGGGCGTAACCGA AATCGG-3'	5'- CATATACCTCACG TCGCA-3'	HPV 16 E6 region	54°C/35cy/2mM	206
HPV 18 typing	5'- CATATACCTCACGT CGCA-3'	5'- CGGTTGCATAAAC TATGTAT-3'	HPV 18 LCR region	58°C/35cy/2mM	361
LIMD1 (RT)	5'- GTAAATTCATCGGA GGACCTG-3'	5'- CCATCCACAGTCA GCTTG-3'	3'UTR	58°C/40 cy	268
VHL (RT)	5'- TCACCTTTGGCCCT CTTCAGAGAT-3'	5'- CTGGCAGTGTGAA TATTGGCAAA-3'	Exon2	58°C/40 cy	122
β 2- microglobu lin (B2M) (RT)	5'- GTGCTCGCGCTACT CTCTCT-3'	5'- TCAATGTTCGGATG GATGAAA-3'	F.P: Exon1 R.P: Exon2	58°C/40 cy	143
miR-135b- 5p CNV primer (P1)	5'- TTCCCTATGAGATT CCTGC-3'	5'- CAAAGCCTCCTTC TGGTG-3'	pre-miR-135b flanking region	56°C/35 cy	204
miR-135b- 5p CNV (P2)	5'- CCTTTGTTACTCAG GCCCA-3'	5'- GGCTGAGCTGTAC CCAAC-3'	miR-135b promoter region	56°C/35 cy	148
β -Actin CNV	5'- TGAAGATCAAGGT GGGTGTCT-3'	5'- GTAAGTTCGCTCA GGAGGA-3'	F.P: Exon5/intron 5-6 junction R.P: Exon 6	56°C/35 cy	150

Table 3.1b: List of primers used for miRNA expression analysis:

Gene Name	Target sequences	PCR conditions
hsa-miR-135b-5p	5'UAUGGCUUUUCAUCCUAUGUGA	56°C/40cy
hsa-miR-21-5p	5'UAGCUUAUCAGACUGAUGUUGA	56°C/40cy

3.3.1.4 Antibodies

List of the antibodies have been detailed here.

a. Primary antibodies:

1. LIMD1 (sc-271448) [Santa Cruz Biotechnology, USA]
2. VHL (sc-135657) [Santa Cruz Biotechnology, USA]

b. Secondary antibody:

HRP-conjugated rabbit anti-mouse secondary Abs (sc-516102) [Santa Cruz Biotechnology, USA]

3.3.1.5 Kit:

Quick-DNATM FFPE kit (Zymo Research, USA) used for isolation of DNA from FFPE samples.

miRNeasy FFPE kit (Qiagen, Maryland, USA) used for isolation of RNA from FFPE samples.

miRCURY[®]LNA[®]RT Kit (Qiagen, Maryland, USA) used for cDNA synthesis of miRNA.

miRCURY LNA SYBR[®]Green PCR Kit (Qiagen, Maryland, USA) used for expression analysis of miRNA.

3.3.2 Collection of Clinical Samples:

For this study, a total of cervical tissue samples (Discovery phase samples; N=42) [fresh biopsy normal cervical epithelium (N=9), formalin-fixed and paraffin-embedded (FFPE) CIN I-III (N=12), and fresh primary CaCx biopsy (N=21)] along with EDTA-treated blood of corresponding patients were collected from the hospital unit of Chittaranjan National Cancer Institute (CNCI), Kolkata, India. In addition, normal cervical epithelium tissues were collected as control from patients who underwent hysterectomy due to other gynecological reasons. Fresh biopsy samples were immediately divided into three fractions for DNA isolation, RNA

isolation, and immunohistochemical (IHC) analysis. On the other hand, 12 CIN stage tissues were collected in FFPE blocks from women attending community-based cervical screening programs conducted by CNCI. Demography of the patients has been shown in **Figure 3.1** and **Table 3.2a** and **3.2b**

Ethics statement: Institutional Ethical Committee clearance (Ref No. CNCI-IEC-72120) was obtained before commencement of this study and written informed consent were obtained from each patient before sample collection.

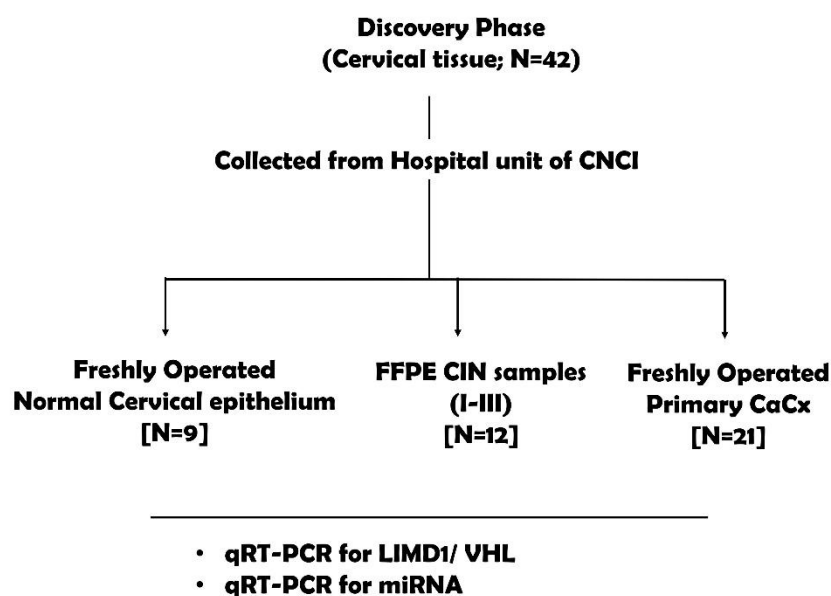


Figure 3.1 Utilization of clinical cervical tissue samples (Discovery Phase) in this study design.

Table 3.2a: Detailed patient history of dysplastic and CaCx samples:

ID	Age	Clinical Stage	Histopathological grade	HPV Status	Age at sexual debut	Parity
28771	60	CIN III	Severe dysplasia	HPV 16	17	2+1
9333	47	CIN II	Moderate dysplasia	HPV 18	16	3+0
18593	51	CIN II	Moderate dysplasia	HPV 16	15	1+1
27347	45	CIN III	Severe dysplasia	HPV 16	16	2+1
27927	55	CIN I	Mild dysplasia	HPV 16	20	2+0
405	30	CIN II	Moderate dysplasia	HPV 18	17	5+1
24897	47	CIN III	Severe dysplasia	HPV 16	21	5+0
16675	43	CIN II	Moderate dysplasia	HPV 16	17	4+2
28764	55	CIN I	Mild dysplasia	HPV 18	17	1+0
24036	32	CIN I	Mild dysplasia	HPV 18	16	3+1
22584	36	CIN I	Mild dysplasia	HPV 16	15	3+0
19635	48	CIN I	Mild dysplasia	HPV 16	16	2+1
7996	34	CaCx IB	WDSCC	HPV 16	14	3+0
7212	52	CaCx IIB	MDSCC	HPV 16	12	2+1
9086	54	CaCx IIIB	PDSCC	HPV 16	16	4+0
173	51	CaCx IIIB	WDSCC	HPV 16	15	3+1
601	48	CaCx IIB	MDSCC	HPV18	16	1+0
770	70	CaCx IIA1	MDSCC	HPV 16	16	2+1
982	45	CaCx IIB	MDSCC	HPV18	18	4+0
1086	30	CaCx IIB	MDSCC	HPV 16	17	3+1
1091	52	CaCx IIB	PDSCC	HPV 16	18	1+0
1293	79	CaCx IIIB	WDSCC	HPV 16	17	2+0
1467	49	CaCx IIB	MDSCC	HPV 16	22	4+0
4457	55	CaCx IIIB	PDSCC	HPV 16	21	1+0
4890	45	CaCx IB2	WDSCC	HPV 16	20	3+1
4897	35	CaCx IIB	MDSCC	HPV 16	17	5+1
4914	46	CaCx IVA	PDSCC	HPV18	17	4+0
5032	60	CaCx IIB	MDSCC	HPV18	15	4+4
5153	46	CaCx IIB	MDSCC	HPV 16	22	1+0
6575	47	CaCx IA1	MDSCC	HPV 16	14	3+1
5958	65	CaCx IIB	MDSCC	HPV 16	16	5+0
1884	60	CaCx IIIB	PDSCC	HPV18	20	9+1
944	62	CaCx IIB	MDSCC	HPV 16	21	5+0

Histology:

WDSCC: Well-differentiated squamous cell carcinoma

MDSCC: Moderately differentiated squamous cell carcinoma

PDSCC: Poorly differentiated squamous cell carcinoma

Table 3.2b: Summary of demography and clinicopathological features of the subjects participated in this study:

Discovery phase samples [Cervical tissue; N=42]		
Clinicopathological features		No. of subjects
Normal Cervical epithelial tissues (Control):		9
	Age range (Mean age): 38-50 yrs (45)	
	HPV status	
	HPV+ve	0
	HPV-ve	9
Dysplastic Cervical epithelial tissues (CIN I-III):		12
	Age range (Mean age): 30-60 yrs (40)	
	HPV status	
	HPV+ve	12
	HPV-ve	0
	Parity	
	<5	9
	≥5	3
	Age at sexual debut	
	Early (12-19)	10
	Late (>19)	2
Cervical Cancer tissues (CaCx):		21
	Age range (Mean age): 30-62 yrs (46)	
	HPV status	
	HPV+ve	21
	HPV-ve	0
	Tumor stage	
	Stage I/II	15
	Stage III/IV	6
	Tumor grade	
	Well differentiated:	4
	Moderate differentiated:	12
	Poor differentiated:	5
	Lymph node	
	Node+	4
	Node-	17
	Parity	
	<5	16
	≥5	5
	Age at sexual debut	
	Early (12-19)	15
	Late (>19)	6

3.3.3 *In vitro* Cell culture:

For this study, HPV16+ve Cervical Cancer cell line (SiHa) and the normal immortalized embryonic kidney epithelial cell line (HEK293T) were purchased from NCCS, Pune, India. The cell lines were grown in humidified chamber at 37°C with 5% CO₂ in Dulbecco's Modified Eagle Medium (DMEM) (Gibco, Carlsbad, CA, USA) supplemented with 10% fetal bovine serum (FBS) (Gibco, Carlsbad, CA, USA) and penicillin/streptomycin antibiotics (Gibco, Carlsbad, CA, USA) [Chen et al., 2014].

3.3.4 DNA isolation:

Normal cervical epithelium (N=9) and primary CaCx biopsy tissue (N=21) were cryo-sectioned and counterstained with Haematoxylin and Eosin. CaCx biopsy tissues with > 30% normal cell infiltration were micro-dissected to enrich tumor cells under a dissecting microscope (Leica MZ16, Germany) [Islam et al., 2020]. Normal cervical epithelium, CaCx tissues and respective peripheral blood lymphocyte (PBL) of discovery phase samples as well as cell lines (SiHa and HEK293T) were further proceeded for DNA isolation by conventional phenol–chloroform extraction method.

Briefly, microdissected tissues and PBLs were first resuspended in TNE buffer (10 mM Tris-HCl, pH 7.4; 10 mM NaCl; 10 mM EDTA). For cell lines, cells were first pelleted down. After washing with PBS, TNE buffer was added to it. Cell lysis was induced by adding SDS at a final concentration of 0.5%, followed by incubation at 65°C for 15 minutes. Subsequently, protein digestion was performed overnight at 37°C using proteinase K (100 µg/mL). Following cell lysis, DNA was extracted from the aqueous phase via phenol–chloroform extraction. Precipitation was achieved by adding 2.5 volumes of chilled ethanol supplemented with 2% potassium acetate. The resulting DNA pellet was dissolved in TE buffer (10 mM Tris-HCl, pH 7.4; 1 mM EDTA). To remove residual RNA, the DNA solution was treated with ribonuclease A (100µg/mL) at room temperature for 2 hours, followed by a second round of phenol–chloroform extraction. DNA was re-precipitated with ethanol and dissolved in TE buffer for long-term storage.

Additionally, DNA was extracted from formalin-fixed, paraffin-embedded (FFPE) tissue blocks using the Quick-DNA™ FFPE kit (Zymo Research, USA) according to the manufacturer's protocol.

DNA concentration was determined spectrophotometrically at an absorbance ratio of A260/280 and DNA integrity was verified via polymerase chain reaction (PCR) of the RAR- β 2 (K2) gene (**Table 3.1a**) [Islam et al., 2020].

3.3.5 HR-HPV detection:

HR-HPV infection in the samples was detected using PCR in a 20 μ L reaction volume, with 35 amplification cycles, using degenerate MY09/11 primers (**Table 3.1a**), designed from the consensus L1 region [Dutta et al., 2016]. The PCR products were subsequently analyzed on a 2% agarose gel for confirmation [Dutta et al., 2016]. For HR-HPV16/18 genotyping, MY09/11-positive samples were further tested using type-specific primers (**Table 3.1a**) targeting the E6 region of HPV16 and the LCR region of HPV18 [Dutta et al., 2016]. Plasmids containing HPV16 and HPV18 sequences served as positive controls for their respective HPV typing assays (**Table 3.1a**). The PCR amplicons were separated by electrophoresis on a 2% agarose gel, stained with ethidium bromide, and visualized using a UV transilluminator.

3.3.6 Copy number variation (CNV) analysis:

Previously, CGH-SNP microarray (high-resolution SurePrint G3 CGH-SNP microarray 2X400K platform, Agilent Technologies, Santa Clara, CA, USA) conducted in a set of clinically advanced CaCx samples (N=11) by Roychowdhury et al, in 2017. We retrieved the CNV data for miRNA and mRNA-encoding genes from this previously reported CGH-SNP microarray data (GSE76911) [Roychowdhury et al., 2017]. Moreover, the chromosomal alteration of LIMD1/ VHL in CaCx was further validated in putative copy number alterations data extracted from The Cancer Genome Atlas (TCGA) [(Cervical Squamous Cell Carcinoma (TCGA, PanCancer Atlas) (N=293) and Cervical Squamous Cell Carcinoma and Endocervical Adenocarcinoma (TCGA, Firehose Legacy) (N=295)] samples through cBioPortal.

Since miR-21-5p expression has already been correlated with HPV integration by Thorland et al. (2003), this study focuses on the mechanisms underlying miR-135b-5p alterations. The validation of MIR135B locus copy number alterations was analyzed by qRT-PCR on genomic DNA isolated from primary cervical tissue samples [Normal cervical epithelium (N=9); FFPE CIN I-III (N=12); CaCx (N=21)] and paired PBL. Two sets of the MIR135B locus-specific primers were designed, one set flanking the pre-miR-135b (P1) and another one from the promoter region (P2) (**Table 3.1a**) (**Figure 3.2**). For CNV analysis of MIR135B locus (1q32.1), approximately 50 ng of genomic DNA from tissue and their respective PBL was amplified in a 15 μ L reaction volume, containing 7.5 μ L of 2X Power SYBR Green master mix (Applied

Biosystems, Foster City, CA, USA) and 1µl of each specific primer. The CNV data was normalized against β -actin locus [Li et al., 2015] and relative copy number was calculated by using the following formula:

$$\text{Relative copy number} = 2^{-dCt \text{ MIR135B locus (Tissue samples)}} / 2^{-dCt \text{ MIR135B locus (Respective blood)}}$$

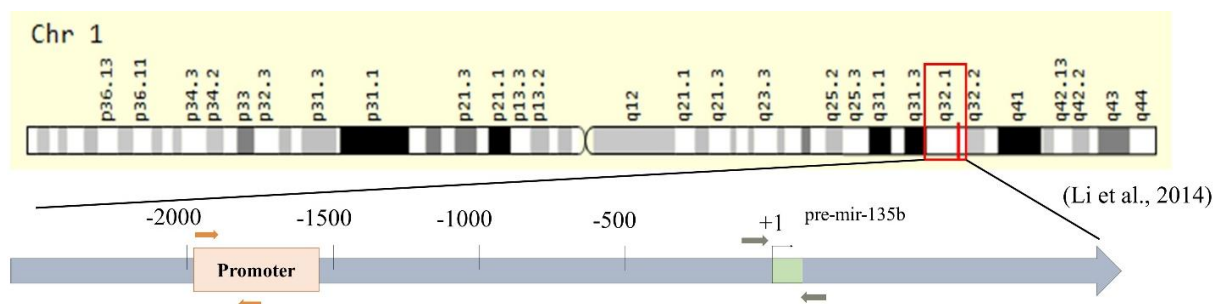


Figure 3.2 Representative image of the location of two primer sets designed for CNV analysis of MIR135B locus: P1 from the pre-miR-135b flanking region (Grey) and P2 from the promoter region (Orange).

3.3.7 Identification of candidate miRNAs through *in silico* analysis:

To identify the reported miRNA differentially expressed during cervical carcinogenesis, two databases viz. The Cancer Genome Atlas (TCGA) and Gene Expression Omnibus (GEO) databases were taken into consideration. The GEO dataset (GSE86100) comprised of HPV-ve normal cervical tissues (N=6) vs. HR-HPV+ve CaCx tissues (N=6) were considered for analysis of differentially expressed miRNAs in cervical tissue samples using GEO2R. Parallely, 308 transcriptomics data including primary tumor (N=306) and normal cervical tissue (N=2) were considered from “TCGA CESC miRNA seq datasets” and analyzed to get deregulated miRNAs in CaCx by using Subio Platform (<https://www.subioplatform.com/>). Consequently, the upregulated miRNAs in TCGA and GEO datasets were identified based on adjusted p-value < 0.05 ($-\log_{10} \text{adj p-value} < 1.301$) and differential Fold Change ≥ 2 ($\log_2 \text{Fold Change} \geq 1$) for up-regulation. In parallel, lists of conserved miRNAs targeting LIMD1 and VHL mRNA were explored using online bioinformatics tools e.g., TargetScan (targetscan.org), miRanda-miRSVR (microrna.org), and miRWalk (mirwalk.umm.uni-heidelberg.de).

3.3.8 RNA expression analysis by quantitative real-time PCR (qRT-PCR):

For this study, total RNA was extracted from 9 normal cervical epithelium samples, 21 CaCx samples, and cell lines (SiHa and HEK293T) using TRIzol Reagent (Invitrogen, USA), following the manufacturer's instructions. Briefly, tumor and normal tissues were homogenized in TRIzol solution (1 mL per 50–100 mg of tissue). For cell lines, cell pellets were thoroughly washed with 1X phosphate-buffered saline (PBS) before adding TRIzol and homogenization. The homogenized suspension was then mixed with an equal volume of chloroform and centrifuged at 12,000 rpm for 15 minutes at 4°C. The aqueous phase was carefully collected. An equal volume of isopropanol was then added to it and incubated at –20°C for one hour to promote RNA precipitation. This was followed by centrifugation at 12,000 rpm for 20 minutes at 4°C. The resulting RNA pellet was washed with 75% chilled ethanol and dissolved in 0.1% diethylpyrocarbonate (DEPC)-treated sterile water. RNA purity was assessed spectrophotometrically by measuring the A260/280 ratio, and concentration was determined from the A260 value [Chakraborty et al., 2018].

Additionally, total RNA from FFPE CIN tissue blocks was extracted using the miRNeasy FFPE kit (Qiagen, Maryland, USA).

a. mRNA expression analysis:

The expression levels of LIMD1 and VHL were assessed using quantitative real-time PCR. Initially, 5µg of total RNA was treated with DNase I to eliminate genomic DNA contamination (if any exists) in the samples and cell line RNA. Subsequently, cDNA synthesis was performed using 1µg of DNase I-treated RNA in a 20µl reaction volume, incubated at 37°C for 30 minutes. The reaction mixture contained 200ng of random hexamers, 40 units of RNase OUT, 1X reverse transcriptase buffer [50 mM Tris-HCl (pH 8.3), 75 mM KCl, 2 mM MgCl₂, 0.005 M DTT], 0.5 mM of each deoxynucleotide triphosphate (dNTP), and 200 units of reverse transcriptase (Promega, USA). The reaction was then incubated at 42°C for 90 minutes, followed by 4°C for 1 minute (Applied Biosystems, USA).

For real-time quantification of mRNA expression, approximately 2µl of synthesized cDNA was amplified in a 15µl reaction containing 7.5µl of 2X Power SYBR Green master mix (Applied Biosystems, Foster City, CA, USA) and 1µl of each specific primer. The primer details were provided in **Table 3.1a** [Chakraborty et al., 2018].

b. miRNA expression analysis:

To analyse the expression of candidate miRNAs, cDNA synthesis was performed on total RNA isolated from tissue samples and cell lines. Next, cDNA was synthesized from the total RNA (20ng) with miRCURY[®]LNA[®]RT Kit (Qiagen, Maryland, USA), followed by quantitative real-time PCR on the synthesized cDNA using miRCURY LNA SYBR[®]Green PCR Kit (Qiagen, Maryland, USA), candidate miRNA primers, and SNORD44 (GenGlobe ID: YP00203902; Qiagen, USA) as endogenous control according to the manufacturer's instruction [Elshelmani et al., 2023; Morata-Tarifa et al., 2017]. Primer lists were tabulated in **Table 3.1b**.

The comparative threshold cycle (Ct) method was used to quantify relative gene expression. The calculation was performed using the following formula [Chakraborty et al., 2018; Elshelmani et al., 2023; Morata-Tarifa et al., 2017]:

$dCt = [(Ct) \text{ target gene} - (Ct) \text{ endogenous control gene}]$, where a higher dCt value indicates lower expression of genes

3.3.9 Protein expression analysis by immunohistochemistry (IHC):

Protein expression levels of LIMD1 and VHL were assessed by IHC in FFPE tissue samples from the discovery phase. The study included normal cervical epithelium (N=9), CIN I-III (N=12), and CaCx (N=21) samples.

Briefly, 5 µm tissue sections were deparaffinized, rehydrated sequentially, and blocked with 3% bovine serum albumin (BSA) for 1 hour. The sections were then incubated overnight at 4°C with primary antibodies targeting LIMD1 (sc-271448) and VHL (sc-135657) at a dilution of 1:100. For detection, HRP-conjugated rabbit anti-mouse secondary Abs (sc-516102) were applied at a dilution of 1:500 [Chakraborty et al., 2018]. The slides were developed using 3,3'-diaminobenzidine (DAB) as the chromogen and counterstained with hematoxylin. To ensure specificity, negative control slides were prepared by substituting the primary antibody with 1X PBS, allowing verification of non-specific secondary antibody binding. Final expression evaluation followed a standardized scoring system [Perrone et al., 2006], where, a total score of 0–2 indicates low expression, 3–5 indicated intermediate expression and 6–7 indicated high expression. The scoring was independently assessed by three observers to ensure consistency and accuracy.

3.3.10 Statistical analysis:

Fisher's exact test was used to assess the statistical significance of categorical variables based on molecular features. To evaluate the significance of differences within groups of a single population, Z-scores were calculated. Data visualization, including histograms, dot plots, and box plots, was performed using GraphPad Prism 8 (GraphPad Software) or Microsoft® Excel 2019. A p-value (P) <0.05 was considered statistically significant. Additionally, Pearson's correlation coefficient was calculated using GraphPad Prism 8 to examine the association between miRNA expression and its corresponding target gene expression.

3.4 RESULT:

3.4.1 Prevalence of HPV 16/18 in samples:

The prevalence of HPV was first assessed in 9 normal cervical biopsy samples, 12 FFPE CIN samples, and 21 primary CaCx biopsy samples. All CIN (12/12, 100%) and CaCx (21/21, 100%) samples tested positive for HPV, while none of the normal cervical tissue samples (0/9) showed HPV infection. Among the 12 HPV-positive CIN samples, 66.6% (8/12) were positive for HPV16, and 33.3% (4/12) were positive for HPV18. Similarly, among the 21 HPV-positive CaCx samples, 76.1% (16/21) were positive for HPV16, whereas 23.8% (5/21) tested positive for HPV18. The distribution of HPV infection across the sample groups is depicted in **Figure 3.3D** and **Table 3.2**.

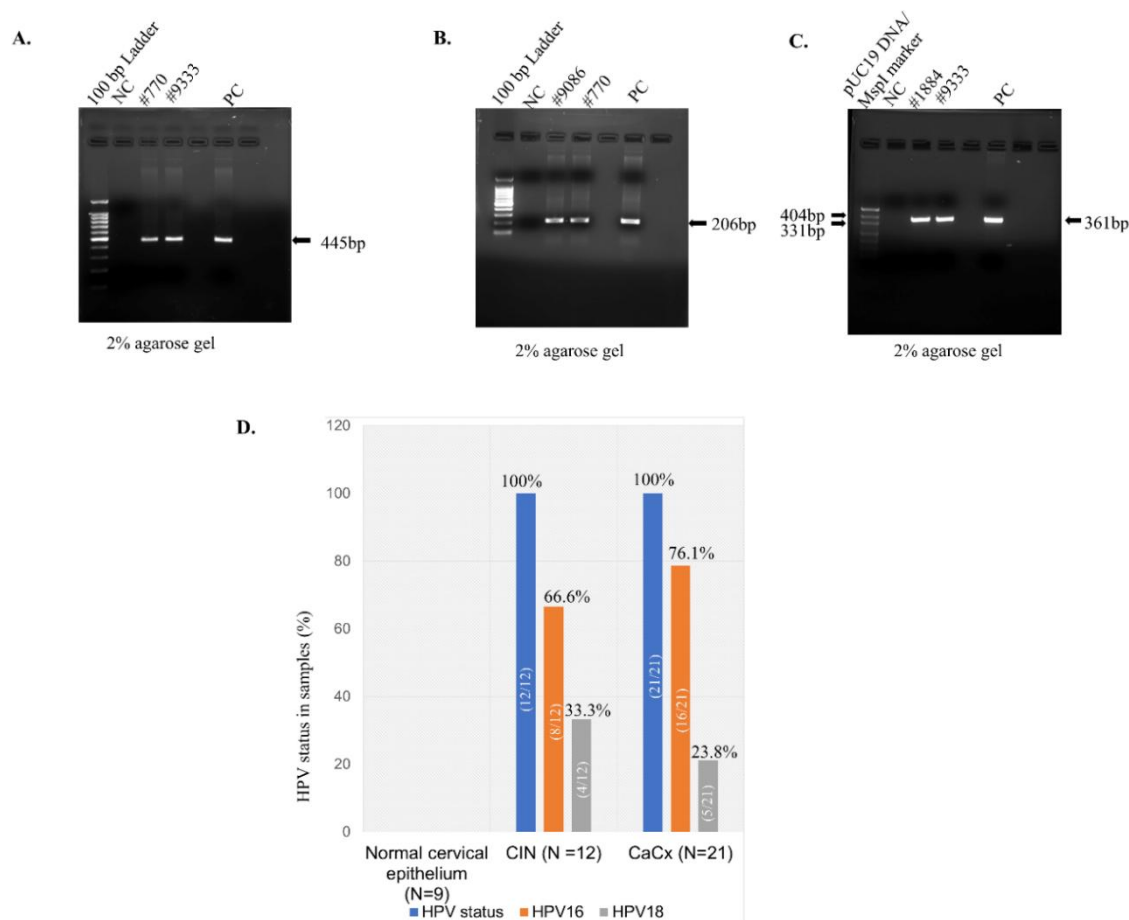


Figure 3.3 HPV detection and typing: Representative images of (A) HPV detection (B) HPV 16 typing and (C) HPV 18 typing in the discovery phases samples. (D) Bar graph representing (%) of HPV prevalence in normal cervical epithelium, CIN and CaCx tissue samples.

3.4.1 Downregulation of LIMD1 and VHL expression during cervical carcinogenesis:

At first, we analyzed the two TSGs, LIMD1 and VHL mRNA expressions in cervical tissue samples [fresh biopsy normal cervical epithelium (N=9), FFPE CIN I-III (N=12), and fresh primary CaCx biopsy (N=21)]. The result showed that the expression of LIMD1 and VHL was significantly decreased ($p=0.043$ and 0.033 , respectively) in CaCx samples (N=21) compared to normal cervical epithelium (N=9) (**Figure 3.4A and 3.4B**). The LIMD1/VHL mRNA expression status correlated with their protein expression status in the same sample sets (**Figure 3.4C**). In normal cervical epithelium, LIMD1 protein showed high/medium expression in the nucleus/cytoplasm of basal-parabasal layers of 56% (5/9) of samples, with a marginal increase in the spinous layers (67%, 6/9) (**Figure 3.4C; Table 3.3**). Conversely, in CIN, only 33% (4/12) of samples showed high/medium expression, followed by a significant decrease in invasive CaCx samples (19%, 4/21) ($p=0.045$) (**Figure 3.4C; Table 3.3**). In contrast, nuclear/cytoplasmic expression (high/medium) of VHL gradually increased from the basal-

parabasal layers (44%; 4/9) to spinous layers (78%, 7/9) of the normal cervical epithelium (Figure 3.4C; Table 3.3). Similar to LIMD1, VHL expression (high/medium) was also reduced in CIN (33%, 4/12), followed by a significant decrease in CaCx (9.5%, 2/21, $p=0.028$) samples (Figure 3.4C; Table 3.3).

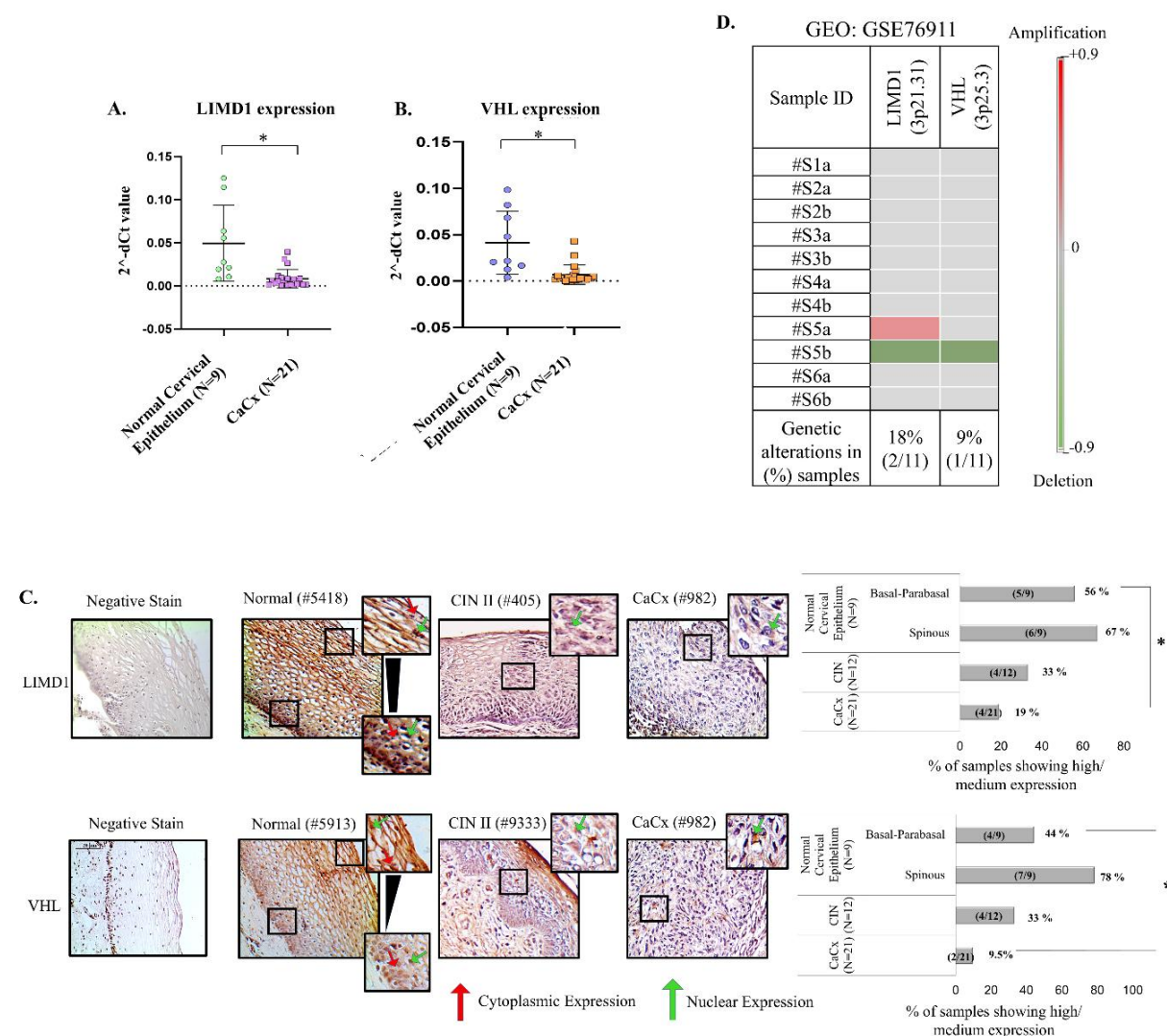


Figure 3.4 Analysis of LIMD1/VHL expression and genetic alterations of their gene locus in cervical tissue samples: Dot-plot displaying the distribution of dCt value of LIMD1 (A) and VHL (B) mRNA in normal cervical epithelium and CaCx samples, the bar line represents mean with SD. (C) Representative images of IHC of LIMD1 and VHL, with a red arrow denoting cytoplasmic staining and a green arrow denoting nuclear staining. All of the photographs have a 20x magnification; the magnification for the inset is 40x. The scale bar is 50 μ m. The histogram plot represents the percentage of samples showing cytoplasmic expression of LIMD1 and VHL. (*, **, and *** represent a significant p -value < 0.05 , < 0.01 , and < 0.001 respectively) (D) Heatmap representing (%) of the sample showing CNVs (amplification and deletion) in LIMD1/ VHL chromosomal locus from microarray data obtained from GEO accession no GSE76911.

Table 3.3: Expression pattern of LIMD1/ VHL protein in normal cervical epithelium, CIN and CaCx tissue samples (%)

Protein Name	Protein Expression	Normal (n=9)		CIN (n=12)	CaCx (n=21)
		Basal-Parabasal	Spinous		
LIMD1	High/Medium	56% (5/9)	67% (6/9)	33% (4/12)	19% (4/21)
	Low	44% (4/9)	33% (3/9)	67% (8/12)	81% (17/21)
VHL	High/Medium	44% (4/9)	78% (7/9)	33.3% (4/12)	9.5% (2/21)
	Low	56% (5/9)	22% (2/9)	66.4% (8/12)	71.5% (15/21)

To further envisage if chromosomal alteration of LIMD1 and VHL locus affects the two TSGs' expression downregulation during cervical carcinogenesis, infrequent CNVs (in 18%, 2/11; and 9%, 1/11 samples, respectively) have been observed in the CGH microarray dataset (GSE76911) (**Figure 3.4D**) that were further validated in TCGA database, where LIMD1 locus showed CNV in 0.3% (1/293) and 2% (6/293) samples in Cervical Squamous Cell Carcinoma (N=293; TCGA, PanCancer Atlas) and Cervical Squamous Cell Carcinoma and Endocervical Adenocarcinoma (N=295; TCGA, Firehose Legacy) datasets, respectively (**Figure 3.5A**). On the other hand, CNV in VHL gene locus was observed in 0.3% (1/293) and 1.4% (4/295) samples in the two TCGA datasets, respectively (**Figure 3.5B**). Hence, it indicates the plausible existence of additional (epigenetic) mechanism for the expression regulation of these two TSGs other than CNVs.

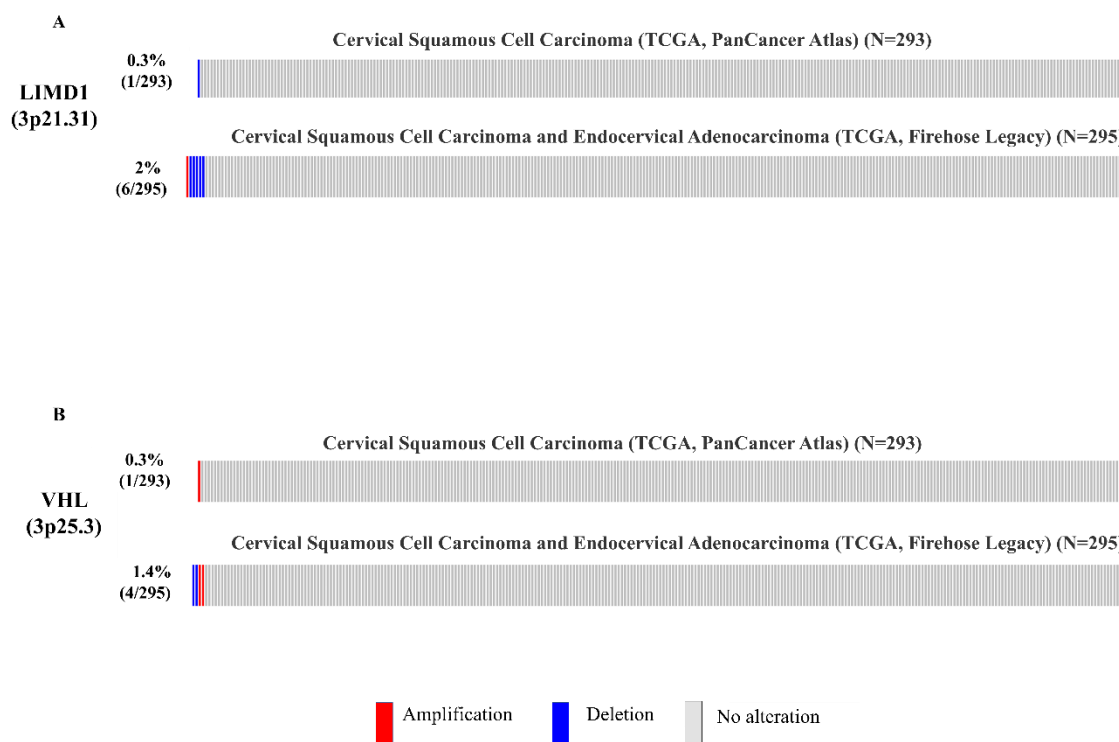


Figure 3.5 Heat map representing (%) of the sample showing CNVs (Amplification/ Deletion) of (A) *LIMD1* and (B) *VHL* chromosomal locus from TCGA data

3.4.2 Identification of *LIMD1* and *VHL* targeting miRNAs *in silico*:

To identify *LIMD1* and *VHL* targeting miRNAs, we produced a Venn diagram using TCGA and GEO databasets (GSE86100) and found 31 upregulated miRNAs in CaCx (**Figure 3.6A**). These shortlisted 31 miRNAs were subsequently examined to determine whether they were targeting either *LIMD1* or *VHL*, using a variety of bioinformatic tools. The lists of *LIMD1* and *VHL* targeting conserved miRNAs were matched with the previously identified upregulated miRNAs to find the candidate miRNAs targeting *LIMD1* and *VHL*. Two miRNAs targeting *LIMD1* were common between TargetScan and miRWalk analysis (viz. miR-224 and miR-135b-5p), while two other miRNAs (viz. miR-21-5p and miR-590-5p) targeting *VHL* were shared between TargetScan and miRanda-miRSVR (**Figure 3.6B and 3.6C**).

In CNV analysis of the 4 selected miRNAs from our CGH microarray data set (GSE76911), the *LIMD1* targeting-miR-135b-5p locus (1q32.1) showed frequent amplification (82%; 9/11). The locus for miR-224-5p (Xq28), whereas, showed amplification in 45.5% of samples (5/11), and only 1 sample (9%, 1/11) showed deletion (**Figure 3.6D**). On the other hand, *VHL* targeting- miR-21-5p (17q23.1) and miR-590-5p (7q11.23) locus showed amplification in 27% (3/11) and 18% (2/11) samples, respectively (**Figure 3.6D**).

Hence, we chose miR-135b-5p and miR-21-5p as the two most frequently amplified miRNAs targeting LIMD1 and VHL, respectively, for our further analysis.

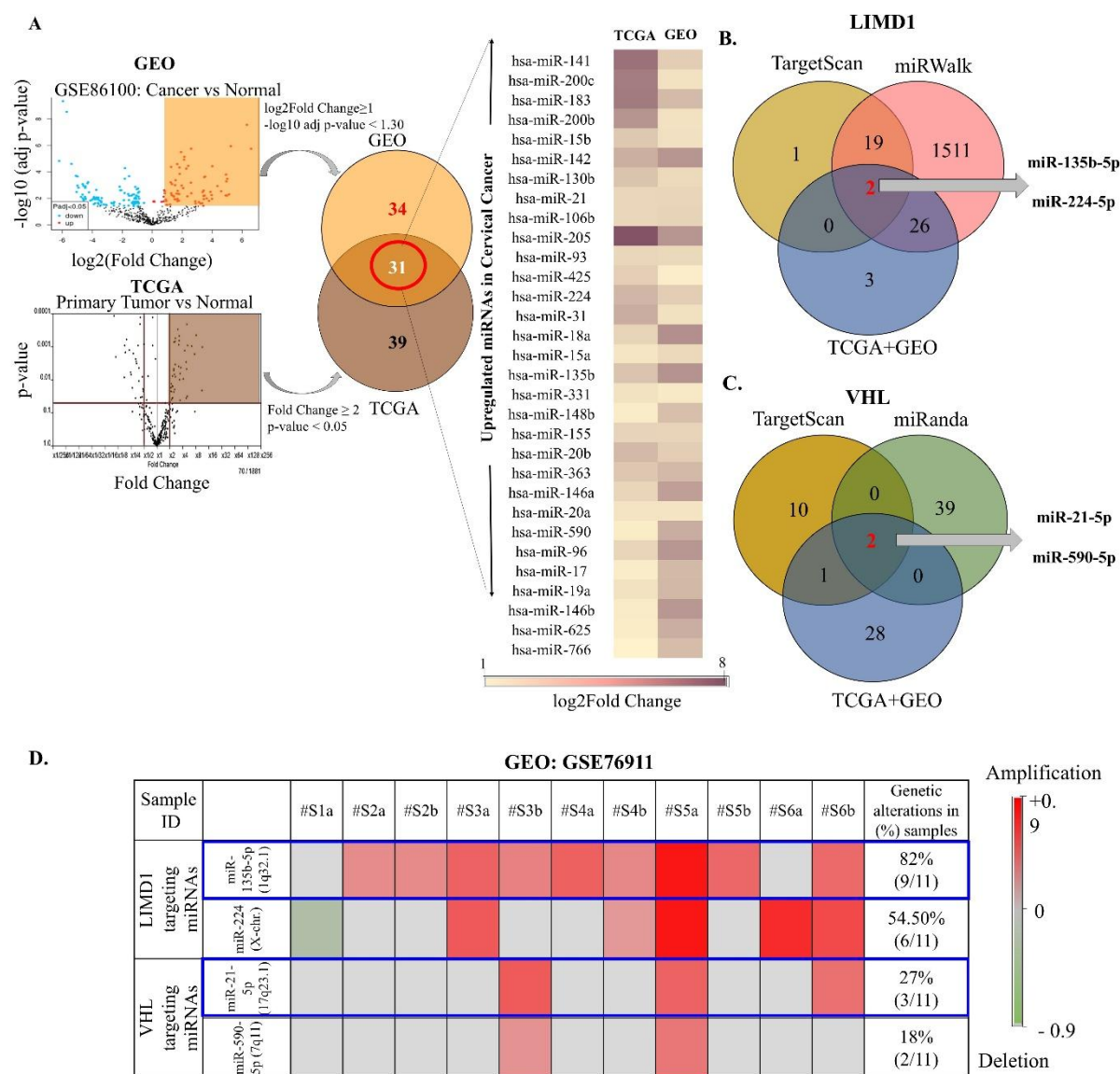


Figure 3.6 Identification of LIMD1-VHL targeting miRNAs through in silico analysis: (A) Venn diagram and heatmap showing upregulated miRNA in CaCx by using publicly available TCGA and GEO (GSE86100) datasets. (B) Venn diagram shortlisting the upregulated miRNAs targeting LIMD1 or VHL by using online bioinformatic tools. (C) Heat map representing (%) of the sample showing CNVs of LIMD1 and VHL targeting miRNAs' chromosomal locus from CGH-microarray data obtained from GEO accession no GSE76911.

3.4.3 Copy number variation (CNV) of MIR135B locus during cervical carcinogenesis:

To further validate the copy number alterations of the MIR135B locus observed in our CGH-microarray data (GSE76911), we analyzed CNV of the locus in an independent set of cervical tissue samples (N=42, Discovery phase) through two independent set of primers, P1 and P2, as described in **section 3.3.6** and **Figure 3.7A**. The data showed amplification for MIR135B locus in 66.6% (8/12) CIN samples, which further increased to 81% (17/21) in CaCx samples (**Figure 3.7B**).

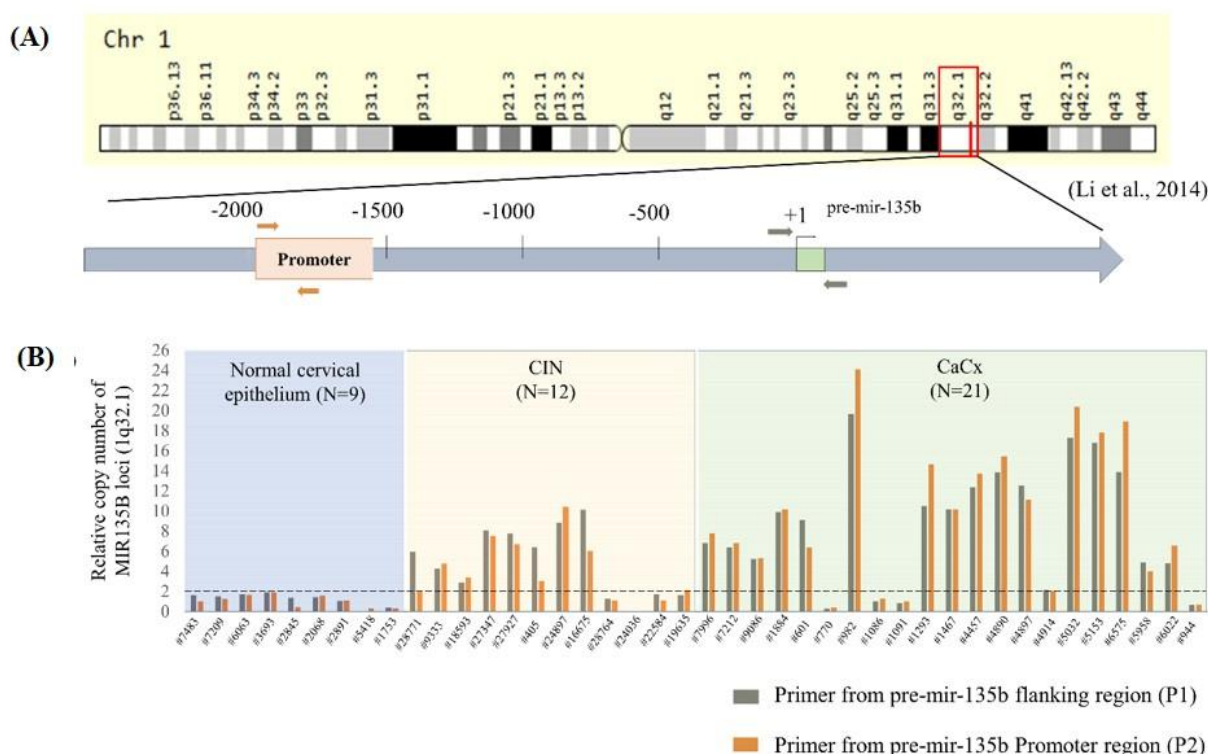


Figure 3.7 CNV of MIR135B locus during cervical carcinogenesis (A) Representative image of the location of two primer sets designed for CNV analysis of MIR135B locus: P1 from the pre-miR-135b flanking region and P2 from the promoter region. (B) Histogram representing the relative copy number of MIR135B loci, analyzed by the P1 and P2 primer sets in the normal cervical epithelium, CIN, and CaCx samples.

3.4.5 Upregulation of miR-135b-5p and miR-21-5p expression during cervical carcinogenesis:

On analysing the expression status of miR-135b-5p and miR-21-5p in the same sample sets of discovery phase (N=42), significantly higher expression of miR-135b-5p and miR-21-5p were found in CIN (p=0.048 and 0.011, respectively) and CaCx (p=0.012 and p=0.005, respectively) samples than normal cervical epithelium (**Figure 3.8A and 3.8B**).

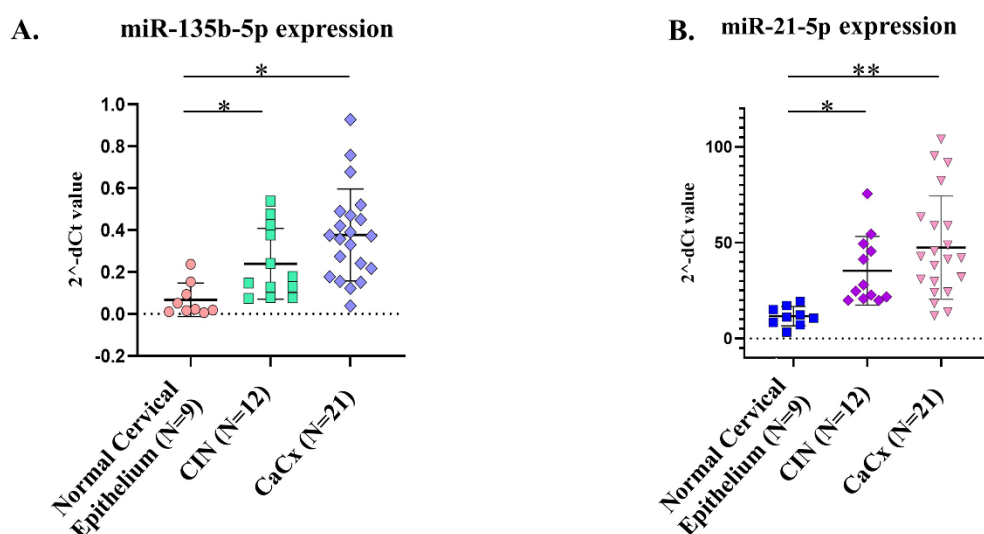


Figure 3.8 Analysis of LIMD1-VHL targeting miRNAs expression in cervical tissue samples: Dot-plot displaying the distribution of dCt values of miR-135b-5p (A) and miR-21-5p (B) in the normal cervical epithelium, CIN, and CaCx tissue samples, the bar line represents the mean with SD. Scatter plot representing Person Correlation coefficient between expression of miRNA and its target gene. (*, and ** represent a significant p-value < 0.05, and <0.01 respectively).

3.4.6 Correlation analysis between CNV of MIR135B locus and its expression during cervical carcinogenesis:

To identify correlation between miR-135b-5p expression and CNVs at its locus in the same sample sets (N=42; Discovery phase), Pearson correlation coefficient was performed. The result revealed a significant positive association (p<0.0001 and p<0.0001, respectively) between amplification of the MIR135B locus and miR-135b-5p expression (**Figure 3.9A**). Further validation in cell lines also showed significantly (p=0.0034) higher expression in SiHa compared to HEK293T cells (**Figure 3.9B**), consistent with its CNV data which indicated a significantly higher copy number (p=0.003 and p=0.027 for P1 and P2 primer sets, respectively) in SiHa cells (**Figure 3.9C**).

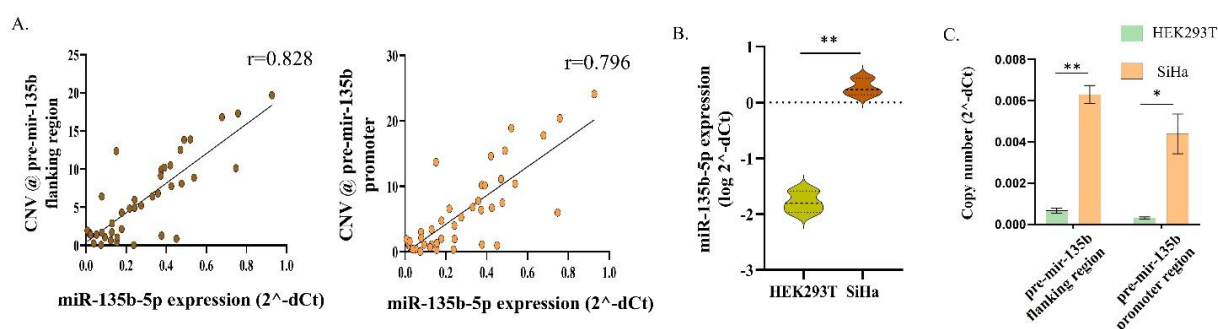


Figure 3.9 Correlation between miR-135b-5p expression upregulation and amplification at MIR135B locus in cervical tissue samples and cell lines. (A) Scatter plot representing the Pearson correlation coefficient between the CNV of miR-135b-5p locus and its expression upregulation. (B) Violin-plot displaying the distribution of $\log 2^{-\Delta\text{Ct}}$ value of miR-135b-5p by qRT-PCR in SiHa and HEK293T cell lines. (C) Histogram representing the CNV of MIR135B locus ($2^{-\Delta\text{Ct}}$), analyzed by the P1 and P2 primer sets in SiHa and HEK293T cell lines. where *, **, *** and **** represents a significant p-value < 0.05, < 0.01, < 0.001 and < 0.0001, respectively.

3.4.8 Inverse correlation between miR-135b-5p/ miR-21-5p and their target genes LIMD1/ VHL expression during cervical carcinogenesis:

Interestingly, Pearson correlation coefficient revealed a significant negative association between LIMD1 mRNA and miR-135b-5p ($p < 0.0001$) expression, as well as between VHL mRNA and miR-21-5p expression ($p < 0.0001$) (Figure 3.10A and 3.10B).

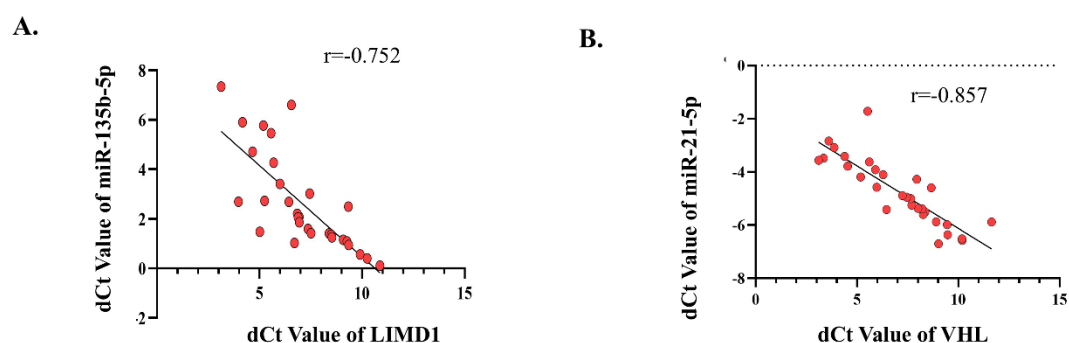


Figure 3.10 Correlation analysis between miRNAs and their respective target genes: Scatter plot representing Person Correlation coefficient between expression of miR-135b-5p and LIMD1 (A); and miR-21-5p and VHL (B). (**** represent a significant p-value < 0.0001)

3.5 Discussion:

We first analyzed the mRNA expression of LIMD1 and VHL in normal cervical epithelium and CaCx samples. Our results revealed a significant downregulation of these two TSGs in CaCx samples (**Figure 3.4A and 3.4B**). This finding was further validated at the protein level (**Figure 3.4C, Table 3.3; Figure 3.11**), consistent with a previous study by Chakraborty et al. (2018), suggesting potential post-transcriptional regulation of LIMD1 and VHL. Although genetic (deletion) and epigenetic (methylation) alterations in the LIMD1 (3p21.31) and VHL (3p25.3) loci have been previously reported in cervical carcinogenesis [Chakraborty et al., 2018], our CGH microarray data indicated infrequent CNVs in these TSGs (**Figure 3.3D**) [Roychowdhury et al., 2017]. This observation was further supported by analysis of TCGA datasets (**Figure 3.5**), suggesting that the downregulation of LIMD1 and VHL may be attributed to miRNA-mediated deregulation.

To explore this possibility, we analyzed the TCGA and GEO databases to identify upregulated miRNAs targeting LIMD1 and VHL. Among these, MIR135B and MIR21 exhibited the most frequent amplifications in their respective loci, as indicated by our CGH microarray data (**Figure 3.6**). Consequently, we selected miR-135b-5p for LIMD1 and miR-21-5p for VHL (**Figure 3.11**). Expression analysis in the same sample set demonstrated significantly elevated levels of miR-135b-5p and miR-21-5p in CIN ($p=0.036$ and $p=0.0214$, respectively) and CaCx samples ($p<0.0001$ for both) compared to normal cervical epithelium (**Figure 3.8A and 3.8B; Figure 3.11**). The upregulation of miR-21-5p was likely due to the proximity of the MIR21 locus (17q23.1) to one of the HPV16 integration sites (FRA17B), as previously reported by Thorland et al. (2003). Since this association is well established, we focused on the mechanisms driving miR-135b-5p alterations. Furthermore, Pearson correlation analysis revealed a significant negative association between LIMD1 and miR-135b-5p ($p=0.0009$), as well as between VHL and miR-21-5p ($p=0.0071$) (**Figure 3.10; Figure 3.11**). These findings strongly suggest that LIMD1 and VHL may be regulated by miR-135b-5p and miR-21-5p, respectively. Although miR-135b-5p overexpression has been reported in various cancers, including CaCx [Nair et al., 2018; Hua et al., 2016; Liu et al., 2022; Chen et al., 2020], the underlying mechanism of its upregulation in CaCx remains unexplored. Therefore, we investigated the genetic mechanisms driving miR-135b-5p upregulation across progressive stages of CaCx, as its CNVs have only been documented in hepatocellular carcinoma [Li et al., 2015]. To the best of our knowledge, this is the first study demonstrating CNV at the MIR135B locus (**Figure**

3.7; Figure 3.11) and its correlation with miR-135b-5p overexpression in both preclinical and clinical CaCx samples, potentially contributing to CaCx progression (**Figure 3.9**).

3.6 Inference points:

- i. LIMD1 and VHL targeting upregulated miRNAs, miR-135b-5p and miR-21-5p, were identified during progression of CaCx.
- ii. Amplification of MIR135B locus was found to be the principal (81%) regulatory mechanism for the upregulation of miR-135b-5p in CaCx, which is consistent with the reported CGH microarray data (GSE76911).
- iii. Amplification of the MIR135B locus was significantly associated with increased expression of miR-135b-5p, as confirmed by analyses of tissue samples and cell lines.
- iv. The mRNA (LIMD1 and VHL) expression showed an inverse correlation with their targeting miRNAs (miR-135b-5p and miR-21-5p, respectively), highlighting miRNA-mediated regulation of these two TSGs.

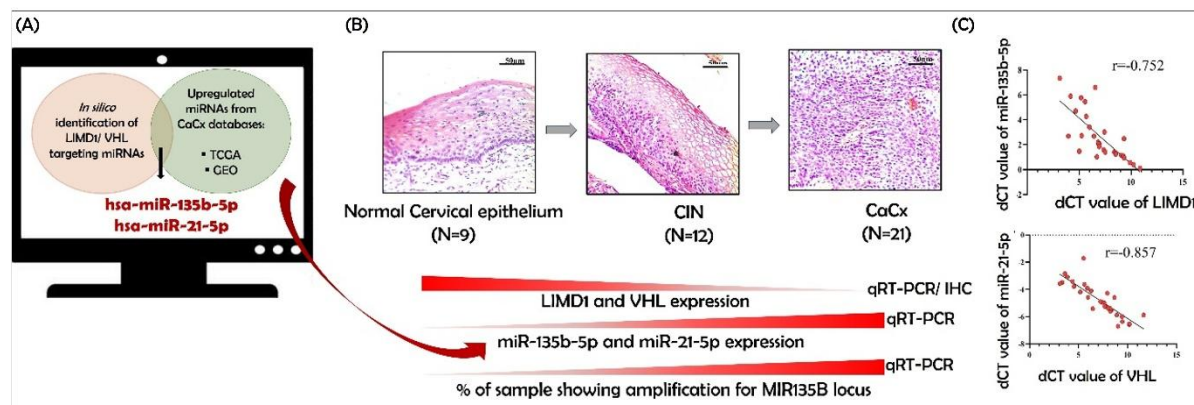


Figure 3.11 Summary of the study in discovery cohort: (A) In silico identification of LIMD1/ VHL targeting upregulated miRNAs, miR-135b-5p and miR-21-5p, in CaCx. (B) Gradual down regulation of LIMD1/VHL and upregulation of their targeting miR-135b-5p/ miR-21-5p expression as well as increasing (%) of samples showing amplification of MIR135B locus during development of CaCx. (C) Inverse correlation between LIMD1/ VHL and their respective targeting miRNAs (miR-135b-5p/ miR-21-5p) expression during the progression of CaCx.

CHAPTER 4

**Evaluation of the candidate
miRNA(s) as molecular
biomarkers in cervical swabs
from population-based cancer
screening**

Chapter 4

Evaluation of the candidate miRNA(s) as molecular biomarkers in cervical swabs from population-based cancer screening

4.1 Introduction:

In the previous chapter, we identified the HIF-1 α stress response pathway associated two miRNAs, miR-135b-5p, targeting LIMD1, and miR-21-5p, targeting VHL, both of which were upregulated during cervical cancer (CaCx) progression. These miRNAs exhibited a negative correlation with their respective target genes. Several reports highlight the oncogenic potential of miR-135b-5p and miR-21-5p, as they regulate genes involved in cancer-related pathways, thereby promoting the progression of various malignancies, including CaCx [Lu et al., 2017; Di et al., 2021; Zhang et al., 2022; Zhang et al., 2017; Tang et al., 2021; Cao et al., 2021; Luo et al., 2020]. Due to its overexpression and functional relevance, miR-21-5p has already been reported in several studies as a diagnostic biomarker for early detection of CaCx from various non-invasive sample types such as plasma, urine, and cervical scrapes [Xin et al., 2016; Aftab et al., 2021; Kawai et al., 2018; Ivanov et al., 2018]. In contrast, studies investigating miR-135b-5p as a biomarker in cervical samples remain limited.

Based on these findings, we hypothesized that if these two miRNAs exhibit similar expression patterns across different clinical stages of cervical swab samples, as observed in cervical tissue samples, they could serve as potential triage biomarkers for the early detection of clinically relevant cervical lesions, a need that remains unmet. Therefore, miRNA based molecular biomarker tests on cervical swabs could be a valuable tool for triaging HR-HPV positive cases with clinically relevant HSIL.

On the other hand, several traditional miRNA detection methods, such as northern blot, microarray chips, and qRT-PCR, are available, but each has limitations [Ye et al., 2019; Lee, 2022]. Among these, qRT-PCR is the most widely used technique for identifying miRNA biomarkers, which we have also utilized in our biomarker studies. However, it requires specialized skills and is time-consuming [Ye et al., 2019; Lee, 2022]. In response to the need

for a simplified technique that can screen larger populations in a shorter timeframe while maintaining sensitivity comparable to qRT-PCR, we also applied a sensor-oligo-based signal amplification method to facilitate miRNA detection from exfoliated cells of cervical swabs (**Figure 4.1**) in a pilot study by following Yoo et al., 2014; thereby highlighting the translational importance of this method.

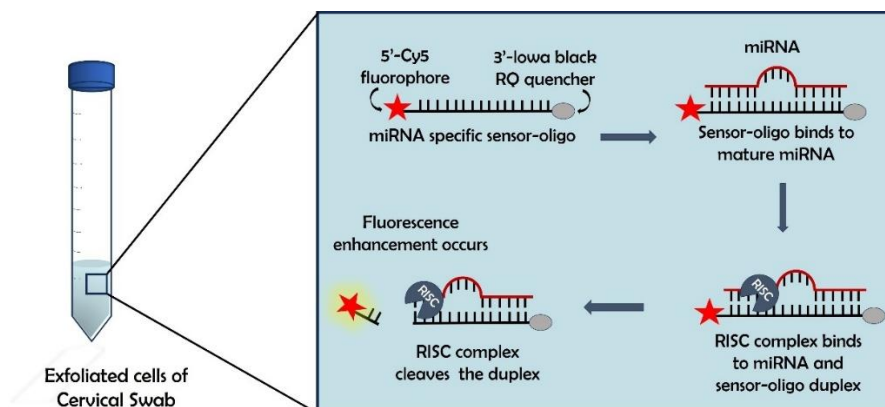


Figure 4.1 Detection of miRNA by sensor-oligo based signal amplification technique from exfoliated cells of cervical swabs

4.2 Objective of the study:

Therefore, this study undertakes the following objectives:

- i. Analysis of LIMD1-VHL targeting miRNA-based triage biomarkers to discern the women with clinically relevant HR-HPV+ve HSIL with the propensity to develop CaCx.
- ii. Detection of miR-135b-5p in intact cervical cells (cell lines), as well as, in a cell-free system (exfoliated cervical swabs and SiHa cell pellet) utilizing a novel and more sensitive sensor-oligo based signal amplification technique: a pilot study.

4.3 Materials and Methods:

4.3.1 Chemical and reagents:

4.3.1.1 Fine chemicals (molecular biology grade) used in the study:

Described in **Section 3.3.1.1**

4.3.1.2 Enzymes

Described in **Section 3.3.1.2**

4.3.1.3 Primers

List of primers used for miRNA expression analysis were tabulated in **Table 3.1b**

4.3.1.4 Antibodies

List of the antibodies have been detailed in **section 3.3.1.4**

4.3.2 Collection of Clinical Samples:

For this study, cervical swab samples were collected from population-based cervical screening camps organized by CNCI, Kolkata. Exfoliated cervical swabs were first screened for HR-HPV by Hybrid Capture 2 (HC2) test [a test that can detect 13 HR-HPV types (types 16, 18, 31, 33, 35, 39, 45, 51, 52, 56, 58, 59, and 68) based on semi-quantitative detection of viral DNA] [Basu et al., 2016]. HC2-ve samples were used as controls (N=54). Participants who tested positive for HC2 were further recalled for cervical examination and treatment at CNCI, during which HC2-positive samples were collected, categorized as follows: HR-HPV+ve asymptomatic (N=52), HR-HPV+ve LSIL (N=50), HR-HPV+ve HSIL (N=52), and HR-HPV+ve CaCx (N=35).

Institutional Ethical Committee clearance and written informed consent were obtained from each participant. The demographic details of the patients are presented in **Figure 4.2; Table 4.1a and 4.1b.**

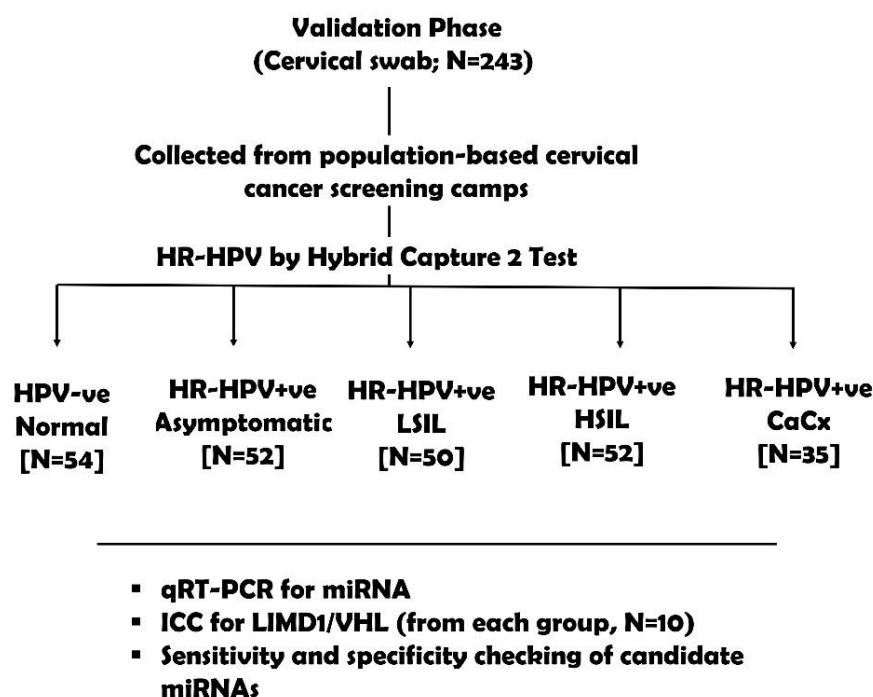


Figure 4.2 Utilization of clinical cervical swab samples (Validation phase) in this study design.

Table 4.1a: Detailed history of the subjects participated in this study:

ID	Age	Sample type	Stage	HPV Status	Age at sexual debut	Parity
18593	33	Normal	Not applicable	-ve	16	2+0
18768	48	Normal	Not applicable	-ve	17	2+1
18787	43	Normal	Not applicable	-ve	18	3+0
28487	50	Normal	Not applicable	-ve	18	4+0
28944	35	Normal	Not applicable	-ve	13	2+1
29272	44	Normal	Not applicable	-ve	17	3+1
29273	40	Normal	Not applicable	-ve	18	2+1
29274	49	Normal	Not applicable	-ve	12	3+0
29275	44	Normal	Not applicable	-ve	18	4+0
29276	40	Normal	Not applicable	-ve	20	3+1
29277	39	Normal	Not applicable	-ve	15	3+1
29278	40	Normal	Not applicable	-ve	24	2+2
29279	55	Normal	Not applicable	-ve	18	5+1
29280	33	Normal	Not applicable	-ve	20	4+1
29281	40	Normal	Not applicable	-ve	17	3+1
29282	35	Normal	Not applicable	-ve	16	2+2
29283	33	Normal	Not applicable	-ve	16	2+1
29284	30	Normal	Not applicable	-ve	15	3+1
29285	35	Normal	Not applicable	-ve	20	5+0
29286	43	Normal	Not applicable	-ve	18	2+1
29287	30	Normal	Not applicable	-ve	20	2+1
29288	35	Normal	Not applicable	-ve	18	3+1
29289	32	Normal	Not applicable	-ve	26	2+0
29290	38	Normal	Not applicable	-ve	17	3+0
29291	30	Normal	Not applicable	-ve	16	3+1
29292	49	Normal	Not applicable	-ve	19	1+2
29293	45	Normal	Not applicable	-ve	17	3+0
29294	32	Normal	Not applicable	-ve	18	4+0
29295	56	Normal	Not applicable	-ve	17	6+0
29296	56	Normal	Not applicable	-ve	20	6+1
29297	53	Normal	Not applicable	-ve	20	3+0
29298	35	Normal	Not applicable	-ve	16	3+1
29299	42	Normal	Not applicable	-ve	18	4+0
29300	32	Normal	Not applicable	-ve	26	2+1
29301	34	Normal	Not applicable	-ve	22	2+0
29302	35	Normal	Not applicable	-ve	18	3+0
29303	42	Normal	Not applicable	-ve	20	3+1
29304	44	Normal	Not applicable	-ve	15	2+0
29305	49	Normal	Not applicable	-ve	12	3+0
29306	55	Normal	Not applicable	-ve	25	3+0
29307	50	Normal	Not applicable	-ve	13	3+1

29308	44	Normal	Not applicable	-ve	18	4+1
29309	46	Normal	Not applicable	-ve	25	4+0
29310	37	Normal	Not applicable	-ve	19	2+1
5546	47	Normal	Not applicable	-ve	20	3+0
33434	45	Normal	Not applicable	-ve	22	2+1
17384	32	Normal	Not applicable	-ve	16	4+0
16995	34	Normal	Not applicable	-ve	16	3+1
17082	35	Normal	Not applicable	-ve	13	3+0
16812	35	Normal	Not applicable	-ve	18	2+2
16849	54	Normal	Not applicable	-ve	20	4+0
11221	53	Normal	Not applicable	-ve	19	2+1
16223	40	Normal	Not applicable	-ve	20	3+1
18865	56	Normal	Not applicable	-ve	23	5+0
3551	45	Asymptomatic	Not applicable	HR-HPV+ve	18	4+0
3650	46	Asymptomatic	Not applicable	HR-HPV+ve	17	3+1
3652	44	Asymptomatic	Not applicable	HR-HPV+ve	18	3+1
3653	54	Asymptomatic	Not applicable	HR-HPV+ve	18	4+0
18090	30	Asymptomatic	Not applicable	HR-HPV+ve	19	1+1
25064	37	Asymptomatic	Not applicable	HR-HPV+ve	22	1+2
25170	35	Asymptomatic	Not applicable	HR-HPV+ve	20	2+0
25222	30	Asymptomatic	Not applicable	HR-HPV+ve	21	1+2
25226	45	Asymptomatic	Not applicable	HR-HPV+ve	19	2+2
25233	33	Asymptomatic	Not applicable	HR-HPV+ve	18	2+1
25255	35	Asymptomatic	Not applicable	HR-HPV+ve	20	2+0
27334	31	Asymptomatic	Not applicable	HR-HPV+ve	21	2+0
27874	45	Asymptomatic	Not applicable	HR-HPV+ve	17	4+1
27885	38	Asymptomatic	Not applicable	HR-HPV+ve	17	3+0
27932	35	Asymptomatic	Not applicable	HR-HPV+ve	15	2+1
27966	55	Asymptomatic	Not applicable	HR-HPV+ve	19	4+1
27969	53	Asymptomatic	Not applicable	HR-HPV+ve	22	4+0
28002	57	Asymptomatic	Not applicable	HR-HPV+ve	21	3+1
28264	35	Asymptomatic	Not applicable	HR-HPV+ve	19	2+1
28271	35	Asymptomatic	Not applicable	HR-HPV+ve	18	3+0
28293	60	Asymptomatic	Not applicable	HR-HPV+ve	18	6+1
28334	30	Asymptomatic	Not applicable	HR-HPV+ve	17	2+0
28496	32	Asymptomatic	Not applicable	HR-HPV+ve	17	2+1
28498	38	Asymptomatic	Not applicable	HR-HPV+ve	19	2+2
18081	33	Asymptomatic	Not applicable	HR-HPV+ve	18	2+2
28768	54	Asymptomatic	Not applicable	HR-HPV+ve	18	4+1
28772	53	Asymptomatic	Not applicable	HR-HPV+ve	15	3+0
28907	41	Asymptomatic	Not applicable	HR-HPV+ve	20	2+1
29783	59	Asymptomatic	Not applicable	HR-HPV+ve	16	5+1
29807	32	Asymptomatic	Not applicable	HR-HPV+ve	22	2+0
30480	44	Asymptomatic	Not applicable	HR-HPV+ve	22	3+1
30743	35	Asymptomatic	Not applicable	HR-HPV+ve	20	2
32655	37	Asymptomatic	Not applicable	HR-HPV+ve	21	2

30957	34	Asymptomatic	Not applicable	HR-HPV+ve	19	2
31157	46	Asymptomatic	Not applicable	HR-HPV+ve	20	3+0
31261	34	Asymptomatic	Not applicable	HR-HPV+ve	19	2+1
31282	37	Asymptomatic	Not applicable	HR-HPV+ve	19	2+1
31684	44	Asymptomatic	Not applicable	HR-HPV+ve	17	3+0
31699	34	Asymptomatic	Not applicable	HR-HPV+ve	20	2+1
31764	36	Asymptomatic	Not applicable	HR-HPV+ve	19	2+2
31770	58	Asymptomatic	Not applicable	HR-HPV+ve	20	5+0
31860	46	Asymptomatic	Not applicable	HR-HPV+ve	19	4+0
32053	55	Asymptomatic	Not applicable	HR-HPV+ve	16	4+2
32055	31	Asymptomatic	Not applicable	HR-HPV+ve	21	2+1
32180	58	Asymptomatic	Not applicable	HR-HPV+ve	16	6+0
32221	58	Asymptomatic	Not applicable	HR-HPV+ve	17	3+0
32359	45	Asymptomatic	Not applicable	HR-HPV+ve	18	3+1
32402	48	Asymptomatic	Not applicable	HR-HPV+ve	17	3+0
33611	41	Asymptomatic	Not applicable	HR-HPV+ve	19	3+1
33625	56	Asymptomatic	Not applicable	HR-HPV+ve	14	4+1
33639	40	Asymptomatic	Not applicable	HR-HPV+ve	17	2+0
33419	35	Asymptomatic	Not applicable	HR-HPV+ve	20	2+1
187	45	LSIL	Not applicable	HR-HPV+ve	17	3+1
2920	40	LSIL	Not applicable	HR-HPV+ve	18	2+0
3098	30	LSIL	Not applicable	HR-HPV+ve	17	2+1
3988	48	LSIL	Not applicable	HR-HPV+ve	19	3+1
4077	46	LSIL	Not applicable	HR-HPV+ve	18	2+1
4969	58	LSIL	Not applicable	HR-HPV+ve	18	5+0
18217	35	LSIL	Not applicable	HR-HPV+ve	22	2+2
19635	48	LSIL	Not applicable	HR-HPV+ve	20	3+0
20200	48	LSIL	Not applicable	HR-HPV+ve	19	2+1
21001	30	LSIL	Not applicable	HR-HPV+ve	15	1+2
22140	30	LSIL	Not applicable	HR-HPV+ve	18	2+0
22557	30	LSIL	Not applicable	HR-HPV+ve	19	1+1
22584	36	LSIL	Not applicable	HR-HPV+ve	18	2+0
22823	30	LSIL	Not applicable	HR-HPV+ve	19	1+1
22885	31	LSIL	Not applicable	HR-HPV+ve	17	1+1
23095	57	LSIL	Not applicable	HR-HPV+ve	15	3+0
23855	33	LSIL	Not applicable	HR-HPV+ve	20	2+1
24036	32	LSIL	Not applicable	HR-HPV+ve	19	2+0
24455	35	LSIL	Not applicable	HR-HPV+ve	19	2+1
25123	52	LSIL	Not applicable	HR-HPV+ve	17	4+0
25852	40	LSIL	Not applicable	HR-HPV+ve	20	2+1
27927	55	LSIL	Not applicable	HR-HPV+ve	14	3+1
28683	41	LSIL	Not applicable	HR-HPV+ve	18	2+0
28764	55	LSIL	Not applicable	HR-HPV+ve	16	4+1
28766	46	LSIL	Not applicable	HR-HPV+ve	20	3+0
29208	45	LSIL	Not applicable	HR-HPV+ve	16	2+2
29414	48	LSIL	Not applicable	HR-HPV+ve	22	3+1

29812	45	LSIL	Not applicable	HR-HPV+ve	17	2+0
30033	44	LSIL	Not applicable	HR-HPV+ve	19	3+0
31308	40	LSIL	Not applicable	HR-HPV+ve	19	2+1
31664	43	LSIL	Not applicable	HR-HPV+ve	20	2+1
31860	46	LSIL	Not applicable	HR-HPV+ve	17	3+1
32924	58	LSIL	Not applicable	HR-HPV+ve	17	5+1
34153	36	LSIL	Not applicable	HR-HPV+ve	19	2+0
35785	45	LSIL	Not applicable	HR-HPV+ve	18	2+0
385	30	LSIL	Not applicable	HR-HPV+ve	18	1+1
26827	41	LSIL	Not applicable	HR-HPV+ve	19	2+0
13922	46	LSIL	Not applicable	HR-HPV+ve	17	2+0
11702	37	LSIL	Not applicable	HR-HPV+ve	18	2+1
18645	30	LSIL	Not applicable	HR-HPV+ve	18	1+0
945	45	LSIL	Not applicable	HR-HPV+ve	18	2+1
33456	49	LSIL	Not applicable	HR-HPV+ve	18	3+0
30967	38	LSIL	Not applicable	HR-HPV+ve	18	1+1
28684	53	LSIL	Not applicable	HR-HPV+ve	17	4+0
28734	55	LSIL	Not applicable	HR-HPV+ve	14	5+1
29207	60	LSIL	Not applicable	HR-HPV+ve	16	5+0
3556	55	LSIL	Not applicable	HR-HPV+ve	17	4+1
35786	42	LSIL	Not applicable	HR-HPV+ve	15	3+0
34310	47	LSIL	Not applicable	HR-HPV+ve	20	2+1
34308	30	LSIL	Not applicable	HR-HPV+ve	18	3+1
28775	47	HSIL	Not applicable	HR-HPV+ve	20	3+1
31724	38	HSIL	Not applicable	HR-HPV+ve	19	2+0
27347	45	HSIL	Not applicable	HR-HPV+ve	17	3+2
28767	49	HSIL	Not applicable	HR-HPV+ve	21	3+0
33955	34	HSIL	Not applicable	HR-HPV+ve	18	2+1
36313	46	HSIL	Not applicable	HR-HPV+ve	16	2+1
33349	46	HSIL	Not applicable	HR-HPV+ve	19	3+1
32528	46	HSIL	Not applicable	HR-HPV+ve	19	3+0
31722	38	HSIL	Not applicable	HR-HPV+ve	20	2+2
22869	30	HSIL	Not applicable	HR-HPV+ve	18	1+2
23299	31	HSIL	Not applicable	HR-HPV+ve	17	1+1
21015	45	HSIL	Not applicable	HR-HPV+ve	16	3+0
21821	35	HSIL	Not applicable	HR-HPV+ve	14	4+0
25600	41	HSIL	Not applicable	HR-HPV+ve	22	2+1
25637	49	HSIL	Not applicable	HR-HPV+ve	17	2+0
24634	37	HSIL	Not applicable	HR-HPV+ve	20	2+2
27343	45	HSIL	Not applicable	HR-HPV+ve	19	3+1
32245	50	HSIL	Not applicable	HR-HPV+ve	18	4+1
18648	30	HSIL	Not applicable	HR-HPV+ve	18	1+2
28771	61	HSIL	Not applicable	HR-HPV+ve	19	5+0
18786	43	HSIL	Not applicable	HR-HPV+ve	17	4+0
25138	46	HSIL	Not applicable	HR-HPV+ve	17	3+1
24289	42	HSIL	Not applicable	HR-HPV+ve	19	3+1

21610	32	HSIL	Not applicable	HR-HPV+ve	20	2+0
18594	51	HSIL	Not applicable	HR-HPV+ve	21	3+2
4949	60	HSIL	Not applicable	HR-HPV+ve	18	2+1
4862	45	HSIL	Not applicable	HR-HPV+ve	18	3+0
5229	45	HSIL	Not applicable	HR-HPV+ve	16	2+1
3801	52	HSIL	Not applicable	HR-HPV+ve	19	5+0
22313	60	HSIL	Not applicable	HR-HPV+ve	17	5+1
36320	44	HSIL	Not applicable	HR-HPV+ve	18	3+2
32530	45	HSIL	Not applicable	HR-HPV+ve	17	4+0
4321	49	HSIL	Not applicable	HR-HPV+ve	19	3+1
26642	49	HSIL	Not applicable	HR-HPV+ve	16	4+0
31859	40	HSIL	Not applicable	HR-HPV+ve	17	3+0
2391	60	HSIL	Not applicable	HR-HPV+ve	21	1+0
2350	74	HSIL	Not applicable	HR-HPV+ve	20	2+0
18756	46	HSIL	Not applicable	HR-HPV+ve	17	1+2
28774	55	HSIL	Not applicable	HR-HPV+ve	18	4+1
19786	60	HSIL	Not applicable	HR-HPV+ve	18	5+0
22877	44	HSIL	Not applicable	HR-HPV+ve	16	4+0
23289	47	HSIL	Not applicable	HR-HPV+ve	19	4+0
21115	49	HSIL	Not applicable	HR-HPV+ve	17	5+1
21901	49	HSIL	Not applicable	HR-HPV+ve	18	4+0
25654	42	HSIL	Not applicable	HR-HPV+ve	17	3+0
25638	60	HSIL	Not applicable	HR-HPV+ve	20	4+1
24644	72	HSIL	Not applicable	HR-HPV+ve	17	5+0
22403	39	HSIL	Not applicable	HR-HPV+ve	18	2+1
35311	46	HSIL	Not applicable	HR-HPV+ve	18	3+1
22345	54	HSIL	Not applicable	HR-HPV+ve	19	3+0
22389	50	HSIL	Not applicable	HR-HPV+ve	17	3+1
24649	48	HSIL	Not applicable	HR-HPV+ve	18	2+2
7212	52	CaCx	CaCx IIB	HR-HPV+ve	19	2+1
7996	34	CaCx	CaCx IB1	HR-HPV+ve	19	3+0
6575	47	CaCx	CaCx IA1	HR-HPV+ve	17	3+1
982	45	CaCx	CaCx IIB	HR-HPV+ve	20	2+1
173	51	CaCx	CaCx IIIB	HR-HPV+ve	19	3+1
5032	60	CaCx	CaCx IIB	HR-HPV+ve	16	4+4
7621	56	CaCx	CaCx III	HR-HPV+ve	19	3+0
1498	45	CaCx	CaCx IIB	HR-HPV+ve	19	2+0
9086	54	CaCx	CaCx IIIB	HR-HPV+ve	20	4+0
601	48	CaCx	CaCx IIB	HR-HPV+ve	18	1+0
770	70	CaCx	CaCx IIA1	HR-HPV+ve	17	2+1
5958	65	CaCx	CaCx IIB	HR-HPV+ve	16	9+1
4738	58	CaCx	CaCx IIB	HR-HPV+ve	15	1+2
1086	30	CaCx	CaCx IIB	HR-HPV+ve	12	3+1
1293	79	CaCx	CaCx IIIB	HR-HPV+ve	25	2+2
4897	35	CaCx	CaCx IIB	HR-HPV+ve	13	5+1
4914	46	CaCx	CaCx IVA	HR-HPV+ve	18	4+0

3548	45	CaCx	CaCx IIB	HR-HPV+ve	25	0
5676	60	CaCx	CaCx IIB	HR-HPV+ve	18	5+0
4801	37	CaCx	CaCx IIB	HR-HPV+ve	18	3+1
1061	72	CaCx	CaCx IIB	HR-HPV+ve	17	4+0
1091	52	CaCx	CaCx IIB	HR-HPV+ve	19	1+1
2868	63	CaCx	CaCx IIB	HR-HPV+ve	16	2+0
5449	65	CaCx	CaCx IIIB	HR-HPV+ve	17	2+1
3557	69	CaCx	CaCx IIB	HR-HPV+ve	19	3+2
4346	64	CaCx	CaCx IIB	HR-HPV+ve	20	2+1
4890	45	CaCx	CaCx IB2	HR-HPV+ve	18	3+1
6022	60	CaCx	CaCx IIIB	HR-HPV+ve	17	5+0
3056	37	CaCx	CaCx IIIB	HR-HPV+ve	14	3+2
611	60	CaCx	CaCX IIB	HR-HPV+ve	16	3+2
4457	55	CaCx	CaCx IIIB	HR-HPV+ve	17	1+0
944	62	CaCx	CaCx IIB	HR-HPV+ve	21	5+0
5406	56	CaCx	CaCxIIIB	HR-HPV+ve	18	3+0
1467	49	CaCx	CaCx IIB	HR-HPV+ve	19	4+0
5153	46	CaCx	CaCx IIB	HR-HPV+ve	22	1+1

Table 4.1b: Summary of the demography and clinicopathological features of the subjects participated in this study:

Validation phase samples [Cervical tissue; N=243]		
Clinicopathological features		No. of subjects
HC2 -ve samples:		
HR-HPV-ve normal		54
Age range (Mean age):	30-56 yrs (40)	
Parity		
	<5	48
	≥5	6
Age at sexual debut		
	Early (12-19)	36
	Late (>19)	18
HC2 +ve samples:		
HR-HPV+ve asymptomatic		52
Age range (Mean age):	30-60 yrs (41)	
Parity		
	<5	43
	≥5	9
Age at sexual debut		
	Early (12-19)	34
	Late (>19)	18

HR-HPV+ve LSIL		50
	Age range (Mean age): 30-60 yrs (40)	
	Parity	
	<5	44
	≥5	6
	Age at sexual debut	
	Early (12-19)	41
	Late (>19)	9
HR-HPV+ve HSIL		52
	Age range (Mean age): 30-74 yrs (46)	
	Parity	
	<5	46
	≥5	6
	Age at sexual debut	
	Early (12-19)	44
	Late (>19)	8
HR-HPV+ve CaCx:		35
	Age range (Mean age): 37-79 yrs (52)	
	Tumor stage	
	Stage I/II	23
	Stage III/IV	12
	Tumor grade	
	Well differentiated:	8
	Moderate differentiated:	18
	Poor differentiated:	9
	Lymph node	
	Node+	4
	Node-	31
	Parity	
	<5	27
	≥5	8
	Age at sexual debut	
	Early (12-19)	25
	Late (>19)	10

4.3.3 Cell culture:

Cell cultures were described in **section 3.3.3**

4.3.4 miRNA expression analysis by quantitative real-time PCR (qRT-PCR):

Samples of exfoliated cervical swabs of different clinical stages and other clinical specimen were first collected in 1x PBS. After pelleting down the cells at 2000 rpm, total RNA was isolated by TriZol reagent (Invitrogen, USA), as described in **section 3.3.8**. Total RNA from FFPE CIN tissue blocks was extracted using the miRNeasy FFPE kit (Qiagen, Maryland, USA). To analyse the expression of candidate miRNAs, cDNA synthesis was performed on total RNA (20ng), as described in **section 3.3.8b**. Primer lists were tabulated in **Table 3.1b**.

4.3.5 Protein expression analysis by immunocytochemistry (ICC) in exfoliated cells of cervical swabs:

For this study, samples of exfoliated cervical swabs were extracted from the validation phase [HPV-ve normal (N=10), HR-HPV+ve asymptomatic (N=10), HR-HPV+ve LSIL (N=10), and HR-HPV+ve HSIL (N=10)]. Briefly, exfoliated cervical swabs were first collected in 1× PBS, followed by centrifugation at 2000 rpm to pellet the cells. The cell pellets were resuspended in the remaining 1× PBS and spread onto albumin-coated slides. The cells were then fixed in methanol at −20°C for 30 minutes. Subsequently, endogenous peroxidase activity was quenched using 0.5% H₂O₂ in 1× PBS. Following quenching, the cells were blocked with 3% BSA in 1× PBS for 1 hour and incubated overnight at 4°C with specific primary antibodies (previously mentioned in **section 3.3.1.4**) at a 1:100 dilution. After washing with 1×PBS, the slides were incubated with FITC-conjugated specific secondary antibodies for 2 hours in the dark at 4°C. Finally, the cells were counterstained with 1 µg/mL DAPI, a fluorescent nuclear staining dye. The slides were then visualized under a fluorescence microscope (Olympus, Model: U-LH100HG). For negative control staining, the same procedure was performed without the addition of any primary antibody [Roy et al., 2019] and the fluorescence intensity of the nucleus and cytoplasm was measured by Image-J software.

4.3.6 Candidate miR-135b-5p specific novel sensor oligonucleotide development:

The sensor oligo was designed against miR-135b-5p (5'-Cy5/rCrArCrArArArUrUrCrGrGrUrUrCrUrArCrArGrGrUrA/IAbRQSp-3'), composed of RNA bases (fully complementary to mature miR-135b-5p) with Cy5 (fluorescent dye) at the 5' and Iowa Black RQ (quencher) at the 3' end, modified after Yoo et al., 2014 (**Figure 4.3**) [Yoo et al., 2014]. Additionally, anti-miR-135b-5p (Qiagen, Gene Globe ID: YI04101769) and scrambled RNA (Qiagen; GeneGlobe ID - YI00199006) were also used to check the specificity of sensor-oligo.

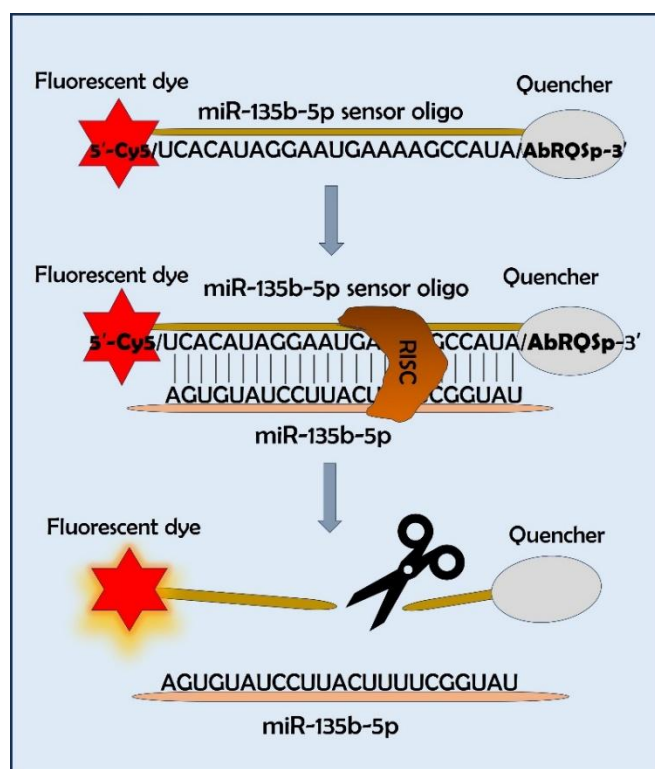


Figure 4.3 Designing strategy of the sensor-oligo for detection of miR-135b-5p using signal amplification technique

4.3.7 Detection of miR-135b-5p by novel sensor oligo in SiHa and HEK293T cell lines:

SiHa and HEK293T cells were cultured on chambered slides at a density of 30,000 cells per well in 0.5 mL of DMEM supplemented with 10% FBS and incubated at 37°C. After 24 hours, the growth medium was discarded and replaced with 0.5 mL of antibiotic-free, serum-free medium. The cells were then transfected with sensor-oligo against miRNA-135b-5p (100 nM) using Lipofectamine 3000 (Invitrogen, California, USA) in accordance with the manufacturer's protocol. Following a 4-hour transfection period, the transfection medium was removed, and complete growth medium was added. After an additional 24-hour incubation, fluorescence was examined in the Cy5 channel using a fluorescence microscope (Olympus, Model: U-LH100HG) and analyzed with ImageJ software (**Figure 4.4**) [Yoo et al., 2014].

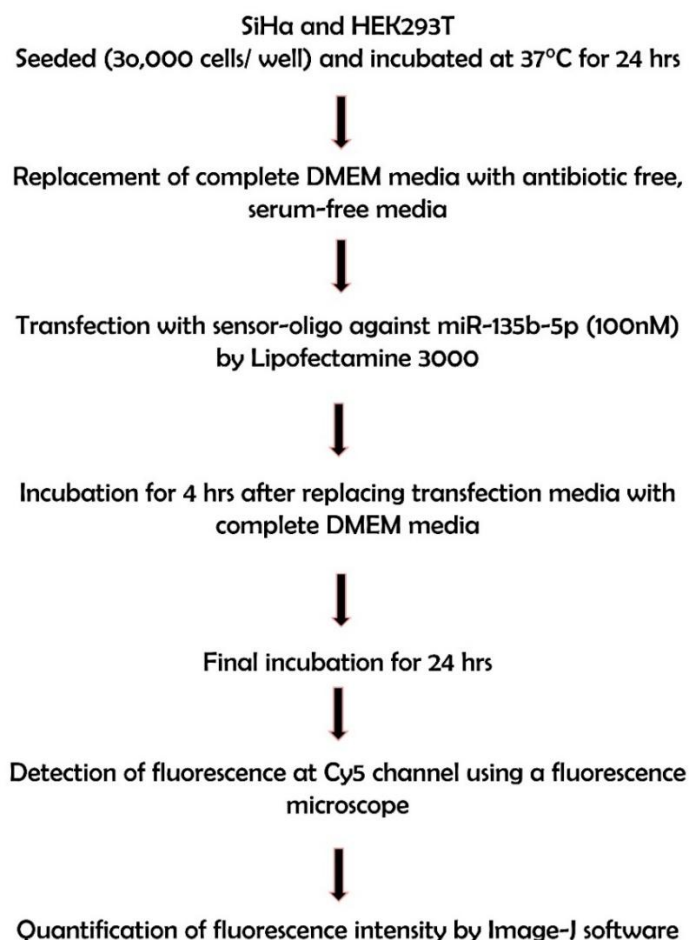


Figure 4.4 Flowchart for direct detection of miR-135b-5p by novel sensor-oligo in intact cells (in cell lines)

4.3.8 Detection of miR-135b-5p by novel sensor-oligo in SiHa and exfoliated cells of cervical swabs:

For detection of miR-135b-5p by novel sensor-oligo in a cell-free system, SiHa cells (culture conditions in DMEM described in **Section 3.3.3**) were pretreated with either scrambled RNA (Qiagen; GeneGlobe ID: YI00199006) or anti-miR-135b-5p (Qiagen; GeneGlobe ID: YI04101769). Pretreated SiHa cells and exfoliated cells of cervical swabs of different clinical stages [HR-HPV+ve asymptomatic (N=10); HR-HPV+ve HSIL (N=12); and HR-HPV+ve CaCx (N=11)] were first placed in ice-cold 1x PBS. After two washes with PBS, the cells were pelleted and lysed by adding four packed cell volumes of lysis buffer, followed by incubation on ice for 10 minutes. To separate the nuclear fraction, the lysates were centrifuged at $760 \times g$ for 10 minutes at 4°C. The resulting supernatant was transferred to a fresh Eppendorf tube and mixed with cold buffer B (0.11 volume). Cytoplasmic extracts were then aliquoted and stored

at -80°C for further analysis. Protein concentration was determined using the Bradford assay [Roy et al., 2019].

To assess the specificity of the sensor-oligo, different concentrations of sensor-oligo (10, 25, 50, and 100 nM) were incubated with cell extracts. The reaction mixture was incubated at 37°C for 2 hours in buffers C and D (composition tabulated in **Table 4.2**), with a final reaction volume of 25 μL containing 40% cell extract (80 μg). To terminate the cleavage reactions, eight volumes (200 μL) of Proteinase K buffer were added, and the mixture was incubated at 37°C for 15 minutes. Fluorescence intensity was subsequently measured using a SpectraMax® i3x device at an excitation wavelength of 649 nm and an emission wavelength of 670 nm (**Figure 4.4**) [Yoo et al., 2014]. The compositions of all buffers used are listed in **Table 4.2**.

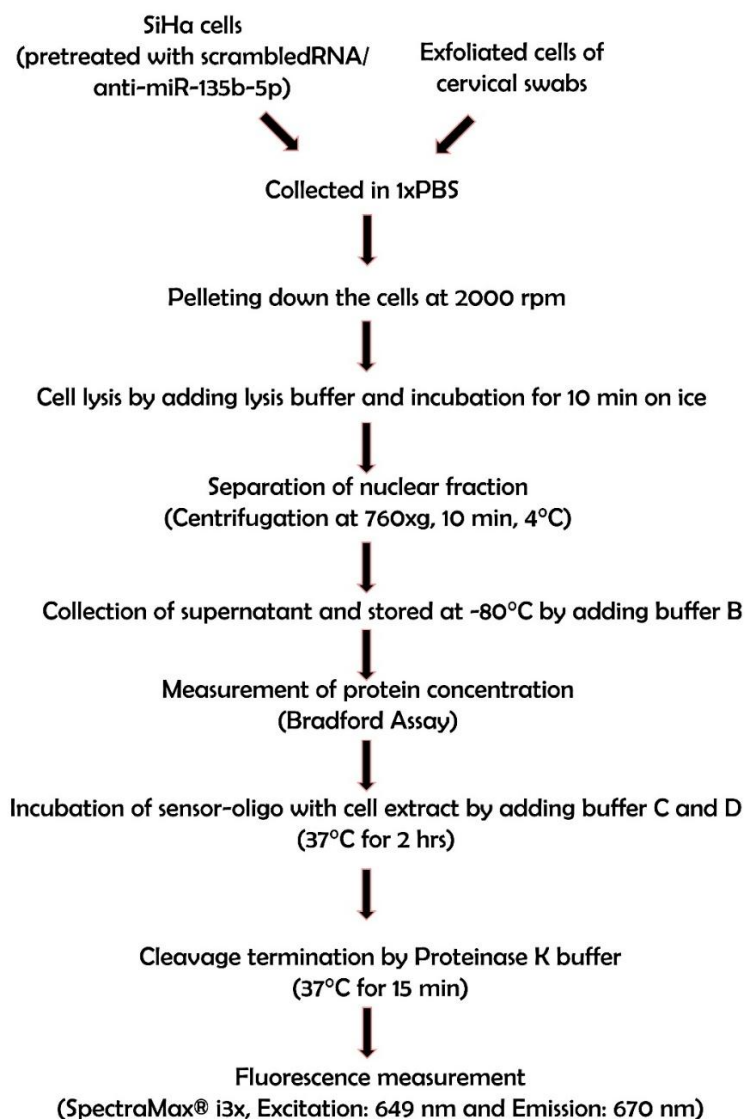


Figure 4.4 Detection of miR-135b-5p by novel sensor-oligo in SiHa cell pellet and exfoliated cells of cervical swabs

Table 4.2: Compositions of all buffers used for detection of miR-135b-5p using sensor-oligo in SiHa and exfoliated cells of cervical swabs:

Used Buffer	Composition	Working Concentration
Cell lysis Buffer	NaCl	10 mM
	MgCl ₂	1 mM
	Sucrose	0.5 M
	EDTA	0.2 mM
	DTT	0.5 mM
	PMSF	0.5 mM
	Triton X-100	0.35% (v/v)
Buffer B	HEPES (pH:7.9)	20 mM
	NaCl	10 mM
	MgCl ₂	1 mM
	Sucrose	0.35 M
	EDTA	0.2 mM
	DTT	0.5 mM
	PMSF	0.5 mM
Buffer C	ATP	1 mM
	GTP	0.2 mM
	Rnasin	1U/ μ l
	Creatine Kinase	30 μ g/ml
	Creatine Phosphate	25 mM
	MgCl ₂	2 mM
	NaCl	20 mM
Buffer D	KCl	100 mM
	HEPES	20 mM
	Glycerol	2% (v/v)
	EDTA	0.2 mM
Proteinase K Buffer	Tris-HCL (pH:7.5)	200 mM
	EDTA	25 mM
	NaCl	300 mM
	SDS	2% (w/v)
	Proteinase K	0.6 mg/ml

4.4 RESULT:

4.4.1 miR-135b-5p/miR-21-5p upregulation and their target genes LIMD1/VHL downregulation in cervical swabs with progressive lesions

To extrapolate our findings (described in **section 3.4**) from cervical tissue samples to non-invasive cervical swab samples, we performed expression analysis of the two candidate miRNAs, miR-135b-5p and miR-21-5p along with their target genes in samples collected from CaCx screening camps.

Gradual upregulation of miR-135b-5p and miR-21-5p was observed during disease progression. Interestingly, significant upregulation of miR-135b-5p ($p=0.002$, $p=0.0096$, and $p=0.006$) and miR-21-5p ($p=0.035$, $p=0.041$, and $p=0.016$) was observed in HSIL samples (N=52) than in HPV-ve normal (N=54)/ HR-HPV+ve asymptomatic (N=52)/ HR-HPV+ve LSIL samples (N=50), respectively (**Figure 4.5A and 4.5B**).

To correlate the effect of miR-135b-5p/miR-21-5p on LIMD1/VHL expression, ICC for LIMD1 and VHL proteins was performed in 20% of samples of each cervical swab type from the validation phase. The nuclear and cytoplasmic expression of LIMD1 was significantly downregulated ($p=0.004$ and $p=0.004$, respectively) in HR-HPV+ve HSIL samples (N=10) compared to earlier stages samples (**Figure 4.5C and 4.5E**). On the other hand, a significant down-expression of VHL was also observed in the nucleus ($p<0.0001$ and $p=0.004$, respectively) and cytoplasm ($p=0.005$ and $p=0.005$, respectively) in HR-HPV+ve HSIL samples (N=10) compared to HPV-ve normal (N=10) and HR-HPV+ve asymptomatic samples (N=10) (**Figure 4.5D and 4.5F**). Furthermore, the nuclear expression of VHL was also significantly decreased ($p=0.003$) in HR-HPV+ve HSIL samples (N=10) compared to HR-HPV+ve LSIL (N=10) (**Figure 4.5D and 4.5F**). Therefore, a similar inverse correlation between miRNAs and their targets was detected in non-invasive cervical swab samples.

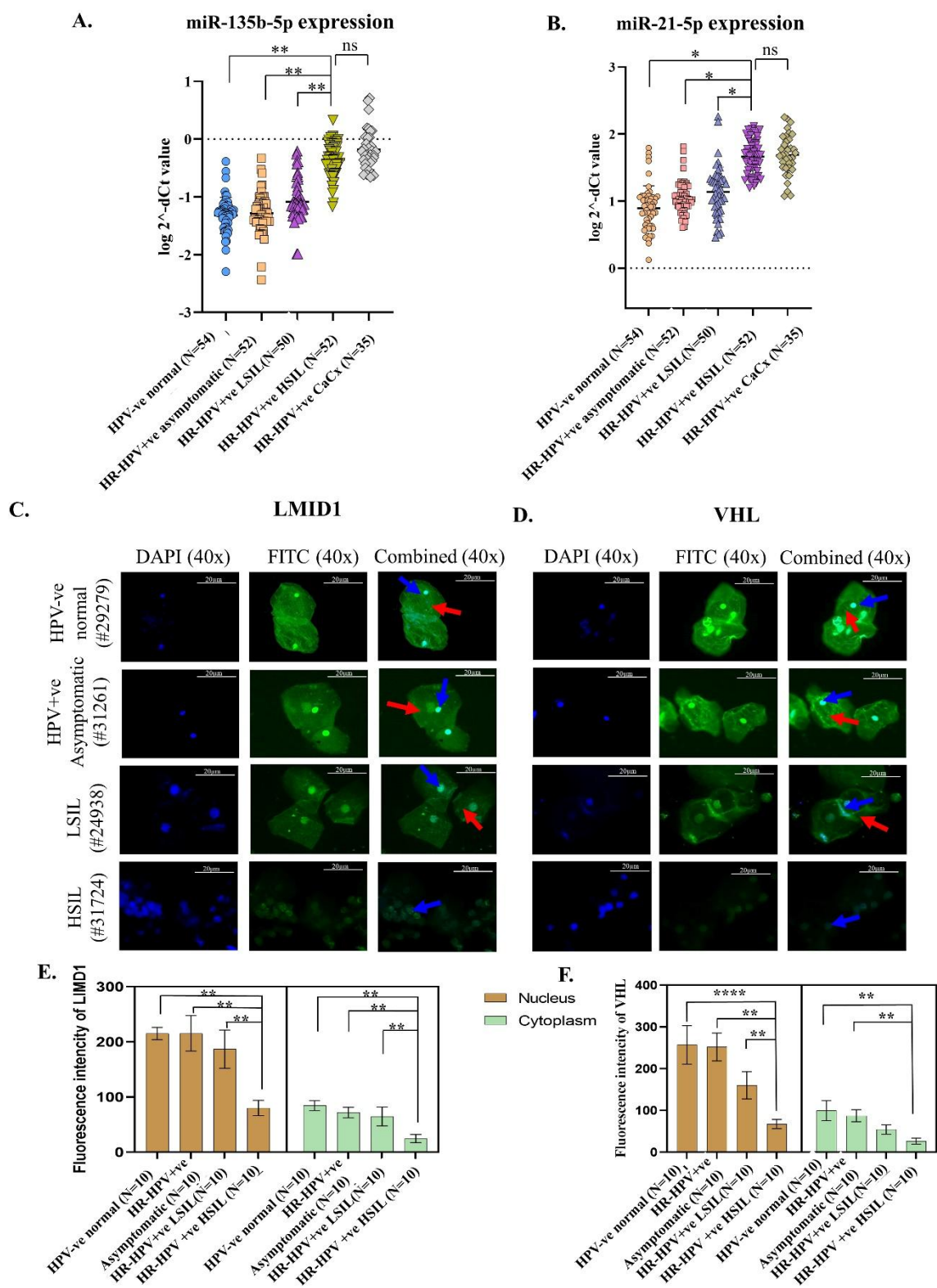


Figure 4.5 Expression validation of miR-135b-5p/ miR-21-5p and their target genes LIMD1/ VHL in cervical swab samples: Dot-plot represents the distribution of $\log 2^{-dCt}$ value of (A) miR-135b-5p and (B) miR-21-5p in HPV-ve normal, HR-HPV+ve asymptomatic, HR-HPV+ve LSIL, HR-HPV+ve HSIL, and HR-HPV+ve CaCx swab samples, the horizontal line represents mean with SD, where, *, and ** indicate a significant p-value <0.05 , and <0.01 respectively and 'ns' represents non-significant. Representative images of immunocytochemical analysis of (C) LIMD1 and (D) VHL in HR-HPV+ve asymptomatic, HR-HPV+ve LSIL, and HR-HPV+ve HSIL swab samples in 40x magnification, where, the scale bar is 20 μ m with red arrow denoting cytoplasmic staining and a blue arrow denoting nuclear staining DAPI: 4', 6-diamidino-2-phenylindole. The histogram represents the quantification of nuclear and cytoplasmic staining intensity of (E) LIMD1 and (F) VHL by Image J (**, and **** represent a significant p-value <0.01 , and <0.0001 , respectively).

4.4.2 Effective diagnosis of HR-HPV+ve HSIL from earlier clinical stages by miR-135b-5p and miR-21-5p:

To identify the diagnostic usefulness of miR-135b-5p and miR-21-5p, ROC curves were evaluated to differentiate HR-HPV+ve HSIL patients (N=52) from those with earlier clinical stages. Heat maps were generated to represent the ability of miR-135b-5p and miR-21-5p for distinguishing different clinical stages by analyzing their concordance and discordance with histopathological reports in a sample-wise manner, based on the ROC curve cut-off value (**Figure 4.6A, 4.6D, and 4.6G**). To distinguish HR-HPV+ve HSIL patients (N=52) from HPV-ve normal (N=54), miR-135b-5p has a sensitivity of 92.6% and a specificity of 96.2% with an AUC of 0.979 (95% confidence interval (CI): 0.958-1). In contrast, miR-21-5p had a higher sensitivity (96.3%) but lower specificity (94.2%) than miR-135b-5p, with an AUC of 0.985 (95% confidence interval (CI): 0.968-1) (**Figure 4.6B; Table 4.3**). To distinguish HR-HPV+ve HSIL patients (N=52) from HR-HPV+ve asymptomatic (N=52), miR-135b-5p revealed 90.4% sensitivity and 94.2% specificity, with an AUC of 0.969 (95% confidence interval (CI): 0.940-0.988), whereas, miR-21-5p demonstrated higher sensitivity (94.2%) and lower specificity (92.3%) than miR-135b-5p, with an AUC of 0.977 (95% CI: 0.956-0.999) (**Figure 4.6E; Table 4.3**). Furthermore, miR-135b-5p and miR-21-5p were also able to distinguish HR-HPV+ve HSIL (N=52) patients from HR-HPV+ve LSIL (N=50) with good sensitivity (86% and 86%, respectively) and specificity (88.5% and 78.8%, respectively), with AUCs of 0.925 and 0.898, respectively (95% confidence interval (CI): 0.874-0.976 and 0.837-0.960, respectively) (**Figure 4.6H; Table 4.3**). More interestingly, when the two miRNAs were used in combination, they showed better AUC values of 0.995 (95% CI: 0.986-1), 0.996 (95% CI): 0.989-1, and 0.969 (95% CI): 0.942-0.996) to distinguish HR-HPV+ve HSIL from HPV-ve normal, HR-HPV+ve asymptomatic, and HR-HPV+ve LSIL, respectively, because of the better

sensitivity of miR-21-5p and better specificity of miR-135b-5p (**Figure 4.6C, 4.6F, and 4.6I; Table 4.3**).

The diagnostic value of miR-21-5p alone was also investigated to distinguish HR-HPV+ve asymptomatic (N=52) from HPV-ve normal (N=54); however, the value (sensitivity of 68.5% and specificity of 65.4% with an AUC of 0.677 (95% CI: 0.57-0.77) was insufficient to distinguish the two types of samples (**Figure 4.7A and 4.7B; Table 4.4**). Moreover, the diagnostic accuracy of miR-135b-5p, miR-21-5p, and their combination was analyzed to differentiate HR-HPV+ve CaCx (N=35) from HR-HPV+ve HSIL (N=52); however, the results did not show any significant differences between these two groups (**Figure 4.7C-4.7E; Table 4.4**). Hence, it can be concluded that the expression of miR-135b-5p, miR-21-5p, and their combination has better diagnostic value for distinguishing HR-HPV+ve HSIL from earlier clinical stages.

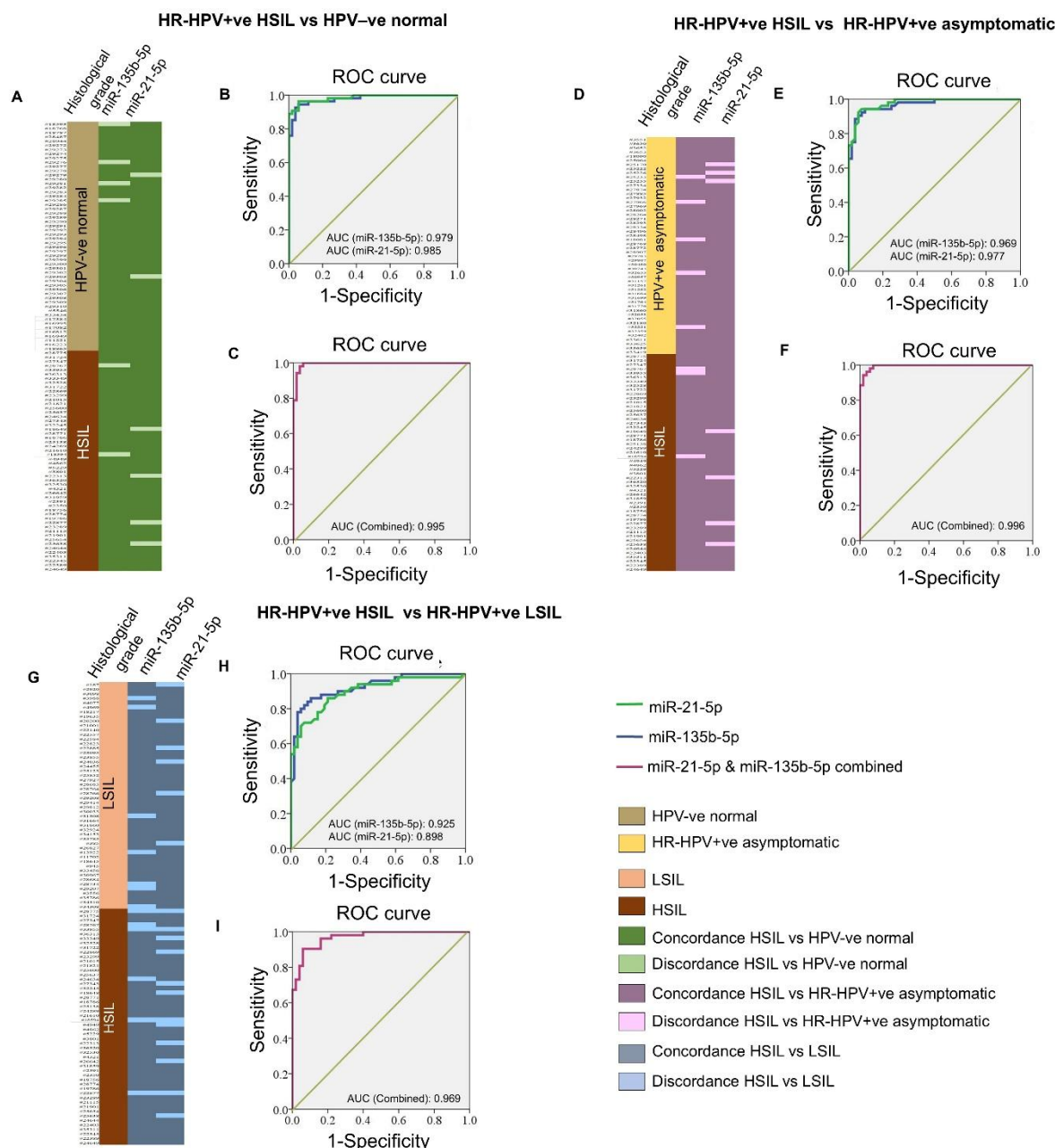


Figure 4.6 The diagnostic performance of miR-135b-5p and miR-21-5p from cervical swabs: The diagnostic usefulness of miR-135b-5p and miR-21-5p was represented to distinguish HR-HPV+ve HSIL from HPV-ve normal (A-C); HR-HPV+ve HSIL from HR-HPV+ve asymptomatic (D-F); HR-HPV+ve HSIL from HR-HPV+ve LSIL (G-I), where the heatmap represents the concordance and discordance of miR-135b-5p and miR-21-5p expression with histopathological reports (A, D, G). The ROC curve represents the sensitivity and specificity of miR-135b-5p and miR-21-5p individually (B, E, H) and in combination (C, F, I).

Table 4.3: Diagnostic value of miR-135b-5p and miR-21-5p to differentiate various clinical stages of cervix

Items	AUC 95% confidence interval (CI)			Sensitivity (%)			Specificity (%)		
	HR-HPV +ve HSIL vs HPV-ve normal	HR-HPV+ve HSIL vs HR-HPV+ve asymptomatic	HR-HPV+ve HSIL vs HR-HPV+ve LSIL	HR-HPV +ve HSIL vs HPV-ve normal	HR-HPV+ve HSIL vs HR-HPV+ve asymptomatic	HR-HPV+ve HSIL vs HR-HPV+ve LSIL	HR-HPV +ve HSIL vs HPV-ve normal	HR-HPV+ve HSIL vs HR-HPV+ve asymptomatic	HR-HPV+ve HSIL vs HR-HPV+ve LSIL
miR-135b-5p	0.979 (0.958-1)	0.969 (0.940-0.988)	0.925 (0.874-0.976)	92.6	90.4	86	96.2	94.2	88.5
miR-21-5p	0.985 (0.968-1)	0.977 (0.956-0.999)	0.898 (0.837-0.960)	96.3	94.2	86	94.2	92.3	78.8
Combined	0.995 (0.986-1)	0.996 (0.989-1)	0.969 (0.942- 0.996)	98.1	96.2	90.4	96.3	96.2	94

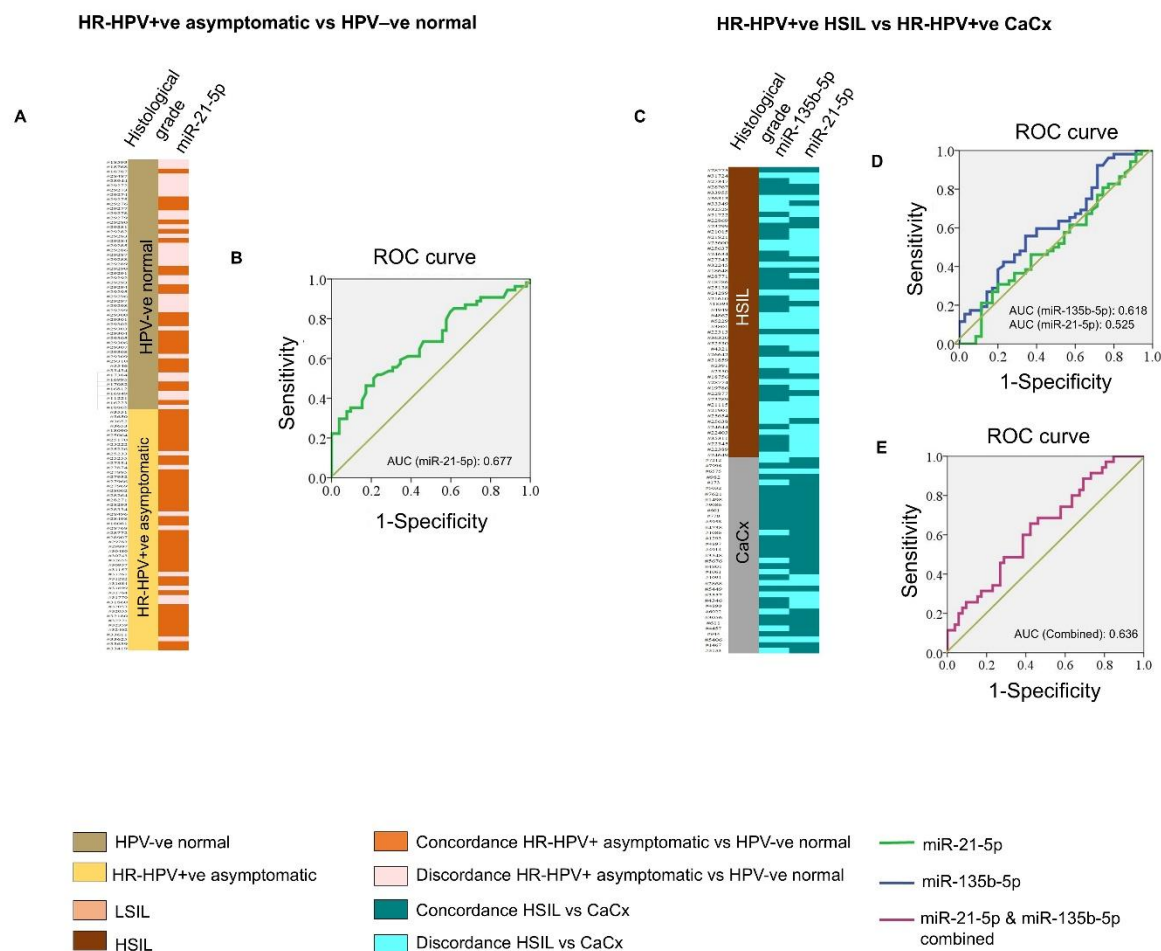


Figure 4.7 The diagnostic performance of miR-135b-5p and miR-21-5p from cervical swabs: The diagnostic usefulness of miR-21-5p alone to distinguish HR-HPV+ve asymptomatic from HPV-ve normal (A-B), where (A) The heatmap represents concordance and discordance of miR-21-5p with histopathological grade and (B) the ROC curve represents the sensitivity and specificity of miR-21-5p alone. The diagnostic usefulness of miR-21-5p and miR-135b-5p to distinguish HR-HPV+ve HSIL from HR-HPV+ve CaCx (C-E), where, the heatmap represents concordance and discordance of these two miRNAs with histopathological grade (C) and the ROC curve represents the sensitivity and specificity of miR-135b-5p and miR-21-5p individually (D) and in combination (E).

Table 4.4: Diagnostic value of miR-135b-5p and miR-21-5p to differentiate various clinical stages of cervix

Items	AUC		Sensitivity (%)		Specificity (%)	
	95% confidence interval (CI)					
miR-135b-5p	HR-HPV+ve asymptomatic vs HPV-ve normal	HR-HPV+ve HSIL vs HR-HPV+ve CaCx	HR-HPV+ve asymptomatic vs HPV-ve normal	HR-HPV+ve HSIL vs HR-HPV+ve CaCx	HR-HPV+ve HSIL vs HR-HPV+ve CaCx	HR-HPV+ve HSIL vs HR-HPV+ve CaCx
miR-21-5p	0.677 (0.968-1)	0.525 (0.400-0.650)	46.3	30.8	82.7	80
Combined	-	0.636 (0.518-0.753)	-	65.7	-	57.7

4.4.3 Detection of miR-135b-5p expression using novel sensor oligo both in cell lines and cell-free system (exfoliated cells of cervical swabs as well as in SiHa cell line):

To further validate miR-135b-5p expression *in vitro*, we have used a novel sensor oligo, labelled with a fluorescent dye-quencher pair, so that upon cleavage of the oligo by the microRNA-RISC, fluorescence enhancement is detected (**Figure 4.8A**). At first, we transfected the SiHa and HEK293T cells with sensor oligo against the endogenous miR-135b-5p. The result showed significantly ($p=0.035$) higher detection of miR-135b-5p by the sensor oligo in SiHa compared to HEK293T cells (**Figure 4.8B**). Furthermore, to confirm the detection sensitivity of sensor oligo for miR-135b-5p, different concentrations of the sensor oligo were titrated into SiHa cells pretreated with anti-miR-135b-5p or Scrambled RNA. When endogenously overexpressed miR-135b-5p was inhibited by anti-miR-135b-5p in SiHa cells, the fluorescence intensity of sensor oligo was lower than the Scrambled RNA-pretreated condition, even with gradually increasing concentrations of the sensor oligo (**Figure 4.8C**).

To translate this miRNA-direct detection method into clinical practice, we detected miR-135b-5p on a few cervical swab samples [i.e. cell-free system, N=33; HR-HPV+ve asymptomatic (N=10); HR-HPV+ve HSIL (N=12); and HR-HPV+ve CaCx (N=11)] that were previously analyzed for miR-135b-5p expression by qRT-PCR. Interestingly, a significant increase in sensor oligo fluorescence intensity was observed in HR-HPV+ve HSIL ($p=0.034$) and HR-HPV+ve CaCx ($p=0.048$) samples, compared to the HR-HPV+ve asymptomatic controls (**Figure 4.8D**). This data showed a significant ($p<0.0001$) positive correlation with our qRT-PCR data (**Figure 4.8E**) showing significant upregulation of miR-135b-5p in the HR-HPV+ve HSIL and CaCx samples, compared to HR-HPV+ve asymptomatic.

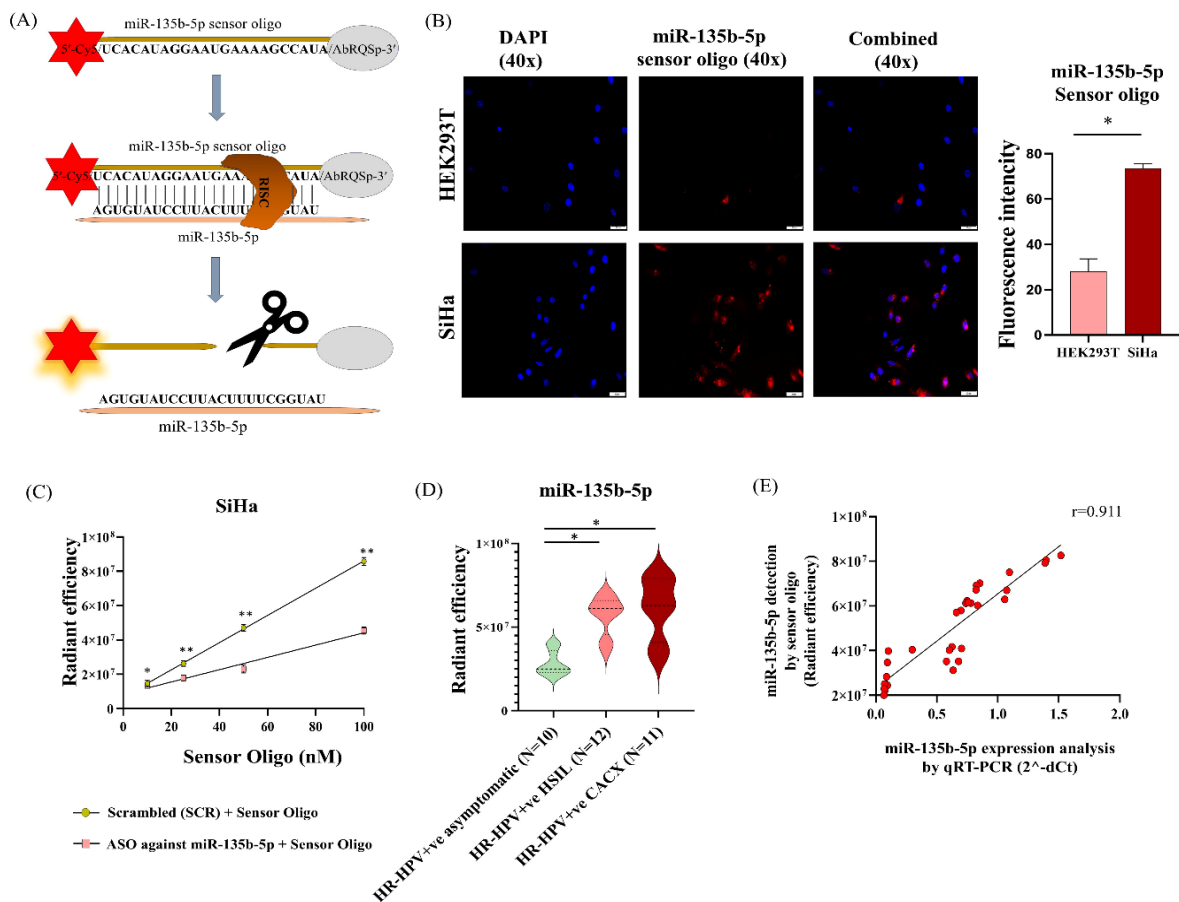


Figure 4.8 Direct detection of miR-135b-5p expression using sensor oligo in intact cells (in vitro) and cell-free system (cervical swab samples). (A) Representative images of the direct detection of miR-135b-5p using sensor oligo, composed of RNA bases, are cleavable around the seed region, and are labeled with a fluorescent dye-quencher pair, so that, upon cleavage of the oligonucleotide by the miRNA-RISC, fluorescence enhancement is observed. (B) Representative image of the detection of miR-135b-5p molecule in SiHa and HEK293T cell line using sensor oligo against miR-135b-5p. Histogram representing the fluorescence intensity of sensor oligo for the detection of miR-135b-5p. (C) Plot representing quantification of radiant efficiency as a function of sensor concentration. (D) Violin plot representing radiant efficiency for the detection of miR-135b-5p molecules in HR-HPV+ve asymptomatic control, HR-HPV+ve HSIL, and CaCx swab samples. (E) Scatter plot representing the Pearson correlation coefficient between miR-135b-5p expression analysis by qRT-PCR and direct detection of miR-135b-5p by sensor-oligo based. where *, **, *** and **** represents a significant p -value < 0.05 , < 0.01 , < 0.001 and < 0.0001 , respectively.

4.5 Discussion:

In this study, we investigated the miRNAs, associated with regulation of the stress-induced proteins LIMD1 and VHL, in relation to HR-HPV infection in transforming cervical lesions to develop miRNA-based triage biomarkers for early detection of CaCx.

Upon validating our findings in a large number of cervical swabs, similar trends of significant over-expression of miR-135b-5p/ miR-21-5p and down expression of LIMD1/VHL were found in HR-HPV+ve HSIL than its earlier clinical stages (**Figure 4.5**).

Even though a number of potential miRNA-based triage biomarkers for CaCx screening have already been reported from various body fluids, such as plasma, urine, and cervical scrapes [Xin et al., 2016; Aftab et al., 2021; Kawai et al., 2018; Ivanov et al., 2018], identification of miRNA from exfoliated cervical cells would be more appropriate because of its extensive use in CaCx screening and for being minimally invasive method [Kawai et al., 2018; Ivanov et al., 2018]. However, a number of miRNAs or their panel in cervical mucus have already been identified as potential biomarkers for differentiating high-grade CIN and CaCx, where the control arm has not always been uniform (HPV status was not reported in every case) [Kawai et al., 2018; Ivanov et al., 2018; Kotani et al., 2022]. There are only a very few reports where miRNA panel from cervical mucus was used to discriminate CIN II+ stages from <CIN II stages, however, with moderate sensitivity and specificity [Ivanov et al., 2018; Kotani et al., 2022]. Therefore, there was a lack of potential biomarkers that could even differentiate LSIL from HSIL, especially from the Indian population where CaCx incidence is very high. Here, we reported the sensitivity and specificity of LIMD1/ VHL stress response pathway associated two miRNAs, miR-21-5p and miR-135b-5p, in cervical swabs to discern HSIL from other earlier stages of CaCx (\leq HSIL) rather than focusing only on CaCx stages. We specifically aimed the HR-HPV+ve CIN II+/HSIL, the critical stage of "no-return" when treatment is essentially required. Though, miR-21-5p is reported as a well-known diagnostic biomarker that has already been reported from plasma, and cervical scrapes for early diagnosis of CaCx [Kotani et al., 2022; Okoye et al., 2019; Wang et al., 2019], individually, miR-21-5p showed comparatively lower specificity (78.8%) to discern HR-HPV+ve HSIL from LSIL which was subsequently overcome by introducing miR-135b-5p (specificity 88.5%). To the best of our knowledge, this is the first report of combined triage application of two miRNAs in discerning HR-HPV+ve pre-malignant (CIN II+/HSIL) lesions from HR-HPV+ve LSIL with considerably enhanced sensitivity (90.4%) and specificity (94%) [**Figure 4.6 and Table 4.3**].

On the other hand, we have also focused on the direct detection of miRNAs from non-invasive samples. While several traditional miRNA detection methods, such as northern blot, microarray chips, and qRT-PCR, were accessible; each had some drawbacks [Ye et al., 2019; Lee, 2022]. The most widely used technique for identifying miRNA biomarkers was qRT-PCR; however, it requires expert skill sets and time [Ye et al., 2019; Lee, 2022]. To facilitate miRNA detection as a screening triage tool, a more facile, quick, and concurrent detection approach is required for accurate detection of candidate miRNA from non-invasive swab samples during CaCx screening. Here, we developed a novel technique to detect miR-135b-5p directly in intact cells and in a cell-free system using a sensor oligo against miR-135b-5p (**Figure 4.8B and 4.8C**), just to check the efficiency of sensor-oligo based signal amplification technique as a preliminary study.

The detection of higher fluorescence intensity in swabs from HR-HPV+ve HSIL and CaCx patients compared to the HR-HPV+ve asymptomatic control implies that this novel technique could be translated into clinical settings for miRNA biomarker detection during high-throughput cervical screening, rapidly and sensitively (**Figure 4.8D**). Validating this technique in a small study setting is a limitation of our study that needs to be overcome by testing in larger sample number at each clinical stage. Due to its high sensitivity in detecting miR-135b-5p, this sensor-oligo-based technique could be extended to other miRNAs, broadening its utility in molecular diagnostics.

4.6 Inference points:

- i. miR-21-5p, miR-135b-5p, and their combination could serve as potential triage biomarkers for HR-HPV+ve, clinically relevant CIN II+/HSIL lesions during cervical screening in low-middle income countries and thus could decrease the CaCx patient burden (**Figure 4.9**).

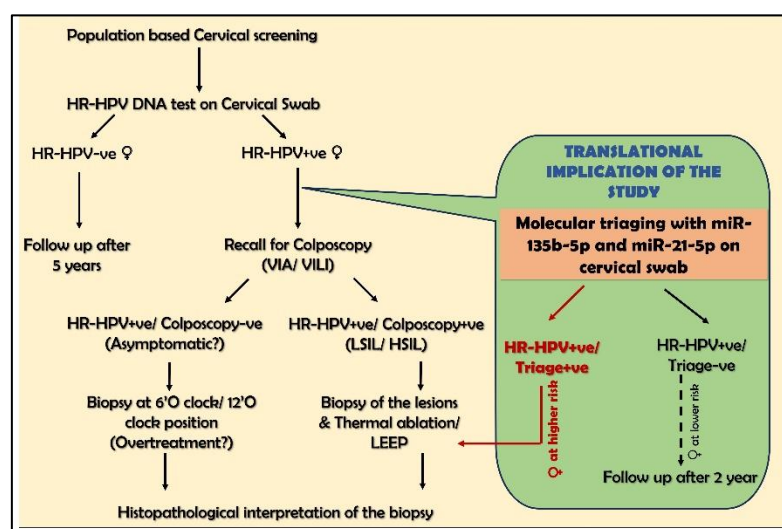


Figure 4.9 Combined application of miR-135b-5p and miR-21-5p as a triage biomarker for detection of HR-HPV+ve women having higher risk of developing cervical cancer

- ii. The novel sensor oligo against miR-135b-5p is able to detect the miRNA both in cell-free system as well as in intact cells, rapidly and sensitively, and could be applied to miRNA biomarker detection directly from non-invasive samples (**Figure 4.10**).

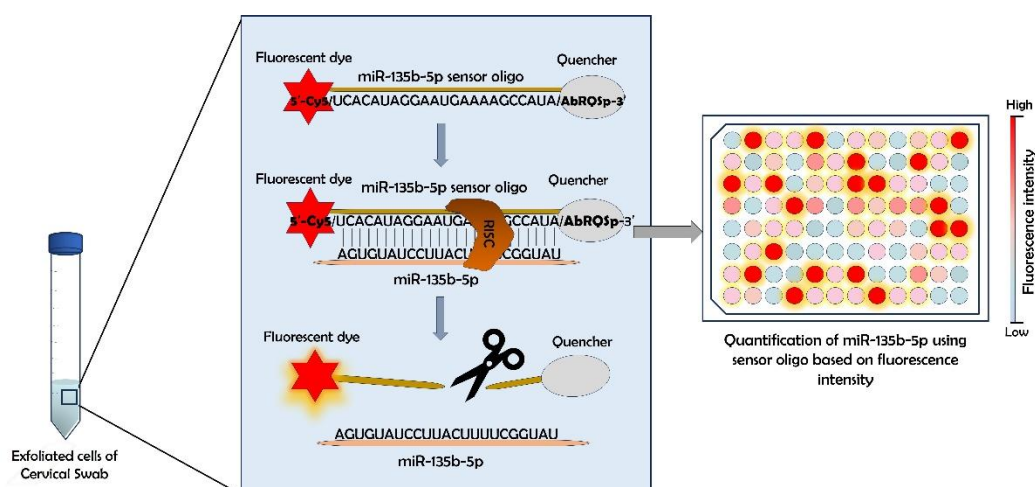


Figure 4.10 Detection of candidate miRNA as biomarker in non-invasive cervical swabs using sensor-oligo based signal amplification technique

CHAPTER 5

***In vitro* functional validation of
the candidate miRNA(s) in
target gene expression**

Chapter 5

In vitro functional validation of the candidate miRNA(s) in target gene expression

5.1 Introduction:

High-risk HPV (HR-HPV) modulates the cellular response to hypoxia by inhibiting HIF-1 α ubiquitylation, leading to its stabilization [Nakamura et al., 2009; Bodily et al., 2011; Ravi et al., 2000]. HIF-1 α , a key transcription factor, regulates the expression of several angiogenic factors, including VEGF, MMP9, and TGF- α , thereby promoting cancer progression [Ziello et al., 2007]. Under normoxic conditions, HIF-1 α is primarily regulated by two tumor suppressor genes (TSGs), LIMD1 and its interacting partner VHL (as described in **Section 1.3.1**). These TSGs, along with prolyl hydroxylase domain-containing proteins (PHDs), facilitate the ubiquitylation and subsequent proteasomal degradation of HIF-1 α [Foxler et al., 2012] (described in **section 1.3.1**). Other tumor-suppressive functions of LIMD1 and VHL are also discussed in **Section 1.3.1**.

In **Chapter 3**, we analyzed data from the TCGA/GEO (GSE86100) and CGH-microarray (GSE76911) databases to identify upregulated and amplified miRNAs involved in cervical cancer (CaCx) progression. Among these, miR-135b-5p (targeting LIMD1) and miR-21-5p (targeting VHL) were linked to the HIF-1 α stress response pathway. We further validated the expression of these miRNAs in primary tissue samples, confirming significant upregulation in CIN and CaCx samples compared to normal cervical epithelium.

Moreover, as detailed in **Chapter 4**, our group proposed the diagnostic potential of these miRNAs as triage biomarkers, both individually and in combination, for the early detection of CaCx in LMICs such as India. By individually targeting several proteins, the upregulation and functional roles of miR-135b-5p and miR-21-5p as oncomiRs have already been reported in various human tumors [Lu et al., 2017; Di et al., 2021; Zhang et al., 2017; Tang et al., 2021; Cao et al., 2021; Luo et al., 2020], including cervical cancer [Xu et al., 2015; Wang et al., 2019;

Cai et al., 2018]. However, the specific regulatory mechanisms of these miRNAs on LIMD1 and VHL, particularly in the context of the HIF-1 α -induced cellular stress response pathway, as well as their potential synergistic effects within this pathway and its downstream signalling, has not been fully elucidated (**Figure 5.1**).

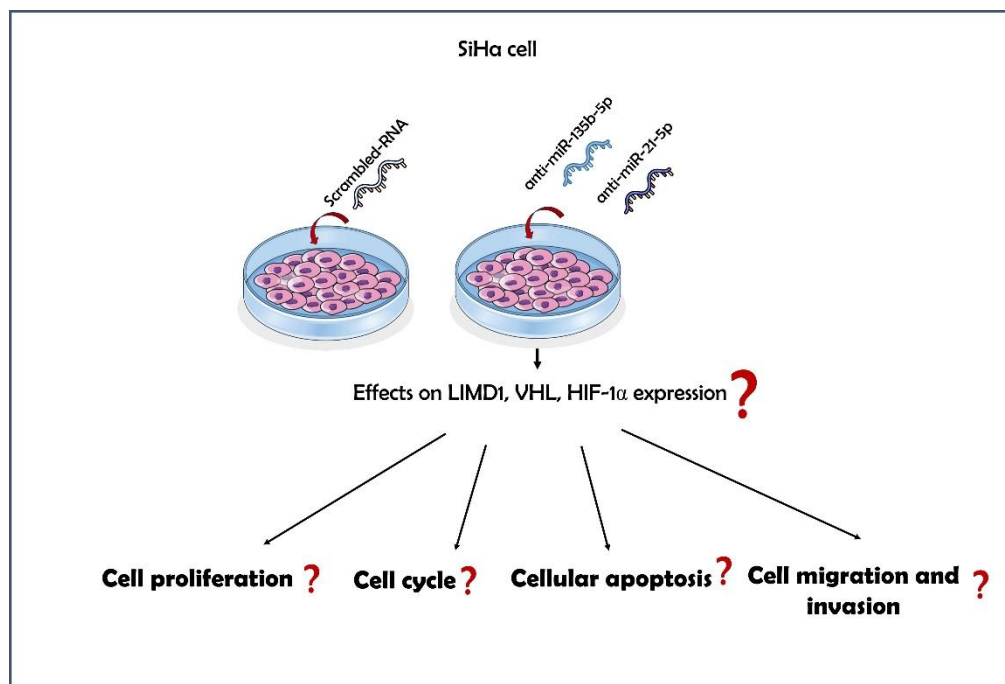


Figure 5.1 Investigating the functional role of miR-135b-5p and miR-21-5p inhibition in regulating different cellular phenotypes of SiHa cells via LIMD1-VHL-HIF-1 α pathway.

5.2 Objective of the study:

Since the activation of the LIMD1-VHL-HIF-1 α pathway is a key event in HR-HPV-induced cervical carcinogenesis, the functional roles of its key regulatory miRNAs, miR-135b-5p (targeting LIMD1) and miR-21-5p (targeting VHL), remain poorly characterized during the development of CaCx. To address this gap, our study focuses on the following aspect:

- (a) Analysis of the effects of miR-135b-5p and miR-21-5p knockdown on the tumorigenicity of SiHa cells, with a focus on cellular proliferation and apoptosis
- (b) Exploring the effects of miR-135b-5p and miR-21-5p knockdown on epithelial-mesenchymal transition (EMT), including migration and invasion, in SiHa cells

5.3 Materials and Methods:

5.3.1 Chemical and reagents:

5.3.1.1 Fine chemicals (molecular biology grade) used in the study:

Described in Section 3.3.1.1

5.3.1.2 Enzymes

Described in Section 3.3.1.2

5.3.1.3 Primers

Table 5.1: List of primers used for mRNA expression analysis

Gene Name	Forward Primers (5'-3')	Reverse Primer (5'-3')	Primer location	PCR conditions	Product Size (bp)
LIMD1 (RT)	5'- GTAAATTCATCGGAGGAC CTG-3'	5'- CCATCCACAGTCAGC TTG-3'	3'UTR	58°C/40 cy	268
VHL (RT)	5'- TCACCTTTGGCCCTCTTC AGAGAT-3'	5'- CTGGCAGTGTGAAT ATTGGCAAA-3'	Exon2	58°C/40 cy	122
TGF- α (RT)	5'- CCATGAAAGGGGGACCA GTCA-3'	5'- GTTTTGTGTTAATAAA GCCGGCAT-3'	3'UTR	58°C/40 cy	180
MMP9 (RT)	5'- TGACAGCGACAAGAAGT G-3'	5'- ACATAGGGTACATG AGCGCC-3'	Exon7- Exon8	58°C/40 cy	131
CyclinD1 (RT)	5'-AACACCAGCTCC TGTGCTGCGAA-3'	5'-GTCTCCTTCATC TTAGAGGCCACG-3'	Exon1- Exon2	60°C/40 cy	343
B2M (RT)	5'- GTGCTCGCGCTACTCTCT CT-3'	5'- TCAATGTGCGGATGG ATGAAA-3'	Exon1- Exon2	58°C/40 cy	143

5.3.1.4 Antibodies

Table 5.2: List of antibodies used for western blot analysis

Sl.No.	Antibody	Primary antibody	Dilution	Secondary antibody	Dilution
1	LIMD1	Mouse, sc-271448	1:500	Rabbit anti-Mouse IgG (sc-516102)	1:10000
2	VHL	Mouse, sc-135657	1:1000	Rabbit anti-Mouse IgG (sc-516102)	1:10000
3	HIF-1A	Mouse, Orb-38400	1:1000	Goat Anti-Rabbit IgG (sc-2004)	1:10000
4	VEGF	Mouse, sc-7269	1:1000	Rabbit anti-Mouse IgG (sc-516102)	1:10000
5	E-cadherin	Mouse, CST14472	1:500	Rabbit anti-Mouse IgG (sc-516102)	1:10000
6	N-cadherin	Mouse, sc-59987	1:500	Rabbit anti-Mouse IgG (sc-516102)	1:10000
7	Cyclin D1	Mouse, sc-20044	1:500	Rabbit anti-Mouse IgG (sc-516102)	1:10000
8	Bax	Mouse, sc-7480	1:1000	Rabbit anti-Mouse IgG (sc-516102)	1:10000
9	Bcl-2	Mouse, sc-7382	1:1000	Rabbit anti-Mouse IgG (sc-516102)	1:10000
10	α -tubulin	Mouse, sc-5286	1:1000	Rabbit anti-Mouse IgG (sc-516102)	1:10000

5.3.1.5 Kit:

CytoSelect™ 24-well Cell Invasion Assay kit (Cell Biolabs, San Diego, California, USA) used to check SiHa cell invasion phenotype

QuickChange Site-Directed Mutagenesis kit (Agilent Technologies, US) used to rapidly and efficiently introduce targeted mutations into double-stranded plasmid DNA.

5.3.2 Cell culture:

Cell cultures were described in **section 3.3.3**

5.3.3 Candidate miRNA knockdown experiments *in vitro*:

To knock down the miRNAs, SiHa cells were first cultured in DMEM medium (as described in **Section 3.3.3**) and seeded into six-well plates for 24 hrs (Corning, NY, USA). Once the cells reached 50%–70% confluence, transfection was performed using Lipofectamine 3000 (Invitrogen, USA) in Opti-MEM (Gibco, Paisley, Scotland, UK) media with varying concentrations (25nM and 50nM) of specific inhibitors: miRCURY LNA anti-miR-135b-5p

(Qiagen; GeneGlobe ID: YI04101769) and anti-miR-21-5p (Qiagen; GeneGlobe ID: YI04100689) [Xu et al., 2015; Tang et al., 2020]. After six hours of treatment, the Opti-MEM media was replaced with complete DMEM, and the expression of target genes was analyzed at different time points (0, 24, and 48 hours) to determine the optimal dose and time for inhibition. Scrambled RNA (negative control A, Qiagen; GeneGlobe ID: YI00199006) was used as a control. Finally, the effects of anti-miR-135b-5p and anti-miR-21-5p were evaluated by transfecting SiHa cells individually or in combination (50 nM each for dual inhibition) to assess various cellular phenotypes. The sequences of the anti-miRs are provided in **Table 5.3**.

Table 5.3: List of anti-miRs used for knock down of candidate miRNAs

anti-miR (miRNA inhibitor)	Inhibitor sequence
anti-miR-135b-5p	5'-UAUGGCUUUUCAUCCUAUGUGA
anti-miR-21-5p	5'-UAGCUUAUCAGACUGAUGUUGA
Scrambled RNA (negative control)	TAACACGTCTATACGCCCA

5.3.4 RNA expression analysis by quantitative real-time PCR (qRT-PCR):

mRNA expression from cell lines (SiHa and HEK293T) were analysed by qRT-PCR, as described in **section 3.3.8a**. List of primers used for mRNA expression analysis were given in **Table 5.1**.

5.3.5 Luciferase Reporter assay for candidate miR-135b-5p target validation:

To check miR-135b-5p mediated deregulation of LIMD1, we identified the region of LIMD1 3'UTR (position 2340-2346 of LIMD1 3' UTR), which could be recognized by miR-135b-5p using TargetScan and performed luciferase reporter assays. We have designed two luciferase constructs by cloning the identified region of LIMD1 3'UTR in psiCHECK2 vector: one containing the wild-type (WT) LIMD1 3' UTR (AAGCCAU) and another containing a mutated (Mut) LIMD1 3' UTR (AATTTAU), generated by QuickChange Site-Directed Mutagenesis kit (Agilent Technologies, US) [**Figure 5.2**]. After sequence confirmation, these cloned vectors were co-transfected with anti-miR-135b-5p (50nM) and scrambled RNA (50nM) within the SiHa cells as described in **section 5.3.3**. After 48 hours of transfection, the relative luciferase activity of each sample was assessed using the Dual-Luciferase Assay Kit (Promega, USA), following the manufacturer's guidelines [Xu et al., 2015]. The activity was determined by

calculating the ratio of Renilla luciferase to Firefly luciferase. All experiments were performed in triplicate.

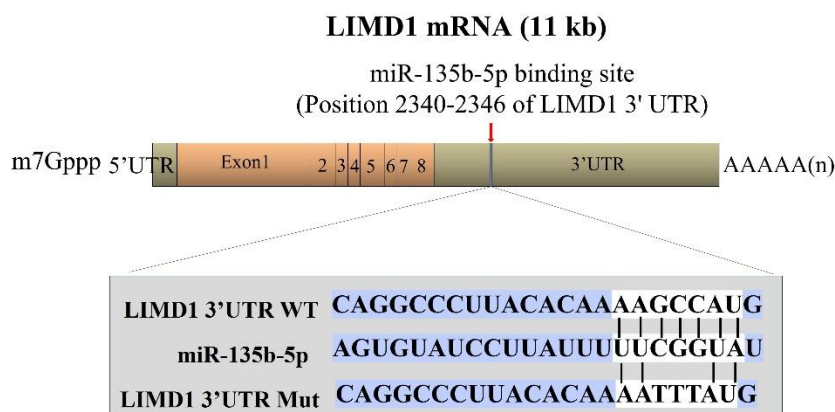


Figure 5.2 Schematic representation of *LIMD1* 3'UTR, highlighting putative miR-135b-5p binding site along with Wild type (WT) and Mutated (mut) seed sequence.

5.3.6 Analysis of the effect of candidate miRNA knockdown on different cellular phenotypes:

To check the effect of candidate miRNA knockdown on different cellular phenotypes, following functional validation has been done:

a. Colony Formation Assay:

To assess the colony-forming ability of SiHa cells, 1,000 cells per well were seeded into six-well plates. After 24 hrs, the cells were transfected with anti-miR-135b-5p (50 nM), anti-miR-21-5p (50 nM), or both (50 nM each for dual inhibition). The medium was refreshed every two days. After 14 days, the colonies were fixed with 4% paraformaldehyde and stained with 0.05% crystal violet. Colony numbers were quantified using ImageJ software. This experiment was performed independently three times [Wang et al., 2021].

b. Cell cycle analysis:

To analyze cell cycle distribution, SiHa cells (3×10^5 per well) were seeded into six-well plates and cultured for 24 hrs. To get a clear picture of cell cycle distribution, cells were first synchronized using 2.5 mM thymidine (Sigma, USA) for 18 hrs, followed by an 8-hrs release in prewarmed DMEM. A second 2.5 mM thymidine treatment was applied for an additional 18 hrs [Amin et al., 2017].

After washing with $1 \times$ PBS, the cells were transfected (as described in **section 5.3.3**) with anti-miR-135b-5p (50nM), anti-miR-21-5p (50nM), or both (50nM each for dual

inhibition) and incubated for 48 hrs. Cells were then fixed in 70% ice-cold ethanol at 4°C for 24 hrs. Following RNase treatment, cell cycle distribution was assessed by staining with 30µL of 0.05g/L propidium iodide (Sigma, USA) and analyzed via flow cytometry (BD Biosciences, Germany) at room temperature. The experiments were performed in triplicate, and cell cycle distribution was quantified using flow cytometry (BD Biosciences) [Hwang et al., 2023].

c. Apoptosis assay:

To assess apoptotic cell fate, SiHa cells (3×10^5 per well) were seeded into six-well plates and cultured for 24 hrs. After 48 hrs of transfection (as described in **Section 5.3.3**) with anti-miR-135b-5p (50 nM), anti-miR-21-5p (50 nM), or both (50 nM each for dual inhibition), apoptosis was analyzed using flow cytometry (BD Biosciences) and FlowJo software with the Annexin V-FITC Apoptosis Detection Kit (Sigma-Aldrich), following the manufacturer's protocol [Pigault et al., 1994]. Cells were harvested and washed twice with \times PBS, then stained with propidium iodide (PI) and Annexin V. After 15 minutes of incubation in the dark at room temperature, apoptotic cells were quantified by flow cytometry (BD Biosciences) using FlowJo software. The experiments were conducted in **triplicate**.

d. Cell viability Assay:

To further verify cellular apoptosis, SiHa cell viability was assessed using the MTT assay (Himedia, India) [Mohammaddoust et al., 2023]. Briefly, 10×10^3 cells per well were seeded into a 96-well plate and cultured for 24 hrs. After 48 hrs of transfection (as described in **Section 5.3.3**), with anti-miR-135b-5p (5 nM), anti-miR-21-5p (50nM), or both (50nM each for dual inhibition), MTT solution (5mg/mL) was added and incubated at 37°C for 4 hrs. Subsequently, 100 µL of DMSO was added to dissolve the formazan crystals. Finally, optical absorbance was measured at 570 nm using a MULTISKAN SkyHigh microplate reader (Thermo Scientific, Waltham, Massachusetts, USA). The experiment was performed independently three times.

e. Wound healing assay:

To assess cellular migration, SiHa cells (0.05×10^6 per well) were seeded into a 24-well plate and cultured for 24 hrs. Once the cells reached 70%–80% confluence, a straight-line was created using a sterile 200 μ L pipette tip [Mohammaddoust et al., 2023]. The cells were then washed with $1 \times$ PBS to remove debris. Next, the cells were transfected (as described in **Section 5.3.3**) with anti-miR-135b-5p (50nM), anti-miR-21-5p (50nM), or both (50nM each for dual inhibition). Images were captured at 0, 24, and 48 hrs using an inverted microscope. Cell migration was quantified by measuring wound closure using ImageJ software. The experiment was performed independently three times.

f. Invasion assay:

The cell invasive ability was assessed using the CytoSelect™ 24-Well Cell Invasion Assay Kit CytoSelect™ 24-well Cell Invasion Assay kit (Cell Biolabs, San Diego, California, USA). Transfected SiHa cells (0.05×10^6 per well) were seeded into the upper chamber containing serum-free DMEM, while the lower chamber was filled with DMEM supplemented with 10% FBS, serving as a chemoattractant. After 48 hrs of incubation at 37°C, non-invasive cells were carefully removed using cotton swabs, and invasive cells were stained with 0.1% crystal violet for 10 minutes at room temperature. Images of the invasive cells were captured using a light microscope (Olympus, Japan). Subsequently, the upper chamber was transferred to an empty well, and extraction solution was added per well, followed by 10 minutes of incubation on an orbital shaker. Finally, optical absorbance was measured at 560 nm using a MULTISKAN SkyHigh microplate reader (Thermo Scientific, Waltham, Massachusetts, USA) [Polo-Generelo et al., 2022].

5.3.7 Protein expression analysis by Western Blot:

To confirm variations in cellular phenotypes, Western blot analysis was performed to assess the protein expression of specific markers. SiHa cells (3×10^5 per well) were cultured until they reached approximately 70%–80% confluence. After transfection for 48 hours with anti-miR-135b-5p (50nM), anti-miR-21-5p (50nM), or a combination of both (50nM each), cells were lysed using ice-cold RIPA buffer. The buffer composition included 25 mM Tris-HCl (pH 7.6), 1 mM EDTA (pH 8.0), 150 mM NaCl, 1% NP-40, 1% sodium deoxycholate, 0.1% SDS, 1 mM PMSF, and 1–2 μ g/ μ L of protease inhibitors (leupeptin and aprotinin). Sonication was used for

lysis, followed by centrifugation at 4°C to collect the supernatant, which was then quantified using the Bradford assay, as previously reported by Roy et al. (2019).

For Western blot analysis, 60 µg of total protein per sample was separated using SDS-PAGE and transferred onto a polyvinylidene difluoride (PVDF) membrane (Millipore, Burlington, MA), following established protocols (Islam et al., 2020). Membranes were then blocked with 3%–5% bovine serum albumin (BSA) at room temperature for one hour. This was followed by overnight incubation at 4°C with specific primary antibodies. Secondary detection was performed using horseradish peroxidase (HRP)-conjugated antibodies (anti-mouse or anti-rabbit), and the labeled protein bands were visualized with luminol reagent (Advansta, San Jose, California). Band intensities were measured using ImageJ software, with normalization to α -tubulin as a loading control. The relative expression levels of the target proteins were graphically represented in comparison to the control group. A detailed list of antibodies and dilutions used for the Western blot analysis is provided in **Table 5.2**.

5.3.6 Statistical analysis:

Fisher's exact *t*-test was used to analyse the level of significance in the samples categorized based on their molecular features. Z-score was used to determine the significance level between the groups of a single population. The histogram, dot plots, and box plots were organized using either GraphPad Prism 8 software (GraphPad Software) or Microsoft® Excel 2019. A probability value (*P*) <0.05 was taken into consideration as statistically significant.

5.4 Result:

5.4.1 Validation of LIMD1 and VHL as direct targets of miR-135b-5p and miR-21-5p, respectively, in SiHa cells:

At first, we have checked the expression of miR-135b-5p and miR-21-5p and their targeting LIMD1/VHL in SiHa and HEK293T cell lines, where HEK293T is used as a control. A significant upregulation of miR-135b-5p and miR-21-5p was observed in SiHa cells (*p*=0.002 and 0.001, respectively) compared to HEK293T cells (**Figure 5.3A and 5.3B**). Whereas, the expression of miR-135b-5p and miR-21-5p respective target genes LIMD1 and VHL was significantly decreased (*p*=0.012 and 0.031) in SiHa cells (**Figure 5.3C and 5.3D**). This indicates that LIMD1 and VHL expression might be regulated by their respective targeting miRNAs, miR-135b-5p and miR-21-5p. To confirm the target of miR-135b-5p, vectors containing either the WT or Mut LIMD1 3' UTR were transfected into SiHa cells along with

anti-miR-135b-5p. After 48 hours, luciferase activity was measured. Interestingly, cells transfected with the WT LIMD1 3' UTR exhibited that downregulation of miR-135b-5p significantly increased ($p=0.012$) the relative luciferase activity compared to control cells (**Figure 5.3E**). Whereas, mutation of the miR-135b-5p binding site in the LIMD1 3'-UTR abolished this effect, indicating that miR-135b-5p directly and specifically binds to LIMD1 3'UTR, regulating mRNA expression. On the other hand, the miR-21-5p-mediated regulation of VHL has already been experimentally proved in cervical cancer cells by Cai et al., 2018. As miR-135b-5p and miR-21-5p were higher in SiHa cells, they were further treated with respective inhibitors against miR-135b-5p and miR-21-5p to check their effect on different SiHa cell phenotypes.

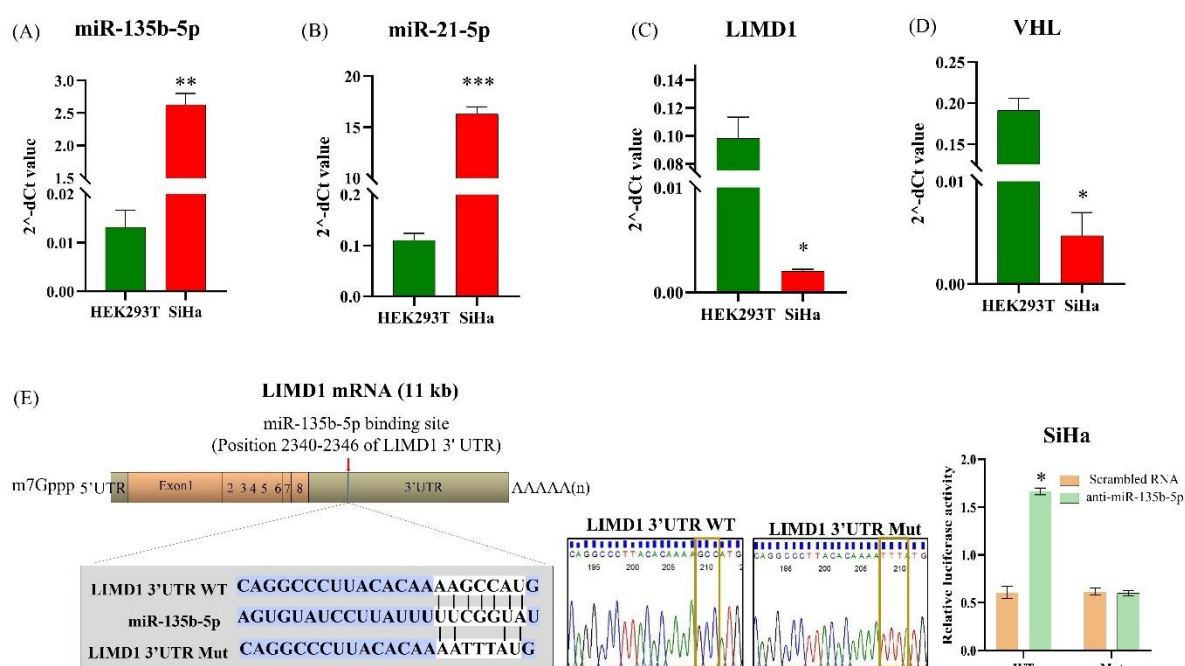


Figure 5.3 Regulation of LIMD1 and VHL expression by their respective targeting miRNAs, miR-135b-5p and miR-21-5p, in SiHa cells: (A-D) The mRNA level of LIMD1 and VHL was determined by real time-PCR in cell lines. Bar-plot displaying the distribution of $2^{-\Delta Ct}$ value of (A) miR-135b-5p, (B) miR-21-5p, (C) LIMD1, and (D) VHL mRNA in SiHa and HEK293T cell lines, where B2M and SNORD44 used as endogenous control for mRNA and miRNA expression, respectively. (E) Schematic representation of LIMD1 3'UTRs showing putative miRNA target site to verify LIMD1 as a direct target of miR-135b-5p. Sequence verification of LIMD1 WT and Mut 3'UTR. The analysis of the relative luciferase activities of LIMD1 WT and LIMD1 Mut in SiHa cells by co-transfecting with anti-miR-135b-5p or anti-miR-NC for 48 hours.

5.4.2 Optimization of anti-miR-135b-5p and anti-miR-21-5p treatment to assess the functional role of the respective miRNAs in SiHa cells:

Initially, the dose and timepoint of anti-miR-135b-5p or anti-miR-21-5p were selected for treatment. For this purpose, two doses of each inhibitor (25nM and 50nM) were taken into consideration through a literature survey to check their effect on LIMD1/ VHL mRNA deregulation in SiHa cells at different time intervals (6 hours, 24 hours, 48 hours, and 72 hours) (**Figure 5.4A and 5.4B**). The inhibitors were most effective at a 50nM dose after 48 hours, as evidenced by a prominent increase in LIMD1 and VHL mRNA expression (**Figures 5.4A and 5.4B**). This finding was further corroborated by corresponding increases in protein expression levels (**Figures 5.4C and 5.4D**), with significant upregulation observed for LIMD1 ($p=0.018$) and VHL ($p=0.003$) at the selected dose and time point (**Figure 5.4C and 5.4D**). Subsequently, treatment with a 50nM concentration of each individual inhibitor, as well as dual inhibition for 48 hours, demonstrated a significantly higher expression of LIMD1/VHL mRNA [$p=0.019$ (individual inhibition) and $p=0.014$ (dual inhibition) for LIMD1, and $p=0.025$ (individual inhibition) and $p=0.032$ (dual inhibition) for VHL] at this dose and timepoint (**Figure 5.4E**). Since these two miRNAs regulate LIMD1 and VHL, thereby affecting HIF-1 α stabilization. Immunoblot analysis demonstrated a significant downregulation ($p=0.025$ and $p=0.022$) of HIF-1 α when the cells were treated with anti-miR-135b-5p and anti-miR-21-5p, respectively. A further significant reduction ($p=0.026$) in HIF-1 α was observed upon dual inhibition of miR-135b-5p and miR-21-5p compared to the control cells (**Figure 5.4F**).

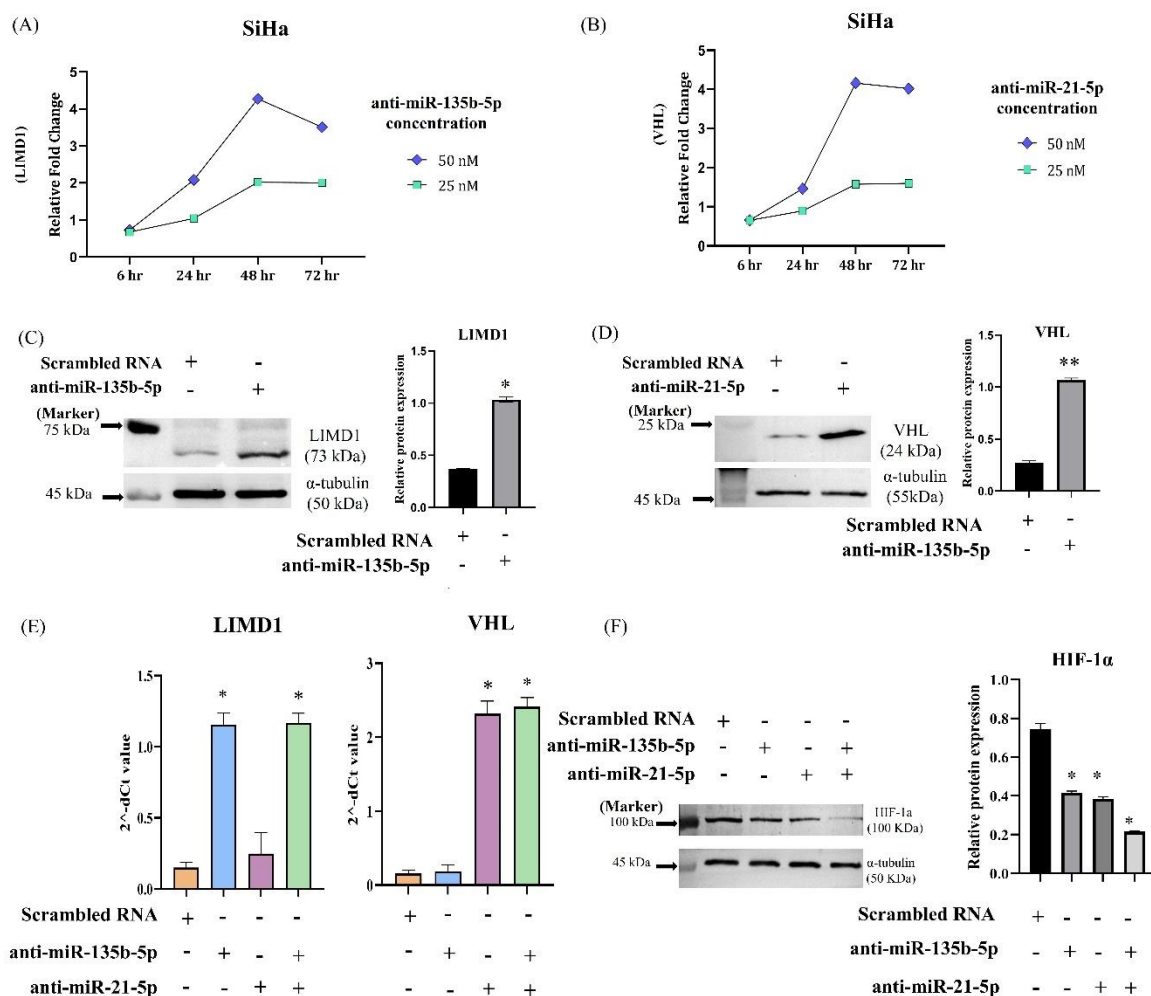


Figure 5.4 Dose selection of anti-miR-135b-5p and anti-miR-21-5p treatment to check functional role of these two miRNAs in SiHa cells: Dot plot showing the relative fold change of (A) LIMD1 and (B) VHL mRNA determined by real-time PCR at different time intervals with two doses (25nM and 50nM). Western blot depicting the protein expression of (C) LIMD1 and (D) VHL at a 50 nM concentration of inhibitor treatment after 48 hours. (E) The mRNA level of LIMD1 and VHL was determined by real time-PCR after 48 hours of anti-miR transfection, where bar-plot displaying the distribution of $2^{-\Delta\Delta Ct}$ value of LIMD1 and VHL mRNAs with B2M used as a loading control. (F) The protein expression of HIF-1 α was determined by Western blot after inhibiting miR-135b-5p and miR-21-5p. Quantification of HIF-1 α band intensities using ImageJ software after normalised with α -tubulin (All data are presented as mean with standard deviation (SD), where Error bars represent the SD; *, ** and *** represent a significant p-value < 0.05, <0.01 and <0.001, respectively)

5.4.3 Effect of anti-miR-135b-5p and anti-miR-21-5p on the proliferation of SiHa cells:

To acquire a better understanding of the roles played by these two miRNAs in the development of cervical cancer, the effect of miR-135b-5p and miR-21-5p, alone and in combination, were evaluated in SiHa cells by treating respective inhibitors against these two miRNAs. To investigate the role of miR-135b-5p and miR-21-5p on SiHa cell growth, the colony-forming ability of these two miRNAs was first studied on SiHa cells. The transfection of anti-miR-135b-5p and anti-miR-21-5p in SiHa cells showed a significantly lower number ($p=0.006$ and $p=0.0003$, respectively) of colonies compared to the scrambled-RNA treated control cells (**Figures 5.5A and 5.4B**). In addition, dual inhibition of these two miRNAs markedly reduced ($p=0.0005$) colony-formation capacity (number of colonies) compared to the control cells (**Figure 5.5A and 5.5B**).

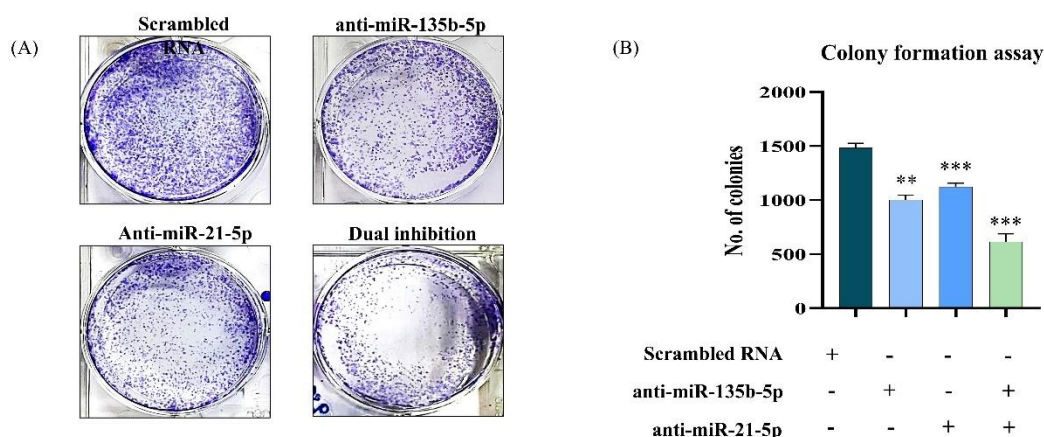


Figure 5.5 Impact of miR-135b-5p and miR-21-5p Suppression on SiHa Cell Proliferation: SiHa cells were transfected with anti-miR-135b, anti-miR-21-5p, or anti-miR-NC to examine their effects on cell proliferation. (A) A colony formation assay was conducted to assess the proliferation of SiHa cells. (B) A histogram illustrates the number of cell colonies, quantified using Image-J software.

5.4.4 Effect of anti-miR-135b-5p and anti-miR-21-5p on cell cycle of SiHa cells:

In light of these observations, it was pertinent to test if miR-135b-5p and miR-21-5p can deregulate the cell cycle, via downregulation of the two TSGs, LIMD1 and VHL, eventually culminating in HIF-1 α accumulation and aid in G1-S transition. At first, SiHa cells were synchronized at G0/G1 phase by double thymidine block (**Figure 5.6A and 5.6B**). A significant arrest ($p=0.002$) was observed in G0/G1 phase upon treatment with double thymidine (**Figure 5.6A and 5.6B**). The synchronized cells were transfected separately with anti-miR-135b-5p and anti-miR-21-5p. Interestingly, a significant increase ($p=0.024$ and $p=0.029$, respectively) in the number of cells in the G1 phase was observed, indicating G1-S cell cycle arrest (**Figure**

5.6C and 5.6D). This observation was further validated by significantly decreased cyclin D1 protein expression ($p=0.048$ and $p=0.027$, respectively) in the cells, upon treatment with anti-miR-135b-5p and anti-miR-21-5p, compared to the control cells (**Figure 5.6E and 5.6F**). This data indicates that miR-135b-5p and miR-21-5p promote cellular proliferation.

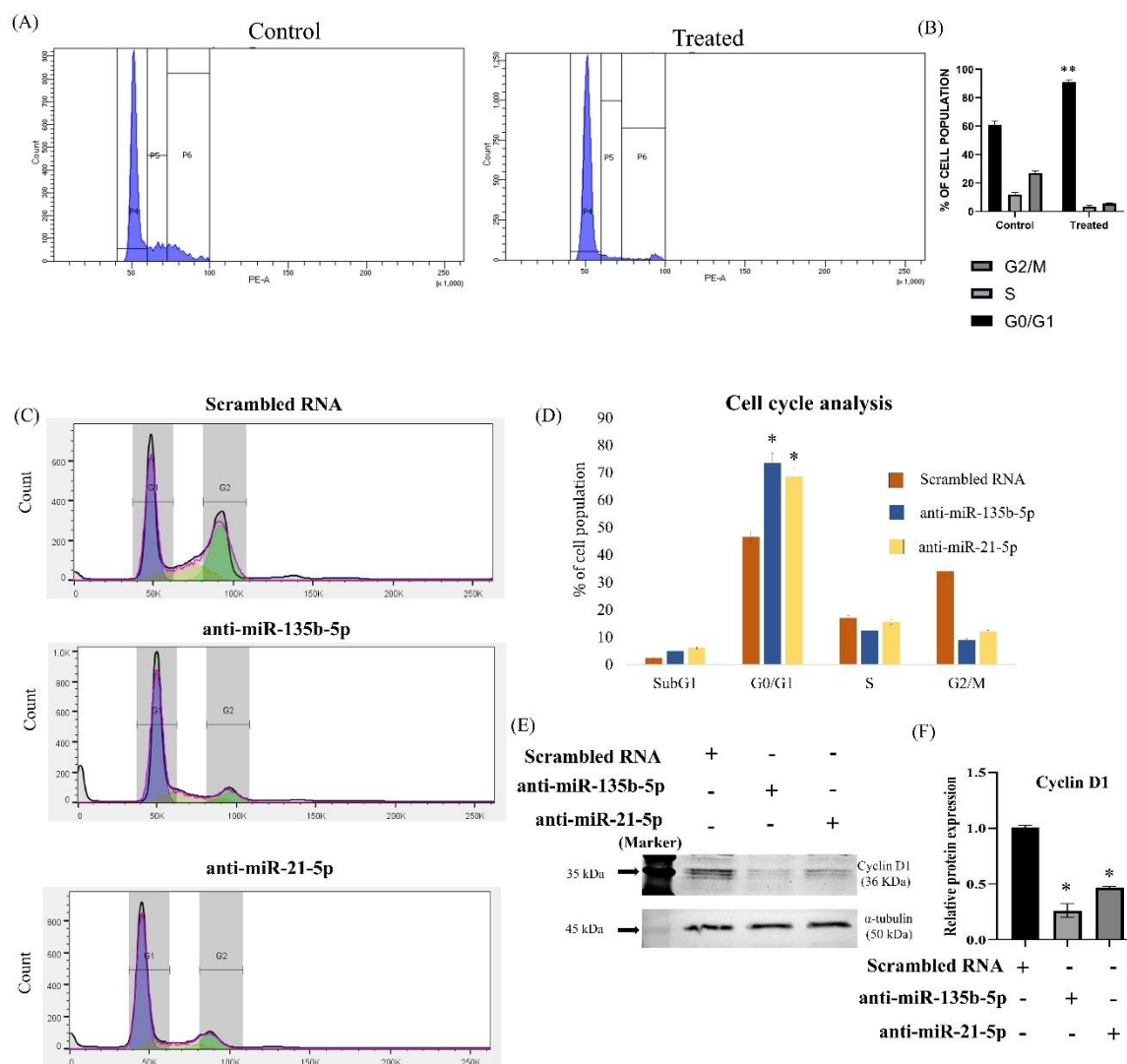


Figure 5.6 Influence of miR-135b-5p and miR-21-5p Inhibition on the SiHa Cell Cycle: (A-B) Cell cycle progression was evaluated using flow cytometry following double thymidine synchronization. (C) Post-synchronization, cells were transfected with anti-miR-135b, anti-miR-21-5p, or anti-miR-NC and analyzed for cell cycle distribution using flow cytometry. (D) A histogram presents the percentage of cells in different phases of the cell cycle. (E) Western blot analysis was performed to assess Cyclin D1 protein expression, using α -tubulin as a loading control. (F) Cyclin D1 protein band intensities were quantified using ImageJ software and normalized to α -tubulin. (All data are shown as the mean \pm standard deviation (SD), with error bars representing SD; *, **, and *** denote statistically significant p -values of < 0.05 , < 0.01 , and < 0.001 , respectively.)

5.4.5 Effect of anti-miR-135b-5p and anti-miR-21-5p on the apoptosis of SiHa cells:

To further analyze the effect of miR-135b-5p and miR-21-5p on the apoptosis of the SiHa cells, annexin V/propidium iodide (PI) staining and flow cytometry analysis were conducted. After transfection of anti-miR-135b-5p and anti-miR-21-5p, the percentages of total apoptotic cell numbers (both early and late apoptotic) were significantly increased ($p=0.017$ and $p=0.03$, respectively) compared to the scrambled-RNA treated cells (**Figure 5.7A and 5.7B**). Interestingly, dual inhibition of the two miRNAs showed a further significant increase ($p=0.007$) in cellular apoptosis, compared to the control cells (**Figure 5.7A and 5.7B**). Together, these data indicate that SiHa cells with individual upregulation of miR-135b-5p and miR-21-5p escape apoptosis, and this cellular phenotype is more prominent upon combined upregulation of the two miRNAs. Conversely, the downregulation of miR-135b-5p and miR-21-5p showed a significant decrease in ($p=0.002$ and $p=0.001$, respectively) SiHa cell viability by MTT assay, compared to the control cells (**Figure 5.7C**). Notably, SiHa cells showed greater reduction ($p=0.008$) in viability upon dual inhibition of miR-135b-5p and miR-21-5p (**Figure 5.7C**), corroborated with cellular apoptosis data discussed previously. Additionally, a significant upregulation of proapoptotic Bax ($p=0.008$ and $p=0.011$, respectively), down expression of anti-apoptotic Bcl-2 ($p=0.002$ and $p=0.014$, respectively) and a significant increase in Bax/Bcl-2 ratio ($P=0.008$ and $p=0.027$, respectively) were observed when the cells were treated with anti-miR-135b-5p and anti-miR-21-5p (**Figures 5.7D, 5.7E and 5.7F**). Moreover, dual inhibition of these two miRNAs resulted in a more pronounced increase in Bax expression ($p=0.021$), a greater reduction in Bcl-2 expression ($p=0.0004$) and a further increase in Bax/Bcl-2 ratio ($p=0.03$) compared to the control cells (**Figures 5.7D, 5.7E and 5.7F**). Thus, our findings suggest that SiHa cells upregulating miR-135b-5p and miR-21-5p can effectively escape cellular apoptosis.

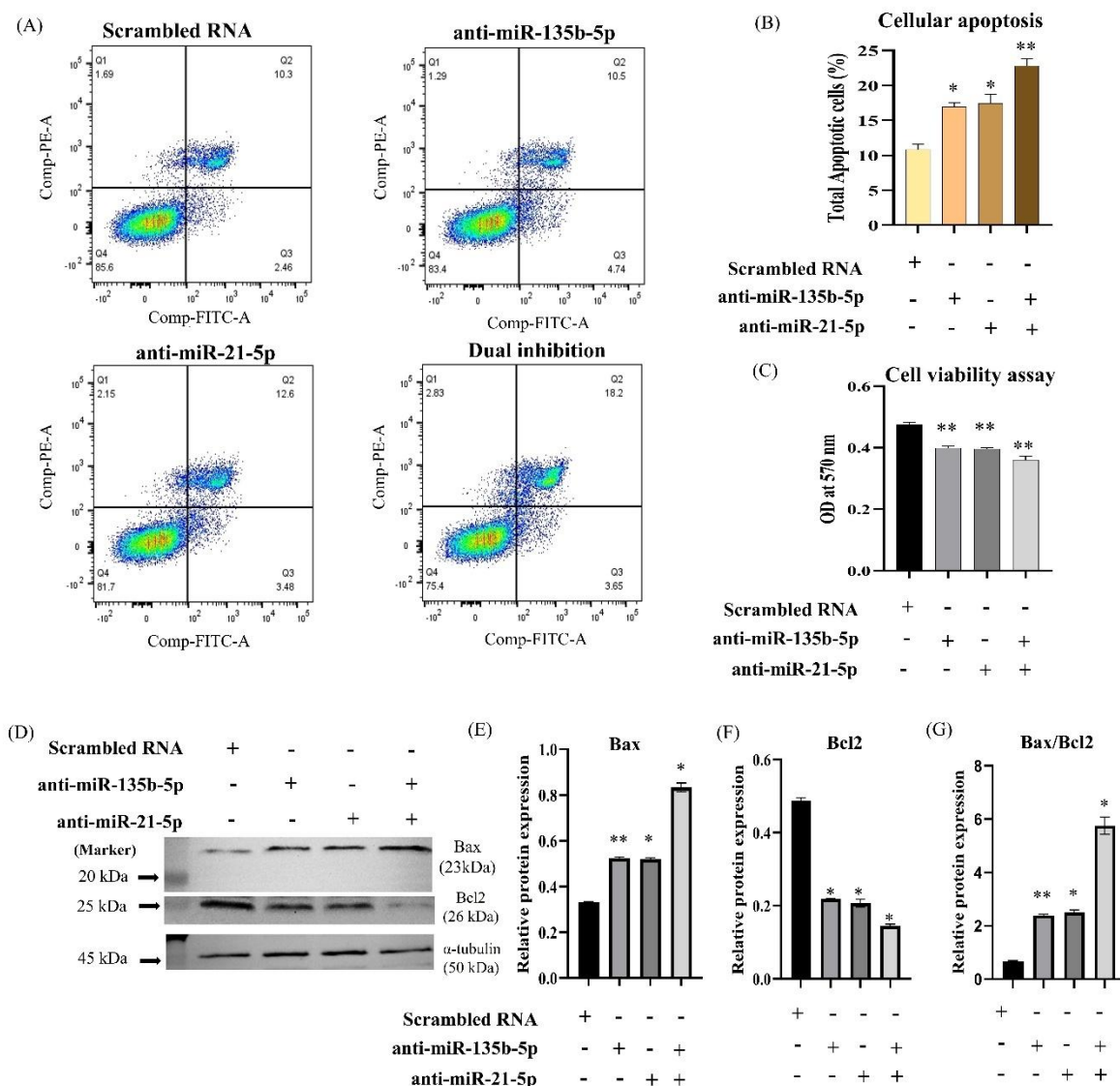


Figure 5.7 Effect of miR-135b-5p and miR-21-5p Inhibition on Apoptosis in SiHa Cells: SiHa cells were transfected with anti-miR-135b, anti-miR-21-5p, or anti-miR-NC to examine their impact on apoptosis. (A) Flow cytometry was used to analyze apoptotic cells. (B) A bar graph quantifies the total number of apoptotic cells (early and late apoptosis) using FlowJo software. (C) An MTT assay was performed to determine cell viability, with a bar graph illustrating the proportion of viable cells. (D) Western blot analysis was conducted to assess the expression of Bax and Bcl-2 proteins, using α -tubulin as a loading control. (E-G) Histograms depict the relative expression levels of (E) Bax, (F) Bcl-2, and (G) the Bax/Bcl-2 ratio. Band intensities were measured using Image-J software and normalized to α -tubulin. (All data are presented as the mean \pm SD, with error bars representing SD; *, **, and *** denote statistically significant p-values of < 0.05 , < 0.01 , and < 0.001 , respectively.)

5.4.6 Effect of anti-miR-135b-5p and anti-miR-21-5p on the epithelial-mesenchymal transition (EMT) in SiHa cells:

Owing to the above observations, it was pertinent to test if miR-135b-5p and miR-21-5p upregulation can further contribute to aggressive malignant phenotypes viz. cellular migration and invasion. The knockdown of miR-135b-5p and miR-21-5p, individually, showed significantly lower wound healing [wound size (%)] capability ($p=0.004$ and $p=0.002$ at 48 hours, respectively) of the SiHa cells compared to the control (**Figure 5.8A and 5.8B**). Interestingly, when the cells were treated with both inhibitors, wound healing capability decreased significantly with progression of time ($p=0.003$ at 24 hours and $p=0.0004$ at 48 hours) (**Figure 5.8A and 5.8B**). Furthermore, the SiHa cells lost their invasiveness when treated with anti-miR-135b-5p and anti-miR-21-5p inhibitors, as we observed significantly fewer cells ($p=0.016$ and $p=0.021$, respectively) at the bottom of the chambers from the invasion assay (**Figure 5.8C and 5.8D**). More interestingly, dual inhibition of miR-135b-5p and miR-21-5p caused a greater decrease ($p=0.004$) in the number of invasive cells than the individual miRNA inhibition (**Figure 5.8C and 5.8D**).

To further verify the effect of miR-135b-5p, and miR-21-5p in the EMT transition of SiHa cells, the expression of the principal key EMT markers were evaluated. Our data confirmed the up-regulation of epithelial marker E-cadherin ($p=0.021$, $p=0.013$, and $p=0.0385$, respectively) and down-expression of mesenchymal marker N-cadherin ($p=0.036$, $p=0.04$ and $p=0.018$, respectively) when the cells were treated with anti-miR-135b-5p, anti-miR-21-5p, individually and in combination by immunoblotting, suggesting a reduction of EMT (**Figures 5.8E-5.8G**). Together, this data indicated that miR-135b-5p and miR-21-5p promote the EMT transition of SiHa cells.

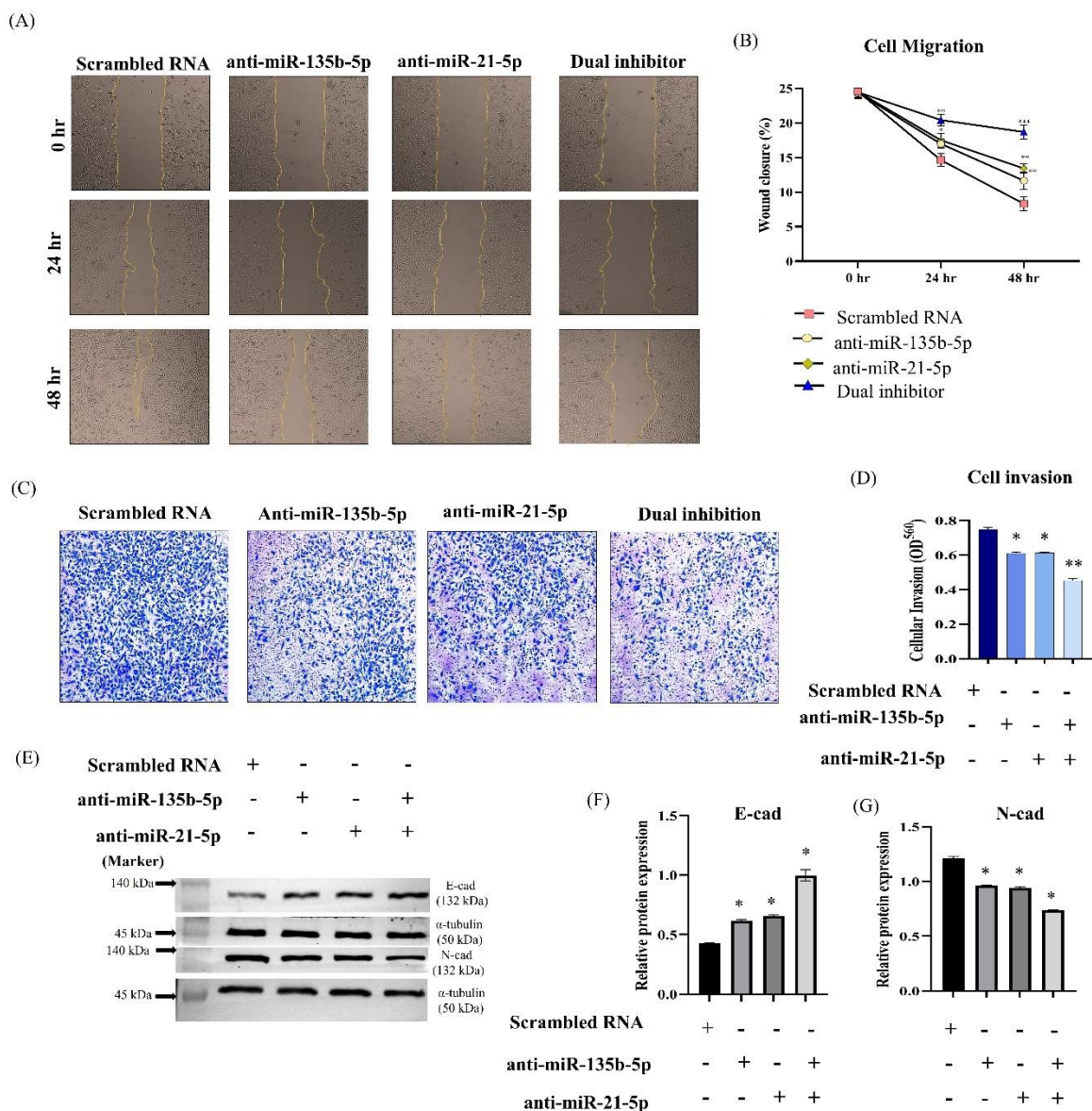


Figure 5.8 Influence of miR-135b-5p and miR-21-5p Suppression on Epithelial-Mesenchymal Transition (EMT) in SiHa Cells: SiHa cells were transfected with anti-miR-135b, anti-miR-21-5p, or anti-miR-NC to examine their effects on EMT. (A) A wound healing assay was performed at 0, 24, and 48 hours to evaluate cell migration. (B) A dot plot represents the wound closure rate after transfection with anti-miR-135b, anti-miR-21-5p, or anti-miR-NC. (C) Cell invasion was assessed using the CytoSelect™ 24-Well Cell Invasion Assay Kit. (D) A bar graph quantifies the number of invasive cells. (E) Western blot analysis was used to evaluate the expression of E-cadherin and N-cadherin, with α -tubulin serving as a loading control. (F-G) The relative band intensities of (F) E-cadherin and (G) N-cadherin were measured using ImageJ software and normalized to α -tubulin. (All data are shown as the mean \pm SD, with error bars representing SD; *, **, and *** indicate statistically significant p-values of < 0.05 , < 0.01 , and < 0.001 , respectively.)

5.4.7 Effect of anti-miR-135b-5p and anti- miR-21-5p on the expression of HIF-1 α target genes expression:

As HIF-1 α expression becomes altered, it was postulated that HIF-1 α target genes may become deregulated following transfection with inhibitors against these two miRNAs. Immunoblot analysis demonstrated a significant decrease in the expression of the downstream angiogenic factor VEGF ($p = 0.025$, $p = 0.023$, and $p = 0.021$, respectively) when cells were treated with anti-miR-135b-5p, anti-miR-21-5p, or the dual inhibition of both miRNAs, compared to control cells (**Figure 5.9A and 5.9B**). Additionally, a significant down-expression of other HIF-1 α target genes that could be used as tumor markers, such as growth factor, TGF- α ($p=0.037$ and $p=0.048$, respectively), proteolysis marker of extracellular matrix wound healing maker, MMP9 ($p=0.034$ and $p=0.016$, respectively); and G1-S cell cycle marker, Cyclin D1 ($p=0.008$ and $p=0.007$, respectively) showed significant down-expression following treatment with anti-miR-135b-5p or anti-miR-21-5p (**Figure 5.9C-5.9E**). A more pronounced decrease in the expression of TGF-1 α ($p=0.033$), MMP9 ($p=0.032$), and Cyclin D1 ($p=0.008$) mRNA was observed with the dual inhibition of these two miRNAs (**Figure 5.9C-5.9E**). Together, this data indicated that miR-135b-5p and miR-21-5p promote cervical cancer progression by inducing HIF-1 α target gene expression.

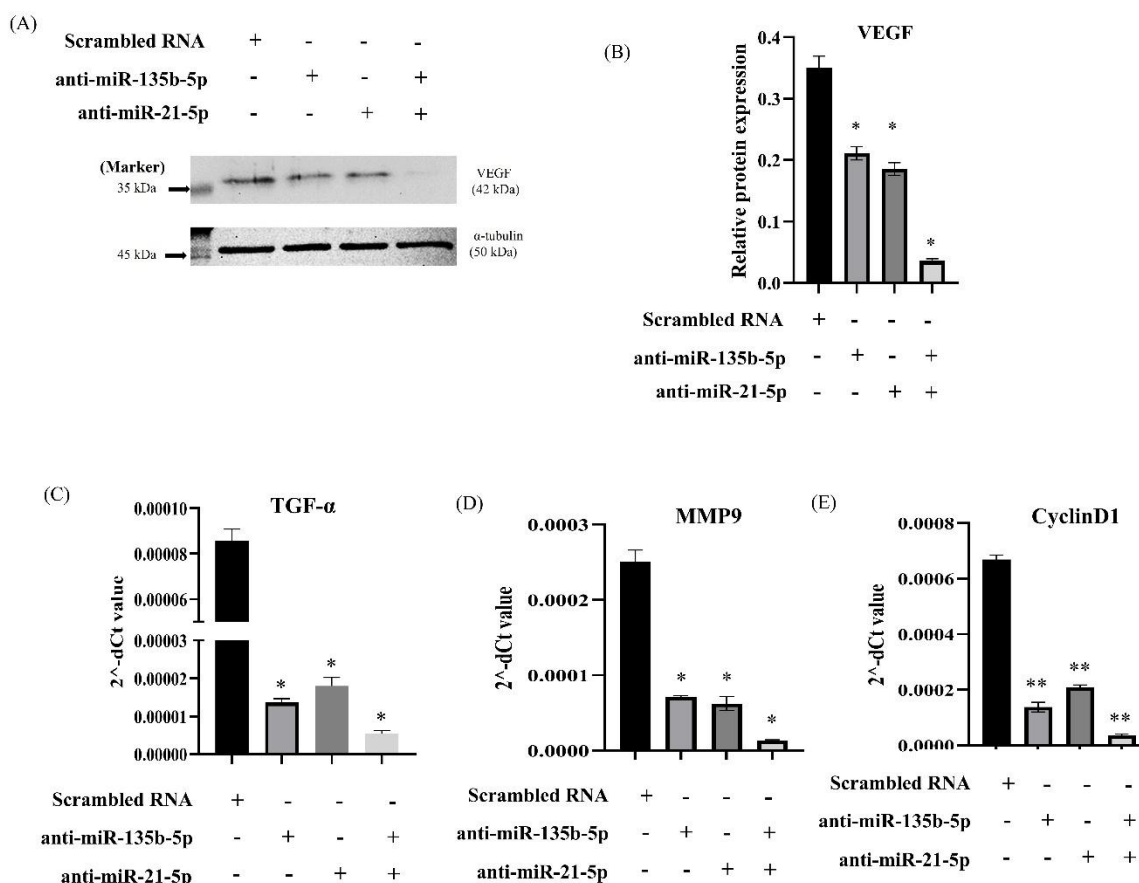


Figure 5.9 Role of miR-135b-5p and miR-21-5p Inhibition in HIF-1 α Target Gene Expression: SiHa cells were transfected with anti-miR-135b, anti-miR-21-5p, or anti-miR-NC to investigate their effects on HIF-1 α target gene expression. (A) VEGF protein expression was analyzed using Western blot, with α -tubulin as a loading control. (B) Band intensities of VEGF were quantified using ImageJ software and normalized to α -tubulin. (C-E) Bar plots display the $2^{-\Delta\text{Ct}}$ values for (C) TGF- α , (D) MMP9, and (E) Cyclin D1 mRNA, with B2M used as an endogenous control. (All data are shown as the mean \pm SD, with error bars representing SD; *, **, and *** indicate statistically significant p -values of < 0.05 , < 0.01 , and < 0.001 , respectively).

5.5 Discussion:

In this study, we demonstrated that anti-miR treatment targeting these miRNAs reduced the metastatic phenotypes of SiHa cells (**Figure 5.10**), offering new insights into the oncogenic roles of miR-135b-5p and miR-21-5p in regulating the LIMD1-VHL-HIF-1 α pathway.

Consistent with previous reports [Chakraborty et al., 2018; Xu et al., 2015; Cai et al., 2018], we confirm that LIMD1 and VHL are downregulated by their respective targeting miRNAs, miR-135b-5p and miR-21-5p, in SiHa cells, as demonstrated by a luciferase reporter assay (**Figure 5.3**). The mechanisms driving tumor initiation and progression are complex and multifactorial, with uncontrolled cell proliferation being a hallmark of malignancy [Swanton et al., 2024]. Investigating molecular mechanisms that disrupt the balance between cell

proliferation and apoptosis provides critical insights for developing targeted therapeutic strategies.

We observed that anti-miR-135b-5p treatment induced G0/G1 cell cycle arrest (**Figure 5.6**), likely due to the restoration of LIMD1, a key tumor suppressor known to stabilize the pRB-E2F interaction, thereby repressing E2F-mediated transcription [Sharp et al., 2004]. Similarly, VHL upregulation following anti-miR-21-5p treatment also induced G0/G1 arrest (**Figure 5.6C and 5.6D**), likely due to HIF-1 α destabilization, which in turn reduced transcription of its downstream target gene CCND1 (cyclin D1) [Wen et al., 2010]. These findings correlate with increased proliferation (**Figure 5.5**) and reduced apoptosis (**Figure 5.7**) in SiHa cells following miR-135b-5p and miR-21-5p upregulation.

Furthermore, knockdown of miR-135b-5p and miR-21-5p reduced the aggressiveness of SiHa cells, as evidenced by increased E-cadherin and decreased N-cadherin expression (**Figure 5.8**), consistent with previous reports [Xu et al., 2015; Cai et al., 2018]. This effect is likely mediated through HIF-1 α destabilization, leading to reduced transcription of Snail and Slug, direct repressors of CDH1 (E-cadherin). Simultaneously, HIF-1 α destabilization reduces CDH2 (N-cadherin) expression, thereby inhibiting epithelial-to-mesenchymal transition (EMT) and reducing the invasive potential of tumor cells (Tam et al., 2020; Shen et al., 2024). Additionally, downregulation of miR-135b-5p and miR-21-5p reduces the expression of other HIF-1 α target genes—VEGF, TGF- α , MMP9, and CCND1 (cyclin D1)—which are known to drive cancer progression (**Figure 5.9**) [Wen et al., 2010; Unwith et al., 2015].

Although previous studies have reported both oncogenic and tumor-suppressive roles of miR-135b-5p in various cancers, including gastric [Lu et al., 2017], esophageal [Di et al., 2021], colorectal [Zhang et al., 2022], pancreatic [Zhang et al., 2017], and breast [Pu et al., 2019] cancers, miR-21-5p has been consistently recognized as an oncogene across multiple malignancies [Tang et al., 2021; Cao et al., 2021; Luo et al., 2020], including cervical cancer [Cai et al., 2018]. While the oncogenic function of miR-135b-5p in cervical cancer has previously been attributed to FOXO1 targeting [Xu et al., 2015], our study expands on this by elucidating its role in LIMD1 regulation. Although miR-21-5p-mediated VHL repression has been previously reported in cervical cancer [Cai et al., 2018], our study is the first to comprehensively detail its functional role, particularly highlighting its downstream effects on HIF-1 α regulation.

In conclusion, miR-135b-5p and miR-21-5p function as dual oncomiRs by downregulation of LIMD1 and VHL along with stabilization of HIF-1 α protein, resulting in enhanced cellular proliferation and migration as well as reduction of apoptosis to promote cervical carcinogenesis.

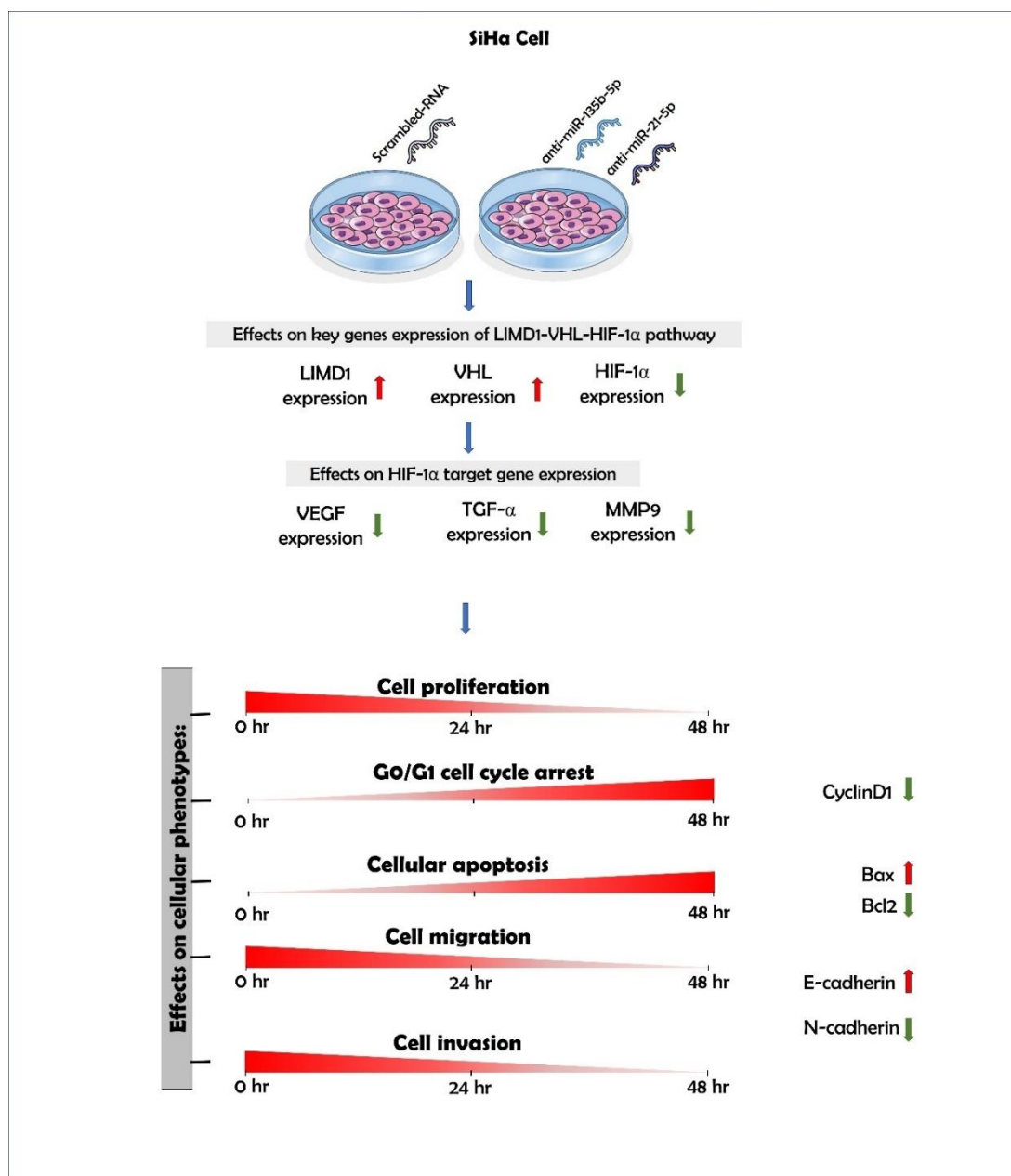


Figure 5.10 A schematic illustration depicting the impact of miR-135b-5p and miR-21-5p inhibition on cervical cancer metastasis through the LIMD1-VHL-HIF-1A pathway. In the diagram, a red upward arrow signifies upregulation, while a green downward arrow represents downregulation.

5.6 Inference points:

- i. miR-135b-5p and miR-21-5p, independently and synergistically exerts its regulatory effect on the LIMD1-VHL-HIF-1 α pathway, thereby, promote cervical cancer metastasis by driving cellular proliferation, transformed cell migration, and invasion, while simultaneously suppressing cellular apoptosis.
- ii. Thus, miR-135b-5p and miR-21-5p acts as oncomiR during cervical carcinogenesis.

CHAPTER 6

General Discussion

Chapter 6

General Discussion

Cervical cancer (CaCx) remains a significant public health concern, particularly in low- and middle-income countries (LMICs), where limited access to early detection and treatment contributes to high mortality rates [Hull et al., 2020]. Persistent infection with high-risk human papillomavirus (HR-HPV) is a prerequisite for CaCx development [Doorbar et al., 2006; Wright et al., 2013; Dueñas-González et al., 2005]. HR-HPV-induced stabilization of hypoxia-inducible factor-1 alpha (HIF-1 α) plays a crucial role in tumor progression by regulating angiogenic factors that promote tumor growth [Ziello et al., 2007]. Under normoxic conditions, HIF-1 α is regulated by the tumor suppressor genes (TSGs) LIMD1 and VHL (described in **section 1.3.1**) [Foxler et al., 2012], which are frequently altered in cervical cancer. While reduced expression of LIMD1 and VHL is often attributed to promoter methylation and genetic deletions, some CaCx samples exhibit low expression of these genes without detectable promoter methylation and genetic deletions [Chakraborty et al., 2018], suggesting the involvement of additional regulatory mechanisms, not yet explored.

Given the pivotal role of the LIMD1-VHL-HIF-1 α pathway in HR-HPV-induced cervical carcinogenesis, we hypothesize that miRNAs targeting these two key TSGs (LIMD1 and VHL) could serve as triage biomarkers for distinguishing HR-HPV+ve pre-malignant lesions, such as CIN II+/HSIL, from less severe stages. This approach could address critical gaps in CaCx screening protocols while also elucidating the molecular mechanisms underlying the deregulation of the LIMD1-VHL-HIF-1 α pathway in cervical carcinogenesis, which remain inadequately documented.

Through *in silico* analysis, this study first identifies miR-135b-5p and miR-21-5p as candidate miRNAs upregulated in CaCx, that target two important TSGs, LIMD1 and VHL, respectively (as discussed in Chapter 3 and Figure 3.6) [**Figure 6.1A**]. We showed that the overexpression of miR-135b-5p and miR-21-5p correlates with the progressive stages of cervical lesion severity, from normal epithelium to CIN to CaCx (as shown in Chapter 3 and Figure 3.8)

[**Figure 6.1B**]. We also explored the genetic mechanisms underpinning upregulation of miR-135b-5p, identifying amplification of MIR135B locus as a primary driver. This novel finding extends our understanding of miRNA regulation in CaCx and reinforces the value of integrating genomic data with functional assays (as evident from Chapter 3 and Figure 3.7) [**Figure 6.1B**].

Moreover, through validation in a large cohort of cervical swabs (N=243), we revealed consistent overexpression of these miRNAs and under-expression of their target genes (LIMD1 and VHL) in HR-HPV+ve HSIL compared to earlier clinical stages (as discussed in Chapter 4 and Figure 4.5) [**Figure 6.1C**]. This underscores the potential of miR-135b-5p and miR-21-5p as triage biomarkers capable of distinguishing LSIL from HSIL, addressing an area where current diagnostic tools often lack precision. While miR-21-5p has been widely reported as an oncogenic miRNA in multiple cancers [Qu et al., 2017; Gao et al., 2016], including CaCx [Okoye et al., 2019; Wang et al., 2019], the combined use of miR-21-5p and miR-135b-5p in our study represents a novel approach. Although miR-21-5p alone exhibited moderate specificity (78.8%) for distinguishing HR-HPV+ve HSIL from LSIL, the addition of miR-135b-5p significantly improved specificity (94%) and sensitivity (90.4%) (**Figure 6.1D**), demonstrating their effectiveness as triage biomarkers through this study (as shown in Chapter 4, Figure 4.6 and Table 4.3) [**Figure 6.1E**]. The use of exfoliated cervical cells rather than tissue biopsies or other body fluids (e.g., serum, urine) highlights the practical and scalable nature of this approach, particularly in population-level screening programme as it provides a precise and non-invasive diagnostic option [Xin et al., 2016; Aftab et al., 2021; Kawai et al., 2018; Ivanov et al., 2018]. Additionally, we introduced a novel sensor-oligo-based fluorescence detection technique for miR-135b-5p by following Yoo et al., 2014, enabling rapid and sensitive detection of miR-135b-5p in both cell lines and exfoliated cells of cervical swabs (as described in Chapter 4 and Figure 4.8) [**Figure 6.1F**]. Hence, our pilot study on novel sensor oligo-based miR-135b-5p detection in clinical settings indicates a significant contribution in high-throughput cervical cancer screening and precise clinical decision.

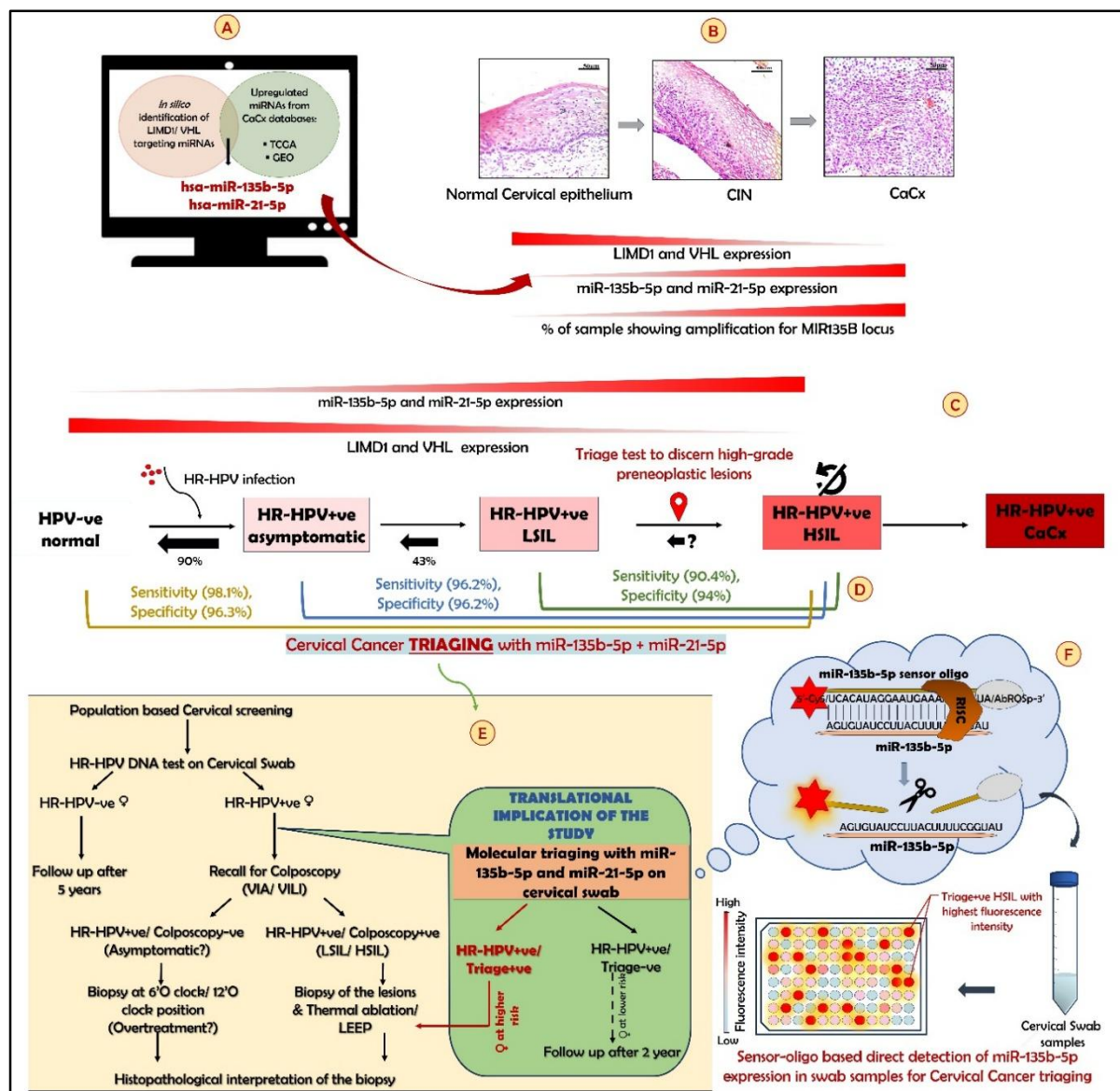


Figure 6.1: The application of miR-135b-5p and miR-21-5p in triaging HR-HPV+ve samples: (A) In silico identification of LIMD1/ VHL targeting upregulated miRNAs, miR-135b-5p and miR-21-5p, in CaCx. (B) Gradual down regulation of LIMD1/VHL and upregulation of their targeting miR-135b-5p/ miR-21-5p expression as well as increasing (%) of samples showing amplification of MIR135B locus during development of CaCx. (C) Validation of miR-135b-5p/ miR-21-5p expression and their targeting LIMD1/ VHL expression in different clinical stages of cervical swab samples. (D) Combined sensitivity and specificity of miR-135b-5p and miR-21-5p to discern HR-HPV+ve HSIL from earlier clinical stages. (E) Molecular triaging with miR-135b-5p and miR-21-5p on cervical swabs (F) Sensor-oligo based direct detection of miR-135b-5p expression in swab samples for CaCx screening.

The dual oncogenic role of miR-135b-5p and miR-21-5p, on the other hand, in modulating the LIMD1-VHL-HIF-1 α pathway provided deeper insights into HR-HPV-induced cervical carcinogenesis. Therefore, we have analyzed the mechanistic role of these two miRNAs in regulating two key TSGs (LIMD1 and VHL) during the progression of CaCx. This analysis demonstrates the impact of these miRNAs on CaCx cell proliferation, invasion, migration, and apoptosis. Dual inhibition of miR-135b-5p and miR-21-5p resulted in G0/G1 cell cycle arrest through the restoration of LIMD1 and VHL expression, enhanced apoptosis, reduced migration, and invasion of CaCx cells (as discussed in Chapter 5) [Figure 6.2A, B]. These effects were mediated by the downregulation of HIF-1 α target genes, including VEGF, MMP9, TGF- α and cyclin D1, elucidating their roles in CaCx progression. Experimental validation through dual-luciferase assays confirmed LIMD1 as direct target of miR-135b-5p, further strengthening the mechanistic understanding of their role in cervical carcinogenesis (as shown in Chapter 5, Figure 5.3).

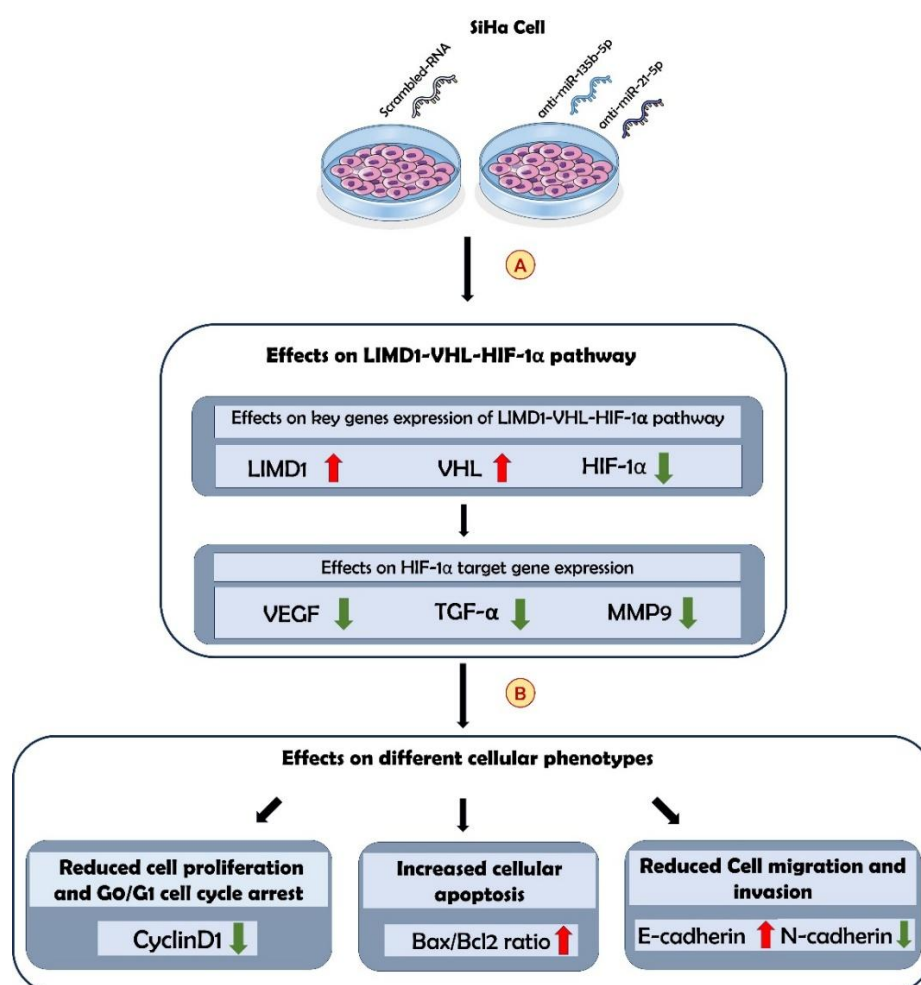


Figure 6.2 Knock down of miR-135b-5p and miR-21-5p on SiHa cells by anti-miR treatment: (A) Effect on LIMD1-VHL-HIF-1 α pathway (B) Effect on different cellular phenotypes of SiHa cells

To conclude, this study identifies miR-135b-5p and miR-21-5p as oncomiRs that drive a more aggressive cervical cancer phenotype by promoting metastasis through HIF-1 α stress response pathway via LIMD1 and VHL deregulation. On the other hand, miR-135b-5p and miR-21-5p could be used as promising triage biomarkers for HR-HPV+ve CIN II+/HSIL detection, particularly in low-resource settings. The novel insights into their mechanistic role in cervical lesion progression and the development of a rapid detection method underscore their translational potential. This dual biomarker strategy bridges the gap between basic research and clinical application, paving the way for more effective, personalized approaches to CaCx management. These two candidate miRNAs could be further investigated for their involvement in additional cellular pathways contributing to cervical carcinogenesis, potentially uncovering new therapeutic targets. Moreover, the sensor-oligo-based technique could be refined and validated for use with other non-invasive sample types, broadening its application in clinical diagnostics and precision medicine. This approach may enhance early detection strategies and personalized treatment options, ultimately improving cervical cancer management and patient outcomes.

REFERENCES

- Aftab, M., Poojary, S. S., Seshan, V., Kumar, S., Agarwal, P., Tandon, S., ... & Das, B. C. (2021). Urine miRNA signature as a potential non-invasive diagnostic and prognostic biomarker in cervical cancer. *Scientific reports*, 11(1), 10323.
- Akagi, K., Li, J., Broutian, T. R., Padilla-Nash, H., Xiao, W., Jiang, B., ... & Gillison, M. L. (2014). Genome-wide analysis of HPV integration in human cancers reveals recurrent, focal genomic instability. *Genome research*, 24(2), 185-199.
- Alles, J., Fehlmann, T., Fischer, U., Backes, C., Galata, V., Minet, M., ... & Meese, E. (2019). An estimate of the total number of true human miRNAs. *Nucleic acids research*, 47(7), 3353-3364.
- Amin, M. A., & Varma, D. (2017). Combining mitotic cell synchronization and high resolution confocal microscopy to study the role of multifunctional cell cycle proteins during mitosis. *JoVE (Journal of Visualized Experiments)*, (130), e56513.
- Arbyn, M., Ronco, G., Anttila, A., Meijer, C. J., Poljak, M., Ogilvie, G., ... & Peto, J. (2012). Evidence regarding human papillomavirus testing in secondary prevention of cervical cancer. *Vaccine*, 30, F88-F99.
- Babion, I., Jaspers, A., van Splunter, A. P., van der Hoorn, I. A., Wilting, S. M., & Steenbergen, R. D. (2019). miR-9-5p exerts a dual role in cervical cancer and targets transcription factor TWIST1. *Cells*, 9(1), 65.
- Babion, I., Snoek, B. C., Novianti, P. W., Jaspers, A., van Trommel, N., Heideman, D. A., ... & Wilting, S. M. (2018). Triage of high-risk HPV-positive women in population-based screening by miRNA expression analysis in cervical scrapes; a feasibility study. *Clinical epigenetics*, 10, 1-10.
- Baker, T. S., Newcomb, W. W., Olson, N. H., Cowser, L. M., Olson, C., & Brown, J. (1991). Structures of bovine and human papillomaviruses. Analysis by cryoelectron microscopy and three-dimensional image reconstruction. *Biophysical journal*, 60(6), 1445-1456.
- Banks, R. E., Tirukonda, P., Taylor, C., Hornigold, N., Astuti, D., Cohen, D., ... & Selby, P. J. (2006). Genetic and epigenetic analysis of von Hippel-Lindau (VHL) gene alterations and relationship with clinical variables in sporadic renal cancer. *Cancer research*, 66(4), 2000-2011.

- Bao, W., Wang, H. H., Tian, F. J., He, X. Y., Qiu, M. T., Wang, J. Y., ... & Wan, X. P. (2013). A TrkB–STAT3–miR-204-5p regulatory circuitry controls proliferation and invasion of endometrial carcinoma cells. *Molecular cancer*, 12, 1-19.
- Basu, P., Muwonge, R., Mittal, S., Banerjee, D., Ghosh, I., Panda, C., ... & Sankaranarayanan, R. (2016). Implications of semi-quantitative HPV viral load estimation by Hybrid capture 2 in colposcopy practice. *Journal of medical screening*, 23(2), 104-110.
- Behm-Ansmant, I., Rehwinkel, J., Doerks, T., Stark, A., Bork, P., & Izaurralde, E. (2006). mRNA degradation by miRNAs and GW182 requires both CCR4: NOT deadenylase and DCP1: DCP2 decapping complexes. *Genes & development*, 20(14), 1885-1898.
- Bergeron, C., Ronco, G., Reuschenbach, M., Wentzensen, N., Arbyn, M., Stoler, M., & von Knebel Doeberitz, M. (2015). The clinical impact of using p16INK4a immunochemistry in cervical histopathology and cytology: An update of recent developments. *International journal of cancer*, 136(12), 2741-2751.
- Bhatla, N., Lal, N., Bao, Y. P., Ng, T., & Qiao, Y. L. (2008). A meta-analysis of human papillomavirus type-distribution in women from South Asia: implications for vaccination. *Vaccine*, 26(23), 2811-2817.
- Bhattacharya, N., Singh, R. K., Mondal, S., Roy, A., Mondal, R., Roychowdhury, S., & Panda, C. K. (2004). Analysis of molecular alterations in chromosome 8 associated with the development of uterine cervical carcinoma of Indian patients. *Gynecologic oncology*, 95(2), 352-362.
- Bierkens, M., Hesselink, A. T., Meijer, C. J., Heideman, D. A., Wisman, G. B. A., van der Zee, A. G., ... & Steenbergen, R. D. (2013). CADM1 and MAL promoter methylation levels in hrHPV-positive cervical scrapes increase proportional to degree and duration of underlying cervical disease. *International journal of cancer*, 133(6), 1293-1299.
- Bodily, J. M., Mehta, K. P., & Laimins, L. A. (2011). Human papillomavirus E7 enhances hypoxia-inducible factor 1-mediated transcription by inhibiting binding of histone deacetylases. *Cancer research*, 71(3), 1187-1195.
- Bonde, J., Floore, A., Ejegod, D., Vink, F. J., Hesselink, A., van de Ven, P. M., ... & Heideman, D. A. (2021). Methylation markers FAM19A4 and miR124-2 as triage strategy for primary

human papillomavirus screen positive women: a large European multicenter study. *International journal of cancer*, 148(2), 396-405.

Boon, S. S., Luk, H. Y., Xiao, C., Chen, Z., & Chan, P. K. S. (2022). Review of the standard and advanced screening, staging systems and treatment modalities for cervical cancer. *Cancers*, 14(12), 2913

Braun, J. E., Huntzinger, E., Fauser, M., & Izaurralde, E. (2011). GW182 proteins directly recruit cytoplasmic deadenylase complexes to miRNA targets. *Molecular cell*, 44(1), 120-133.

Bray, F., Laversanne, M., Sung, H., Ferlay, J., Siegel, R. L., Soerjomataram, I., & Jemal, A. (2024). Global cancer statistics 2022: GLOBOCAN estimates of incidence and mortality worldwide for 36 cancers in 185 countries. *CA: a cancer journal for clinicians*, 74(3), 229-263.

Bruning, U., Cerone, L., Neufeld, Z., Fitzpatrick, S. F., Cheong, A., Scholz, C. C., ... & Taylor, C. T. (2011). MicroRNA-155 promotes resolution of hypoxia-inducible factor 1 α activity during prolonged hypoxia. *Molecular and cellular biology*, 31(19), 4087-4096.

Bumrunghai, S., Ekalaksananan, T., Evans, M. F., Chopjitt, P., Tangsiriwatthana, T., Patarapadungkit, N., ... & Pientong, C. (2015). Up-regulation of miR-21 is associated with cervicitis and human papillomavirus infection in cervical tissues. *PloS one*, 10(5), e0127109.

Cai, L., Wang, W., Li, X., Dong, T., Zhang, Q., Zhu, B., ... & Wu, S. (2018). MicroRNA-21-5p induces the metastatic phenotype of human cervical carcinoma cells in vitro by targeting the von Hippel-Lindau tumor suppressor. *Oncology letters*, 15(4), 5213-5219.

Campos-Viguri, G. E., Peralta-Zaragoza, O., Jiménez-Wences, H., Longinos-González, A. E., Castañón-Sánchez, C. A., Ramírez-Carrillo, M., ... & Fernández-Tilapa, G. (2020). MiR-23b-3p reduces the proliferation, migration and invasion of cervical cancer cell lines via the reduction of c-Met expression. *Scientific reports*, 10(1), 3256.

Cao, J., Zhang, Y., Mu, J., Yang, D., Gu, X., & Zhang, J. (2021). Exosomal miR-21-5p contributes to ovarian cancer progression by regulating CDK6. *Human Cell*, 34, 1185-1196.

Caraway, N. P., Khanna, A., Dawlett, M., Guo, M., Guo, N., Lin, E., & Katz, R. L. (2008). Gain of the 3q26 region in cervicovaginal liquid-based pap preparations is associated with squamous intraepithelial lesions and squamous cell carcinoma. *Gynecologic Oncology*, 110(1), 37-42.

- Cha, S. T., Chen, P. S., Johansson, G., Chu, C. Y., Wang, M. Y., Jeng, Y. M., ... & Kuo, M. L. (2010). MicroRNA-519c suppresses hypoxia-inducible factor-1 α expression and tumor angiogenesis. *Cancer research*, 70(7), 2675-2685.
- Chakraborty, C., Mitra, S., Roychowdhury, A., Samadder, S., Dutta, S., Roy, A., ... & Panda, C. K. (2018). Deregulation of LIMD1–VHL–HIF-1 α –VEGF pathway is associated with different stages of cervical cancer. *Biochemical Journal*, 475(10), 1793-1806.
- Chen, C. Y. A., Zheng, D., Xia, Z., & Shyu, A. B. (2009). Ago–TNRC6 triggers microRNA-mediated decay by promoting two deadenylation steps. *Nature structural & molecular biology*, 16(11), 1160-1166.
- Chen, J., Yao, D., Zhao, S., He, C., Ding, N., Li, L., & Long, F. (2014). MiR-1246 promotes SiHa CaCx cell proliferation, invasion, and migration through suppression of its target gene thrombospondin 2. *Archives of gynecology and obstetrics*, 290, 725-732.
- Chen, Y., Song, Y., Mi, Y., Jin, H., Cao, J., Li, H., ... & Zou, Z. (2020). microRNA-499a promotes the progression and chemoresistance of cervical cancer cells by targeting SOX6. *Apoptosis*, 25, 205-216.
- Chen, Y., Wu, Q., Lin, J., & Wei, J. (2020). DARS-AS1 accelerates the proliferation of cervical cancer cells via miR-628-5p/JAG1 axis to activate Notch pathway. *Cancer cell international*, 20, 1-11.
- Chen, Z., Gao, Y., Gao, S., Song, D., & Feng, Y. (2020). MiR-135b-5p promotes viability, proliferation, migration and invasion of gastric cancer cells by targeting Krüppel-like factor 4 (KLF4). *Archives of Medical Science*, 16(1), 167-176.
- Cheng, C. W., Chen, P. M., Hsieh, Y. H., Weng, C. C., Chang, C. W., Yao, C. C., ... & Shen, C. Y. (2015). Foxo3a-mediated overexpression of microRNA-622 suppresses tumor metastasis by repressing hypoxia-inducible factor-1 α in ERK-responsive lung cancer. *Oncotarget*, 6(42), 44222.
- Cheung, T. H., Man, K. N. M., Yu, M. Y., Yim, S. F., Siu, N. S., Lo, K. W., ... & Wong, Y. F. (2012). Dysregulated microRNAs in the pathogenesis and progression of cervical neoplasm. *Cell Cycle*, 11(15), 2876-2884.

- Choi, P. W., Liu, T. L., Wong, C. W., Liu, S. K., Lum, Y. L., & Ming, W. K. (2022). The Dysregulation of MicroRNAs in the Development of Cervical Pre-Cancer—An Update. *International Journal of Molecular Sciences*, 23(13), 7126.
- Chu, C. Y., & Rana, T. M. (2006). Translation repression in human cells by microRNA-induced gene silencing requires RCK/p54. *PLoS biology*, 4(7), e210.
- Clarke, M. A., Wentzensen, N., Mirabello, L., Ghosh, A., Wacholder, S., Harari, A., ... & Burk, R. D. (2012). Human papillomavirus DNA methylation as a potential biomarker for cervical cancer. *Cancer Epidemiology, biomarkers & prevention*, 21(12), 2125-2137.
- Condrat, C. E., Thompson, D. C., Barbu, M. G., Bugnar, O. L., Boboc, A., Cretoiu, D., ... & Voinea, S. C. (2020). miRNAs as biomarkers in disease: latest findings regarding their role in diagnosis and prognosis. *Cells*, 9(2), 276.
- Conrad, M., Bubb, V. J., & Schlegel, R. (1993). The human papillomavirus type 6 and 16 E5 proteins are membrane-associated proteins which associate with the 16-kilodalton pore-forming protein. *Journal of virology*, 67(10), 6170-6178.
- Contreras-Paredes, A., De la Cruz-Hernández, E., Martínez-Ramírez, I., Dueñas-González, A., & Lizano, M. (2009). E6 variants of human papillomavirus 18 differentially modulate the protein kinase B/phosphatidylinositol 3-kinase (akt/PI3K) signaling pathway. *Virology*, 383(1), 78-85.
- Correia de Sousa, M., Gjorgjieva, M., Dolicka, D., Sobolewski, C., & Foti, M. (2019). Deciphering miRNAs' action through miRNA editing. *International journal of molecular sciences*, 20(24), 6249.
- Costa, V., Dico, A. L., Rizzo, A., Rajata, F., Tripodi, M., Alessand, R., & Conigliaro, A. (2017). MiR-675-5p supports hypoxia induced epithelial to mesenchymal transition in colon cancer cells. *Oncotarget*, 8(15), 24292.
- Crow, J. M. (2012). HPV: The global burden. *Nature*, 488(7413), S2-S3.
- Cuzick, J., Myers, O., Hunt, W. C., Robertson, M., Joste, N. E., Castle, P. E., ... & Wheeler, C. M. (2014). A population-based evaluation of cervical screening in the United States: 2008–2011. *Cancer epidemiology, biomarkers & prevention*, 23(5), 765-773.

- Dasgupta, S., Chakraborty, S. B., Roy, A., Roychowdhury, S., & Panda, C. K. (2003). Differential deletions of chromosome 3p are associated with the development of uterine cervical carcinoma in Indian patients. *Molecular Pathology*, 56(5), 263.
- de Freitas, A. C., Gurgel, A. P. A. D., Chagas, B. S., Coimbra, E. C., & do Amaral, C. M. M. (2012). Susceptibility to CaCx: an overview. *Gynecologic oncology*, 126(2), 304-311.
- De Strooper, L. M., van Zummeren, M., Steenberg, R. D., Bleeker, M. C., Hesselink, A. T., Wisman, G. B. A., ... & Meijer, C. J. (2014). CADM1, MAL and miR124-2 methylation analysis in cervical scrapes to detect cervical and endometrial cancer. *Journal of clinical pathology*, 67(12), 1067-1071.
- De Villiers, E. M., Fauquet, C., Broker, T. R., Bernard, H. U., & Zur Hausen, H. (2004). Classification of papillomaviruses. *Virology*, 324(1), 17-27.
- Del Pino, M., Svanholm-Barrie, C., Torné, A., Marimon, L., Gaber, J., Sagasta, A., ... & Ordi, J. (2015). mRNA biomarker detection in liquid-based cytology: a new approach in the prevention of cervical cancer. *Modern Pathology*, 28(2), 312-320.
- Di, Y., Jiang, Y., Shen, X., Liu, J., Gao, Y., Cai, H., ... & Jin, S. (2021). Downregulation of miR-135b-5p suppresses progression of esophageal cancer and contributes to the effect of cisplatin. *Frontiers in Oncology*, 11, 679348.
- Diez, H., Fischer, A., Winkler, A., Hu, C. J., Hatzopoulos, A. K., Breier, G., & Gessler, M. (2007). Hypoxia-mediated activation of Dll4-Notch-Hey2 signaling in endothelial progenitor cells and adoption of arterial cell fate. *Experimental cell research*, 313(1), 1-9.
- Disbrow, G. L., Hanover, J. A., & Schlegel, R. (2005). Endoplasmic reticulum-localized human papillomavirus type 16 E5 protein alters endosomal pH but not trans-Golgi pH. *Journal of virology*, 79(9), 5839-5846.
- Doghish, A. S., Ali, M. A., Elyan, S. S., Elrebehy, M. A., Mohamed, H. H., Mansour, R. M., ... & Moustafa, H. A. M. (2023). miRNAs role in cervical cancer pathogenesis and targeted therapy: Signaling pathways interplay. *Pathology-Research and Practice*, 244, 154386.
- Dolman, L., Sauvaget, C., Muwonge, R., & Sankaranarayanan, R. (2014). Meta-analysis of the efficacy of cold coagulation as a treatment method for cervical intraepithelial neoplasia: a

systematic review. *BJOG: An International Journal of Obstetrics & Gynaecology*, 121(8), 929-942.

Doorbar, J. (2006). Molecular biology of human papillomavirus infection and cervical cancer. *Clinical science*, 110(5), 525-541.

Dueñas-González, A., Lizano, M., Candelaria, M., Cetina, L., Arce, C., & Cervera, E. (2005). Epigenetics of cervical cancer. An overview and therapeutic perspectives. *Molecular cancer*, 4, 1-24.

Dutta, S., Begum, R., Mazumder, D., Mandal, S. S., Mondal, R., Biswas, J., ... & Basu, P. (2012). Prevalence of human papillomavirus in women without cervical cancer: a population-based study in Eastern India. *International journal of gynecological pathology*, 31(2), 178-183.

Dutta, S., Singh, R. K., Mandal, R. K., Roychoudhury, S., Basu, P., & Panda, C. K. (2016). Alteration of Human Papillomavirus Type 16 Genetic and Epigenetic Profiles in Cervical Cancer Patients Is Indicative of Poor Disease Prognosis: A Cohort Analysis. *International journal of gynecological cancer: official journal of the International Gynecological Cancer Society*, 26(4), 750–757.

Egawa, N., Egawa, K., Griffin, H., & Doorbar, J. (2015). Human papillomaviruses; epithelial tropisms, and the development of neoplasia. *Viruses*, 7(7), 3863-3890.

Elshelmani, H., Keegan, D., & Rani, S. (2022). Serum MicroRNAs Profiling in Age-Related Macular Degeneration. In *MicroRNA Profiling: Methods and Protocols* (pp. 123-135). New York, NY: Springer US.

Fabian, M. R., Mathonnet, G., Sundermeier, T., Mathys, H., Zipprich, J. T., Svitkin, Y. V., ... & Sonenberg, N. (2009). Mammalian miRNA RISC recruits CAF1 and PABP to affect PABP-dependent deadenylation. *Molecular cell*, 35(6), 868-880.

Fan, Y., Li, H., Ma, X., Gao, Y., Bao, X., Du, Q., ... & Zhang, X. (2016). Dicer suppresses the malignant phenotype in VHL-deficient clear cell renal cell carcinoma by inhibiting HIF-2 α . *Oncotarget*, 7(14), 18280.

- Farzanehpour, M., Mozhgani, S. H., Jalilvand, S., Faghihloo, E., Akhavan, S., Salimi, V., & Azad, T. M. (2019). Serum and tissue miRNAs: potential biomarkers for the diagnosis of cervical cancer. *Virology journal*, 16, 1-9.
- Fedele, A. O., Whitelaw, M. L., & Peet, D. J. (2002). Regulation of gene expression by the hypoxia-inducible factors. *Molecular interventions*, 2(4), 229.
- Finkel, T., Serrano, M., & Blasco, M. A. (2007). The common biology of cancer and ageing. *Nature*, 448(7155), 767-774.
- Forman, J. J., Legesse-Miller, A., & Collier, H. A. (2008). A search for conserved sequences in coding regions reveals that the let-7 microRNA targets Dicer within its coding sequence. *Proceedings of the National Academy of Sciences*, 105(39), 14879-14884.
- Foxler, D. E., Bridge, K. S., James, V., Webb, T. M., Mee, M., Wong, S. C., ... & Sharp, T. V. (2012). The LIMD1 protein bridges an association between the prolyl hydroxylases and VHL to repress HIF-1 activity. *Nature cell biology*, 14(2), 201-208.
- Franceschi, S., Rajkumar, R., Snijders, P. J. F., Arslan, A., Mahe, C., Plummer, M., ... & Weiderpass, E. (2005). Papillomavirus infection in rural women in southern India. *British journal of cancer*, 92(3), 601-606.
- Fukaya, T., & Tomari, Y. (2012). MicroRNAs mediate gene silencing via multiple different pathways in *Drosophila*. *Molecular cell*, 48(6), 825-836.
- Gao, Y., Cai, Q., Huang, Y., Li, S., Yang, H., Sun, L., ... & Wang, Y. (2016). MicroRNA-21 as a potential diagnostic biomarker for breast cancer patients: a pooled analysis of individual studies. *Oncotarget*, 7(23), 34498.
- Gnarra, J. R., Tory, K., Weng, Y., Schmidt, L., Wei, M. H., Li, H., ... & Linehan, W. M. (1994). Mutations of the VHL tumour suppressor gene in renal carcinoma. *Nature genetics*, 7(1), 85-90.
- Grabe, N., Lahrmann, B., Pommerenke, T., von Knebel Doeberitz, M., Reuschenbach, M., & Wentzensen, N. (2010). A virtual microscopy system to scan, evaluate and archive biomarker enhanced cervical cytology slides. *Analytical Cellular Pathology*, 32(1-2), 109-119.

- Guo, Z. Z., Ma, Z. J., He, Y. Z., Jiang, W., Xia, Y., Pan, C. F., ... & Chen, Y. J. (2020). miR-550a-5p functions as a tumor promoter by targeting LIMD1 in lung adenocarcinoma. *Frontiers in Oncology*, 10, 570733.
- Gurumurthy, R. K., Koster, S., Kumar, N., Meyer, T. F., & Chumduri, C. (2022). Patient-derived and mouse endo-ectocervical organoid generation, genetic manipulation and applications to model infection. *Nature Protocols*, 17(7), 1658-1690.
- Haedicke, J., & Iftner, T. (2016). A review of the clinical performance of the Aptima HPV assay. *Journal of Clinical Virology*, 76, S40-S48.
- Hao, Z., Yang, J., Wang, C., Li, Y., Zhang, Y., Dong, X., ... & Qian, J. (2015). MicroRNA-7 inhibits metastasis and invasion through targeting focal adhesion kinase in cervical cancer. *International journal of clinical and experimental medicine*, 8(1), 480.
- Harris, C. P., Lu, X. Y., Narayan, G., Singh, B., Murty, V. V., & Rao, P. H. (2003). Comprehensive molecular cytogenetic characterization of cervical cancer cell lines. *Genes, Chromosomes and Cancer*, 36(3), 233-241.
- Hasan, M. T., Islam, M. R., Islam, M. R., Altahan, B. R., Ahmed, K., Bui, F. M., ... & Moni, M. A. (2023). Systematic approach to identify therapeutic targets and functional pathways for the cervical cancer. *Journal of Genetic Engineering and Biotechnology*, 21(1), 10.
- Hausen, H. Z. (2000). Papillomaviruses causing cancer: evasion from host-cell control in early events in carcinogenesis. *Journal of the National Cancer Institute*, 92(9), 690-698.
- He, Y., Lin, J., Ding, Y., Liu, G., Luo, Y., Huang, M., ... & Wang, K. (2016). A systematic study on dysregulated microRNA s in cervical cancer development. *International journal of cancer*, 138(6), 1312-1327.
- Herman, J. G., Latif, F., Weng, Y., Lerman, M. I., Zbar, B., Liu, S., ... & Linehan, W. M. (1994). Silencing of the VHL tumor-suppressor gene by DNA methylation in renal carcinoma. *Proceedings of the National Academy of Sciences*, 91(21), 9700-9704.
- Hou, X., Li, T., Ren, Z., & Liu, Y. (2016). Novel BRCA2-interacting protein, LIMD1, is essential for the centrosome localization of BRCA2 in esophageal cancer cell. *Oncology Research*, 24(4), 247.

- Hu, Z., Zhu, D., Wang, W., Li, W., Jia, W., Zeng, X., ... & Ma, D. (2015). Genome-wide profiling of HPV integration in cervical cancer identifies clustered genomic hot spots and a potential microhomology-mediated integration mechanism. *Nature genetics*, 47(2), 158-163.
- Hua, K., Jin, J., Zhao, J., Song, J., Song, H., Li, D., ... & Fang, L. (2016). miR-135b, upregulated in breast cancer, promotes cell growth and disrupts the cell cycle by regulating LATS2. *International journal of oncology*, 48(5), 1997-2006.
- Huang, Y., Li, Y., Wang, F. F., Lv, W., Xie, X., & Cheng, X. (2016). Over-expressed miR-224 promotes the progression of cervical cancer via targeting RASSF8. *PLoS One*, 11(9), e0162378.
- Huggins, C. J., & Andrulis, I. L. (2008). Cell cycle regulated phosphorylation of LIMD1 in cell lines and expression in human breast cancers. *Cancer letters*, 267(1), 55-66.
- Hull, R., Mbele, M., Makhafola, T., Hicks, C., Wang, S. M., Reis, R. M., ... & Dlamini, Z. (2020). Cervical Cancer in low and middle-income countries. *Oncology letters*, 20(3), 2058-2074.
- Human protein atlas database: www.proteinatlas.org
- Huntzinger, E., & Izaurralde, E. (2011). Gene silencing by microRNAs: contributions of translational repression and mRNA decay. *Nature Reviews Genetics*, 12(2), 99-110.
- Huntzinger, E., Braun, J. E., Heimstädt, S., Zekri, L., & Izaurralde, E. (2010). Two PABPC1-binding sites in GW182 proteins promote miRNA-mediated gene silencing. *The EMBO journal*, 29(24), 4146-4160.
- Hwang, T. I. S., Cui, Y. C., Chen, Y. C., Chen, P. C., Tsai, T. F., Chou, K. Y., ... & Chang, A. C. (2023). Tumor suppressive functions of hsa-miR-34a on cell cycle, migration and protective autophagy in bladder cancer. *International Journal of Oncology*, 62(5), 66.
- Ilahi, N. E., & Bhatti, A. (2020). Impact of HPV E5 on viral life cycle via EGFR signaling. *Microbial pathogenesis*, 139, 103923.
- International Agency for Research on Cancer. (2005). Cervix cancer screening. In *Cervix cancer screening* (pp. 302-302).
- International Agency for Research on Cancer. (2006). Human papillomaviruses. *IARC monographs on the evaluation of carcinogenic risks to humans*, 90.

- Ipsaro, J. J., & Joshua-Tor, L. (2015). From guide to target: molecular insights into eukaryotic RNA-interference machinery. *Nature structural & molecular biology*, 22(1), 20-28.
- Islam, M. S., Dasgupta, H., Basu, M., Roy, A., Alam, N., Roychoudhury, S., & Kumar Panda, C. (2020). Reduction of nuclear Y654-p- β -catenin expression through SH3GL2-mediated downregulation of EGFR in chemotolerance TNBC: Clinical and prognostic importance. *Journal of Cellular Physiology*, 235(11), 8114-8128.
- Ivanov, M. K., Titov, S. E., Glushkov, S. A., Dzyubenko, V. V., Malek, A. V., Arkhangelskaya, P. A., et al. (2018). Detection of high-grade neoplasia in air-dried cervical PAP smears by a microRNA-based classifier. *Oncology reports*, 39(3), 1099–1111.
- Iwakawa, H. O., & Tomari, Y. (2015). The functions of microRNAs: mRNA decay and translational repression. *Trends in cell biology*, 25(11), 651-665.
- James, V., Zhang, Y., Foxler, D. E., De Moor, C. H., Kong, Y. W., Webb, T. M., ... & Sharp, T. V. (2010). LIM-domain proteins, LIMD1, Ajuba, and WTIP are required for microRNA-mediated gene silencing. *Proceedings of the National Academy of Sciences*, 107(28), 12499-12504.
- Kadrmaz, J. L., & Beckerle, M. C. (2004). The LIM domain: from the cytoskeleton to the nucleus. *Nature reviews Molecular cell biology*, 5(11), 920-931.
- Kai, A. K. L., Chan, L. K., Lo, R. C. L., Lee, J. M. F., Wong, C. C. L., Wong, J. C. M., & Ng, I. O. L. (2016). Down-regulation of TIMP2 by HIF-1 α /miR-210/HIF-3 α regulatory feedback circuit enhances cancer metastasis in hepatocellular carcinoma. *Hepatology*, 64(2), 473-487.
- Kawai, S., Fujii, T., Kukimoto, I., Yamada, H., Yamamoto, N., Kuroda, M., ... & Iwata, A. (2018). Identification of miRNAs in cervical mucus as a novel diagnostic marker for cervical neoplasia. *Scientific reports*, 8(1), 7070.
- Kendrick, J. E., Conner, M. G., & Huh, W. K. (2007). Gene expression profiling of women with varying degrees of cervical intraepithelial neoplasia. *Journal of Lower Genital Tract Disease*, 11(1), 25-28.
- Kersemaekers, A. M. F., Fleuren, G. J., Kenter, G. G., Van den Broek, L. J., Uljee, S. M., Hermans, J., & Van de Vijver, M. J. (1999). Oncogene alterations in carcinomas of the uterine

cervix: overexpression of the epidermal growth factor receptor is associated with poor prognosis. *Clinical Cancer Research*, 5(3), 577-586.

Kim, S. H., Juhnn, Y. S., Kang, S., Park, S. W., Sung, M. W., Bang, Y. J., & Song, Y. S. (2006). Human papillomavirus 16 E5 up-regulates the expression of vascular endothelial growth factor through the activation of epidermal growth factor receptor, MEK/ERK1, 2 and PI3K/Akt. *Cellular and Molecular Life Sciences CMLS*, 63, 930-938.

Kim, S. H., Oh, J. M., No, J. H., Bang, Y. J., Juhnn, Y. S., & Song, Y. S. (2009). Involvement of NF- κ B and AP-1 in COX-2 upregulation by human papillomavirus 16 E5 oncoprotein. *Carcinogenesis*, 30(5), 753-757.

Kiviat, N. B., Hawes, S. E., & Feng, Q. (2008). Screening for cervical cancer in the era of the HPV vaccine—the urgent need for both new screening guidelines and new biomarkers. *Journal of the National Cancer Institute*, 100(5), 290-291.

Koliopoulos, G., Nyaga, V. N., Santesso, N., Bryant, A., Martin-Hirsch, P. P., Mustafa, R. A., ... & Arbyn, M. (2017). Cytology versus HPV testing for cervical cancer screening in the general population. *Cochrane database of systematic reviews*, (8).

Kong, W., He, L., Richards, E. J., Challa, S., Xu, C. X., Permuth-Wey, J., ... & Cheng, J. Q. (2014). Upregulation of miRNA-155 promotes tumour angiogenesis by targeting VHL and is associated with poor prognosis and triple-negative breast cancer. *Oncogene*, 33(6), 679-689.

Kotani, K., Iwata, A., Kukimoto, I., Nishio, E., Mitani, T., Tsukamoto, T., et al. (2022). Nomogram for predicted probability of cervical cancer and its precursor lesions using miRNA in cervical mucus, HPV genotype and age. *Scientific reports*, 12(1), 16231.

Krutilina, R., Sun, W., Sethuraman, A., Brown, M., Seagroves, T. N., Pfeffer, L. M., ... & Fan, M. (2014). MicroRNA-18a inhibits hypoxia-inducible factor 1 α activity and lung metastasis in basal breast cancers. *Breast Cancer Research*, 16, 1-16.

Kulshreshtha, R., Davuluri, R. V., Calin, G. A., & Ivan, M. (2008). A microRNA component of the hypoxic response. *Cell Death & Differentiation*, 15(4), 667-671.

Kulshreshtha, R., Ferracin, M., Wojcik, S. E., Garzon, R., Alder, H., Agosto-Perez, F. J., ... & Ivan, M. (2007). A microRNA signature of hypoxia. *Molecular and cellular biology*, 27(5), 1859-1867.

- Laikangbam, P., Sengupta, S., Bhattacharya, P., Duttagupta, C., Singh, T. D., Verma, Y., ... & Mukhopadhyay, S. (2007). A comparative profile of the prevalence and age distribution of human papillomavirus type 16/18 infections among three states of India with focus on northeast India. *International Journal of Gynecologic Cancer*, 17(1).
- Langer, E. M., Feng, Y., Zhao, H., Rauscher, F. J., Kroll, K. L., & Longmore, G. D. (2008). Ajuba LIM proteins are snail/slug corepressors required for neural crest development in *Xenopus*. *Developmental cell*, 14(3), 424-436.
- Latif, F., Tory, K., Modi, W. S., Graziano, S. L., Gamble, G., Douglas, J., ... & Lerman, M. I. (1992). Molecular characterization of a large homozygous deletion in the small cell lung cancer cell line U2020: a strategy for cloning the putative tumor suppressor gene. *Genes, Chromosomes and Cancer*, 5(2), 119-127.
- Lazaros, K., Adam, S., Krokidis, M. G., Exarchos, T., Vlamos, P., & Vrahatis, A. G. (2025). Non-Invasive Biomarkers in the Era of Big Data and Machine Learning. *Sensors*, 25(5), 1396.
- Lazo, P. A. (1999). The molecular genetics of cervical carcinoma. *British journal of cancer*, 80(12), 2008-2018.
- Lee, C. (2022). A Combinational Approach for More Efficient miRNA Biosensing. *Current Genomics*, 23(1), 5.
- Leung, C. O., Deng, W., Ye, T. M., Ngan, H. Y., Tsao, S. W., Cheung, A. N., ... & Yeung, W. S. (2014). miR-135a leads to cervical cancer cell transformation through regulation of β -catenin via a SIAH1-dependent ubiquitin proteosomal pathway. *Carcinogenesis*, 35(9), 1931-1940.
- Li, B., Hu, Y., Ye, F., Li, Y., Lv, W., & Xie, X. (2010). Reduced miR-34a expression in normal cervical tissues and cervical lesions with high-risk human papillomavirus infection. *International Journal of Gynecologic Cancer*, 20(4).
- Li, J. H., Xiao, X., Zhang, Y. N., Wang, Y. M., Feng, L. M., Wu, Y. M., & Zhang, Y. X. (2011). MicroRNA miR-886-5p inhibits apoptosis by down-regulating Bax expression in human cervical carcinoma cells. *Gynecologic oncology*, 120(1), 145-151.
- Li, M. Y., & Hu, X. X. (2015). Meta-analysis of microRNA expression profiling studies in human cervical cancer. *Medical oncology*, 32, 1-9.
- Li, N., Cui, T., Guo, W., Wang, D., & Mao, L. (2019). MiR-155-5p accelerates the metastasis of cervical cancer cell via targeting TP53INP1. *OncoTargets and therapy*, 3181-3196.

- Li, T., Zhou, W., Li, Y., Gan, Y., Peng, Y., Xiao, Q., ... & Yin, G. (2019). MiR-4524b-5p/WTX/ β -catenin axis functions as a regulator of metastasis in cervical cancer. *PloS one*, 14(4), e0214822.
- Li, Y., Wang, F., Xu, J., Ye, F., Shen, Y., Zhou, J., ... & Xie, X. (2011). Progressive miRNA expression profiles in cervical carcinogenesis and identification of HPV-related target genes for miR-29. *The Journal of pathology*, 224(4), 484-495.
- Li, Y., Xu, D., Bao, C., Zhang, Y., Chen, D., Zhao, F., ... & He, X. (2015). MicroRNA-135b, a HSF1 target, promotes tumor invasion and metastasis by regulating RECK and EVI5 in hepatocellular carcinoma. *Oncotarget*, 6(4), 2421.
- Li, Y., Zhang, D., Wang, X., Yao, X., Ye, C., Zhang, S., ... & Ying, H. (2015). Hypoxia-inducible miR-182 enhances HIF1 α signaling via targeting PHD2 and FIH1 in prostate cancer. *Scientific reports*, 5(1), 12495.
- Liang, H., Zhao, Y., Pi, J., & Luo, R. (2021). MiR-875-5p suppresses cervical cancer cell proliferation and metastasis via negative regulation of EGFR. *Tropical Journal of Pharmaceutical Research*, 20(5), 939-946.
- Liu, C. J., Tsai, M. M., Hung, P. S., Kao, S. Y., Liu, T. Y., Wu, K. J., ... & Chang, K. W. (2010). miR-31 ablates expression of the HIF regulatory factor FIH to activate the HIF pathway in head and neck carcinoma. *Cancer research*, 70(4), 1635-1644.
- Liu, D., Jin, Y., Wu, J., Zhu, H., & Ye, D. (2022). MiR-135b-5p is an oncogene in pancreatic cancer to regulate GPRC5A expression by targeting transcription factor KLF4. *Cell death discovery*, 8(1), 23.
- Liu, L., Wang, Y., Bai, R., Yang, K., & Tian, Z. (2016). MiR-186 inhibited aerobic glycolysis in gastric cancer via HIF-1 α regulation. *Oncogenesis*, 5(5), e224-e224.
- Liu, N., Xia, W. Y., Liu, S. S., Chen, H. Y., Sun, L., Liu, M. Y., ... & Gao, J. X. (2016). MicroRNA-101 targets von Hippel-Lindau tumor suppressor (VHL) to induce HIF1 α mediated apoptosis and cell cycle arrest in normoxia condition. *Scientific Reports*, 6(1), 20489.
- Liu, S. S., Chan, K. K., Chu, D. K., Wei, T. N., Lau, L. S., Ngu, S. F., ... & Ngan, H. Y. (2018). Oncogenic microRNA signature for early diagnosis of cervical intraepithelial neoplasia and cancer. *Molecular oncology*, 12(12), 2009-2022.

- Liu, T., Zhao, L., Chen, W., Li, Z., Hou, H., Ding, L., & Li, X. (2014). Inactivation of von Hippel-Lindau increases ovarian cancer cell aggressiveness through the HIF1 α /miR-210/VMP1 signaling pathway. *International journal of molecular medicine*, 33(5), 1236-1242.
- Liu, Y., Tan, J., Ou, S., Chen, J., & Chen, L. (2019). Adipose-derived exosomes deliver miR-23a/b to regulate tumor growth in hepatocellular cancer by targeting the VHL/HIF axis. *Journal of physiology and biochemistry*, 75, 391-401.
- Lockwood, W. W., Coe, B. P., Williams, A. C., MacAulay, C., & Lam, W. L. (2007). Whole genome tiling path array CGH analysis of segmental copy number alterations in cervical cancer cell lines. *International journal of cancer*, 120(2), 436-443.
- Lorincz, A. T. (2016). Virtues and weaknesses of DNA methylation as a test for cervical cancer prevention. *Acta cytologica*, 60(6), 501-512.
- Lu, M., Gao, Q., Wang, Y., Ren, J., & Zhang, T. (2022). LINC00511 promotes cervical cancer progression by regulating the miR-497-5p/MAPK1 axis. *Apoptosis*, 27(11), 800-811.
- Lu, M., Huang, Y., Sun, W., Li, P., Li, L., & Li, L. (2017). miR-135b-5p promotes gastric cancer progression by targeting CMTM3. *International journal of oncology*, 52(2), 589-598.
- Lu, Y., Ji, N., Wei, W., Sun, W., Gong, X., & Wang, X. (2017). MiR-142 modulates human pancreatic cancer proliferation and invasion by targeting hypoxia-inducible factor 1 (HIF-1 α) in the tumor microenvironments. *Biology open*, 6(2), 252-259.
- Luo, T., Liu, Q., Tan, A., Duan, L., Jia, Y., Nong, L., ... & Liu, Y. (2020). Mesenchymal stem cell-secreted exosome promotes chemoresistance in breast cancer via enhancing miR-21-5p-mediated S100A6 expression. *Molecular Therapy-Oncolytics*, 19, 283-293.
- Macville, M., Schröck, E., Padilla-Nash, H., Keck, C., Ghadimi, B. M., Zimonjic, D., ... & Ried, T. (1999). Comprehensive and definitive molecular cytogenetic characterization of HeLa cells by spectral karyotyping. *Cancer research*, 59(1), 141-150.
- Makino, S., Mishima, Y., Inoue, K., & Inada, T. (2015). Roles of mRNA fate modulators Dhh1 and Pat1 in TNRC6-dependent gene silencing recapitulated in yeast. *Journal of Biological Chemistry*, 290(13), 8331-8347.

- Maranchie, J. K., Vasselli, J. R., Riss, J., Bonifacino, J. S., Linehan, W. M., & Klausner, R. D. (2002). The contribution of VHL substrate binding and HIF1- α to the phenotype of VHL loss in renal cell carcinoma. *Cancer cell*, 1(3), 247-255.
- Mattoscio, D., Medda, A., & Chiocca, S. (2018). Human papilloma virus and autophagy. *International journal of molecular sciences*, 19(6), 1775.
- Maxwell, P. H., Wiesener, M. S., Chang, G. W., Clifford, S. C., Vaux, E. C., Cockman, M. E., ... & Ratcliffe, P. J. (1999). The tumour suppressor protein VHL targets hypoxia-inducible factors for oxygen-dependent proteolysis. *Nature*, 399(6733), 271-275.
- Mazumder Indra, D., Mitra, S., Roy, A., Mondal, R. K., Basu, P. S., Roychoudhury, S., ... & Panda, C. K. (2011). Alterations of ATM and CADM1 in chromosomal 11q22. 3–23.2 region are associated with the development of invasive cervical carcinoma. *Human genetics*, 130, 735-748.
- Mazumder, D., Singh, R. K., Mitra, S., Dutta, S., Chakraborty, C., Basu, P. S., ... & Panda, C. K. (2011). Genetic and epigenetic changes of HPV16 in cervical cancer differentially regulate E6/E7 expression and associate with disease progression. *Gynecologic oncology*, 123(3), 597-604.
- McBee Jr, W. C., Gardiner, A. S., Edwards, R. P., Lesnock, J. L., & Bhargava, R. (2011). MicroRNA analysis in human papillomavirus (HPV)-associated cervical neoplasia and cancer. *J Carcinogene Mutagene*, 1(1).
- McCredie, M. R., Sharples, K. J., Paul, C., Baranyai, J., Medley, G., Jones, R. W., & Skegg, D. C. (2008). Natural history of cervical neoplasia and risk of invasive cancer in women with cervical intraepithelial neoplasia 3: a retrospective cohort study. *The lancet oncology*, 9(5), 425-434.
- Mirabello, L., Sun, C., Ghosh, A., Rodriguez, A. C., Schiffman, M., Wentzensen, N., ... & Burk, R. D. (2012). Methylation of human papillomavirus type 16 genome and risk of cervical precancer in a Costa Rican population. *Journal of the National Cancer Institute*, 104(7), 556-565.
- Mishima, Y., Giraldez, A. J., Takeda, Y., Fujiwara, T., Sakamoto, H., Schier, A. F., & Inoue, K. (2006). Differential regulation of germline mRNAs in soma and germ cells by zebrafish miR-430. *Current biology*, 16(21), 2135-2142.

- Mitra, A. B., Murty, V. V. V. S., Li, R. G., Pratap, M., Luthra, U. K., & Chaganti, R. S. K. (1994). Allelotype analysis of cervical carcinoma. *Cancer research*, 54(16), 4481-4487.
- Mitra, S., Mazumder, D., Basu, P. S., Mondal, R. K., Roy, A., Roychoudhury, S., & Panda, C. K. (2010). Amplification of CyclinL1 in uterine cervical carcinoma has prognostic implications. *Molecular carcinogenesis*, 49(11), 935-943.
- Mitra, S., Mazumder, D., Basu, P. S., Mondal, R. K., Roy, A., Roychoudhury, S., & Panda, C. K. (2012b). Alterations of RASSF1A in premalignant cervical lesions: clinical and prognostic significance. *Molecular Carcinogenesis*, 51(9), 723-733.
- Mitra, S., Mazumder-Indra, D., Mondal, R. K., Basu, P. S., Roy, A., Roychoudhury, S., & Panda, C. K. (2012a). Inactivation of SLIT2-ROBO1/2 pathway in premalignant lesions of uterine cervix: clinical and prognostic significances. *PLoS One*, 7(6), e38342.
- Modis, Y., Trus, B. L., & Harrison, S. C. (2002). Atomic model of the papillomavirus capsid. *The EMBO journal*.
- Mohammaddoust, S., & Sadeghizadeh, M. (2023). Mir-183 functions as an oncogene via decreasing PTEN in breast cancer cells. *Scientific Reports*, 13(1), 8086.
- Montz, F. J. (2000). Management of high-grade cervical intraepithelial neoplasia and low-grade squamous intraepithelial lesion and potential complications. *Clinical obstetrics and gynecology*, 43(2), 394-409.
- Morata-Tarifa, C., Picon-Ruiz, M., Griñan-Lison, C., Boulaiz, H., Perán, M., Garcia, M. A., & Marchal, J. A. (2017). Validation of suitable normalizers for miR expression patterns analysis covering tumour heterogeneity. *Scientific Reports*, 7(1), 39782.
- Morgan, E. L., & Macdonald, A. (2020). Manipulation of JAK/STAT signalling by high-risk HPVs: Potential therapeutic targets for HPV-associated malignancies. *Viruses*, 12(9), 977.
- Mosciciki, A., Schiffman, M., Kajer, S., et al. (2006). Chapter 5: Updating the natural history of HPV and anogenital cancer. *Vaccine*, 24: S42-S51.
- Mullokandov, M. R., Kholodilov, N. G., Atkin, N. B., Burk, R. D., Johnson, A. B., & Klinger, H. P. (1996). Genomic alterations in cervical carcinoma: losses of chromosome heterozygosity and human papilloma virus tumor status. *Cancer research*, 56(1), 197-205.

- Muñoz, N., Bosch, F. X., De Sanjosé, S., Herrero, R., Castellsagué, X., Shah, K. V., ... & Meijer, C. J. (2003). Epidemiologic classification of human papillomavirus types associated with cervical cancer. *New England journal of medicine*, 348(6), 518-527.
- Murillo, R., Almonte, M., Pereira, A., Ferrer, E., Gamboa, O. A., Jerónimo, J., & Lazcano-Ponce, E. (2008). Cervical cancer screening programs in Latin America and the Caribbean. *Vaccine*, 26, L37-L48.
- Nair, V. B., Manasa, V. G., Sinto, M. S., Jayasree, K., James, F. V., & Kannan, S. (2018). Differential expression of microRNAs in uterine cervical cancer and its implications in carcinogenesis; an integrative approach. *International Journal of Gynecologic Cancer*, 28(3).
- Nakamura, M., Bodily, J. M., Beglin, M., Kyo, S., Inoue, M., & Laimins, L. A. (2009). Hypoxia-specific stabilization of HIF-1 α by human papillomaviruses. *Virology*, 387(2), 442-448.
- Nanda, K., McCrory, D. C., Myers, E. R., Bastian, L. A., Hasselblad, V., Hickey, J. D., & Matchar, D. B. (2000). Accuracy of the Papanicolaou test in screening for and follow-up of cervical cytologic abnormalities: a systematic review. *Annals of internal medicine*, 132(10), 810-819.
- Narayan, G., & Murty, V. V. (2010). Integrative genomic approaches in cervical cancer: implications for molecular pathogenesis. *Future oncology (London, England)*, 6(10), 1643–1652.
- Nayar, R., & Wilbur, D. C. (2015). The Pap Test and Bethesda 2014 “The reports of my demise have been greatly exaggerated.” (after a quotation from Mark Twain). *Acta cytologica*, 59(2), 121-132.
- Nelson, C. W., & Mirabello, L. (2023). Human papillomavirus genomics: Understanding carcinogenicity. *Tumour Virus Research*, 15, 200258.
- Nguyen, H. C., Yang, H., Fribourgh, J. L., Wolfe, L. S., & Xiong, Y. (2015). Insights into Cullin-RING E3 ubiquitin ligase recruitment: structure of the VHL-EloBC-Cul2 complex. *Structure*, 23(3), 441-449.
- Nishihara, T., Zekri, L., Braun, J. E., & Izaurralde, E. (2013). miRISC recruits decapping factors to miRNA targets to enhance their degradation. *Nucleic acids research*, 41(18), 8692-8705.

- Nishimura, T., Padamsi, Z., Fakim, H., Milette, S., Dunham, W. H., Gingras, A. C., & Fabian, M. R. (2015). The eIF4E-binding protein 4E-T is a component of the mRNA decay machinery that bridges the 5' and 3' termini of target mRNAs. *Cell reports*, 11(9), 1425-1436.
- Okoye, J. O., Ngokere, A. A., Onyenekwe, C. C., & Erinle, C. A. (2019). Comparable expression of miR-let-7b, miR-21, miR-182, miR-145, and p53 in serum and cervical cells: Diagnostic implications for early detection of cervical lesions. *International journal of health sciences*, 13(4), 29–38.
- Olsen, P. H., & Ambros, V. (1999). The lin-4 regulatory RNA controls developmental timing in *Caenorhabditis elegans* by blocking LIN-14 protein synthesis after the initiation of translation. *Developmental biology*, 216(2), 671-680.
- Origoni, M., Cristoforoni, P., Carminati, G., Stefani, C., Costa, S., Sandri, M. T., ... & Preti, M. (2015). E6/E7 mRNA testing for human papilloma virus-induced high-grade cervical intraepithelial disease (CIN2/CIN3): a promising perspective. *Ecancermedicalscience*, 9.
- Pang, R. T., Leung, C. O., Ye, T. M., Liu, W., Chiu, P. C., Lam, K. K., ... & Yeung, W. S. (2010). MicroRNA-34a suppresses invasion through downregulation of Notch1 and Jagged1 in cervical carcinoma and choriocarcinoma cells. *Carcinogenesis*, 31(6), 1037-1044.
- Pardini, B., De Maria, D., Francavilla, A., Di Gaetano, C., Ronco, G., & Naccarati, A. (2018). MicroRNAs as markers of progression in cervical cancer: a systematic review. *BMC cancer*, 18, 1-17.
- Patel, N. S., Li, J. L., Generali, D., Poulsom, R., Cranston, D. W., & Harris, A. L. (2005). Up-regulation of delta-like 4 ligand in human tumor vasculature and the role of basal expression in endothelial cell function. *Cancer research*, 65(19), 8690-8697.
- Pereira, P. M., Marques, J. P., Soares, A. R., Carreto, L., & Santos, M. A. (2010). MicroRNA expression variability in human cervical tissues. *PloS one*, 5(7), e11780.
- Perrone, F., Suardi, S., Pastore, E., Casieri, P., Orsenigo, M., Caramuta, S., ... & Pilotti, S. (2006). Molecular and cytogenetic subgroups of oropharyngeal squamous cell carcinoma. *Clinical cancer research*, 12(22), 6643-6651.

- Petit, M. M., Crombez, K. R., Vervenne, H. B., Weyns, N., & Van de Ven, W. J. (2005). The tumor suppressor Scrib selectively interacts with specific members of the zyxin family of proteins. *FEBS letters*, 579(22), 5061-5068.
- Pett, M., & Coleman, N. (2007). Integration of high-risk human papillomavirus: a key event in cervical carcinogenesis?. *The Journal of Pathology: A Journal of the Pathological Society of Great Britain and Ireland*, 212(4), 356-367.
- Pigault, C., Follenius-Wund, A., Schmutz, M., Freyssinet, J. M., & Brisson, A. (1994). Formation of two-dimensional arrays of annexin V on phosphatidylserine-containing liposomes. *Journal of molecular biology*, 236(1), 199-208.
- Pillai, R. S., Bhattacharyya, S. N., Artus, C. G., Zoller, T., Cougot, N., Basyuk, E., ... & Filipowicz, W. (2005). Inhibition of translational initiation by Let-7 MicroRNA in human cells. *Science*, 309(5740), 1573-1576.
- Pim, D., Massimi, P., Dilworth, S. M., & Banks, L. (2005). Activation of the protein kinase B pathway by the HPV-16 E7 oncoprotein occurs through a mechanism involving interaction with PP2A. *Oncogene*, 24(53), 7830-7838.
- Poli, U. R., Bidinger, P. D., & Gowrishankar, S. (2015). Visual inspection with acetic acid (via) screening program: 7 years experience in early detection of cervical cancer and pre-cancers in rural South India. *Indian Journal of Community Medicine*, 40(3), 203-207.
- Poli, U. R., Bidinger, P. D., & Gowrishankar, S. (2015). Visual inspection with acetic acid (via) screening program: 7 years experience in early detection of Cervical Cancer and pre-cancers in rural South India. *Indian Journal of Community Medicine*, 40(3), 203-207.
- Polo-Generelo, S., Torres, B., Guerrero-Martínez, J. A., Camafeita, E., Vázquez, J., Reyes, J. C., & Pintor-Toro, J. A. (2022). TGF- β -Upregulated lnc-nr6a1 acts as a reservoir of miR-181 and mediates assembly of a glycolytic complex. *Non-coding RNA*, 8(5), 62.
- Pontén, J., & Guo, Z. (1998). Precancer of the human cervix. *Cancer surveys*, 32, 201-229.
- Prowse, A. H., Webster, A. R., Richards, F. M., Richard, S., Olschwang, S., Resche, F., ... & Maher, E. R. (1997). Somatic inactivation of the VHL gene in Von Hippel-Lindau disease tumors. *American journal of human genetics*, 60(4), 765.

- Pu, T., Shen, M., Li, S., Yang, L., Gao, H., Xiao, L., ... & Bu, H. (2019). Repression of miR-135b-5p promotes metastasis of early-stage breast cancer by regulating downstream target SDCBP. *Laboratory Investigation*, 99(9), 1296-1308.
- Qiao, Y. L., Jeronimo, J., Zhao, F. H., Schweizer, J., Chen, W., Valdez, M., ... & Castle, P. E. (2014). Lower cost strategies for triage of human papillomavirus DNA-positive women. *International journal of cancer*, 134(12), 2891-2901.
- Qin, W., Dong, P., Ma, C., Mitchelson, K., Deng, T., Zhang, L., ... & Cheng, J. (2012). MicroRNA-133b is a key promoter of cervical carcinoma development through the activation of the ERK and AKT1 pathways. *Oncogene*, 31(36), 4067-4075.
- Qu, K., Zhang, X., Lin, T., Liu, T., Wang, Z., Liu, S., ... & Wu, Z. (2017). Circulating miRNA-21-5p as a diagnostic biomarker for pancreatic cancer: evidence from comprehensive miRNA expression profiling analysis and clinical validation. *Scientific reports*, 7(1), 1692.
- Ramírez-Moya, J., & Santisteban, P. (2019). miRNA-directed regulation of the main signaling pathways in thyroid cancer. *Frontiers in Endocrinology*, 10, 430.
- Ravi, R., Mookerjee, B., Bhujwalla, Z. M., Sutter, C. H., Artemov, D., Zeng, Q., ... & Bedi, A. (2000). Regulation of tumor angiogenesis by p53-induced degradation of hypoxia-inducible factor 1 α . *Genes & development*, 14(1), 34-44.
- Ronco, G., Dillner, J., Elfström, K. M., Tunesi, S., Snijders, P. J., Arbyn, M., ... & Meijer, C. J. (2014). Efficacy of HPV-based screening for prevention of invasive cervical cancer: follow-up of four European randomised controlled trials. *The lancet*, 383(9916), 524-532.
- Rotondo, J. C., Bosi, S., Bassi, C., Ferracin, M., Lanza, G., Gafà, R., ... & Martini, F. (2015). Gene expression changes in progression of cervical neoplasia revealed by microarray analysis of cervical neoplastic keratinocytes. *Journal of Cellular Physiology*, 230(4), 806-812.
- Roy, R., Pal, D., Sur, S., Mandal, S., Saha, P., & Panda, C. K. (2019). Pongapin and Karanjin, furanoflavanoids of *Pongamia pinnata*, induce G2/M arrest and apoptosis in Cervical Cancer cells by differential reactive oxygen species modulation, DNA damage, and nuclear factor kappa-light-chain-enhancer of activated B cell signaling. *Phytotherapy research*, 33(4), 1084-1094.
- Roychowdhury, A., Samadder, S., Das, P., Mandloi, S., Addya, S., Chakraborty, C., et al. (2017). Integrative genomic and network analysis identified novel genes associated with the

- development of advanced cervical squamous cell carcinoma. *Biochimica et biophysica acta. General subjects*, 1861(1 Pt A), 2899–2911.
- Sankaranarayanan, R., Nene, B. M., Dinshaw, K. A., Mahe, C., Jayant, K., Shastri, S. S., ... & Parkin, D. M. (2005). A cluster randomized controlled trial of visual, cytology and human papillomavirus screening for cancer of the cervix in rural India. *International journal of cancer*, 116(4), 617-623.
- Sankaranarayanan, R., Nene, B. M., Shastri, S. S., Jayant, K., Muwonge, R., Budukh, A. M., ... & Dinshaw, K. A. (2009). HPV screening for cervical cancer in rural India. *New England Journal of Medicine*, 360(14), 1385-1394.
- Sankaranarayanan, R., Wesley, R. S., & World Health Organization. (2003). A practical manual on visual screening for cervical neoplasia. (*No Title*).
- Sapp, M., Volpers, C., Müller, M., & Streeck, R. E. (1995). Organization of the major and minor capsid proteins in human papillomavirus type 33 virus-like particles. *Journal of General Virology*, 76(9), 2407-2412.
- Sasagawa, T., Takagi, H., & Makinoda, S. (2012). Immune responses against human papillomavirus (HPV) infection and evasion of host defense in cervical cancer. *Journal of Infection and Chemotherapy*, 18(6), 807-815.
- Sathyanarayanan, A., Chandrasekaran, K. S., & Karunakaran, D. (2016). microRNA-146a inhibits proliferation, migration and invasion of human cervical and colorectal cancer cells. *Biochemical and biophysical research communications*, 480(4), 528-533.
- Sauvaget, C., Fayette, J. M., Muwonge, R., Wesley, R., & Sankaranarayanan, R. (2011). Accuracy of visual inspection with acetic acid for cervical cancer screening. *International Journal of Gynecology & Obstetrics*, 113(1), 14-24.
- Sawai, S., Wong, P. F., & Ramasamy, T. S. (2022). Hypoxia-regulated microRNAs: the molecular drivers of tumor progression. *Critical Reviews in Biochemistry and Molecular Biology*, 57(4), 351-376.
- Scheffner, M., Werness, B. A., Huibregtse, J. M., Levine, A. J., & Howley, P. M. (1990). The E6 oncoprotein encoded by human papillomavirus types 16 and 18 promotes the degradation of p53. *cell*, 63(6), 1129-1136.

- Schiffman, M., & Wentzensen, N. (2013). Human papillomavirus infection and the multistage carcinogenesis of cervical cancer. *Cancer epidemiology, biomarkers & prevention*, 22(4), 553-560.
- Schmitz, M., Driesch, C., Jansen, L., Runnebaum, I. B., & Dürst, M. (2012). Non-random integration of the HPV genome in cervical cancer. *PloS one*, 7(6), e39632.
- Serocki, M., Bartoszewska, S., Janaszak-Jasiecka, A., Ochocka, R. J., Collawn, J. F., & Bartoszewski, R. (2018). miRNAs regulate the HIF switch during hypoxia: a novel therapeutic target. *Angiogenesis*, 21, 183-202.
- Sharp, T. V., Munoz, F., Bourboulia, D., Presneau, N., Darai, E., Wang, H. W., ... & Boshoff, C. (2004). LIM domains-containing protein 1 (LIMD1), a tumor suppressor encoded at chromosome 3p21. 3, binds pRB and represses E2F-driven transcription. *Proceedings of the National Academy of Sciences*, 101(47), 16531-16536.
- Shen, Z., Yu, N., Zhang, Y., Jia, M., Sun, Y., Li, Y., & Zhao, L. (2024). The potential roles of HIF-1 α in epithelial-mesenchymal transition and ferroptosis in tumor cells. *Cellular Signalling*, 122, 111345.
- Singh, R. K., Dasgupta, S., Bhattacharya, N., Chunder, N., Mondal, R., Roy, A., ... & Panda, C. K. (2005). Deletion in chromosome 11 and Bcl-1/Cyclin D1 alterations are independently associated with the development of uterine cervical carcinoma. *Journal of cancer research and clinical oncology*, 131, 395-406.
- Singh, R. K., Indra, D., Mitra, S., Mondal, R. K., Basu, P. S., Roy, A., ... & Panda, C. K. (2007). Deletions in chromosome 4 differentially associated with the development of cervical cancer: evidence of slit2 as a candidate tumor suppressor gene. *Human genetics*, 122, 71-81.
- Snijders, P. J., Steenbergen, R. D., Heideman, D. A., & Meijer, C. J. (2006). HPV-mediated cervical carcinogenesis: concepts and clinical implications. *The Journal of Pathology: A Journal of the Pathological Society of Great Britain and Ireland*, 208(2), 152-164.
- Snijders, P. J., Steenbergen, R. D., Heideman, D. A., & Meijer, C. J. (2006). HPV-mediated cervical carcinogenesis: concepts and clinical implications. *The Journal of Pathology: A Journal of the Pathological Society of Great Britain and Ireland*, 208(2), 152-164.
- Snoek, B. C., Verlaet, W., Babion, I., Novianti, P. W., van de Wiel, M. A., Wilting, S. M., ... & Steenbergen, R. D. (2019). Genome-wide microRNA analysis of HPV-positive self-samples

yields novel triage markers for early detection of cervical cancer. *International journal of cancer*, 144(2), 372-379.

Sohn, E. J., Won, G., Lee, J., Lee, S., & Kim, S. H. (2015). Upregulation of miRNA3195 and miRNA374b mediates the anti-angiogenic properties of melatonin in hypoxic PC-3 prostate cancer cells. *Journal of Cancer*, 6(1), 19.

Song, T., Zhang, X., Wang, C., Wu, Y., Cai, W., Gao, J., & Hong, B. (2011). MiR-138 suppresses expression of hypoxia-inducible factor 1alpha (HIF-1alpha) in clear cell renal cell carcinoma 786-O cells. *Asian Pac J Cancer Prev*, 12(5), 1307-11.

Sopov, I., Sörensen, T., Magbagbeolu, M., Jansen, L., Beer, K., Kühne-Heid, R., ... & Dürst, M. (2004). Detection of cancer-related gene expression profiles in severe cervical neoplasia. *International journal of cancer*, 112(1), 33-43.

Srivastava, A. N., Misra, J. S., Srivastava, S., Das, B. C., & Gupta, S. (2018). Cervical cancer screening in rural India: Status & current concepts. *Indian Journal of Medical Research*, 148(6), 687-696.

Subtelny, A. O., Eichhorn, S. W., Chen, G. R., Sive, H., & Bartel, D. P. (2014). Poly (A)-tail profiling reveals an embryonic switch in translational control. *Nature*, 508(7494), 66-71.

Sureshkumar, B. T., Shanmughapriya, S., Das, B. C., & Natarajaseenivasan, K. (2015). A population-based study of the prevalence of HPV in three districts of Tamil Nadu, India. *International Journal of Gynecology & Obstetrics*, 129(1), 58-61.

Swanton, C., Bernard, E., Abbosh, C., André, F., Auwerx, J., Balmain, A., ... & Hanahan, D. (2024). Embracing cancer complexity: Hallmarks of systemic disease. *Cell*, 187(7), 1589-1616.

Tam, S. Y., Wu, V. W., & Law, H. K. (2020). Hypoxia-induced epithelial-mesenchymal transition in cancers: HIF-1 α and beyond. *Frontiers in oncology*, 10, 486.

Tang, J., Li, X., Cheng, T., & Wu, J. (2021). miR-21-5p/SMAD7 axis promotes the progress of lung cancer. *Thoracic Cancer*, 12(17), 2307-2313.

Tang, T., Wong, H. K., Gu, W., Yu, M. Y., To, K. F., Wang, C. C., ... & Choy, K. W. (2013). MicroRNA-182 plays an onco-miRNA role in cervical cancer. *Gynecologic oncology*, 129(1), 199-208.

- Tang, Y., Zhao, Y., Ran, J., & Wang, Y. (2020). MicroRNA-21 promotes cell metastasis in cervical cancer through modulating epithelial-mesenchymal transition. *Oncology letters*, 19(4), 3289-3295.
- Thakur, M. D., Feng, Y., Jagannathan, R., Seppa, M. J., Skeath, J. B., & Longmore, G. D. (2010). Ajuba LIM proteins are negative regulators of the Hippo signaling pathway. *Current Biology*, 20(7), 657-662.
- Thorland, E. C., Myers, S. L., Gostout, B. S., & Smith, D. I. (2003). Common fragile sites are preferential targets for HPV16 integrations in cervical tumors. *Oncogene*, 22(8), 1225-1237.
- Thun, M., Linet, M. S., Cerhan, J. R., Haiman, C. A., & Schottenfeld, D. (Eds.). (2017). *Cancer epidemiology and prevention*. Oxford University Press.
- Tian, Q., Li, Y., Wang, F., Li, Y., Xu, J., Shen, Y., ... & Xie, X. (2014). MicroRNA detection in cervical exfoliated cells as a triage for human papillomavirus-positive women. *Journal of the National Cancer Institute*, 106(9), dju241.
- Till, S., Lejeune, E., Thermann, R., Bortfeld, M., Hothorn, M., Enderle, D., ... & Ladurner, A. G. (2007). A conserved motif in Argonaute-interacting proteins mediates functional interactions through the Argonaute PIWI domain. *Nature structural & molecular biology*, 14(10), 897-903.
- Tommasino, M., & Crawford, L. (1995). Human papillomavirus E6 and E7: proteins which deregulate the cell cycle. *Bioessays*, 17(6), 509-518.
- Torres-Poveda, K., Piña-Sánchez, P., Vallejo-Ruiz, V., Lizano, M., Cruz-Valdez, A., Juárez-Sánchez, P., ... & Manzo-Merino, J. (2020). Molecular markers for the diagnosis of high-risk human papillomavirus infection and triage of human papillomavirus-positive women. *Revista de investigación clínica*, 72(4), 198-212.
- Umez, T., Tadokoro, H., Azuma, K., Yoshizawa, S., Ohyashiki, K., & Ohyashiki, J. H. (2014). Exosomal miR-135b shed from hypoxic multiple myeloma cells enhances angiogenesis by targeting factor-inhibiting HIF-1. *Blood, The Journal of the American Society of Hematology*, 124(25), 3748-3757.
- Unwith, S., Zhao, H., Hennah, L., & Ma, D. (2015). The potential role of HIF on tumour progression and dissemination. *International journal of cancer*, 136(11), 2491-2503.

- Valdez, M., Jeronimo, J., Bansil, P., Qiao, Y. L., Zhao, F. H., Chen, W., ... & Castle, P. E. (2016). Effectiveness of novel, lower cost molecular human papillomavirus-based tests for cervical cancer screening in rural china. *International Journal of Cancer*, 138(6), 1453-1461.
- Valencia-Cervantes, J., & Sierra-Vargas, M. P. (2024). Regulation of Cancer-Associated miRNAs Expression under Hypoxic Conditions. *Analytical Cellular Pathology*, 2024(1), 5523283.
- Vogelstein, B., Papadopoulos, N., Velculescu, V. E., Zhou, S., Diaz Jr, L. A., & Kinzler, K. W. (2013). Cancer genome landscapes. *science*, 339(6127), 1546-1558.
- Walboomers, J. M., Jacobs, M. V., Manos, M. M., Bosch, F. X., Kummer, J. A., Shah, K. V., ... & Muñoz, N. (1999). Human papillomavirus is a necessary cause of invasive cervical cancer worldwide. *The Journal of pathology*, 189(1), 12-19.
- Wang, F., Liu, M., Li, X., & Tang, H. (2013). MiR-214 reduces cell survival and enhances cisplatin-induced cytotoxicity via down-regulation of Bcl2l2 in cervical cancer cells. *FEBS letters*, 587(5), 488-495.
- Wang, F., Zhang, H., Xu, N., Huang, N., Tian, C., Ye, A., ... & Zhang, Y. (2016). A novel hypoxia-induced miR-147a regulates cell proliferation through a positive feedback loop of stabilizing HIF-1 α . *Cancer biology & therapy*, 17(8), 790-798.
- Wang, H., Zhang, D., Chen, Q., & Hong, Y. (2019). Plasma expression of miRNA-21, -214, -34a, and -200a in patients with persistent HPV infection and cervical lesions. *BMC cancer*, 19(1), 986.
- Wang, L. H., Wu, C. F., Rajasekaran, N., & Shin, Y. K. (2019). Loss of tumor suppressor gene function in human cancer: an overview. *Cellular Physiology and Biochemistry*, 51(6), 2647-2693.
- Wang, W., Li, Y., Zhi, S., Li, J., Miao, J., Ding, Z., ... & Chen, S. (2021). LncRNA-ROR/microRNA-185-3p/YAP1 axis exerts function in biological characteristics of osteosarcoma cells. *Genomics*, 113(1), 450-461.
- Wang, Y., Zhou, S., Fan, K., & Jiang, C. (2019). MicroRNA-21 and its impact on signaling pathways in cervical cancer. *Oncology Letters*, 17(3), 3066-3070.

- Wei, Y. Q., Jiao, X. L., Zhang, S. Y., Xu, Y., Li, S., & Kong, B. H. (2019). MiR-9-5p could promote angiogenesis and radiosensitivity in cervical cancer by targeting SOCS5. *European Review for Medical & Pharmacological Sciences*, 23(17).
- Wen, C. X., Tian, H. L., Chen, E., Liu, J. F., & Liu, X. X. (2021). MiRNA-873-5p acts as a potential novel biomarker and promotes cervical cancer progression by regulating ZEB1 via notch signaling pathway. *Dose-Response*, 19(1), 15593258211001255.
- Wen, W., Ding, J., Sun, W., Wu, K., Ning, B., Gong, W., ... & Wang, H. (2010). Suppression of cyclin D1 by hypoxia-inducible factor-1 via direct mechanism inhibits the proliferation and 5-fluorouracil-induced apoptosis of A549 cells. *Cancer research*, 70(5), 2010-2019.
- Wentzensen, N., Fetterman, B., Castle, P. E., Schiffman, M., Wood, S. N., Stiemerling, E., ... & Kinney, W. (2015). p16/Ki-67 dual stain cytology for detection of cervical precancer in HPV-positive women. *Journal of the National Cancer Institute*, 107(12), djv257.
- Wentzensen, N., Fetterman, B., Tokugawa, D., Schiffman, M., Castle, P. E., Wood, S. N., ... & Kinney, W. (2014). Interobserver reproducibility and accuracy of p16/Ki-67 dual-stain cytology in cervical cancer screening. *Cancer cytopathology*, 122(12), 914-920.
- Whitlock, E. P., Vesco, K. K., Eder, M., Lin, J. S., Senger, C. A., & Burda, B. U. (2011). Liquid-based cytology and human papillomavirus testing to screen for cervical cancer: a systematic review for the US Preventive Services Task Force. *Annals of internal medicine*, 155(10), 687-697.
- Wightman, B., Ha, I., & Ruvkun, G. (1993). Posttranscriptional regulation of the heterochronic gene lin-14 by lin-4 mediates temporal pattern formation in *C. elegans*. *Cell*, 75(5), 855-862.
- Wilting, S. M., Snijders, P. J. F., Verlaet, W., Jaspers, A. V., Van De Wiel, M. A., Van Wieringen, W. N., ... & Steenbergen, R. D. M. (2013). Altered microRNA expression associated with chromosomal changes contributes to cervical carcinogenesis. *Oncogene*, 32(1), 106-116.
- World Health Organization. (2013). WHO guidance note: comprehensive cervical cancer prevention and control: a healthier future for girls and women.
- World Health Organization. (2020). *Global strategy to accelerate the elimination of cervical cancer as a public health problem*. World Health Organization.

World Health Organization. (2021). WHO Guideline for Screening and Treatment of Cervical Pre-cancer Lesions for Cervical Cancer Prevention: web annex A: syntheses of evidence. In *WHO guideline for screening and treatment of cervical pre-cancer lesions for cervical cancer prevention: web annex A: syntheses of evidence*.

World Health Organization. WHO Guidelines Approved by the Guidelines Review Committee. In *Comprehensive Cervical Cancer Control: A Guide to Essential Practice*; World Health Organization: Geneva, Switzerland, 2014.

Wright, A. A., Howitt, B. E., Myers, A. P., Dahlberg, S. E., Palescandolo, E., Van Hummelen, P., ... & Hirsch, M. S. (2013). Oncogenic mutations in cervical cancer: genomic differences between adenocarcinomas and squamous cell carcinomas of the cervix. *Cancer*, *119*(21), 3776-3783.

Wright, T. C., Ferenczy, A., & Kurman, R. J. (1994). Carcinoma and other tumors of the cervix. In *Blaustein's pathology of the female genital tract* (pp. 279-326). New York, NY: Springer New York.

Wu, F., Huang, W., & Wang, X. (2015). microRNA-18a regulates gastric carcinoma cell apoptosis and invasion by suppressing hypoxia-inducible factor-1 α expression. *Experimental and therapeutic medicine*, *10*(2), 717-722.

Wu, Z., Cai, X., Huang, C., Xu, J., & Liu, A. (2016). miR-497 suppresses angiogenesis in breast carcinoma by targeting HIF-1 α . *Oncology reports*, *35*(3), 1696-1702.

Xiao, B., Zhou, X., Ye, M., Lv, S., Wu, M., Liao, C., ... & Zhu, X. (2016). MicroRNA-566 modulates vascular endothelial growth factor by targeting Von Hippel-Landau in human glioblastoma in vitro and in vivo. *Molecular medicine reports*, *13*(1), 379-385.

Xie, H., Norman, I., Hjerpe, A., Vladic, T., Larsson, C., Lui, W. O., ... & Andersson, S. (2017). Evaluation of microRNA-205 expression as a potential triage marker for patients with low-grade squamous intraepithelial lesions. *Oncology Letters*, *13*(5), 3586-3598.

Xin, F., Liu, P., & Ma, C. F. (2016). A circulating serum miRNA panel as early detection biomarkers of cervical intraepithelial neoplasia. *European review for medical and pharmacological sciences*, *20*(23), 4846-4851.

- Xin, F., Liu, P., & Ma, C. F. (2016). A circulating serum miRNA panel as early detection biomarkers of cervical intraepithelial neoplasia. *European review for medical and pharmacological sciences*, 20(23), 4846–4851.
- Xu, J., Zhang, W., Lv, Q., & Zhu, D. (2015). Overexpression of miR-21 promotes the proliferation and migration of cervical cancer cells via the inhibition of PTEN. *Oncology reports*, 33(6), 3108-3116.
- Xu, Q., Liu, L. Z., Qian, X., Chen, Q., Jiang, Y., Li, D., ... & Jiang, B. H. (2012). MiR-145 directly targets p70S6K1 in cancer cells to inhibit tumor growth and angiogenesis. *Nucleic acids research*, 40(2), 761-774.
- Xu, Y., Zhao, S., Cui, M., & Wang, Q. (2015). Down-regulation of microRNA-135b inhibited growth of cervical cancer cells by targeting FOXO1. *International journal of clinical and experimental pathology*, 8(9), 10294.
- Xue, D., Yang, Y., Liu, Y., Wang, P., Dai, Y., Liu, Q., ... & Tan, Z. (2016). MicroRNA-206 attenuates the growth and angiogenesis in non-small cell lung cancer cells by blocking the 14-3-3 ζ /STAT3/HIF-1 α /VEGF signaling. *Oncotarget*, 7(48), 79805.
- Xue, T. M., Tao, L. D., Zhang, M., Zhang, J., Liu, X., Chen, G. F., ... & Zhang, P. J. (2015). Clinicopathological significance of MicroRNA-20b expression in hepatocellular carcinoma and regulation of HIF-1 α and VEGF effect on cell biological behaviour. *Disease markers*, 2015(1), 325176.
- Yamakuchi, M., Lotterman, C. D., Bao, C., Hruban, R. H., Karim, B., Mendell, J. T., ... & Lowenstein, C. J. (2010). P53-induced microRNA-107 inhibits HIF-1 and tumor angiogenesis. *Proceedings of the National Academy of Sciences*, 107(14), 6334-6339.
- Yang, Y. S., Smith-McCune, K., Darragh, T. M., Lai, Y., Lin, J. H., Chang, T. C., ... & Cheng, S. (2012). Direct human papillomavirus E6 whole-cell enzyme-linked immunosorbent assay for objective measurement of E6 oncoproteins in cytology samples. *Clinical and Vaccine Immunology*, 19(9), 1474-1479.
- Ye, J., Xu, M., Tian, X., Cai, S., & Zeng, S. (2019). Research advances in the detection of miRNA. *Journal of pharmaceutical analysis*, 9(4), 217-226.

- Yeh, Y. M., Chuang, C. M., Chao, K. C., & Wang, L. H. (2013). MicroRNA-138 suppresses ovarian cancer cell invasion and metastasis by targeting SOX4 and HIF-1 α . *International journal of cancer*, 133(4), 867-878.
- Yin, Y., Yan, Z. P., Lu, N. N., Xu, Q., He, J., Qian, X., ... & Liu, L. Z. (2013). Downregulation of miR-145 associated with cancer progression and VEGF transcriptional activation by targeting N-RAS and IRS1. *Biochimica et Biophysica Acta (BBA)-Gene Regulatory Mechanisms*, 1829(2), 239-247.
- Yoo, B., Kavishwar, A., Ghosh, S. K., Barteneva, N., Yigit, M. V., Moore, A., & Medarova, Z. (2014). Detection of miRNA expression in intact cells using activatable sensor oligonucleotides. *Chemistry & biology*, 21(2), 199-204.
- Zang, C., Sun, J., Liu, W., Chu, C., Jiang, L., & Ge, R. (2019). miRNA-21 promotes cell proliferation and invasion via VHL/PI3K/AKT in papillary thyroid carcinoma. *Human cell*, 32, 428-436.
- Zhai, Y., Kuick, R., Nan, B., Ota, I., Weiss, S. J., Trimble, C. L., ... & Cho, K. R. (2007). Gene expression analysis of preinvasive and invasive cervical squamous cell carcinomas identifies HOXC10 as a key mediator of invasion. *Cancer research*, 67(21), 10163-10172.
- Zhang, F., Liu, J., & Xie, B. B. (2019). RETRACTED: Downregulation of microRNA-205 inhibits cell invasion and angiogenesis of cervical cancer through TSLC1-mediated Akt signaling pathway. *Journal of cellular physiology*, 234(10), 18626-18638.
- Zhang, H., Yan, T., Liu, Z., Wang, J., Lu, Y., Li, D., & Liang, W. (2018). MicroRNA-137 is negatively associated with clinical outcome and regulates tumor development through EZH2 in cervical cancer. *Journal of cellular biochemistry*, 119(1), 938-947.
- Zhang, J., Zhou, W., Liu, Y., Liu, T., Li, C., & Wang, L. (2018). Oncogenic role of microRNA-532-5p in human colorectal cancer via targeting of the 5'UTR of RUNX3. *Oncology letters*, 15(5), 7215-7220.
- Zhang, R., Zhao, J., Xu, J., Wang, J., & Jia, J. (2016). miR-526b-3p functions as a tumor suppressor in colon cancer by regulating HIF-1 α . *American Journal of Translational Research*, 8(6), 2783.

- Zhang, S., Zhou, X., Wang, B., Zhang, K., Liu, S., Yue, K., ... & Wang, X. (2014). Loss of VHL expression contributes to epithelial–mesenchymal transition in oral squamous cell carcinoma. *Oral oncology*, 50(9), 809-817.
- Zhang, Y., Zhang, W., Xia, W., Xia, J., Zhang, H., & Liu, H. (2022). Downregulation of hsa-miR-135b-5p Inhibits Cell Proliferation, Migration, and Invasion in Colon Adenocarcinoma. *Genetics Research*, 2022, e16.
- Zhang, Z., Che, X., Yang, N., Bai, Z., Wu, Y., Zhao, L., & Pei, H. (2017). miR-135b-5p Promotes migration, invasion and EMT of pancreatic cancer cells by targeting NR3C2. *Biomedicine & Pharmacotherapy*, 96, 1341-1348.
- Zhou, A. D., Diao, L. T., Xu, H., Xiao, Z. D., Li, J. H., Zhou, H., & Qu, L. H. (2012). β -Catenin/LEF1 transactivates the microRNA-371-373 cluster that modulates the Wnt/ β -catenin-signaling pathway. *Oncogene*, 31(24), 2968-2978.
- Zhou, J., Xu, D., Xie, H., Tang, J., Liu, R., Li, J., ... & Cao, K. (2015). miR-33a functions as a tumor suppressor in melanoma by targeting HIF-1 α . *Cancer biology & therapy*, 16(6), 846-855.
- Zhou, Y., An, Q., Guo, R. X., Qiao, Y. H., Li, L. X., Zhang, X. Y., & Zhao, X. L. (2017). miR424-5p functions as an anti-oncogene in cervical cancer cell growth by targeting KDM5B via the Notch signaling pathway. *Life sciences*, 171, 9-15.
- Zhou, Y., Yang, C., Wang, K., Liu, X., & Liu, Q. (2017). MicroRNA-33b inhibits the proliferation and migration of osteosarcoma cells via targeting hypoxia-inducible factor-1 α . *Oncology research*, 25(3), 397.
- Ziello, J. E., Jovin, I. S., & Huang, Y. (2007). Hypoxia-Inducible Factor (HIF)-1 regulatory pathway and its potential for therapeutic intervention in malignancy and ischemia. *The Yale journal of biology and medicine*, 80(2), 51.
- Zou, W., & Cheng, J. (2020). MiR-887 promotes the progression of hepatocellular carcinoma via targeting VHL. *Technology in cancer research & treatment*, 19, 1533033820940425.

**Paper published/
Communicated**

PAPERS RELATED TO THE THESIS:

[1] **Farhin Sultana**, Ananya De1, Dr. Sreeya Bose, Anirban Roychowdhury, Masmuda Khatun, Puja Chatterjee, Manisha Vernekar Roy, Dipanwita Banerjee, Jayanta Chakrabarti, Ranajit K. Mandal, Chinmay Kumar Panda, Sankhadeep Dutta “Clinical evaluation of microRNA biomarkers miR-135b-5p and miR-21-5p on self-collected cervical swab samples for triaging HR-HPV-positive high-grade preneoplastic lesions (**Communicated, Under review**)

[2] **Farhin Sultana**, Sreeya Bose, Puja Chatterjee, Manisha Vernekar, Dipanwita Banerjee, Jayanta Chakrabarti, Ranajit Kumar Mandal, Chinmay Kumar Panda, Sankhadeep Dutta “Sensor-oligo-based direct detection of miR-135b-5p upregulation due to amplification of MIR135B locus during cervical carcinogenesis: A pilot non-invasive approach” (**Communicated, Under review**)

- **PATENT FILED (App no. – 202531022775)**

[3] **Farhin Sultana**, Nilanjana Chatterjee, Debica Mukherjee, Chinmay Kumar Panda, Sankhadeep Dutta “MiR-135b-5p and miR-21-5p: a double-tap gunshot to LIMD1 and VHL to promote metastasis of cervical cells by deregulating HIF-1 α stress response pathway” (**Communicated, Under review**)

PAPERS PUBLISHED AS CO-AUTHOR:

[1] Rituparna Roy, Nilanjana Chatterjee, Md Sadi Khan, **Farhin Sultana**, Arindam Roy, Sukanya Naskar, Rajdeep Guha, Sagar Sen, Jayanta Chakrabarti, Bishnu Pada Chatterjee, Chinmay Kumar Panda & Sankhadeep Dutta (2024). “High prevalence of CD44 and its ligand low molecular weight hyaluronan in plasma of HNSCC patients: clinical significance”. *Molecular Biology Reports*, 51(1), 157.

[2] Nilanjana Chatterjee, **Farhin Sultana**, Rituparna Roy, Samyadip Dey, Sukanya Naskar, Aniruddha Dam, Anup K. Bhowmick, Rakiba Begum, Shyam S. Mandal, Ranajit K. Mandal, Jayanta Chakrabarti, Chinmay K. Panda, Massimo Tommasino, Tarik Gheit, Sankhadeep Dutta (2023) “Prevalence of novel gamma HPV Types 223 and 225 in oral cavity and skin of indian normal and neoplastic participants. *Journal of Medical Virology*, 95(8), p.e29019”.

[3] Sudipta Mondal, **Farhin Sultana**, Dr. Sankhadeep Dutta, Dr. Mohabul A. Mondal (2023) “Synthesis of Luotonin and Rutaecarpine Analogues by One-Pot Intramolecular

Dehydrogenative Cross-Coupling and Benzylic C–H Oxidation, and In Vitro Cytotoxicity Assay”. *Chemistry Select*, **8**(25), p.e202300980.

[4] Sudipta Mondal, Rwitabrita Panda, Soumya Das, **Farhin Sultana**, Sankhadeep Dutta, Mohabul A. Mondal (2023) “Synthesis and ct-DNA binding study of a donor- π -acceptor dihydropyrimidinone fluorophore”. *Journal of Molecular Structure*, **1285**, 135438.

[5] Priyanka Dutta, Debolina Pal, **Farhin Sultana**, Ranajit Kumar Mandal, Anup Roy & Chinmay Kumar Panda (2023). “Down-regulation of FA-BRCA Pathway in Cervical Carcinoma Gradually Reversed During the Development of Chemo-tolerance: Clinical Implications”. *Reproductive Sciences*, 1-17.

[6] Md Asrafuddoza Hazari, Gautam Kannan, Akash Kumar Jha, Musale Pavan, Subrata Dasgupta, **Farhin Sultana**, Soumya Pujahari, Simran Singh, Sarbajeet Dutta, Sai Pydi, Sankhadeep Dutta, Prasenjit Bhaumik, Hamim Zafar, Ashutosh Kumar, Shamik Sen “Faster amylin aggregation on fibrillar collagen hastens diabetic progression through β cell death and and loss of function” (Manuscript Under review).

Seminars / Conferences attended

1. Delivered an **oral presentation** on “*Deregulation in expression of LIMD1 protein in the transforming epithelium during cervical carcinogenesis*” **at the 90th Annual Session of the National Academy of Sciences, India and Symposium on ‘Towards a New Healthcare regime for the Nation’, on February 25-27, 2021 on WEB.**
2. Presented a **poster** on “*MiRNA-135b-5p deregulate expression of LIMD1 mRNA during HPV associated cervical carcinogenesis*” **at the 34th International Papillomavirus Virtual Conference, November 15-19, 2021**
3. Delivered an **oral presentation** on “*Molecular triaging of cervical preneoplastic lesions by non-invasive detection of miRNA from cervical swab samples*” in the one-day symposium on Integrated Approach in S&T for Sustainable future on the occasion of **National Science Day, 28th February, 2022, held at Chittaranjan National Cancer Institute.**
4. **Awarded for best oral presentation on “LIMD1 targeting miR-135b-5p as biomarker for non-invasive detection of clinically relevant preneoplastic cervical lesions”. at the 11th General Assembly of Asian Pacific Organization for Cancer Prevention (APOCP11) held in Kolkata from December 8-10, 2022.**
5. Presented a **poster** on “*MiR-135b-5p dysregulation promotes cellular transformation during HR-HPV-induced cervical carcinogenesis*” **at the 43rd Annual Conference of the Indian Association for Cancer Research, on January 19-22, 2024, held at IISER**